ISSN 1831-9424 (PDF)
ISSN 1018-5593 (Printed)

European Commission

Performance-based earthquake engineering analysis of short-medium span steel-concrete composite bridges

(SEQBRI)

Research and Innovation

EUR 28455 EN

EUROPEAN COMMISSION
Directorate-General for Research and Innovation
Directorate D — Industrial Technologies
Unit D.4 — Coal and Steel

E-mail: rtd-steel-coal@ec.europa.eu
RTD-PUBLICATIONS@ec.europa.eu

Contact: RFCS Publications

European Commission
B-1049 Brussels

European Commission

Research Fund for Coal and Steel

Performance-based earthquake engineering analysis of short-medium span steel-concrete composite bridges

(SEQBRI)

Dr. Fabrizio Paolacci
Roma Tre University
161, Via Ostiense, 00154 Roma, ITALY

Prof. O.S. Bursi
University of Trento
12, Via Belenzani, 38100 Trento, ITALY

Dr. N. Popa
Arcelormittal Belval & Differdange s.a.
66, rue de Luxembourg, 4009 Esch-sur-Alzette, LUXEMBOURG

Dr. C. Cremona
Centre d'études et d'expertise sur les risques, l'environnement, la mobilité et l'aménagement
110, Rue de Paris, 77171 Sourdun, FRANCE

Dr. S. Stathopoulos
S. Stathopoulos - K. Farros Cconsulting Engineers
14, Korgialeniou, 11526 Athens, GREECE

Prof. B. Hoffmeister
Rheinisch-Westfaelische Technische Hochschule Aachen
55, Templergraben, 52062 Aachen, GERMANY

Grant Agreement RFSR-CT-2012-00032
1 July 2012 to 30 June 2015

Final report

Directorate-General for Research and Innovation

2017 EUR 28455 EN

Europe Direct is a service to help you find answers to your questions about the European Union

Freephone number (*)**:**

00 800 6 7 8 9 10 11

(*) Certain mobile telephone operators do not allow access to 00 800 numbers or these calls may be billed.

More information on the European Union is available on the Internet (http://europa.eu).

Cataloguing data can be found at the end of this publication.

Luxembourg: Publications Office of the European Union, 2017

Print	ISBN 978-92-79-65611-8	ISSN 1018-5593	doi:10.2777/17191	KI-NA-28-455-EN-C
PDF	ISBN 978-92-79-65612-5	ISSN 1831-9424	doi:10.2777/48012	KI-NA-28-455-EN-N

TABLE OF CONTENTS

1 FINAL SUMMARY

Nowadays, short-medium span steel-concrete composite I-girder bridges made of hot rolled steel beams are very popular, owing to their short construction time and reduced costs. Moreover, they are particularly suitable for seismic areas due to their limited weight. With regard to static loading, these bridges exhibit a favourable behaviour testified by recent research projects. However, seismic loading has not been yet fully investigated. For this reason, SEQBRI project aimed to fill this gap investigating the applicability a new design/assessment methodology (PBEE) to a new typology of steel concrete composite bridges with S355M/N-S460M/N fine grain steel and concrete cross beams, through a comprehensive experimental and numerical investigation. The results have been used to provide the foundation for a new generation of European seismic codes for bridges and to extend Eurocodes. To successfully reach this goal SEQBRI project has been articulated in 5 work packages (WP) and 20 technical tasks (T), (Fig. 1-1).

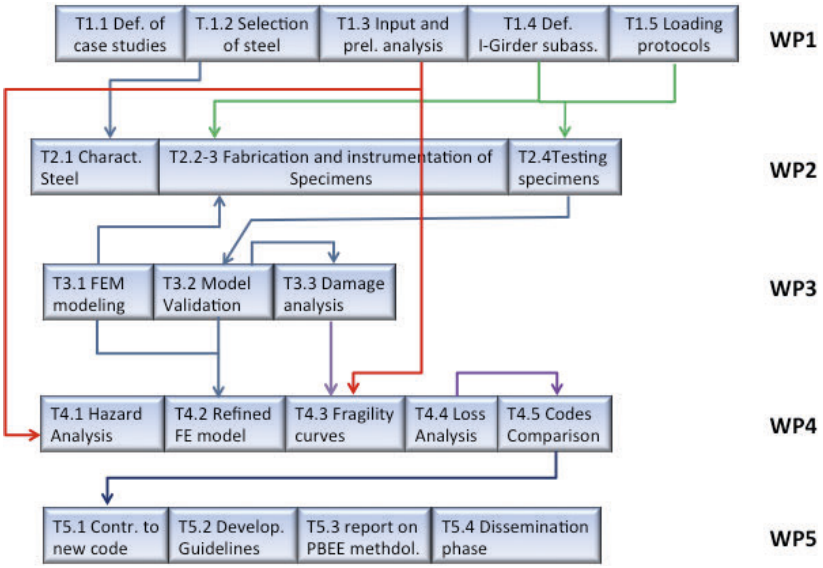

Fig. 1-1 Structure of the SEQBRI project

The research program consists of a combination of actions performed by experts in different fields (Academic Institutions (UNIRM3, UNITN, RWTH), designers (DOMI SA), a Center of excellence in Infrastructure and Transportation engineering (CEREMA, ex SETRA), a world's number one Steel Company (ARCELOR MITTAL) for the purpose of developing guidelines for the application of PBEE methodology for the design/assessment of steel concrete composite (SCC) bridges with concrete cross beams (CCB).

Towards this purpose, an extensive experimental (WP2), analytical (WP1, WP4), and numerical work (WP3) has been conducted within the project, under the synergy of all partners. The proposed guidelines are novel incorporating modern aspects of earthquake-resistant design for the design/assessment of SCC bridges with CCB (WP5).

PBEE is certainly a complex framework that needs time to be fully employed in a national code, therefore, in addition to the above guidelines, specific provisions for improving Eurocodes with some integration that could help technician in designing SCC bridges with CCB, have been finally proposed.

The results of the investigations are summarised below, demonstrating the achievements of project objectives, work package per work package.

1.1 WP 1: Definition of representative case studies. Selection of I-girder subassemblies to be tested

The Work Package 1 deals with the definition and selection of case studies to be designed and investigated through the Performance Based Earthquake Engineering methodology in WP4. As shown

in the planning of the project, the activities foreseen in this work package were limited to the first year of the project, which correspond to the Phase I.

The main objectives of WP1 are:

- Definition and design of representative case studies and preliminary numerical analyses for Engineering Demand Parameters (EDP) and Damage Measures (DM) estimation.
- Selection of I-girder subassemblies and preliminary numerical analyses for EDP and DM estimation at deck level.
- Definition of proper testing setup and protocols for I-girder subassemblies tests

Task 1.1 and 1.2 were dedicated to select and design of representative case studies of a new typology of steel concrete composite bridges with rolled I-girder deck that uses concrete cross beams as transversal connection element at piers and abutments. In particular, 3 different case studies were selected among different possibilities, which are characterized by different span numbers (i.e. 2, 3 and 6) and maximum span lengths (i.e. 20, 35 and 40m). Moreover, different reinforced concrete pier typologies (shear wall and multi-column piers) have been selected to include different deck-pier stiffness ratio that, as well-known, characterizes the seismic behaviour of this kind of bridges. The selection was carried out accounting for the current European and worldwide state of the art of steel concrete composite bridges. In addition, to show the sustainability of the selected typologies a cost operation evaluation of the selected case studies was also presented. All relevant details have been described and included in the Deliverable D1.1 (2013).

Task 1.3 was dedicated to the selection of the seismic input for Code-based and PBEE-based analysis of the selected case studies and to their preliminary analysis. In detail, natural records extracted and selected using the strong motion database of the Pacific Earthquake Engineering Research Centre. The selection was carried out according to the response spectra provided by the EC8. The selection procedure was based on the minimization of the error between the target spectrum and the spectrum of each accelerogram with a further modification of the frequency content using the wavelets transformation method. Four groups of 14 records compatible with EC8 spectra type 1 and 2 were selected and subdivided into two groups: Far Field and Near Fault records, respectively.

The modelling issue was extensively analysed including the most recent models proposed in literature. For a preliminary analysis of the selected case studies, refined and simplified models were used and each case study was accurately designed and checked according to Eurocodes. Consequently, the main engineering demand parameters (EDP) were identified and evaluated. In addition, a detailed cost analysis of each case study was performed. All relevant details have been described and included in the Deliverable D1.1 (2013).

In task 1.4, the criteria for the selection the I-girder subassemblies to be tested were shown, which are based on the result of task 1.3. After the description of possible Concrete Cross Beam configurations, three possible solutions were adopted. One is the DIN FB104 type C; the other variants (DOMI-1, DOMI-2) that include the presence of a low or a significant tensile stress at the CCB bottom. The case study of a straight overpass of 2x20m spans, with monolithic connection between deck and pier (i.e. CS-2.1.2), was selected as the most suitable configuration to be tested both in longitudinal and transversal direction.

In task 1.5 several possible testing protocols for I-girder subassemblies were described and analysed. The most suitable is identified with the classical ECCS procedure, given that the other ones are based on a realistic prediction of non-linear behaviour of the bridge and thus difficult to be easily implemented. The details of activities performed within task 1.4 and 1.5 are reported in Deliverable D1.2 (2013).

1.2 WP2: Tests on scaled I-girder subassembly specimens

In this WP the experimental evaluation of the transversal and longitudinal capacity of intermediate concrete crossbeams related to prototype I-girder subassemblies analysed in Task 1.3, have been performed in accordance with the following objectives of WP2:

- Experimental evaluation of the transverse capacity of intermediate concrete crossbeams in I-girder subassemblies.
- Experimental evaluation of the longitudinal capacity of intermediate concrete crossbeams in I-girder subassemblies.
- Investigation of the residual capacity after an earthquake of a damaged intermediate concrete crossbeam subject to traffic loads.

In particular 15 different experimental tests were carried on specimens with intermediate crossbeams in the UNITN and UNIRM3 Laboratories. Tests allowed to investigate both transversal and longitudinal behaviour of deck-I-girder sub-assemblages under monotonic/cyclic loading and to evaluate their residual capacity against vertical loads. As a result refined and stick FE models have been calibrated and validated (see WP3).

Task 2.1 has been devoted to the mechanical characterization of fine grain steel (S460M, S355J2W, S355J2+M). The activities have been successfully performed and concluded (Deliverable D1.2, 2013, Mid Term Report, 2014). In particular, a series of tests to mechanically characterize different steel types (S355J2W, S355J2+M, S460), including the one used for the specimens, were carried out in Task 2.1 by UNIRM3 and RWTH. In particular, monotonic tests were performed by UNIRM3 using 3-point bending configuration with the goal to characterize each type of steel, including force and deformation at yielding and the force and displacement at ultimate condition. The remaining cyclic tests have been used for the fatigue evaluation of each steel grade. A similar characterization has been performed by RWTH using tension/compression tests on round bar specimens. In both the cases, the cyclic tests allowed to calibrate the non-linear isotropic/kinematic hardening parameters of the Lemaitre-Chaboche function for the steel modelling in ABAQUS.

Task 2.2 concerns the design and construction of I-Girder specimens to test by UNIRM3 and UNITN. In particular, 8 specimens tested along the longitudinal direction (UNIRM3) and 6 speciemens tested along the transversal direction (UNITN) were built. The first set of specimens is a test subassembly that represents the deck-pier joint of Case Study 2.1.2 (Monolithic solution), whereas the second set represent the deck-pier joint of Case Study 2.1.1 (simply supported deck). A specimen has been also tested in vertical direction to characterize its residual vertical capacity for traffic loads for a given level of seismic damage. In order to minimize the scaling effects, especially for the concrete slab in terms of cracking pattern, a scale factor 1:2 has been adopted.

All specimens have been designed according to the selected CCB typologies defined in the WP1. Specifically, in longitudinal direction the following specimen typologies were adopted: 2 specimens equipped with DIN-FB104 Type C concrete cross beam, 2 specimens equipped with a DOMI-1 CCB and 4 specimens equipped with a DOMI-2 CCB. The same typologies have been adopted for the specimens to be tested in the transversal direction. In this case, 2 specimens for each typology have been built. Finally a specific test setup has been properly designed and built for each test typology. This activity has been designed using numerical simulation performed with linear and non-linear models. A simplified fiber-based model has been adopted for a preliminary simulation of the cyclic behaviour of the specimens. This model has been validetd through the experimental results and used in WP4 for the applications of the PBEE approach. In addition a refined 3D model has been implemented in ABQUS and used for a more detailed numerical-experimental comparison, whose results have been developed in WP3.

This comprehensive experimental campaign allowed to identify the relatioship between the Engineering Demand Parameters (EDP) selected in WP1 and WP4 and the Damage Measures (DM) identified in WP4 and adopetd for the PBEE analysis (Deliverable D4.3, 2015, and second annual report, 2015). All observed damage states, both in transversal and longitudinal direction, were identified and the related demand parameters (DM) quantified. These latter are in good agreement with the values adopetd for the PBEE calculation (Deliverable D4.3, 2015).

From the monotonic and cyclic tests in transversal direction (Task 2.3) the main conclusions are the following:

- The transversal displacement at which collapse of the specimen occurs varies slightly between the tests. Thus, the type of construction appears not to be responsible for the capacity of the specimens;
- The collapse mechanism developed primarily inside the concrete slab at the girder-cross beam interface;
- The transversal force at collapse appears particularly high and higher than the values expected applying the seismic design action prescribed by the Eurocode. This is mainly due to the particular configuration analysed (deck on bearings), which therefore, appear not particularly vulnerable to seismic actions.

The monotonic and cyclic tests in longitudinal direction (Task 2.4) shown instead a higher dependency from the CCB type of the vulnerability of SCC bridiges with monolithic configuration. In particular, the cyclic behavior of DOMI2 CCB shown in general the better performance with respect to the other two configurations. The main reasons are related to:

- a more ductile behaviour and a reduced level of damage in the CCB and in the steel girdes (buckling phenomenon);

- the presence of prestressing bars in the DOMI2 specimen avoided any pull-out phenomenon in the CCB in correspondence of the bottom flange of the steel girders. This latter was clearly present in the DIN-FB104 Type C and DOMI1 specimen with an irreversible damage condition;
- the possibility to recover the prestressing level or substitute the prestressing bars after a seismic event, makes the DOMI2 joint superior in case of steel concrete composite bridges located in high seismic zones;

Additional tests to evaluate the residual vertical load-carrying capacity for a given level of damage have been performed (Task 2.5). In particular, one of the specimens cyclically tested at UNITN was subjected to a monotonic vertical load till the collapse. The level of seismic damage imposed during the cyclic tests (ADS2) was determined by using an energy-based methodology. This tests points out that the residual vertical capacity available for traffic loads of the intermediate concrete crossbeam (CCB) is sufficient for a specific target limit state, more precisely the SLS\frequent. It was also noticed that the CCB, with that damage level reached, is able to satisfy not only the loading corresponding to the ULS, but, almost twice that load value. Additional details can be found in (Deliverable D2.4, 2015, 2nd Annual report, 2015).

1.3 WP3: Numerical simulations and damage analysis of I-girder subassemblies

In this WP detailed 3-dimensional finite element models have been implemented in the ABAQUS software package. All the three different joint typologies – DINF-FB 104, DOMI-1 and DOMI-2 – have been modelled. The available constitutive models have been studied and modified based on the conducted material tests – concrete cube tests as well monotonic and cyclic tests on the steel round bar specimens – done in WP2. Thus, reliable material parameters have been used as input for the numerical simulations. Before test data has been available, preliminary numerical simulations have been conducted, in order to assess the needed force and displacement capacities of the load actuators and gain preliminary insight into the behaviour of the specimens. Different modelling strategies have been investigated in order to find the optimum approach regarding detailed discretization but also computational efficiency and convergence robustness. Mesh sensitivity studies have been conducted to find out an acceptable compromise in both respects.

Both the transversally loaded specimens tested at UNITN as well the longitudinally loaded ones tested at UNIRM3 have been modelled. A special focus was given to the surrounding test setup which showed to play an important role especially for the transversally loaded specimens. Based on analytical considerations and parametric studies it was found out that much of the measured flexibility was origined by the surrounding setup rather than the specimen itself. This issue arises due to the fact that the specimen is indeed very stiff, and thus flexibility and slip effects of the setup – although very small in absolute values – have a large impact in relative terms. In order to compare simulation outcomes with test results, the setup effects needed to be excluded by post processing the test results or alternatively by including these effects in the numerical model. Both approaches have been followed in the calibration of the numerical model. Finally, the calibrated model could very well reproduce the test observations in both quantitative but also qualitative terms. Stiffness of the specimen and load displacement curves regarding reaction loads in direction of the applied load but also in perpendicular direction could be reproduced. Also the failure mode, crushing of the concrete at the transition of slab and CCB was the same as observed during the tests. Cracking patterns and reinforcement yielding have also been in very good agreement. With the calibrated model, the influence of several parameters has been investigated by parametric studies. Finally, cyclic simulations have been conducted.

For the longitudinally tested specimens damage patterns could also be reproduced very well. Cracking in the pier and in the slab and damage in the CCB resembled that one of the tests. Using in general the strength material parameters, which were determined for the calibrated model of the transversal tests, the peak load could be captured very well. However, in the pre-peak region stiffness of the numerical model is higher than in the tests. Some further effort is needed to assess on this issue and to further refine the models, especially concerning the detailed joint behaviour. Convergence issues must be solved to accomplish this task.

In sum the damage patterns observed during the tests could very well be reproduced both in the transversally loaded specimens and the longitudinally loaded specimens. Peak loads at failure of the simulations equal that one of the tests. Whereby the transversally loaded specimen matches very well the test load displacement curve, some differences exist for the longitudinally loaded specimen regarding stiffness. Parametric studies have been conducted for both test campaigns in order to assess on the influence of several parameters and modelling approaches. Cyclic

simulations have been conducted, albeit numerical convergence and computational time issues proved to be a challenging task.

1.4 WP4: Application of the PBEE methodology to selected Case Studies

In this WP, the probabilistic analysis of some case studies selected in task 1.1, subject to seismic loading has been carried out by means of the PBEE methodology. This WP is of paramount importance for the project because it realizes the fourth element of the PEER methodology, namely the Loss or Cost-effective risk analysis. As a result, economic losses have been estimated in terms of Repair Cost Ratio (RCR).

Consequently, five different tasks were dedicated to the above-mentioned aspects.

Task 4.1 has been devoted to the definition of seismic hazard relationships, the annual rate of exceeding a certain intensity measure p(IM), based on natural records matching design target spectra. They can be derived using classical hazard analyses with appropriate recurrence (e.g. Gutemberg-Richter, etc..) and proper attenuation laws, in order to establish the mean annual frequency of exceedance – Hazard– for each Intensity Measure (IM). For the scope of SEQBRI a high seismicity zone has been selected that is located in Priolo Gargallo (Italy). For the evaluation of the hazard curve and the corresponding uniform hazard spectra the Mathazard program developed by UNIRM3 (Giannini, 2015) has been employed. In particular, the uniform hazard spectrum corresponding to a probability of exceeding of 10% in 50 years has been built. The normalized form of this spectrum fits well the response spectrum of EC8 type 1. Therefore, the selection of natural records carried out in task 1.3 appears reasonable and represents well the frequency content of the structural response. To represent the damage potentiality of the seismic action the PGA is used as intensity measure (IM). However, many work dedicated to the efficiency of this IM demonstrated the weakness of this choice. Thus, a different IM has been specifically defined for SEQBRI. In particular, it is defined as the acceleration at zero period of the target response spectrum scaled at a specific PGA value. Consequently, the selected accelerograms are affected by the same scaling factor. This scaling procedure has been adopted in task 4.3 for the probabilistic seismic demand analysis of the SEQBRI bridges. More details can be found in the Mid Term Report (2014) and Deliverable D4.1 (2014).

Task 4.2 has been devoted to the refinement of FE models for the probabilistic seismic analysis of case studies. During the first period of SEQBRI project, simplified models were developed within WP1, in order to perform a preliminary response analysis of the selected bridges designed according to EC8. In order to assess the seismic performance of the bridges according to PBEE methodology refined models were developed for predicting non-linear behaviour of SCC bridges with CCB in longitudinal and transversal direction. In particular, a component-based mechanical model of the connection between the I-girder steel beam and the CCB of a deck, under lateral and longitudinal loading, was proposed.

The mechanical model developed in the OpenSEES environment and validated on the basis of experimental results is capable of taking into account the behaviour of the main mechanical components in a complementary way; thus, the interaction between the various parts of the concrete cross beam can be well characterized. Furthermore, it allows for the evaluation of the dissipated energy by the connection components during a seismic event. The model has been fully validated through the results of the experimental campaign at UNIRM3 and UNITN laboratories. Finally, these models have been integrated in a 3D model of the entire bridge. Its full description is reported in Deliverable D4.1 (2014).

In task 4.3 nonlinear time history analyses have been conducted to estimate the structural response in terms of engineering demand parameters (EDP), using the ground motions defined in task 4.1 at various levels of intensity measures (IM). In this respect, a series of Engineering Demand Parameters (global, intermediate, local) have been selected and used to perform Incremental Dynamic Analyses (IDA) for different valued of PGA.

The results highlighted that for the selected bridges the damage is mainly concentrated in the piers and that significant damage in the CCBs may start after significant levels of IM. In detail, CS1.1 and CS1.2 lead to similar conclusions. The two solutions are quite similar although different support configurations are used. The reason of this similarity lies in the fact that both case studies were designed in order to reduce the seismic action: CS 1.1 with an appropriate isolation system whilst CS 1.2 by plastic dissipation in the piers along the longitudinal direction (behavior factor q=3.5). All the EDPs present a smaller mean response value in the CS 1.1 than in the CS 1.2. For 2 spans bridge with deck monolithically connected to the pier (CS 2.1.2), it has been noticed that for

events with a PGA of 0.3 g or under, the critical part of the bridge is the pier with the formation of a plastic hinge at the base, whilst the concrete crossbeam does not seem to be affected by any relevant damage.

First level of damage within the intermediate CCB starts for values of PGA for which the lower group of studs within the CCB yield (PGA=0.5-0.6g). For the CS2 (skew bridge) the results show that the solution of deck on bearings protects the piers from excessive damage as well as the CCB. In fact, in this case the CCB and the pier remain elastic in design condition. This is due to the imposed unitary behaviour factor. The skewness seems to have a secondary role due to the isolation effect of the bearings. The analyses confirmed these conclusions also for the CS3. More details can be found in Deliverable D4.1 (2014).

In task 4.4 the main results in terms of damage analysis and fragility curves of the bridges selected in WP1 have been presented and discussed. Firstly, the definition of damage measures (DM) has been discussed. According to literature results and the main conclusions presented in Deliverable 4.1 (2014), a series of global, intermediated and local damage measures (DM) have been identified. In particular, for the piers the consolidated approach proposed by Pacific Earthquake Engineering Research Center have been adopted. This is based on experimental evidences and mainly relies on drift measures of different pier typologies.

Concerning one of the crucial aspects of the problem: the selection of representative DM for CCB, an analytical approach has been adopted, which is based on the proposed numerical models for the CCB defined in the Deliverable D4.1. Measures of the relative rotation between girder and CCB have been adopted as intermediate DM, whereas the slip of shear studs of CCB has been used as local DM. The main conclusions reported in Deliverable D2.3 (2015) confirmed the reliability of this choice.

Damage Analysis has been performed to evaluate the probabilistic relationship between the identified DMs and EPDs. Special attention has been paid on the formulation of the problem to account for the mutual exclusivity of the several DM levels. Consequently, a new approach in the formulation of the probability functions P(DM|EDP) and P(DM|IM) has been provided. The fragility curves P(DM|IM) built for the above DMs has shown again how the effects of earthquakes on this type of bridges are limited, especially in terms of CCB damage for which the probability of occurrence is rather low.

Task 4.5 has been devoted to loss analysis of the case studies analyzed in tasks 4.3 and 4.4. The work has been subdivided in several parts. The first part was dedicated the development of loss analysis of bridges in the framework of PBEE analysis. In particular decision models and variables for bridges have been identified and discussed and the loss calculation has been formulated in accordance to the PEER methodology. In order to show the potentiality of the method and to have an immediate application to the SEQBRI case studies the repair cost to total cost ratio has been assumed as Decision Variable (DV), to judge the goodness of the design. In this context, the unit costs have been considered as deterministic, leaving to future researches the evaluation of the influence of the cost randomness. Subsequently, a specific loss analysis method has been formulated for Steel Concrete Composite (SCC) bridges with Concrete Cross Beam (CCB). It is a revisited version of the Loss analysis method proposed in (Mackie et al 2008) and adapted for the special case of SEQBRI bridges. The method includes the definition of Damage States, Performance Groups, Damage Scenarios and Unit Repair Costs and it is specially dedicated to the evaluation of direct costs, even though indirect costs could be included and for which some general considerations have been provided only.

The method has been effectively implemented in Excel which uses the unit repair costs as input for each damage state and the probability of exceedance the damage states for each Intensity measure. Subsequently, according to each damage scenario definition the expected repair cost is evaluated as function of IM. In addition, the special formulation of the problem allows the disaggregation of this cost for the several Performance Groups. Finally, the probability of each scenario is provided along with overall expected repair cost conditioned to IM.

The method has been fully applied to the case study 2.1.2 showing that:

- Significant probability of occurrence of the minor damage scenario are due to 0.3g < PGA < 0.6 g;
- Significant probability of occurrence of the major damage scenario are due to PGA > 0.7 g;
- An overall expected repair ratio between 5-8 % is obtained for the minor damage scenario and >20% for PGA > 0.2 g for major damage scenario

- PG1, PG2 (pier) and PG3 (CCB) mainly govern the decision-making analysis given that their associated costs results particularly important. Therefore, any optimization action should act on these elements

Finally, the design optimization problem by using PBEE approach has been addressed identifying the most suitable methods. More details on task 4.5 can be found in deliverable D4.3 (2015).

1.5 WP5: Issuing of design guidelines and recommendations for improving European seismic code for bridges

WP5 represents the finalization of the technical achievements of the SEQBRI project. In this respect, a contribution to a new generation of seismic codes for design bridges is provided and design guidelines and recommendation for the extension of Eurocodes have been developed.

The main objectives of WP5 are:

- Contribution to the foundation of a new generation of European seismic codes for bridges (task 5.1)

  Performance-Based Earthquake Engineering (PBEE) is a concept that permits the design and construction of structures with a realistic and reliable understanding of the risk of life, occupancy, and economic loss that may occur as a result of future earthquakes. PBEE is based on an assessment of a structures' design to determine the probability of experiencing different types of losses, considering the range of potential earthquakes that may affect the structure. General performance-based provisions are issued for seismic design of bridges according to the PBEE approach, whose response under common and extreme earthquake loads would comply, with diverse needs and objectives of owners, users and society.

  On this basis, code-writing bodies could base the development of a new generation of European seismic codes for bridges. An attempt to collect all the aspects of Performance Based Earthquake Engineering (PBEE) methodology (Seismic Hazard, Modeling and Seismic Response Analysis, Damage Analysis, Decision Making analysis), is proposed, specializing the approach for the case of Steel Concrete Composite Bridges endowed with Concrete Cross Beam. All these aspects are presented in the form of guidelines to help code-writing bodies in implementing it in a new generation seismic code.

- Development of design guidelines and recommendations for extension of Eurocodes (task 5.2)

  PBEE is certainly a complex framework that needs time to be fully employed in a national code, therefore, the contribution to a new generation of European seismic codes for SCC bridges with CCB can be successfully used to improve current codes with some integration that could help technician in designing. Thus, design guidelines in seismic prone areas are developed. At this purpose experimental data and numerical simulations are organized in recommendations that will contribute to the improvement of Eurocodes. In particular, the main effort is devoted to the selection of proper models and analysis methods for the seismic analysis of this type of bridges and the design of the Concrete Cross Beam.

- Dissemination of project results (Task 5.3, Task 5.4).

  The transfer of knowledge and expertise gained within SEQBRI project was achieved through a round table, attended by all partners and invited experts, as well as dissemination of documents and other information through a dedicated webpage, developed and maintained for this purpose.

- Comparison of SSC and RC bridges performance in terms of fragility and RCR with the aim to show the benefits in using the proposed SCC bridge typology.

The activities of this WP concerning the first two objectives are presented in detail in Deliverable D5.1 (2016), whereas the dissemination results are included in Deliverables D5.2 (2016) and D5.3 (2016).

1.6 WP6: Project Coordination and Management

The main objectives of WP6 were to establish an efficient management process (task 6.1), to define the standard protocols (task 6.2), SWOT evaluation (task 6.3) and the monitoring of the activities of the project in different activities (task 6.4). In this respect, some difficulties mainly due

to the experimental activities have created some delays. Nevertheless, these difficulties have been overcome and the project has been successfully concluded. This consolidates the results obtained in applying PBEE procedure that has been successfully used for the assessment of a case study. Consequently, the management process has provided good results and allowed to conclude successfully the project with the organization of a round table in Paris at the end of the project where expert in seismic design of bridges have been invited.

1.7 Conclusions and main results

SEQBRI can be considered a pioneering project within RFCS funding program. In fact, it is the first time that the next-generation probabilistic earthquake engineering (PBEE) approach has been employed for the design/assessment of bridges and, in particular, for a new type of steel concrete composite (SCC) bridges endowed with a special pier-to-deck connection (Concrete Cross Beam, (CCB)). At this purpose, typical bridge typologies were selected and analysed. All steps of the PBEE approach were developed, which include: a) seismic hazard analysis by using the PSHA, b) implementation of refined non-linear models, c) probabilistic seismic demand analysis of the bridges, d) damage analysis and fragility curves development, e) cost-effective analysis and decision making analysis based on the concept of the Repair Cost Ratio (RCR).

This complex procedure has been possible thanks to a wide experimental and numerical activity undertaken on selected I-girder subassemblies. At this purpose a monolithic pier-to-deck connection has been chosen because never tested before and because it is considered a vulnerable detail. The main outcomes were a comprehensive damage analysis with the definition of proper limit states and the proposal of a component-based model.

The collaboration of experts on infrastructure engineering and design of bridges allowed the identification of the repair actions and costs for this new bridge typology under moderate and severe earthquakes. Accordingly, the cost effective analysis of a selected case study has been perform with the calculation of the global RCR and the identification of the elements that provide the higher contribution to the repair cost. A comparison with the most diffused RC bridges in terms of seismic fragility and RCR showed the benefits in using SCC bridges with CCB.

The development of the PBEE framework for SCC bridges can be considered a contribution to the foundation of a new generation of seismic engineering codes for bridges, currently based on a simplified and deterministic performance-based approach rather than a full probabilistic-based method like PBEE. However, given that it will need time to be fully employed in a national code, it has been used to improve current codes with some integration that could help technician in designing. Thus, specific design guidelines of SCC bridges with CCB in seismic prone areas have been developed.

The organization of a final round table in which experts on seismic bridge design have been invited provided a useful feedback about the correctness of the road maps suggested in SEQBRI project and its novelty.

2 SCIENTIFIC DESCRIPTION OF THE RESULTS

2.1 Objects of the project

SEQBRI project intended to achieve the following main goals:

1. Development of a Performance-Based Earthquake Engineering (PBEE) procedure applied to short-medium span steel-concrete composite I-girder bridges made of hot rolled fine grain steel beams, that includes seismic input randomness, probabilistic demand evaluation and damage analysis as well as economic cost-benefit estimations. It is based on the premise that performance can be predicted and evaluated with confidence to make, together with clients, intelligent and informed trade-offs based on cost-effective risk management rather than design and construction costs alone.
2. Optimal application of high performance hot rolled (S355M/N-S460M/N) fine grain steel beams obtained with Thermo-Mechanical (M) or Normalisation (N) control processes and characterized by improved mechanical properties of a) tensile resistance –possible use of higher strength-, b) toughness, c) ductility, d) weldability –possible elimination of preheating and e) wear resistance and by a wider range of thicknesses in view of the enlargement of market-share.
3. Development of representative prototype case studies for short-medium span I-girder bridges systematically designed and optimized according to the PBEE approach, whose performance under common and extreme earthquake loads would respond to the diverse needs and objectives of owners, users and society.
4. Provision of a background foundation for a new generation of European seismic codes for bridges on which code-writing bodies could base the development of transparent performance based provisions.
5. Issuing of design guidelines and recommendations for improving Eurocodes for the design of SCC bridges with CCB.

2.2 Comparison of initially planned activities and work accomplished

All the above objectives, reported in the Technical Annex, have been successfully accomplished in the course of the relevant work packages of **SEQBRI** project.

2.3 Description of activities and discussion

In what follow the description of the activities and the main results is provided along with the discussion of the aspects of the problem. In order to be effective in reporting the main results obtained in SEQBRI project, the description is provided work package per work package. In particular, the following WP have been developed:

- WP1: Definition of representative case studies. Selection of I girder subassemblies to be tested
- WP2: Tests on scaled I-girder subassembly specimens
- WP3: Numerical simulations and damage analysis of I-girder subassemblies
- WP4: Application of the PBEE methodology to the selected Case Studies
- WP5: Issuing of design guidelines and recommendations for improving European seismic code for bridges
- WP6: Project coordination and management

2.3.1 Work Package 1: Definition of representative case studies. Selection of I-girder subassemblies to be tested

The first work package is devoted to the definition of relevant Case Studies for short-medium span steel-concrete composite bridges to be investigated through the Performance Based Earthquake Engineering methodology. Using properly selected response natural records as input, preliminary design and numerical analyses were carried out. Moreover, refined analyses were carried out on I-

girder subassemblies in view of specimen definitions and proper testing protocols, which have been used in WP2.

The main objectives of WP1 are:

- Definition and design of representative case studies and preliminary numerical analyses for Engineering Demand Parameters (EDP) and Damage Measures (DM) estimation.
- Selection of I-girder subassemblies and preliminary numerical analyses for EDP and DM estimation at deck level.
- Definition of proper testing setup and protocols for I-girder subassemblies tests

Task 1.1 and 1.2 were dedicated to select and design representative case studies of a new typology of steel concrete composite bridges with rolled I-girder deck that use concrete cross beams as transversal connection element at piers and abutments. Three major Case Studies were selected among straight and skew, multi-span bridge typologies of ordinary (e.g. overpasses) and strategic (e.g. highway) bridge types, with 2, 3 and 6 spans, and maximum span length ranging between 20 to 40 m. Task 1.3 was dedicated to the selection of the seismic input for Code-based and PBEE-based analysis of the selected case studies and to their preliminary analysis. The selection was carried out according to the response spectra provided by the EC8 (CEN Eurocode8a, 2005). Four groups of 14 records compatible with EC8 spectra were selected and subdivided into two groups: Far Field and Near Fault records, respectively. The modelling issue was extensively analysed including the most recent models proposed in literature; refined and simplified models were used and each case study was accurately designed and checked according to Eurocodes. In task 1.4, for the selection of the I-girder subassemblies to be tested, three possible configurations were finally adopted. One is the DIN FB104 type C; the other new variants (DOMI-1, DOMI-2) include the presence of a low or a significant tensile stress at the CCB bottom. The case study of a straight overpass of 2x20m spans, with monolithic connection between deck and pier (CS-2.1.2), was selected as the most suitable configuration to be tested both in longitudinal and transversal direction. In task 1.5 several possible testing protocols for I-girder subassemblies were described and analysed. The most suitable one was identified with the classical ECCS procedure.

2.3.1.1 Definition of representative case studies and selection of steel grade and steel beams (Task 1.1 and Task 1.2)

In order to define the relevant Case Studies for short-medium span steel-concrete composite (SCC) bridges, a comprehensive overview of the state of the art of steel-concrete composite bridges worldwide, particularly in the USA, Japan, China, South-Korea and Europe was performed. Different solutions were investigated. A comparison among relevant design documents considering seismic design of bridges was performed. Moreover, current design practice and trends of steel concrete composite bridges in the USA as well as example bridges were presented. Given that on the First annual report a comprehensive worldwide state of the art was already provided, the main aspects of the European state of the art are described herein.

European practice in short-medium span steel-concrete composite (SCC) bridges

Since the end of the 1990s numerous composite bridges have been successfully built with a high level of prefabrication identified as an economic solution in the span range between 20 to 80 m. From the beginning, attempts they have been undertaken to optimize not only the steel structure but also the way how to fabricate the concrete slab. For multi-span valley bridges a formwork carriage is often used, which is usually not an appropriate solution for bridges in the small and medium span range. Thus, two innovative approaches evolved, which are both combined with in-situ concrete: (a) steel girders and precast concrete elements, and (b) prefabricated composite girders. The main girders are welded or rolled steel cross-sections completely prefabricated in the shop. The typical reinforced concrete deck consists of partially prefabricated elements and additional in-situ concrete. Only cross beams at supports are used and these beams are normal reinforced concrete members. This solution allows a simple erection to minimize or eliminate welding or bolting on side (Fig. 2-1). The reinforced concrete crossbeams over intermediate supports of multiple span bridges may be designed as splices of longitudinal girders. This construction method combines the following advantages:

- the longitudinal girders are erected as single span girders
- there is no need for welded or bolted splices

Continuity is achieved by the use of vertical end plates and additional reinforcing bars in the deck slab. During concreting loads due to the dead weight of steel girders, formwork and wet concrete are

carried by simply supported beams. After the concrete has hardened, moment resistance is provided at splices and subsequent loads are supported by continuous girders. Thus hogging bending is produced at supports only by super-imposed dead loads and variable actions.

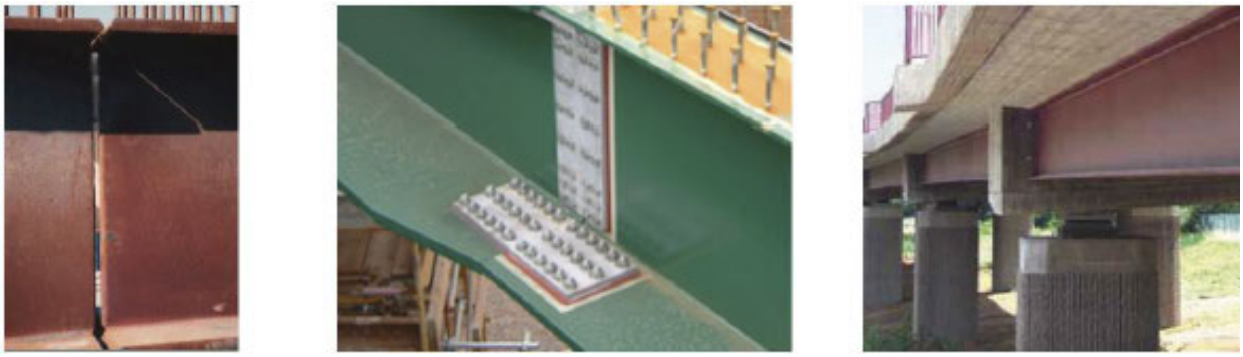

(a) (b) (c)

Fig. 2-1 a) Welded splice, b) Bolted splice, c) Concrete Cross Beam (CCB) splice

Forces are transmitted as follows: The compressive force is directed through the end plate from the lower flange to the concrete. The tensile force flows from the upper beam flange through the shear studs into the longitudinal slab reinforcement. Studs welded to the vertical end plates transfer the shear force from the steel beams to the concrete bracing. In the German design code DIN-FB104 proposals for the configuration of the connection between steel girder and reinforced cross beams as well as minimum dimensions are given (Fig. 2-2). However, these provisions are based on the assumption that CCB suffers mainly, if not exclusively, from vertical, static loads.

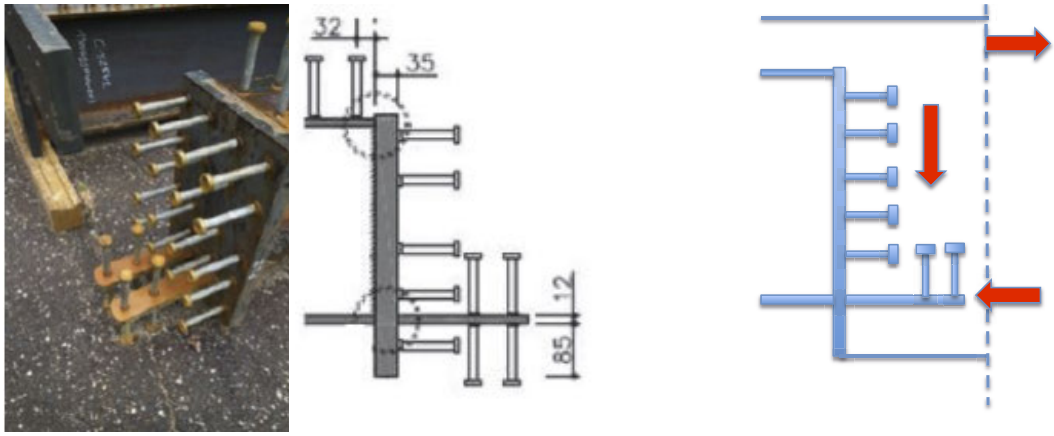

(a) (c)

Fig. 2-2 DIN-FB104 Var C - a) Typical geometry, b) Static functioning

Based on this concept, three representative case studies were selected, among straight and skew overpasses and multi span typologies. The case studies are presented in detail in Deliverable D1.1 (2013). A brief description is following, while corresponding longitudinal sections and typical span cross sections are presented at Annex of WP1 (Figs A3.1-1 to A3.1-6)

Case study 1: straight 3-span bridge over national road

The total length of the bridge is 96.20m, which consists of 3 spans of 28.60+40.00+28.60m. The skew angle is equal to 0 deg (straight bridge, Fig. 2-3). It covers typical span lengths of 25-30m as well as an 'upper' limit of 40m for such kind of steel-concrete composite bridges. The total width of the bridge is 10.60m, with carriageway 6.50m wide and 2 sidewalks 2.05m wide. This is a typical overpass cross-section with 2 traffic lanes. One of the targets of the project is the application of hot-rolled (S355/S460) steel beams, instead of welded sections (in order to simplify fabrication on shop). Due to the limited dimensions of such profiles combined with the large length of the central span, 5 main

girders HLB-1000 of S460 steel grade are used, with 2.15m in-between distance. Transverse steel beams are not foreseen. The thickness of the concrete slab is equal to 25cm.

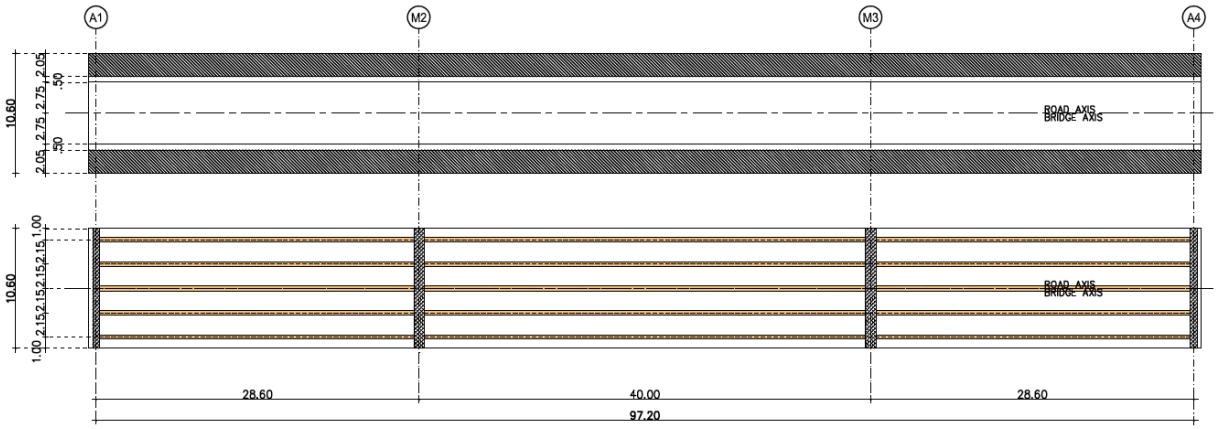

Fig. 2-3 Plan view of case study CS1.1 and CS 1.2

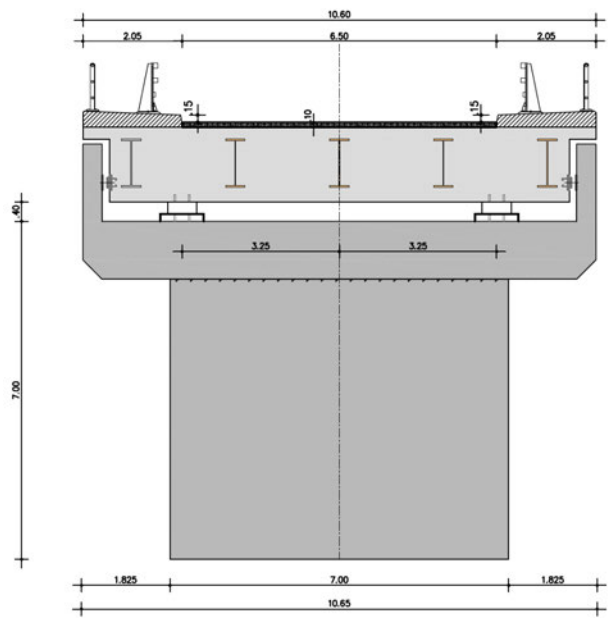

Fig. 2-4 Wall type pier – Deck on bearings (CS 1.1)

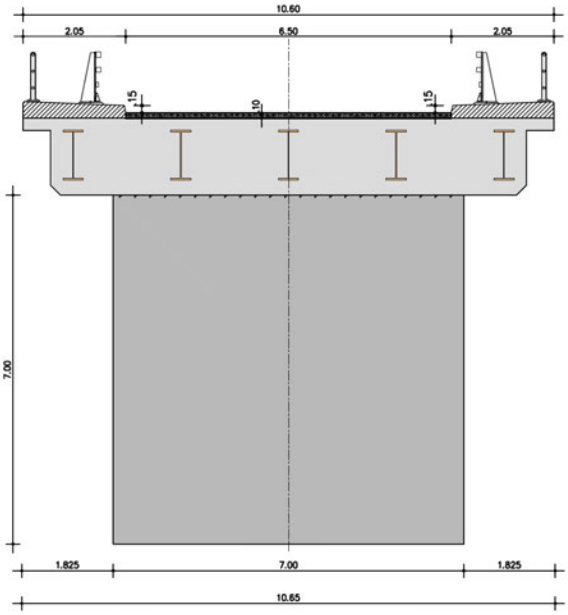

Fig. 2-5 Wall type pier – Deck monolithically connected to pier (CS 1.2)

The steel girders are fixed to an end reinforced concrete crossbeam 0.80m wide at the abutments; thus, the deck is simply supported on normal damping rubber bearings. The monolithic connection between deck and abutment is not examined in order to avoid the soil-structure interaction. At the intermediate piers, the steel girders are fixed to intermediate reinforced concrete crossbeams. Two different types of deck's support at the intermediate piers are examined: (a) deck with crossbeams 0.90m wide, on low damping rubber bearings NDRB ($\xi \leq 6\%$), and (b) deck with crossbeams 1.20m wide, monolithically connected with the two intermediate piers (Fig. 2-4 and Fig. 2-5). At steel-concrete composite bridges with steel crossbeams, bearings are usually aligned under each steel girder. However, by using concrete crossbeams the number of bearings can be minimized up to 2, which reduces the construction as well as the maintenance costs. The use of 3 NDRB per crossbeam is adopted at Case Study 1, such devices offer a low-cost, reliable seismic isolation system, suitable for the seismic requirements for the category of bridges under investigation.
The pier's (clear) height is 7.00m. A wall type pier 0.90m thick and 7.00m wide is used. It is chosen to use the same deep-foundation type for every sub-case, in order to provide a stiff support at the piers, which minimizes the soil-structure interaction (SSI) and its influence to the seismic response of the superstructure. The effects of SSI tend to be beneficial to lower the earthquake force demand; however it may increase the displacement demand, which may also require large isolation devices

Case study 2: straight and skew 2-span bridges over national road

The Case Study 2 is devoted to the typical 2-span overpasses. It is divided into two main sub-categories: straight and skewed overpasses. The straight bridge is 40.00m long and consists of 2 spans of 20.00m (Fig. 2-6). On the other hand, according to EN1998-2, highly skewed bridges should be avoided in high seismicity regions. Thus, for the skewed bridge of this case study, a skew angle equal to 30deg is selected (Fig. 2-7). Based on the assumption that the two bridges overpass the same national road, for the chosen angle, the total length of the skewed bridge is 46.00m and consists of 2 spans of 23.00m. For both sub-categories, the total width of the road cross-section is 10.60m, with carriageway 6.50m wide and 2 sidewalks 2.05m wide. This is a typical overpass cross-section with 2 traffic lanes, same as for the Case Study 1.

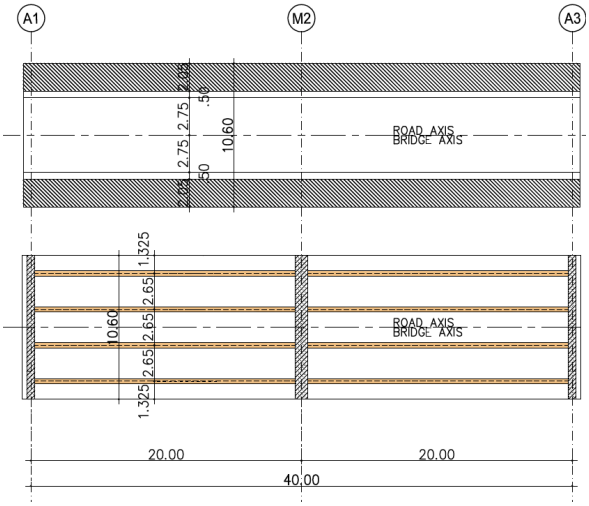

Fig. 2-6 Plan view of case study CS2.1

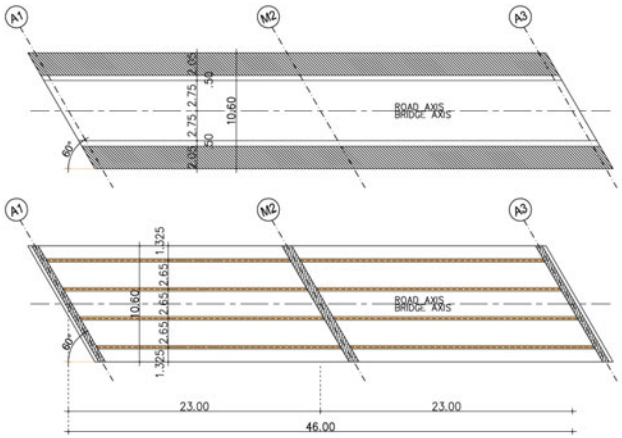

Fig. 2-7 Plan view of case study CS2.2

Based on the selected steel grade, the skewness and the supporting system of the deck, four different configurations are examined, using 4 main girders, with 2.65m in-between distance as follows: Straight overpass (sub-cases 2.1.1-2.1.2): (a) 4 x HLB 600 of S460 steel grade, (b) 4 x HLB 700 of S355 steel grade. Skew overpass (sub-case 2.2): (a) 4 x HLB 700 of S460 steel grade, (b) 4 x HLB 800 of S355 steel grade. Transverse steel beams are not foreseen. The thickness of the concrete slab is equal to 25cm.

At the abutments the steel girders are fixed to an end reinforced concrete crossbeam 0.80m wide. By this diaphragm, the deck is simply supported on normal damping rubber bearings. The monolithic connection between deck and abutment is not examined, in order to avoid the soil-structure interaction. At the intermediate piers the steel girders are fixed to intermediate reinforced concrete crossbeams 0.90m wide. Two different types for the deck's support at the intermediate pier are examined: (a) deck on low damping rubber bearings NDRB ($\xi \leq 6\%$), (b) deck monolithically connected with the intermediate pier (only for the straight sub-cases) The use of 2 normal damping rubber bearings per crossbeam is adopted at Case Study 2. The pier's (clear) height is 7.00m. A wall type pier 0.60m thick and 7.00m wide is used for the straight (Fig. 2-8) and circular columns 3xD100 are used for the skewed overpass (Fig. 2-9). Deep foundation of the piers is chosen for every sub-case.

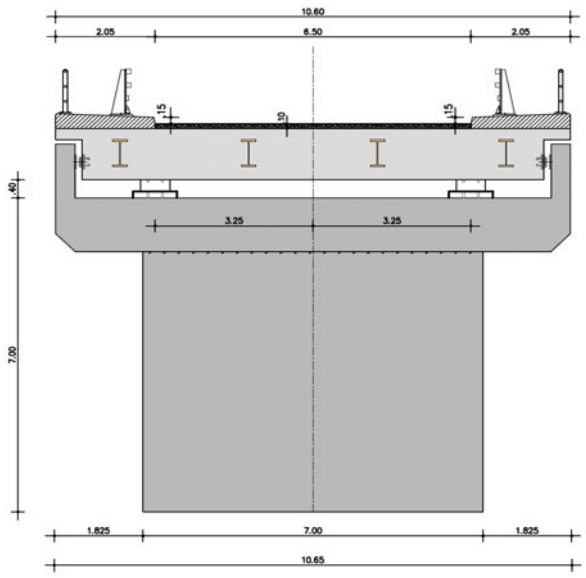

Fig. 2-8 Wall type pier – Deck on bearings (CS 2.1.1)

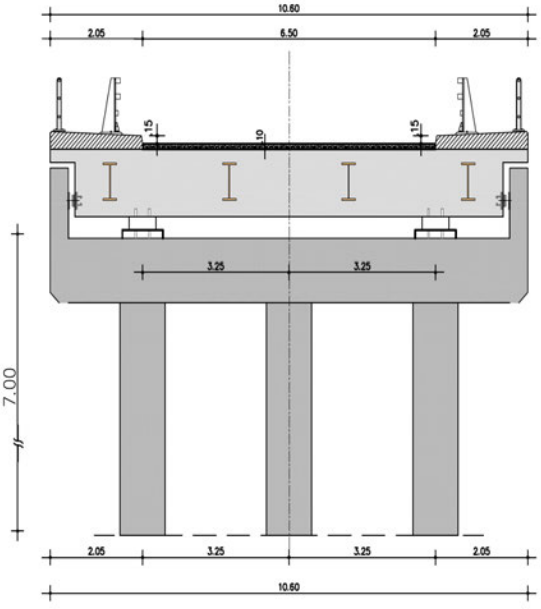

Fig. 2-9 Column type pier – Deck monolithically connected to pier (CS 2.2)

Case study 3: straight multi-span highway bridge

The Case Study 3 describes a multi-span straight bridge carrying one branch of a national highway. The total length of the bridge is 193.60m, which consists of 6 spans with lengths 26.80+4x35.00+26.80m (Fig. 2-10). The total width of the bridge is 15.75m, with carriageway 12.75m wide and 2 sidewalks 1.50m wide. This is a typical cross-section with 3 lanes of traffic for the right branch of a national highway. Thus, the response of wider decks is also investigated. Two different configurations are examined: (a) 6 main girders HLB 1100 of S460 steel grade, with 2.65m in-between distance, (b) 7 main girders HLB 1100 of S355 steel grade, with 2.25m in-between distance

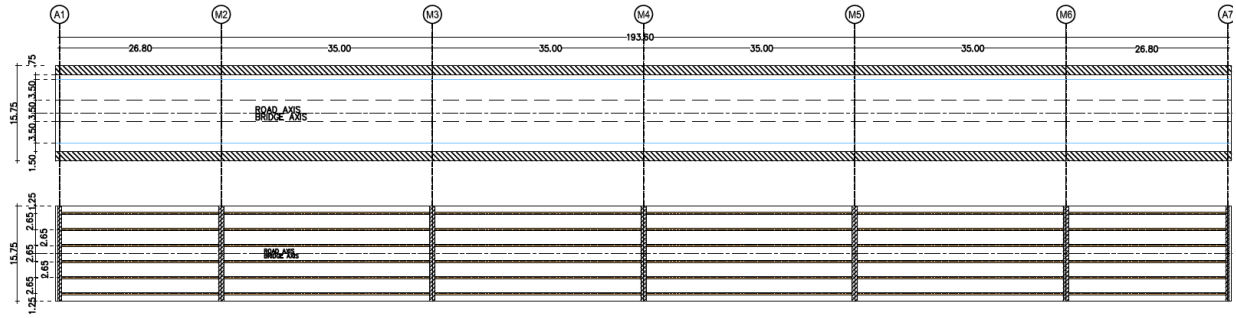

Fig. 2-10 – Plan view of case study CS3

At the abutments, the steel girders are fixed to an end reinforced concrete crossbeam 0.80m wide. By this diaphragm, the deck is simply supported on normal damping rubber bearings. The monolithic connection between deck and abutment is not examined in order to avoid the soil-structure interaction. At the intermediate piers, the steel girders are fixed to intermediate reinforced concrete crossbeams. Two different types of deck's support at the intermediate pier are examined: (a) deck with crossbeams 0.90m wide, on low damping rubber bearings NDRB ($\xi \leq 6\%$), (b) deck with crossbeams 1.20m wide, monolithically connected with the piers M3, M4 and M5. The use of 3 normal damping rubber bearings per crossbeam is adopted at Case Study 2. In order to avoid vertical curvatures, unequal stiffness distribution etc, the clear structural height is fixed to a constant value for all piers equal to 9.0m. Each pier comprises 5 circular columns D100. Deep foundation of the piers is chosen for every sub-case (Fig. 2-11,
Fig. 2-12).

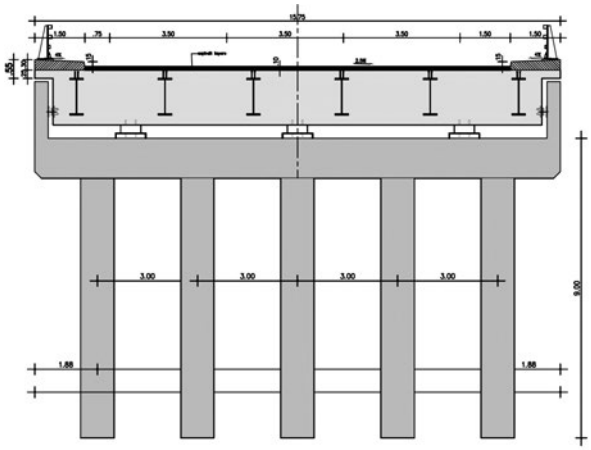

Fig. 2-11 Column type pier – Deck on bearings

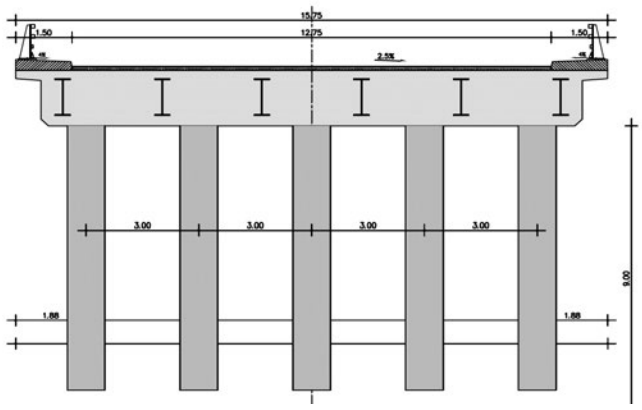

Fig. 2-12 Column type pier – Deck monolithically connected to pier

2.3.1.2 Selection of seismic input for Case Studies and preliminary numerical analyses for EDP and DM estimations (Task 1.3)

In this section the results of preliminary numerical analysis of the selected bridges (CS.1, 2, 3) are described in details and analysed. In particular, to comply with the content of the project proposal the first part is dedicated to the selection criteria of seismic input for the case studies. Additionally, a discussion on simplified models for the simulation of the seismic behaviour of short-medium span steel-concrete composite bridges (SCC) in non-linear filed is addressed. For each case study a simplified numerical model has been proposed and used to perform preliminary seismic analysis. They have been performed to get information about the most relevant engineering demand parameter.

Using these models each case has been analysed for the assumed sequence of the construction phases, taking into account which elements are active (steel or composite cross-section), the appropriate modulus of elasticity for the concrete (long- or short-term loading etc. as discussed earlier) and the active supports (temporary or permanent with continuous beams). By adding the results of each phase, the final forces and stresses are derived, which are used for performing the required checks. Summarized results obtained using refined elastic models have been presented, whose detailed results are provided in Deliverable D1.1 (2013). In what follows a summary of the results is presented and commented.

This part has been extensively illustrated in the First Annual Report, in which for each case study the response to seismic action using the response spectrum method has been carried out (SEQBRI, 2013).

2.3.1.2.1 Seismic Input selection for Case Studies

One of the key issues in non-linear dynamic analysis of structures is the selection of appropriate seismic input signals, which should allow for an accurate estimation of the seismic performance on the basis of the seismic hazard at the site where the structure is located. Assessment of seismic demands and their uncertainties need the availability of sets of acceleration time histories that represent the seismic hazard at different return periods and describe intensity, frequency content and duration with sufficient comprehensiveness so that values and measures of dispersion of the demand parameters can be determined with confidence and efficiency. They should provide a statistical sample of the response of the structure to the variability in phasing and spectral shape of ground motions.

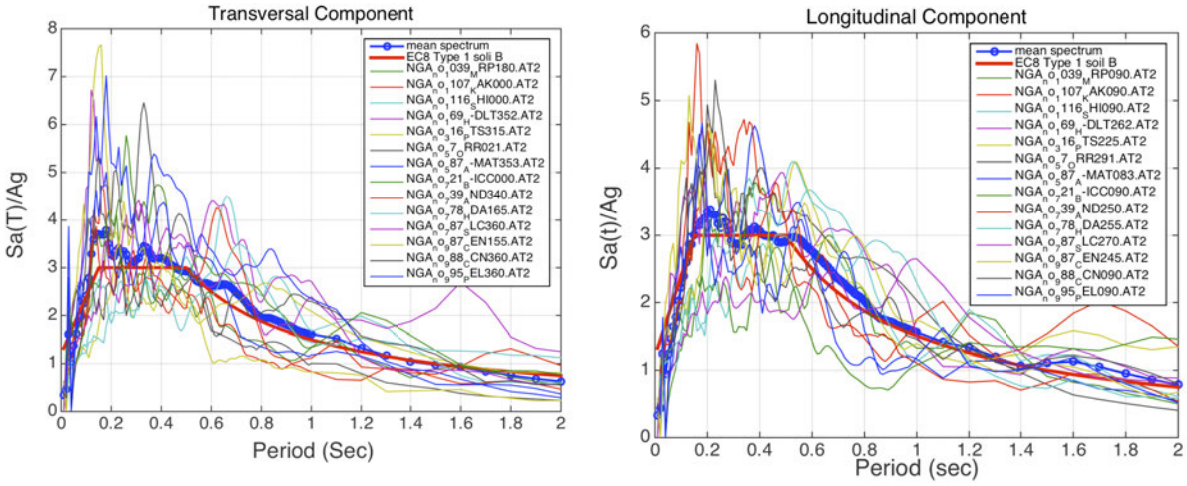

Fig. 2-13 Normalized response spectra of the 14 selected accelerograms and the relevant mean spectrum (dashed line) after it was matched with the reference spectrum (solid line)

Eurocodes allows the use of any form of accelerograms for structural design of bridges; i.e. real, artificial or obtained by simulation of seismic source, propagation and site effects (CEN Eurocode 8b, 2005). The mean spectrum of the records should fit as better as possible the EN1998:2 spectrum and in the range of periods between 0.2 $T_1$and $2T_1$ (where T_1 is the fundamental period of the structure in the direction where the accelerograms will be applied) no value of the mean 5% damping elastic spectrum calculated from all time histories should be less than 90% of the corresponding value of the 5% damping elastic response spectrum.

In Eurocode 8 (CEN Eurocode 8b, 2005) the hazard is described with a single parameter: the value of the reference peak ground acceleration on type A ground (that may be derived from the zonation maps of individual Countries) corresponding to the reference return period of the seismic action for the no-collapse prevention (or equivalently the reference probably of exceedance in 50 years). Two different types of spectra are considered: Type 1 if the earthquakes that contribute most to the seismic hazard defined for the site have a surface-wave magnitude, M_s, greater than 5.5 and Type 2 for smaller values. For the goals of task 1.3 and according to the code prescriptions, that impose the best matching with code spectrum respecting the minimum requirements in terms of intensity and frequency content, four groups of 14 pairs of accelerograms (2 components) have been selected extracting them from the PEER ground motion database. However, given that for the goals of the project strong seismic events are more important, in the following only the spectra Type 1 have been considered. In detail:

- The PEER ground motion database web application has been used to select natural time history records (http://peer.berkeley.edu/smcat/). The mean squared error between the spectrum of each registration and the target spectrum is evaluated and the best 30 pairs of records have been selected. The parameters of the records taken into account were the magnitude M_w, the distance from the fault rupture D_R and the local soil type. In particular, a range of Magnitude M_w = 5.8–7.0 has been selected using far-field earthquakes whose distance D_R ranges between 15 and 40 *km*.

- Among the 30 pairs of registrations chosen by the PEER ground motion database, 14 have been selected so that the mean spectrum of the two components best approximate the target spectrum according to Eurocode 8 (CEN Eurocode 8b). In order to improve the match to the target spectrum, the records have been also scaled. Fig. 2-13 depicts the response spectra of the longitudinal and transversal components.

In Table 2-1 the list of selected records, including seismic event, date, recording station, ground velocity and PGA for both NS and WE components is reported.

Table 2-1 Selected records

Event	Country	Date	Station	M	RB (km) (*)	R_{rup} (km) (**)	V30 (cm/sec)	PGA (g) comp EW	PGA (g) comp NS
San Fernando	USA	1971	Castaic - Old Ridge Route	6.6	19.33	22.63	450.28	0.32	0.27
Imperial Valley-06	USA	1979	Delta	6.5	22.03	22.03	242.05	0.35	0.24
Westmorland	USA	1981	Parachute Facility	5.9	16.7		349	0.16	0.24
New Zealand-02	N. Z	1987	Matahina Dam	6.6	16.09	16.09	551.3	0.34	0.26
Superstition Hills-02	USA	1987	El Centro Imp. Co. Cent	6.5	18.2	18.2	192.05	0.36	0.26
Loma Prieta	USA	1989	Anderson Dam (Downstream)	6.9	19.9	20.26	488.77	0.24	0.24
Loma Prieta	USA	1989	Hollister Differential Array	6.9	24.52	24.82	215.54	0.27	0.28
Loma Prieta	USA	1989	Palo Alto - SLAC Lab	6.9	30.62	30.86	425.3	0.28	0.19
Northridge-01	USA	1994	LA - Centinela St	6.7	20.36	28.3	277.98	0.47	0.32
Northridge-01	USA	1994	LA - Century City CC North	6.7	15.53	23.41	277.98	0.22	0.26
Northridge-01	USA	1994	LA - Hollywood Stor FF	6.7	19.73	24.03	316.46	0.36	0.23
Northridge-01	USA	1994	Moorpark - Fire Sta	6.7	16.92	24.76	341.58	0.29	0.19
Kobe	JAPAN	1995	Kakogawa	6.9	22.5	22.5	312	0.25	0.34
Kobe	JAPAN	1995	Shin-Osaka	6.9	19.14	19.15	256	0.24	0.21

2.3.1.2.2 Preliminary numerical analysis

In what follows preliminary numerical results obtained using models with different refining levels are reported. Main issues concerning modeling and the main results of numerical simulations are presented and discussed.

Modeling issues of SCC bridges with CCB

According to the goals of task 1.3 two different levels of modelling were used:

- A refined model in which the deck is modelled using elastic shell elements for the slab and elastic beam element for the steel girder. The steel beams are connected to the centroid of a transverse beam, representing the CCB, by using rigid links. The cross beam is connected to the CCB, modelled as an elastic beam as well, by a series of elastic springs representing the bearings used to support the deck on piers and abutments. In case of monolithically connection between piers and deck they have been rigidly connected. Finally, the piers are modelled as elastic beam elements connected to the CCB using rigid link again. Single or multiple beams are used respectively to model column or shear wall type piers.
- A stick model in which the deck is represented by an elastic beam element rigidly connected to the cross beam in a certain number of points. The remaining parts are modelled exactly as in the refined model

In the refined model the deck is modeled with beams elements for the main steel girders and concrete cross-beams and with shell elements for the concrete slab. The beams and shell elements are placed at different levels having though common nodes, which results in the successful

modeling of the composite action between the two types of elements. In case of stick model the deck is considered an elastic beam element, whose section is the transversal section of the deck.

In both models, the bearings are modeled by linear springs with shear stiffness $K=GA/\Sigma t_i$, where $G=900$ *kPa* for static loads. In order to take account the variation of the bearing characteristics with the seismic response, the analysis of each sub-case has been carried out with two different values of the shear modulus, *G=990kPa or 1485kPa*.

The reinforced concrete piers is modeled by beam elements. This type of modeling is adopted also for shear wall piers. For the dynamic analyses, the flexural stiffness of the piers is reduced according to Eurocode 8 (CEN Eurocode 8 – Part 2).

The deep foundation is modeled by a stiffness matrix, which allows investigation of the soil-structure interaction's influence to the seismic response of the selected case studies. According to the parametric analyses, the use of deep foundation has small influence to the bridge's response, as its stiffness approximates (about 80% for soil type B) the fully fixed support. Thus, conservatively for the stress state, it is assumed for every case study that the piers are fixed at their base. This was also confirmed by previous works on the seismic behavior of steel concrete composite bridges (Tubaldi et al 2010).

At first, an un-cracked analysis is carried out, and it is derived that the tensile stress of the top fiber of the concrete slab at the region of the internal supports, for the characteristic combination of actions, is $\sigma_c > 2\ f_{ctm} = 6.4$ MPa. As a result, it is required that cracked analysis must be performed, meaning that for those the regions where the above-mentioned criterion is satisfied, cracked stiffness must be taken into account for the composite beams, which is modeled by changing the properties of the finite elements accordingly. For simplicity and according to EN1994-2 (CEN Eurocode 4, 2004), a length of 0.15L at each side of the supports is considered as cracked concrete zone.

To account for seismic (horizontal) actions, more reliable criteria should be used. For this purpose, proper software (e.g. OpenSEES, McKenna et al. 2007) able to model nonlinearities of materials, including steel and reinforced concrete, could be used. However, only linear analyses, with the above indications, have been performed with stick models implemented in SAP2000 (2000). An example of refined and stick models for case study CS3 are shown in Fig. 2-14.

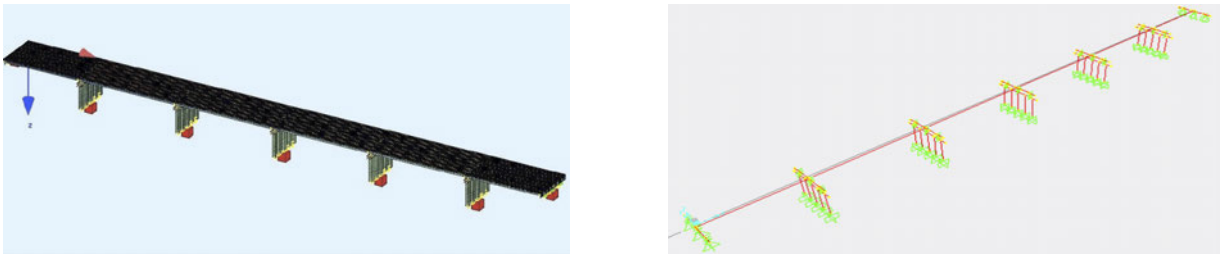

Fig. 2-14 Models for Case Study 3, a) refined model (Sofistik), b) stick model (SAP2000)

Performance-based earthquake engineering requires lots of non-linear analysis, especially in the evaluation of the probabilistic response of the bridge for which Incremental Dynamic Analysis have been used in WP4 (task 4.2 and 4.3). Consequently suitable computationally efficient models should be adopted. In this respect, the stick models previously proposed has been employed.

In order to show the reliability of stick models in predicting the seismic response of steel-concrete composite bridges, a preliminary comparison between refined and stick models has been carried out. The models are considered fully elastic and the seismic response is calculated by using the response spectrum method. As transversal modulus of bearings has been selected the lower (G=0.9 MPa). It is noticed the good capability of the stick model in reproducing (at least in the elastic field) the modal response of the bridge with a limited margin of error. In particular, for case study C2.2 a maximum difference of 1% in the estimation of fundamental vibration period in longitudinal direction is found, whereas only 2.2% for the vibration period in transverse direction. For case C3.1 similar differences were found. More details can be found in Deliverable D1.1 (2013).

Concerning higher modes, the corresponding vibration periods of stick and refined models are slightly different. Given their participating masses are quite limited, this error can be still considered acceptable. In Fig. 2-15 the vibration modes of the CS 3.1 bridges using refined and stick models are shown, from which the good agreement of the two modelling levels can be noticed.

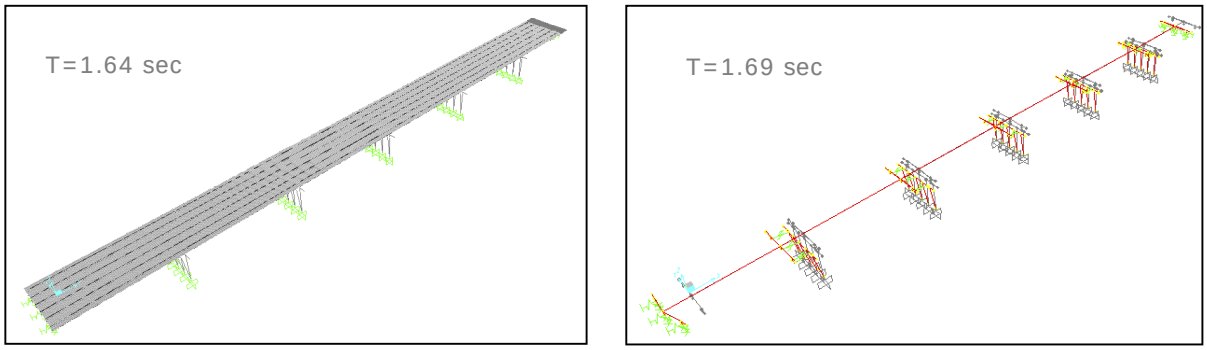

(a) (b)

Fig. 2-15 – 1st vibration mode of a) refined model, b) stick model

Analysis and design of case studies

In this section a summary of the results obtained using linear elastic models of the bridges implemented in Sofisitk (2013), the refined model, are presented and discussed. More details can be found in Deliverable D1.1 (2013). In case of deck supported on NDRB no constraints are used both in longitudinal and transversal direction. Only the presence of stoppers, (here not modelled), avoids any possible loss of support. In case of monolithic solution NDRBs are used only to support the deck at the abutments

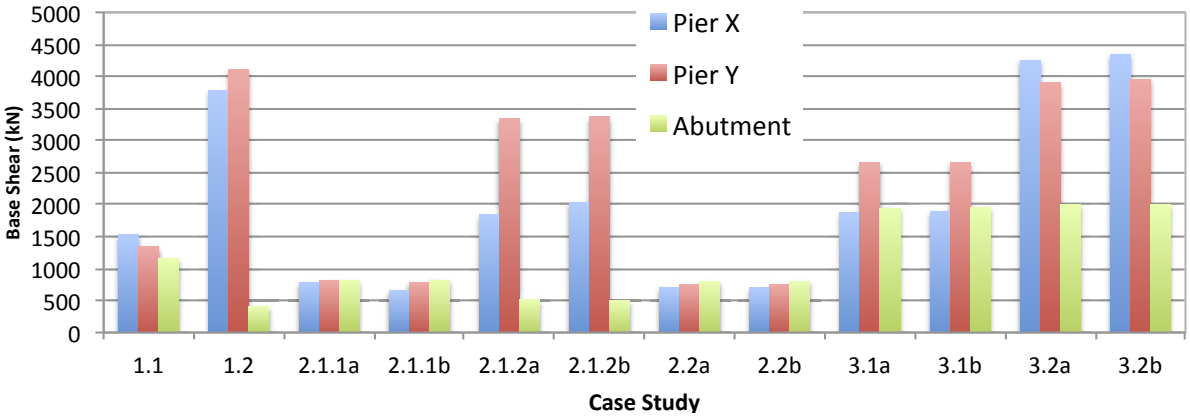

Fig. 2-16 Maximum base shear of pier and abutment for the several case studies

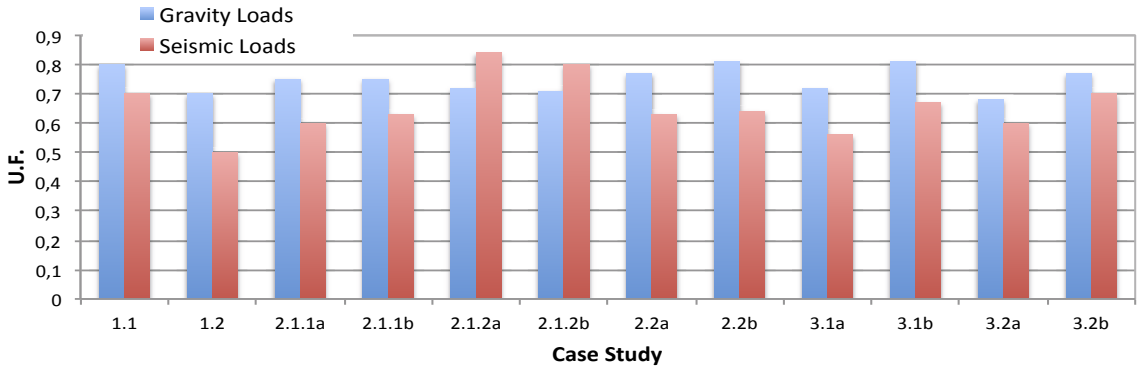

Fig. 2-17 Utilization Factor (U.F.) for the several case studies

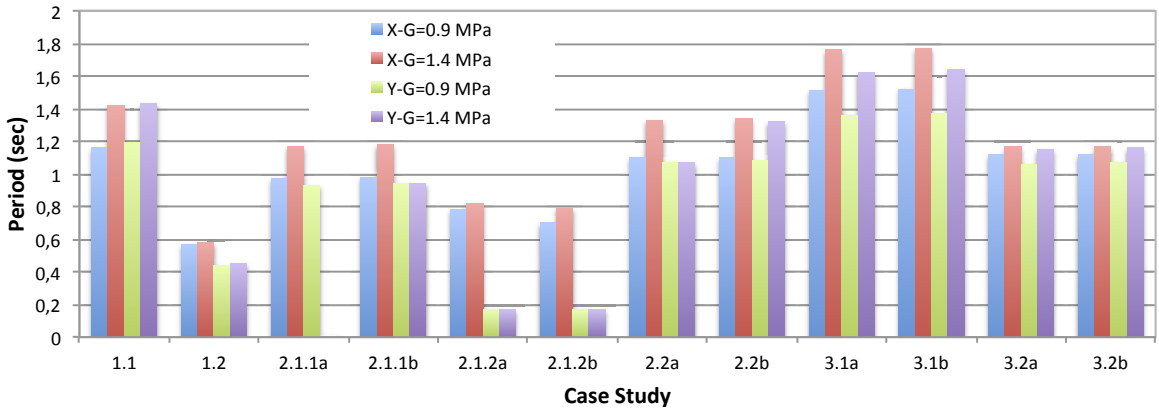

Fig. 2-18 Vibration Period for the several case studies: y(longitudinal), x (transversal)

A summary of the several response parameters is reported in Fig. 2-16, Fig. 2-17 and Fig. 2-18. Based on the aforementioned preliminary design of the selected case studies, the following general conclusions can be drawn.

- The capacity of S355 hot-rolled profiles seems to be limited for spans up to 35-40m. The use of higher steel grade S460 decreases the structural steel consumption 20% to 25% and the overall cost of the structure approximately 10%, especially at large span lengths.

- The two different structural systems, which are investigated, exhibit dissimilar seismic response and follow different design approaches:

  The integral configuration (deck monolithically connected to the piers) forms a stiff frame-type structure. The reduced fundamental period increases the seismic forces and the whole structure is designed according to the capacity design philosophy by using behavior factor up to 3.5. This configuration offers the advantages of a hyperstatic system and minimizes the superstructure displacements, gaining reduced requirements for bearings and expansion joints. On the other hand, the concrete crossbeam is subjected to dynamic cycling loading, even for low levels of ground acceleration, the foundation is significantly burdened and after the design seismic event, the structure will have to deal with extended but repairable damages. Even though the expected damages to the piers are well known, the response of the integral crossbeam under seismic actions is not yet clear and needs to be analytically and experimentally investigated in detail.
  The configuration where the deck is fully supported on normal damping rubber bearings practically leads to a seismic isolated structure. Due to the increased fundamental period the seismic actions are reduced and the whole structure is designed to behave elastically, limiting the damage development to minor cracks. The deck responds practically as a rigid body, minimizing the imposed seismic actions to the crossbeams. On the other hand, large displacements are exhibited, increasing the capacity requirements for the bearings and the expansion joints.

- In terms of construction cost, the two structural configurations are almost equivalent. Thus, the criteria for the choice should set by the needs for simple and rapid construction as well as the maintenance and repair requirements.

Operation cost evaluation of case studies

Evaluation of operation costs is based on the method used in the SBRI project (Maier et al. (2012)). SBRI project proposes a holistic approach for the steel-composite bridge by combining analysis of Lifecycle Assessment (LCA), Lifecycle Cost (LCC) and Lifecycle Performance (LCP). For the Lifecycle Cost, a significant work has been done for the compilation of data on the construction costs, on the operation cost (inspection and maintenance) and demolition costs. So the assumptions and data of the SBRI project are used to evaluate the operation costs of case studies (SBRI, (2013)).
The operation phase contains two significant actions: inspection and maintenance. The construction costs, the inspection costs and the maintenance costs are considered at different times of the bridge service life. So, they have to be discounted by a discount rate to obtain the present net value of future maintenance activities. The assessment of costs is very sensitive to assumptions: inspection scenario, maintenance scenario and discount rate. Therefore, it should rather be seen as a way to compare the

different solutions and not an accurate assessment of maintenance costs during the bridge of service life.
Thus, according to this evaluation the cumulative operations cost for bridges with integral crossbeam (at 100 years) is almost 10% lower than bridges where the deck is simply supported, due to the lack of maintenance actions concerning bearings for the intermediate piers. Concerning the use of higher steel grade, its effect can be considered as negligible on the maintenance cost. In general, bridges which have a lower construction cost also have lower operation costs (Fig. 2-19, Fig. 2-20). The benefits procured by the conception with integral concrete cross beam (less bearings and a reduction of the opening range of the expansion joints) reduce maintenance cost. The operation cost evaluation of case studies is presented in detail in the Mid-Term Report (2014).

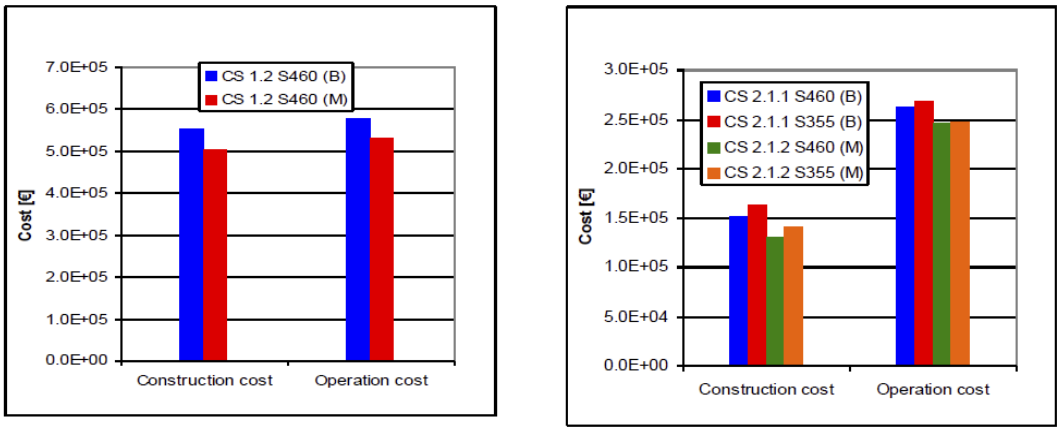

Fig. 2-19 Comparisons between construction costs and operation costs for case studies

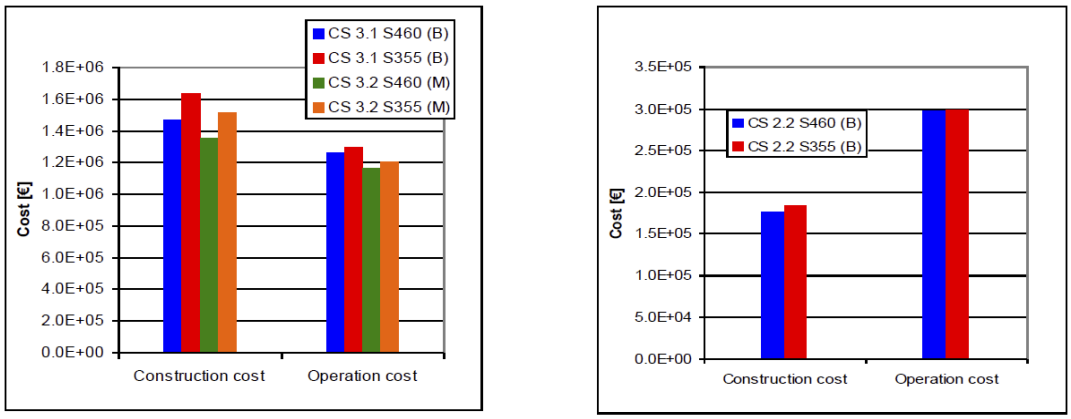

Fig. 2-20 Comparisons between construction costs and operation costs for case studies

2.3.1.2.3 Selection of I-girder subassemblies to be tested and preliminary numerical analyses (Task 1.4)

The activities developed within Task 1.1 allowed the identification of I-girder subassemblies, associated to the Concrete Cross Beams (CCB) technique, which have been tested in WP2. Particular attention was dedicated to the interconnection arrangement of the steel girders with the CCBs on piers and at abutments. In view of a better understanding of part of these systems preliminary 3D FE analyses of the interconnections were conducted, generally considering elastic material behaviour supplemented by basic nonlinear elements at the structural element scale. These latter were used for the identification and characterization of the relevant EDPs at the deck level, which was used for the PBEE procedure. The selection of the I-girder subassemblies to be tested and their preliminary numerical analyses are described in detail in Deliverable D2.1 and Mid-Term Report.

Selection and design of CCB configuration

Considering that the CCB configuration is the most crucial detail, especially for composite bridges in seismic prone areas, the widely used DIN-FB104 variant C (DIN-Fachbericht 104, 2009) is chosen to be analytically as well as experimentally investigated, avoiding variants DIN FB104 A and B (Fig. 2-21), which require significant in-situ welding in order to transfer tensile stresses at the bottom flange of the steel girder due to hogging moments.

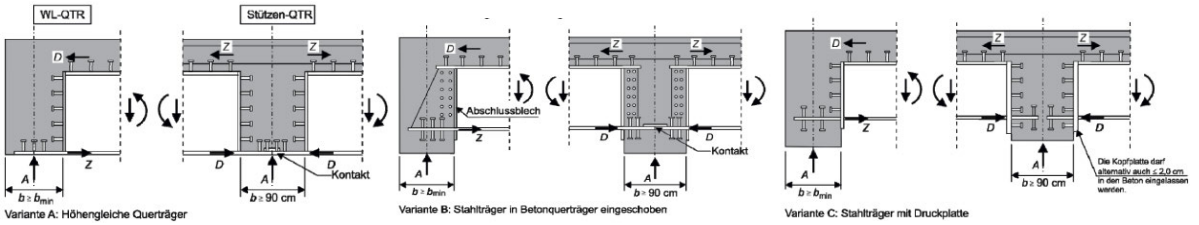

Fig. 2-21 DIN Fachberichte 104 Concrete Cross Beam variants A, B and C

Furthermore, trying to exploit the advantages and avoid the disadvantages of the three typical configurations, a new variant is formed and investigated, especially for, the most critical, intermediate CCB. This new configuration of the intermediate CCB is closer to the DIN-FB-104 variant B, however the steel flanges are not inserted into the CCB and the height of the head plate is limited. The idea is to transfer the forces from the composite girder to the CCB through contact and dedicated groups of shear studs. The tensile force at the top flange is transferred gradually to the longitudinal reinforcement (or reversely a potential compression force to the concrete slab) through a group of vertical studs, which are placed on the top flange of the girder before the CCB. The top flange does not enter into the CCB. The shear force is transferred to the CCB through a group of horizontal studs, transversally placed at the sides of the girder's web, which is inserted into the CCB. This group of studs is subjected only to pure shear, action, which is compatible to their actual function. Holes for the placement of reinforcement are foreseen at the web. Finally, regarding the magnitude of the tensile stress, which might be exhibited at the bottom flange of the steel girder, the following three cases are distinguished:

- Bottom steel flange always in compression. The bottom flange ends before the CCB and the compression force is inserted to the CCB by contact through a thick head steel plate. Only for constructional reasons 4 to 6 studs are placed at the head plate (Fig. 2-22a). This case is common for bridges with medium spans, fully supported on bearings (e.g. CS1).
- Bottom flange in compression or in light tension. The compression force is inserted to the CCB by contact through a thick head steel plate, as in the previous case. In order to transfer the light tension which might be exhibited at the bottom flange, an appropriate number of longitudinal studs are placed at the head plate (Fig. 2-22a). This case could be met at bridges with short to medium spans, fully supported on bearings (e.g. CS2 and CS3). It is noted that the web's shear studs are designed to resist the total shear force and the head plate's shear studs the total tensile force. Nevertheless, due to the fact that part of the shear force is inevitably transferred also to the head plate's studs, this group should be conservatively designed.
- Bottom flange in compression or in significant tension. The compression force is inserted to the CCB by contact through a thick head steel plate, as in the previous cases. On the other hand, significant tensile force at the bottom flange is covered by prestressed bolts or anchor bars (Fig. 2-22b). This case could be met at bridges with monolithic connection between CCB and pier. It is very beneficial that the duct of each anchor is filled with grease, offering the opportunity for inspection, re-tension or even replacement in case of an extreme seismic event.

These configurations provide significant advantages, compared to the types of the DIN FB-104: (a) the static behavior is straight forward without interactions, (b) the fabrication of the steel girders and the constructability of the CCB is simplified, (c) the inspection and maintenance of the interconnection between steel girder and CCB are facilitated.

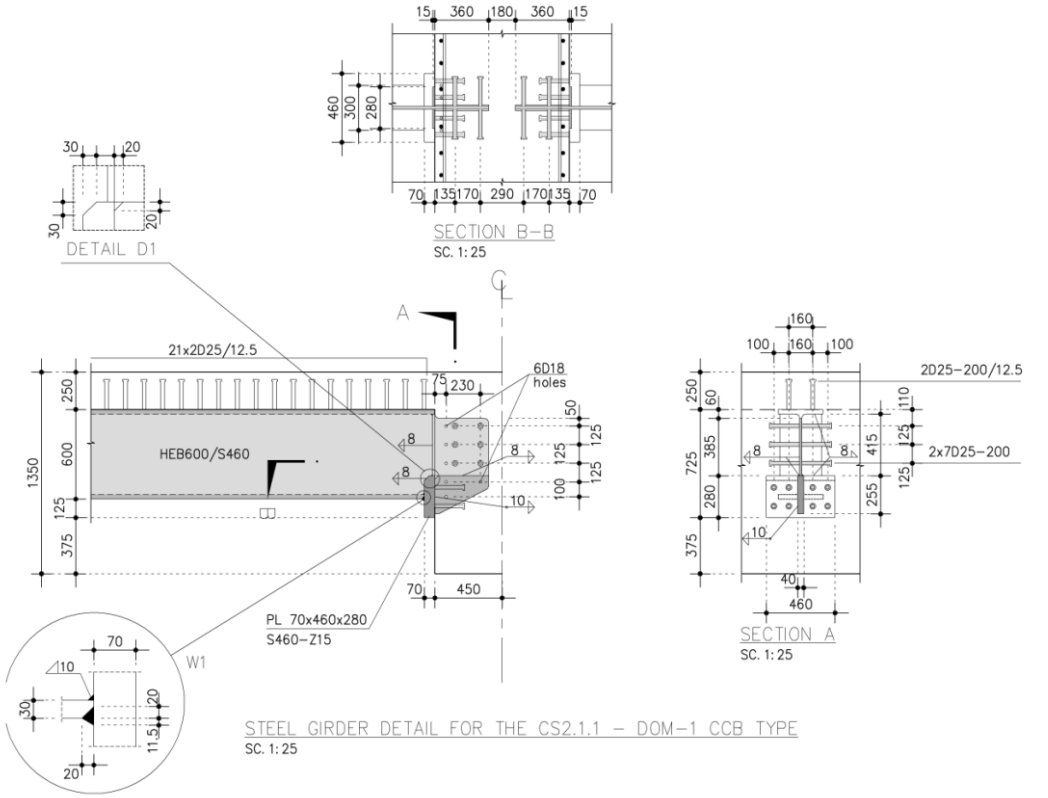

(a)

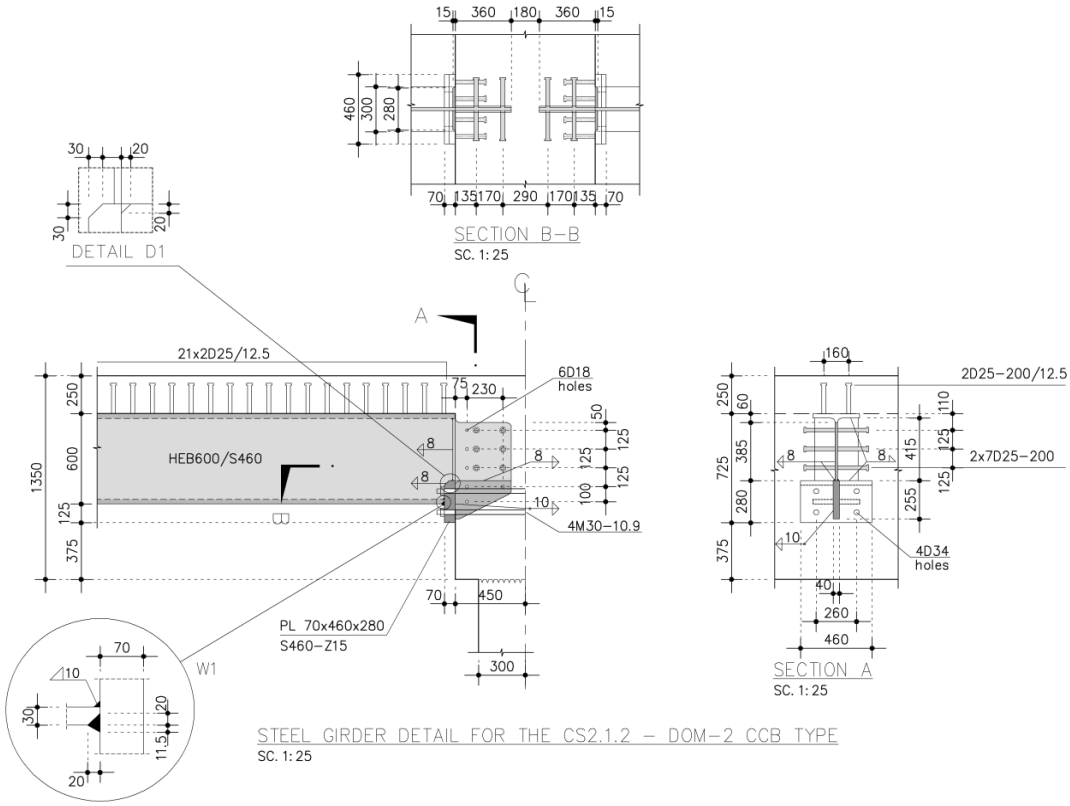

(b)

Fig. 2-22 New CCB variant (a) DOMI-1 (b) DOMI-2

Definition of the properties for the full-scale CCBs

From the Case Studies already defined in Task 1.1 it has been possible to identify the I-girder subassemblies, associated to the Concrete Cross Beams technique to be subject to testing in WP2. Particular attention is dedicated to the interconnection arrangement of the steel girders with the CCBs on piers and at abutments. For these reasons, the test subassemblies for the longitudinal and transversal direction were identified based on simplified modelling considerations. Both vertical and horizontal loads were analysed. The idea was to identify an isostatic portion of the bridge that includes the cross beam–deck joint, the object of tests foreseen in Task 2.2-2.4 of WP2.

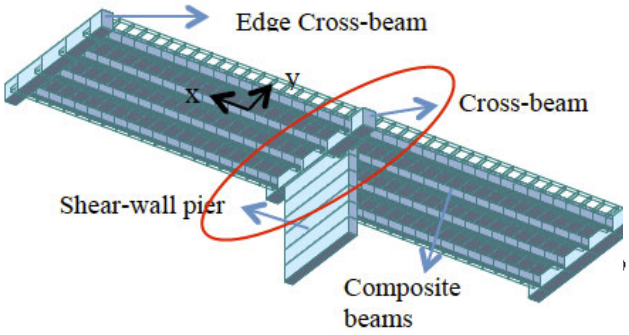

Fig. 2-23 Stick model of the case study 2.1.2.

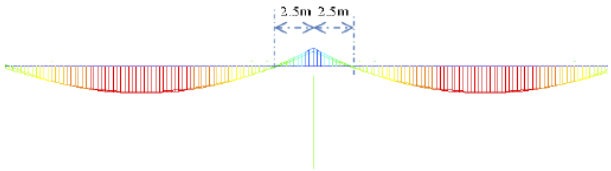

Fig. 2-24 Bending moment distribution due to vertical and seismic loads

According to these F.E. analyses for both directions, it was found that the required load to be applied to a specimen composed by the entire deck was too large, impossible to be reproduced with the existing actuators in the laboratory. Thus, a single beam model was investigated. For the transversal direction the CS2.1.1 (simply supported deck on bearings), was utilized (Fig. 2-25).

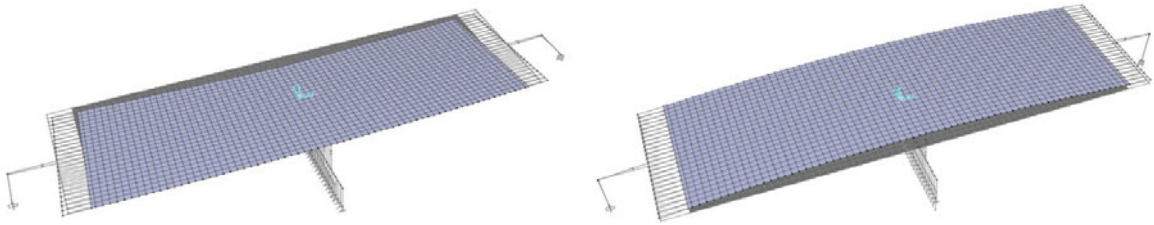

Fig. 2-25 F.E. model of the final specimen subject to (a) horizontal transversal load, and (b) to vertical load

On the contrary in longitudinal direction, it became obvious that the CS2.1.1 couldn't provide information regarding the CCB damage caused by seismic actions, as it would require the development of extremely high displacement beyond the laboratory capacity, and with rather uncertain results, as the damage would be exhibited in the bearings rather than in the CCB. Thus, the CS2.1.2 of the monolithic connection between CCB and pier was utilized in longitudinal direction (Fig. 2-23 and Fig. 2-24).

Based on this procedure, which is described in detail in Deliverable D2.1 (2013) and Mid-Term Report (2014), and after selecting a proper scaling factor equal to 1:2, compatible with the two laboratories' capabilities and able to produce a contained scaling effect, the specimens to be tested were fully defined. The static schemes for vertical and horizontal loads are presented in Fig. 2-26.

For a typical problem involving time-dependent loading, since there are three fundamental dimensions, namely, mass M, length L, and time T, three independent scale factors may be selected for the true modelling. The others scale factors can then be derived according to the principles of dimensional analysis. The fundamental idea is that the actual model and the reduced model have the same material thus the factors have to guarantee the same value of stress in order to evaluate the resistance of elements. There are two possibilities according to Kumar et al. (1997); they correspond to a selection of the most convenient factors for mass and time with respect to the type of problem and to the relevance of gravity loads. In the **SEQBRI** case, the gravity loads are predominant and therefore, the scaling of specimens will be designed by following the Procedure 1. The scale factor S chosen for the subassembly test is 1:2; the dimensions of all elements will be multiplied by this value while the mass and others components will be modified as shown in Table 2-2.

Table 2-2 Scale factor for each dimension in the two procedures

Quantity	Procedure 1	Procedure 2
Length	S	S
Mass	S^3	S
Stress	1	1
Stiffness	S	S
Force	S^2	S^2

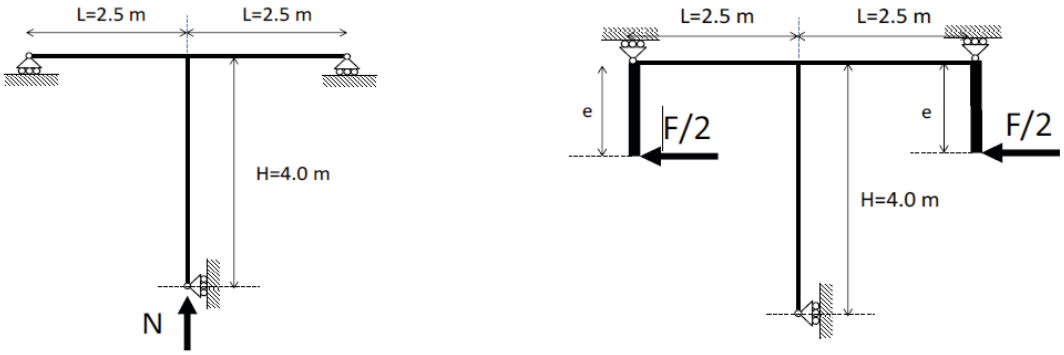

Fig. 2-26 Static scheme for vertical and horizontal longitudinal loads

Geometric and mechanical characteristics of the full-scale prototypes

Based on the intermediate pier's geometry of the CS 2.1.1 and 2.1.2 and applying the three selected CCB variants, the full scale prototypes were formed. These prototypes were designed according to the relevant Eurocodes (EN 1992, 1993, 1994, 1998)) and considering also the MIKTI procedure, (Lashal and Aribert 2002), against permanent, live and seismic actions.
Many details have already been provided in the Deliverable D2.1 (2013), even though some slight modifications and improvements were provided at Mid-Term Report. The final detailing of the full-scale prototypes is presented in the Appendix 3.1 (Figs A3.1-7, A3.1-8 and A3.1-9).
For both the concrete slab and the concrete cross-beam, concrete C35/45 and reinforcing steel B450C are used. The structural steel of the I-girders is S460M, and Nelson type S235-J2G3+C450 shear stud connectors are used. For the DOMI-2 type configuration, prestressing bolts 10.9 with elongated body or Dywidag-type prestressing bars 835/1030 are used.

2.3.1.2.4 Definition of proper testing protocols for I-girder subassemblies tests (Task 1.5)

The definition of an appropriate testing procedure is a key aspect of an experimental activity. Many procedures have proposed criteria for identify loading protocols capable of reproducing the actual behaviour of the structure under seismic actions. In **SEQBRI** project three different procedure have been evaluated:

- ECCS - European Convention for Constructional Steelwork (1986)
- ATC-24 - Applied Technology Council (1992)
- Drift Protocol for Seismic Performance Evaluation (Hutchinson, 2011)

The first procedure considered is in ECCS, (1986). This protocol is composed by two steps in relation to the characteristics of the specimens. The two steps give different information, in particular, the first is relevant to the characterization of the material, while the second is relevant to the cyclic behaviour investigation. The first, a monotonic test, provides the Force-displacement law that after a suitable manipulation gives the parameters of yielding force and displacement. After the definition of the parameters it is possible to set the history of cyclic tests; the amplitude of each cycle is related to the yielding displacement. The limit of this procedure lies in the fact that the actual damage evolution of the specimen is not properly taken into account during the test.
With respect to the ECCS procedure, a more elaborated method was developed by ATC-24 (Applied Technology Council) in 1992 (ATC-24, 1992). As explained in the ATC-24 Guidelines, for the special test case, the damage is considered with a coefficient that modify the amplitude of each single cycle in relation to the amplitude of the previous cycle and to the total number of cycles. Even

though for this procedure the first step is represented again by a monotonic test, in order to define the material properties, this procedure is completely different with respect to the previous one.
After this step, from the ECCS procedure, the values of F_y and e_y are defined. Recommendations for numerical values of these parameters and details of the loading history are provided in the ATC-24 Guidelines. With this procedure, the ATC-24 Guidelines introduces the case of special testing program in which damage is considered. The testing program depends on the postulated cumulative damage model; the simplest model of this type is the one based on the two assumptions of Manson-Coffin relationship and Miner's rule
The third method includes all the previous positive characteristics and seems to be the best method to evaluate the seismic behaviour of composite substructures. The characterization of the cycle history is done following the indications of Hutchinson (Hutchinson et al. 2011); the objective is to design the cycles after an accurate analysis of the structure response. The procedure includes three extra steps above the standard tests to characterize the material mechanical property: (i) seismic hazard definition; (ii) structure modelling and analysis; (iii) final development of the drift protocol. In a greater detail, after the selection of seismic hazard and ground motion, including the motion scaling, the non-linear FE model is set and the structural response with respect to the selected ground motion is evaluated. Based on the calculation of a damage index based on dissipated energy, the generation of cycles is done.
Given that the experimental test campaign is mainly devoted to the evaluation of the capacity and the calibration of refined and simplified numerical models, the adoption of ECCS method appears the most appropriate. The definition of predefined cycles based on yielding conditions of the specimen allows for a better and continuous control of the damage conditions during all phases of the test.

2.3.2 Work Package 2: Tests on scaled I-girder subassembly specimens

WP2 has been devoted to the experimental evaluation of the transverse and longitudinal capacity of intermediate concrete crossbeams related to prototype I-girder subassemblies analysed in Task 1.3. In detail, 15 different experimental tests were performed on specimens with intermediate crossbeams at the UNITN and UNIRM3 Laboratories. In order to investigate both transversal and longitudinal behaviour of deck-I-girder sub-assemblages under seismic actions and to evaluate their residual capacity against vertical loads, monotonic and cyclic loading tests were carried out.

This section is organised as follows. Firstly, the mechanical characterization of fine grain steels for both S355 and S460 grades is presented; secondly, the design and construction of subassembly specimens conducted at the Laboratories of UNIRM3 and UNITN Universities is descripted. Then, the experimental campaign on specimen subassemblies and relevant outcomes in both transversal and longitudinal directions are reported and discussed. Finally, the evaluation of the residual vertical load capacity of the damaged specimen is analysed and discussed.

2.3.2.1 Mechanical characterization of fine grain (S355, S460) steels (Task 2.1)

In this section results of low-cycle fatigue tests both in monotonic and cyclic conditions are presented and discussed. The specimens tested were hereafter described as well as the relevant results. Steel grades S355J2+M as well as S460M have been tested monotonically as well as cyclically. With reference to Fig. 2-27, the object of the test was a 3-point bending cross-shape specimen with curvature at every corner after Ohata and Toyoda (2004). The sample is shaped in order to concentrate cracks and the plastic hinges in the two sides of the specimen. The test has been executed using the universal machine MTS 810 with a maximum capacity of 500 kN capable to impose displacements or forces, both read by an inner LVDT and a Load cell respectively (Fig. 2-29). Given that relative displacements between the grips and the steel work of the setup cannot be excluded, a couple of Linear Potentiometers have also been used. With reference to Fig. 2-28, the tests have been made on smooth round bar specimens. Monotonic tests were made with a "Zwick/Roell Z100 Allround Line" material testing machine or "MTS" hydraulic machine whereby all cyclic tests were made with the hydraulic machine. Moreover, dimensions of the round bar specimen are in compliance with current codes concerning cyclic material testing ([ISO 12106, 2003], [ASTM E606-04, 2004]). Table 2-3 summarises the testing program that has been adopted to perform the Fatigue Test campaign. More specifically, 2 monotonic tests were executed on each steel typology within the experimental campaign at UNIRM3, whilst other 3 tests were provided by RWTH campaign. The goal is to characterize each type of steel, including force and deformation at yielding and the force and displacement at ultimate condition. Actually the deformation ε was measured (with Strain gauges) only for one specimen, which was used to detect the displacement corresponding to the yielding condition. In fact, beyond a certain level of deformation $<\varepsilon_U$ (ultimate

deformation) the strain gauges does not work anymore. Consequently, the ultimate deformation will be evaluated only numerically. The remaining tests are cyclic and have been used for the Fatigue evaluation of each steel grade. Monotonic tensile tests have been conducted for each steel grade – 2 on the Zwick testing machine which used a clip gage for strain measuring and 1 on the MTS testing machine which used a laser extensometer for strain measuring. Results are shown in Fig. 2-30. These data were evaluated to determine a true stress-strain curve which were used as input for monotonic calculations of the bridge subassemblies modelled in ABAQUS software. An example of monotonic response obtained for the two types of specimens is shown in Fig. 2-27 and Fig. 2-28.

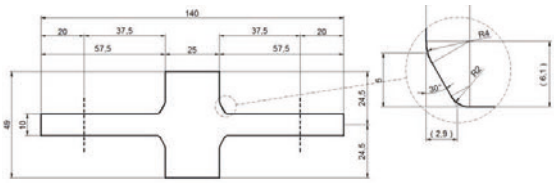

Fig. 2-27 Plane view of the cross-shape specimen (dimension are in mm)

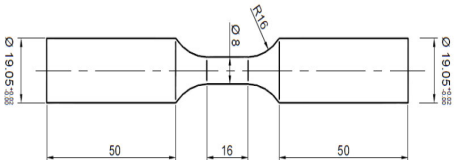

Fig. 2-28 Geometry of round bar specimen (dimension are in mm)

Table 2-3 Fatigue Tests – Testing Program – UNIRM3 and RWTH

	N° specimens				
Test Type	**Monotonic**	**Cyclic [±1.0 %]**	**Cyclic [±1.5 %]**	**Cyclic [±2.0 %]**	
S355J2W (Arcorox)	2	1	1	2	UNIRM3 tests
S355J2+M	2	1	1	2	
S460M	2	1	1	2	
S355J2+M	3	1	1	1	*RWTH tests*
S460M	3	1	1	1	

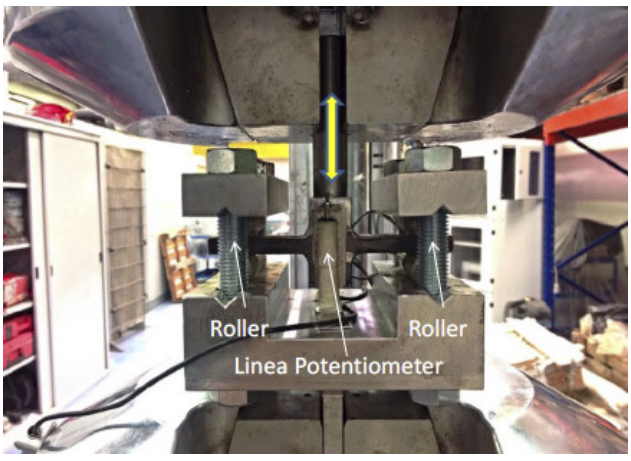

Fig. 2-29 Setup of the 3-points bending test

Fig. 2-30 Setup of the test on round bars

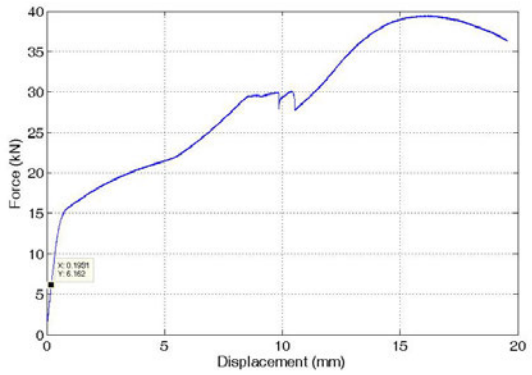

Fig. 2-31 Time history of force - NPC1

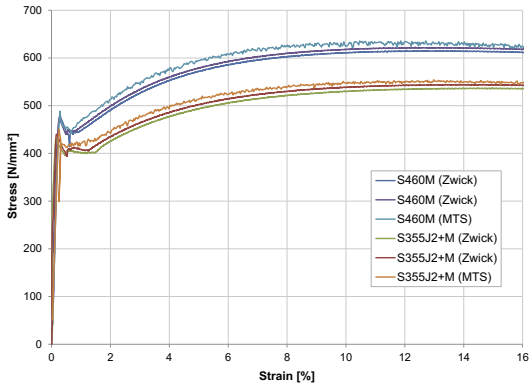

Fig. 2-32 Monotonic tension test results as engineering stress-strain curves for steel grades S355J2+M and S460M conducted on different testing machines (Zwick and MTS)

Cyclic tests allowed to calibrate the non-linear isotropic/kinematic hardening parameters of the Lemaitre-Chaboche function. For example, in Fig. 2-33 the result of the cyclic test on steel with grade S460 and the comparison with the numerical model in ABAQUS is presented. With reference to low cycle fatigue tests on round bar specimens, for each steel grade 3 single step tests have been conducted with strain amplitudes of ±1.0 %, ±1.5 % and ±2.0 % at zero mean strain. The tests have been terminated after a drop-down of force of 10 kN. The main cracks, which caused failure, can be clearly seen but also at other spots minor cracks were visible. Cyclic engineering stress-strain data is shown in Fig. 2-34 for S355J2+M (left) and for S460M steel (right). Further details about the multistep tests and compression after initial tension tests can be found in the Mid-Term report

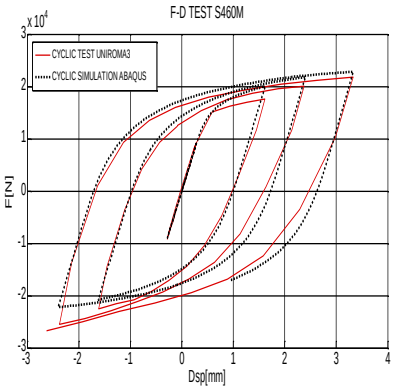

Fig. 2-33 Cyclic test of S460: comparison between experimental and numerical results

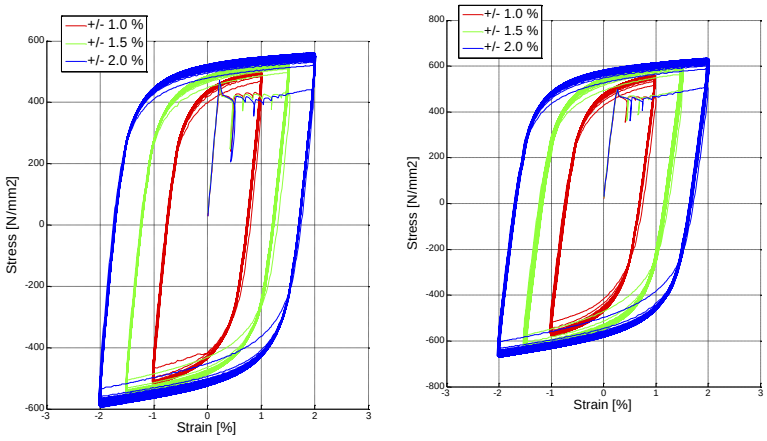

Fig. 2-34 Cyclic engineering stress-strain data for S355J2+M (left) and S460M (right) steel grades

2.3.2.2 Design and construction of I-girder subassembly specimens (Task 2.2)

Specimens have been designed according to the selected CCB typologies defined in the WP1 where three different type of connection solutions between steel I-girder and concrete-cross beam have been considered, as shown in Fig. 2-35. In particular, two specimens with DIN-FB104 Type C concrete cross beam, two specimens equipped with a CCB - DOMI-1 and four specimens equipped with a CCB – DOMI-2 have been built for the experimental campaign of UNIRM3, whilst two specimens for each joint configuration were built for UNITN tests.

(a) (b) (c)

Fig. 2-35 Detail of connections based on (a) DIN FB104 Var.C, (b) DOMI-1, and (c) DOMI-2

Each specimen has been accurately designed in accordance with a selected scaling criterion proposed to minimize the scaling effect, especially for the concrete slab in terms of cracking pattern. Consequently, the adopted scale factor is 1:2. They are made of a single steel girder with its tributary concrete slab 1.325 m wide and a portion of pier. All the girders are 50 cm longer than the necessary, in order to simplify the realization of the appropriate boundary conditions in the laboratory. All the relevant aspects of the specimens are alredy described in the Mid-Term report. All the devices and instruments placed in and on specimens that measure displacements and deformations are reported in the Annex 2. The construction phase for the monolithic connection and the simply supported connection tested in UNIRM3 and UNITN are shown in Fig. 2-36 and Fig. 2-37, respectively

Fig. 2-36 Pier and CCB reinforcements for monolithic joint configuration

Fig. 2-37 CCB formwork detail view for simply supported connections (all specimens)

2.3.2.3 Experimental evaluation of the capacity of I-girder subassemblies subjected to transversal actions (Task 2.3)

The test setup, as depicted in Fig. 2-38, was designed based on the results of a preliminary finite element analysis of test specimens. The necessary forces to induce failure of the specimens were applied through a couple of actuators of 1000 kN capacity each.

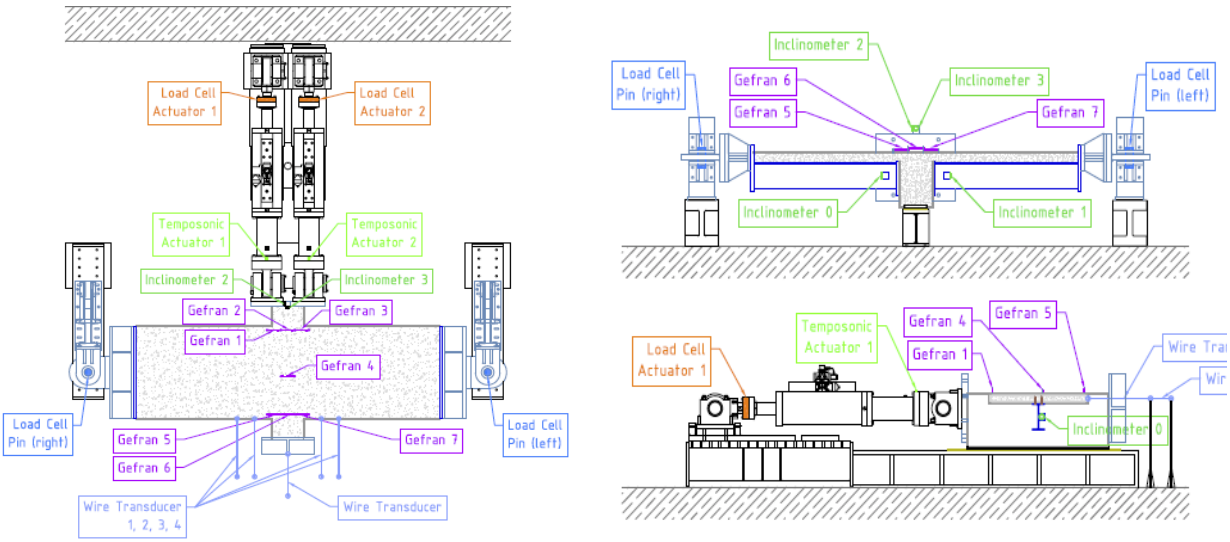

(a) Measuring instruments (top view)

(b) Measuring instruments (front and lateral view)

Fig. 2-38 Position of measuring instruments for UNITN tests

The actuators' heads through which the force was transferred to the specimen were connected using a 1050×850×80 mm steel plate. It allowed the actuators to act in parallel and thus to apply the resultant force on a clearly defined surface. The specimen was positioned on top of a steel basement aligned with the actuators and connected to the strong floor.

The aim of the experimental campaign was the characterization of specimen behaviours under transversal loads. In particular, the connection between I-girder steel beams and the concrete cross-beam was investigated. Three different joint solutions were proposed, and two types of loading protocol were adopted, monotonic and cyclic, respectively. With regards some preliminary consideration about the mechanism of collapse of the specimen, the best position of device instruments was chosen. Main results in terms of force-displacement and strain on some important elements of connection registered during tests are collected hereinafter and in the Annex 2. Table 2-4 reports the testing program carried out in the Laboratory of the UNITN University.

Table 2-4 Numbering and denomination of specimen for transversal tests

Typology	Testing protocol	Number (#)	Name of Specimen
DIN FB-104	Monotonic	1	SQ1M
DIN FB-104	Cyclic	2	SQ1C
DOMI 1	Monotonic	3	SQ2M
DOMI 1	Cyclic	4	SQ2C
DOMI 2	Monotonic	5	SQ3M
DOMI 2	Cyclic/Monotonic	6	SQ3C/3V

In order to evaluate the maximum value of strength and strain of the specimen, as well as the maximum force and displacement at the failure condition, three monotonic tests were carried out, one for each joint solution proposed. The aim of these tests was twofold: to check if the global behaviour of specimen was influenced or not by different joint details between I-girder steel beams and the concrete cross-beam, and to calculate the yielding point of each specimen. An energy-balanced method for steel-concrete structures for the calculation of the yielding point of each specimen was adopted (Bursi et al, 2002); the reason can be found on the high non-linear behaviour of specimens, which make difficult the evaluation of the yielding point and suggests the adoption of more efficient methods.

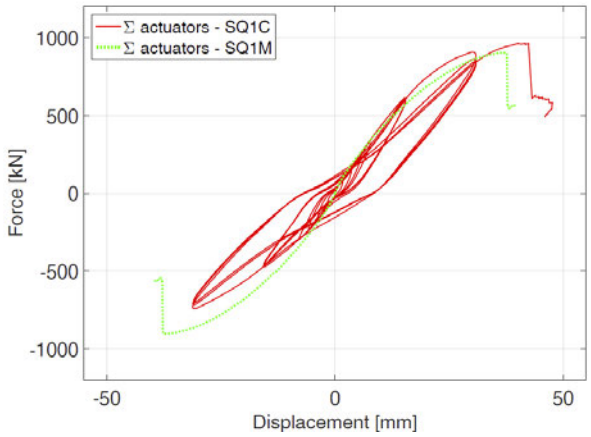

Fig. 2-39 Force - Displacement response of SQ1M and SQ1C tests

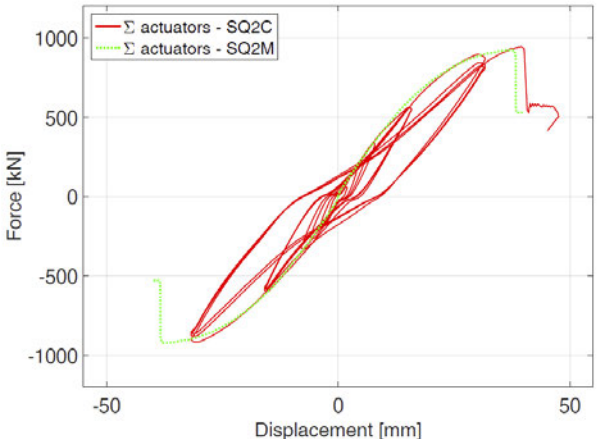

Fig. 2-40 Force - Displacement response of SQ2M and SQ2C tests

This yielding parameter was used to calibrate the cyclic test displacement history in accordance with the ECCS (1986) procedure. Cyclic tests are crucial, on one hand because they provide inside into the specimens' structural behaviour, which obviously represents the primary goal, on the other hand because the test for the evaluation of the vertical load bearing capacity leans onto SQ3C test results. The tests SQ1C and SQ2C carried out on specimens respectively with DIN FB 104 (Var. C) and DOMI1 detail type were characterized by collapse of specimen. With reference to the forces measured at the actuators' load cells and transmitted to the hinges, the maximum values registered in every test are comparable, as shown in Fig. 2-39, Fig. 2-40, Fig. 2-42 and summarised in Table 2-5 and Table 2-6. Furthermore, the transversal displacement for which collapse of the specimen occurs varies slightly between the tests. Thus, the CCB connection type appears not to be responsible for the ultimate capacity of the specimens. In fact, the collapse mechanism develops primarily in the concrete slab at the girder-cross beam interface, as shown in Fig. 2-43.

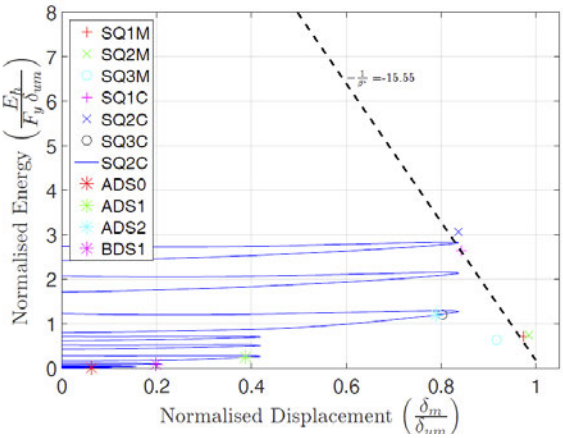

Fig. 2-41 Damage domain for SEQBRI experimental tests

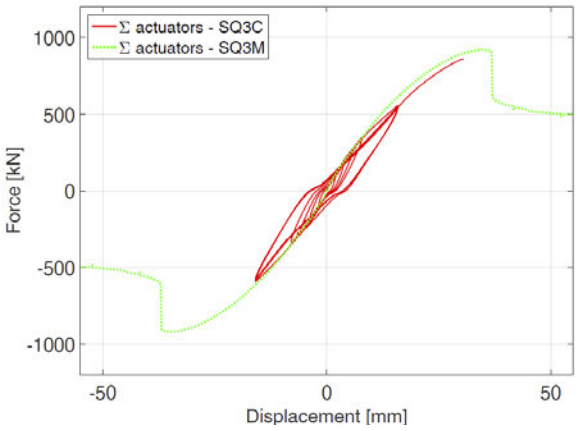

Fig. 2-42 Force - Displacement response of SQ3M and SQ3C tests

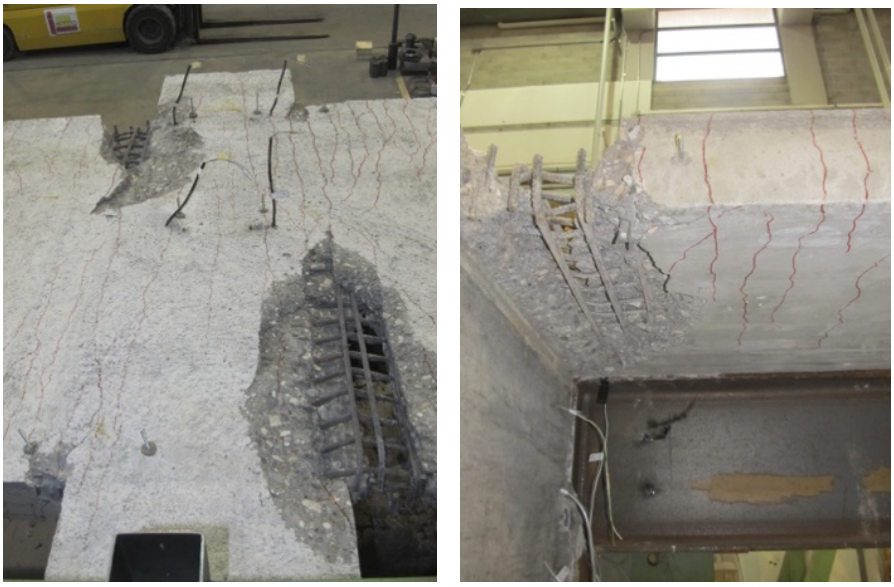

Fig. 2-43 Damage condition of the specimen after the conclusion of the SQ2C test

With regard to the SQ3C test, the maximum transversal displacement of the concrete cross-beam was limited to a specific value. This threshold derived from the damage evaluation performed on the first two cyclic tests. An energy-based methodology (Chai et al., 1995; Bursi et al., 2002) for the assessment of structural damage induced by seismic loading was adopted. The hysteretic energy calculation was done for the three monotonic tests and for the first two cyclic tests (see Fig. 2-41). It is can be note that the major contribution to the damage of the substructure is due to the normalised displacement. Last, for each test is possible to calculate the damage index with the following formula:

$$D_i = \frac{d_m}{d_{um}} + \beta^* \frac{\left(E_H - E_{hm}\right)}{F_y d_{um}} \tag{2.1}$$

where d_m is the maximum displacement, d_{um} is the maximum displacement under a monotonic loading, E_h is the plastic strain energy dissipated during the cycles, E_{hm} is the plastic strain energy dissipated by the structure under a monotonic loading, F_y is the yield strength of the structure, and β^* is the strength deterioration parameter calibrated for the modified model, which characterize the damage contribution due to cumulative plastic strain energy. In this case, the model converges to D_i = 1 for monotonic loading.

Table 2-5 Summary of monotonic experimental test results

Test	d_y (mm)	F_y (kN)	d_{max} (mm)	F_{max} (kN)
SQ1M	7.43	467.30	36.90	906.00
SQ2M	12.87	836.50	37.40	922.00
SQ3M	9.60	625.07	34.80	922.00
Average	*9.97*	*642.96*	*36.37*	*916.67*

Table 2-6 Maximum force and displacement at the failure point for SQ1C and SQ2C tests

Test name	F_{max} (kN)	$d(F_{max})$ (mm)	d_{max} (mm)
SQ1C	963.80	40.20	42.40
SQ2C	948.30	39.50	40.20

Table 2-7 Deck damage limit states according to Makie et al. (2008)

Limit State	Damage State Description
DS0	2% of spalling strain
DS1	25% of spalling strain
DS2	50% of spalling strain

Damage threshold values were found from literature and normative documents analysis. These concepts were applied to experimental result obtained from previously cyclic tests. From literature, some indications were gathered in a PEER report (Mackie et al, 2008), as reported in Table 2-7. Here, each macro-element of the bridge is analysed in term of damage, and each Limit State is related to a measurable quantity like displacement, deformation, ect.

The SQ3C test was conducted as follows: i) the same cyclic history of displacement of previously cyclic test was used; ii) the crushing of concrete was calculated as the average value from the first two cyclic tests (thus this is the 100% of the crushing deformation); iii) according to experimental results, deformations of the concrete corresponding to Limit State defined in Table 2-8 were estimated; iv) values of displacement associated with these Limit States were defined; v) when the deformation of the concrete was equal to the 50% of the deformation of crushing, the test was stopped. The corresponding limit state is called ADS2.

With reference to the maximum force of 859.3 kN registered by the actuators, the corresponding transversal displacement of the concrete cross-beam was 30.3 mm. These values are associated to the ADS2 damage state, as 50% of concrete spalling strain was reached during the test at the left or right slab – CCB interface.

Table 2-8 Damage Limit States and corresponding Damage Index

Limit State	Damage index Di	Structural conditions
ADS0	0.05	No irreversible damage/yielding on structural elements, no visible effect/crack on section.
ADS1	0.47	Reinforcement yielding of more than 25% of section, concrete cracking (crack width ≈ 0.2 mm).
ADS2	0.75	Reinforcement yielding of more than 50% of section, concrete cracking (crack width ≈ 0.7 mm). Concrete cracking in compression.
BDS1	0.20	Reinforcement yielding of more than 10% of section, concrete cracking (crack width ≈ 0.2 mm).

2.3.2.4 Experimental evaluation of the capacity of I-girder subassemblies subjected to longitudinal actions (Task 2.4)

The lateral view of the setup is shown in Fig. 2-44. In this configuration, the horizontal actuator is directly connected to the level arm on the right. The setup is made of a rectangular steel frame lying in the horizontal plane, whose elements are mutually hinged (horizontal trusses). This horizontal frame is bolted to two vertical steel beams (lever arms) linked to the specimen, by a connection steel plate, allowing transmitting to both the sides of axial force, shear force and bending moment. The bonding effect at the end of the reinforcing bars is reproduced using a special clamping system. The vertical force is transmitted through a couple of hydraulic jacks, aligned under the wall pier and placed at a mutual distance of 500 mm, in order to obtain a uniform diffusion of the compressive force in the pier. Before positioning the specimen, in order to allow only vertical displacements at the bottom of the pier, two couples of horizontal trusses are assembled under the steel basement, on the top of the two load cells placed to record the vertical

load. Additional details on the measure devices installed on specimens can be found in the Deliverable 2.3 (2015).

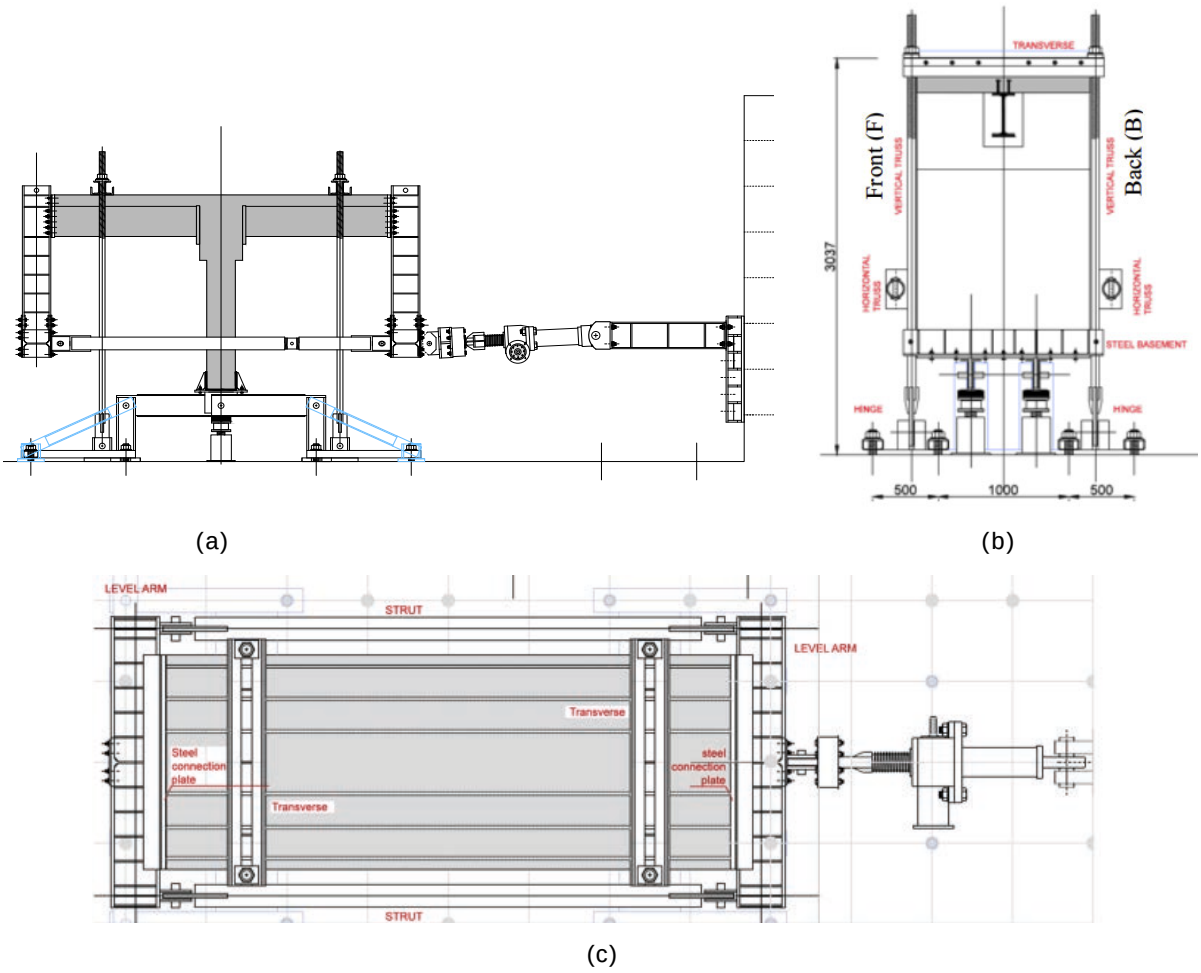

Fig. 2-44 Lateral (a), front (b) and plan (c) views of the setup

Table 2-9 shows the testing program, involving the 8 specimens described in section 1. In particular, one monotonic test is performed for each typology of CCB in order to calibrate the subsequently cyclic tests. In particular, for the CCB typology DIN FB104 and DOMI1 two specimens have been tested, the first one in monotonic conditions and the second one under cyclic loading. DOMI2 specimens were firstly tested monotonically. Then three full cyclic tests were performed on the remaining specimens. The DOMI-2 specimen tested under monotonic condition has been also tested under vertical loads to evaluate the residual vertical load-carrying capacity.

The tests consist in a first phase in which the vertical load is imposed. According to the analysis presented in Deliverable 1.1 (2013) and Deliverable 1.2 (2013) the imposed maximum vertical load was equal to F_v=220 kN. Subsequently a cyclic history, has been applied at the top of the specimen by using the sensor Crtl. In this way the control system imposed the necessary force through the electro-mechanical actuator, in order to reach time by time the desired displacement. Fig. 2-45 and Fig. 2-46 show damage limit states for the DIN FB 104 Var. C and DOMI 1 specimens, respectively. These tests provide indications on the damage pattern with the growing of both lateral displacement and force and allow to calibrate the cyclic test displacement history protocol (in this case the ECCS (1986) procedure was used).

Concerning the cyclic tests, even though the specimen FB104 and DOMI2 have shown a similar global behaviour in terms of maximum force and displacement (see Fig. 2-47 and Fig. 2-50), a different local behaviour was identified. In particular, the CCB cracking was anticipated for the specimen FB104 with respect to DOMI2. In addition, for the FB104 specimen the failure of the CCB was anticipated with respect to DOMI2 (Fig. 2-54). The presence of prestressing bars in the DOMI2 specimen avoided any pull-out phenomenon in the CCB in correspondence of the bottom flange of the steel girders. This latter was clearly present in the FB104 and DOMI1 specimen with

an irreversible damage condition (Fig. 2-52). The possibility to recover the prestressing level or substitute the prestressing bars after a seismic event makes the DOMI2 joint superior in case of SCC bridges located in high seismic zones.

Table 2-9 Type of test for longitudinal loading conditions of SEQBRI Specimens

Typology of specimen	Number (#)	Name of Specimen	Type of test	Name of test
DIN FB-104	1	A2	Monotonic	FBA2M
DIN FB-104	2	A1	Cyclic	FBA1C
DOMI - 1	3	B2	Monotonic	D1B2M
DOMI - 1	4	B1	Cyclic	D1B1C
DOMI - 2	5	C1	Cyclic	D2C1C
DOMI - 2	6	C2	Cyclic	D2C2C
DOMI - 2	7	C4	Cyclic	D2C4C
DOMI - 2	8	C3	Monotonic	D2C3M
DOMI - 2	9	C3	Vertical	D2C3MV

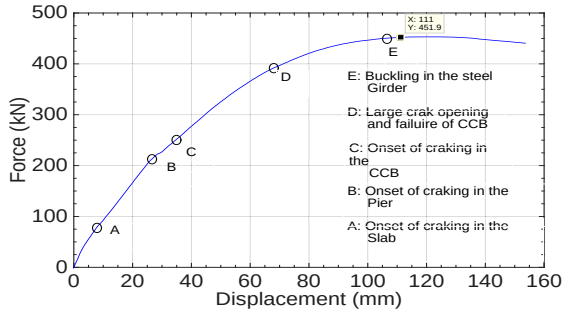

Fig. 2-45 Damage states in the A2 (DIN FB104 Var C) under monotonic loading condition

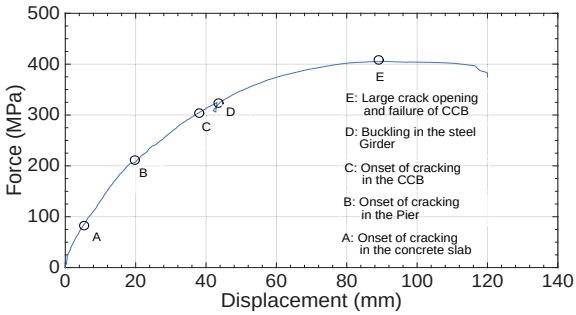

Fig. 2-46 Damage states in the DOMI1 specimen under monotonic loading condition

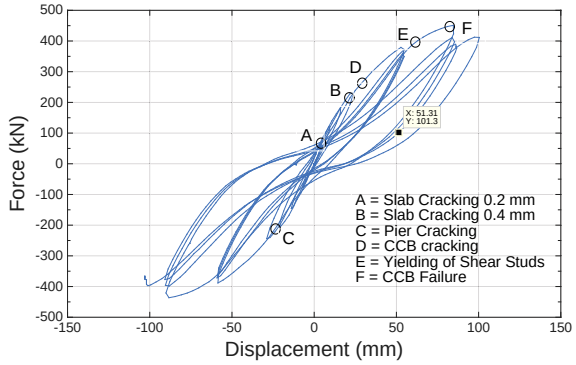

Fig. 2-47 Damage states in the DIN-FB104 specimen under cyclic loading condition

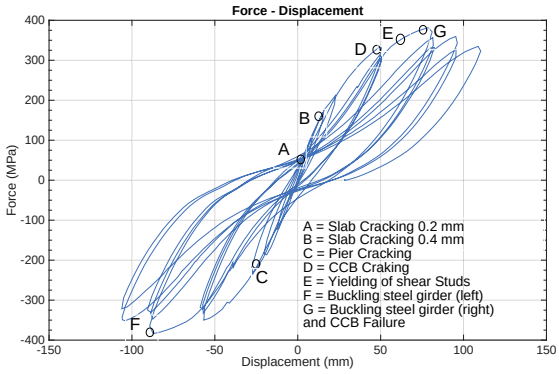

Fig. 2-48 Damage states in the DOMI1 B2 specimen under cyclic loading condition

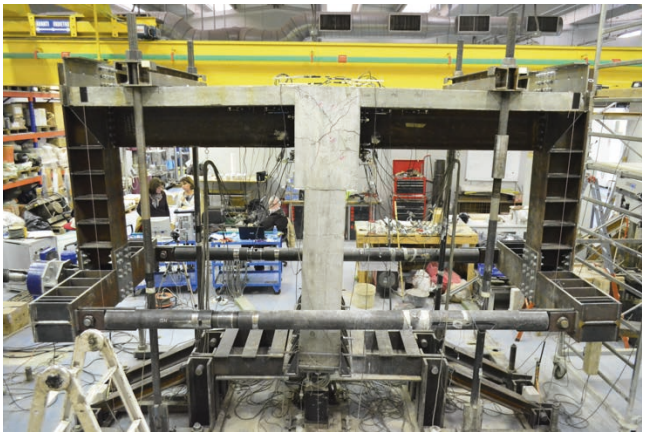

Fig. 2-49 Final deformation of the specimen D2C4C and cracking in the CCB

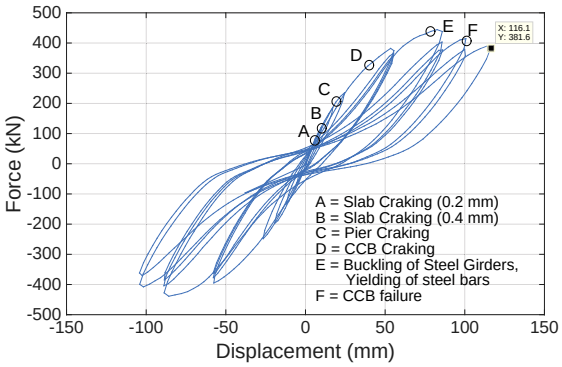

Fig. 2-50 Damage states in the DOMI2 specimen under cyclic loading condition (D2C1C)

Fig. 2-51 Buckling phenomenon in the steel girder (DOMI1)

Fig. 2-52 Detachment of the steel girder end plate

Fig. 2-53 Cracks in concrete slab and CCB

Fig. 2-54 Crack pattern in the CCB

DOMI1 solution showed a less effective behaviour both with respect to specimen DOMI2 and FB104, as illustrated in Fig. 2-48. In fact, an anticipated failure condition of the CCB was noticed. In addition, the longitudinal shear studs yielded earlier than the shear studs in FB104 specimen. In addition, it is not negligible the obtained lower strength with DOMI1 specimen both in monotonic and cyclic conditions.

Table 2-10 Limit states (LS) for the different joint typologies

	FB104		DOMI1		DOMI2 – C1		DOMI2 C4	
Limit State	δ(mm)	F(kN)	δ(mm)	F(kN)	δ(mm)	F(kN)	δ(mm)	F(kN)
A. Crack Slab (0.2 mm)	7	50	5	45	7.5	23	5	15
B. Crack Slab (0.4 mm)	22	210	15	170	22	120	10	102
C. Onset of Cracking in the Pier	25	220	23	212	20	200	15	150
D. Onset of Cracking in the CCB	30	260	49	331	40	320	50	350
E. Yielding of Shear Studs	64	400	60	350	-	-	-	-
F. Buckling of Steel Girders	84	440	75	382	75	450	70	390
G. Failure of CCB	84	440	75	382	100	450	100	380

A phenomenon common to all specimens is the buckling present in the bottom flange of the steel girders (Fig. 2-51). However, no clear indications were identified about the conditions in which it develops. In fact, it depends on the level of imperfection of the steel plates. In any case, it was clearly noticed a more pronounced level of buckling for both DOMI1 and FB104 specimens. This is certainly another positive aspect in favour of DOMI2 joints. The final configuration of the specimen after the test is shown in Fig. 2-49. The development of cracks in the slab was similar for all three CCB typologies (Fig. 2-53). Values of force and displacements for each identified limit state are reported in Table 2-10.

Table 2-11 Limit states for the PG3 (CCB)

	DM	Joint Rotation (mrad)
FB104	Yielding	0.10
	Ultimate	23
DOMI1	Yielding	0.25
	Ultimate	20
DOMI2	Yielding	0.3
	Ultimate	19

Table 2-12 Limit states for the PG4 (Slab)

	Drift (%)		
DM	FB104 (%)	DOMI1 (%)	DOMI2 (%)
Crack opening 0.2 mm	0.35	0.25	0.38
Crack opening 0.4 mm	1.10	0.75	1.10
Yielding of rebars	4.50	4.50	5.0%

In order to quantify the limit states to be used in a PBEE approach for the quantification of the suitable Damage Measures, Table 2-11 and Table 2-12 report the level of DM and EDP for each identified limit state evaluated from the cyclic tests for performance groups P3 (CCB) and P4 (Slab). For more details on the definition of performance groups see section 2.3.4.5.5.

Similarly to the test campaign in transversal direction, to analytically quantify the damage level in the specimens, the damage index D_i defined by Eq (1) was also quantifies. Table 2-13 reports the value of D_i for the three different subassemblies and for each limit state indicated in Table 2-10.

Table 2-13 – Damage index D_i for the different limit states

Limit State	DIN-FB-104 A1	DOMI1 B1	DOMI2 C1
A	0.0654	0.0701	0.0467
B	0.215	0.141	0.117
C	0.244	0.218	0.188
D	0.379	0.442	0.314
E	0.731	0.727	0.662
F	0.833	0.968	1.00
G	1.00	1.00	1.00

The damage index D_i shows the superiority of DOMI2 with respect to both DOMI1 and DIN-FB104 CCD type. Additional comments and detailed information about the outcomes of the experimental campaign in longitudinal direction can be found in Deliverable 2.3 (2015).

2.3.2.5 *Experimental evaluation of a I-girder subassembly residual capacity against vertical loads (Task 2.5)*

The aim of these tests is to check the residual load capacity of the SQ3C specimens after that it was subjected to a certain level of damage. This test required some modifications of the original setup used to monotonic and cyclic tests. Additional dead loads, i.e. steel plates and heavy steel beams put on the concrete slab, were removed. Moreover, two counter columns have been replaced by two stiff steel plates that were connected to the heavy steel beams.

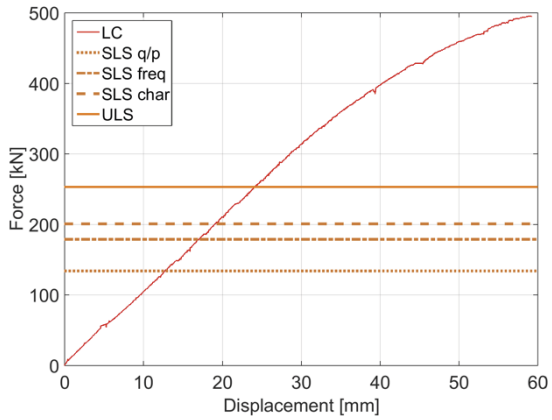

Fig. 2-55 Force-Displacement response of the SQ3V test

Fig. 2-56 Cracks on concrete slab and cross-beam at the ULS

After that, the pin hinges at the end of the specimen were turned of 90° around the y-axis. The vertical load was applied to the specimen thought a hydraulic jack of 1000 kN capacity, with a maximum stroke of 70 mm, placed under the bottom of the concrete cross-beam (CCB). A load cell of 1000 kN capacity and a steel plate of dimensions 350x250x25 mm were allocated between the jack and the CCB.

This additional test points out that the residual vertical capacity available for traffic loads of the intermediate concrete crossbeam (CCB) is sufficient for a specific target limit state, more precisely the SLS\frequent. It could also be noted that the CCB, with that damage level reached, is able to satisfy not only the loading corresponding to the ULS, but also almost twice that load value, as shown in Fig. 2-55 and Fig. 2-56. Additional details can be found in the 2nd Annual report (SEQBRI, 2015).

2.3.3 *Work Package 3: Numerical simulations and damage analysis of I-girder subassemblies*

During the project the experimental tests conducted at UNITN (transversally loaded specimens) as well as at UNIRM3 (longitudinally loaded specimens) were modelled and simulated in detailed finite element models. The aim was the development of a model which was capable to reproduce the observed response quantitatively, regarding e.g. load-displacement performance, as well as qualitatively, e.g. to identify and verify the relevant failure modes and limit states. Such a calibrated finite element model allows for more insight into the specimen behaviour and extends the amount and quality of information obtained from tests by the (limited) number of measurement devices as well as from visual observations which can be gathered only on and close to the surface of the tests specimens, so far the visibility was not limited by other obstructions like test set-up or load applications. Moreover, comprehensive sensitivity and parametric analyses can be made using the virtual model to study the influence of several influence parameters, what was not possible within the laboratory tests due to cost, time and workload constraints.

For the finite element modelling the general-purpose finite element package ABAQUS was used. It is one of the most capable and widely used finite elements software, which was initially designed for highly nonlinear problems and was often used for similar applications in the past. Moreover it provides a Python scripting interface, which gives the possibility to develop Python scripts to execute cumbersome and repetitive tasks automatically. The software also offers good possibilities to describe the material behaviour (concrete, steel, reinforcement) under monotonous and cyclic loading; the already available constitutive material laws can also be modified and adopted to the boundary conditions and calibrated by data achieved from material tests.

2.3.3.1 FE-modelling of I-girder subassemblies (Task 3.1)

General modelling approach

Three different concrete material models are implemented in ABAQUS: “smeared crack concrete model”, “brittle cracking model” and “concrete damaged plasticity model”. The first two constitutive models have some restriction which is the reason why they are only applicable to monotonic loading. However, the concrete damaged plasticity model, or shortly CDP model, is very well suited for cyclic loading conditions. For this reason, it has been chosen for the simulations conducted in the SEQBRI project. The CDP model is based on the Drucker-Prager strength hypothesis and uses isotropic plasticity combined with an isotropic damage elasticity approach. The theoretical background of the CDP model is described in (Lee and Fenves, 1998) and (Lubliner et al., 1898). The general stress strain curves in tension and compression are sketched in Fig. 2-57. The two predominant failure modes in concrete materials are taken into account: concrete crushing due to compressive stresses and concrete cracking due to tensile stresses. During cyclic loading, the elastic stiffness both in tension and compression is reduced to account for degradation effects. Stiffness recovery effects at load reversals form tension to compression conditions (e.g. due to closure of micro-cracks) can be accounted for. The following several input parameters are needed to completely define the CDP model: Young's modulus E; Poisson's ratio υ. Nonlinear stress-strain curve – separately for tension and compression; Damage variables d_c for compression and d_t for tension, each as function of inelastic strain; Stiffness recovery factors w_c for compression and w_t for tension; biaxial/uniaxial compression plastic strain ratio f_{b0}/f_{c0}; invariant stress ratio K_c; flow potential eccentricity ε; dilation angle Ψ; viscosity μ. All the parameters were chosen based on the expected default values for the concrete class used herein. A more detailed description of each parameter can be found in Deliverable 3.1 (2016) of the SEQBRI project.

For the second material of interest, steel, structural steel as well as reinforcing steel, the classical Chaboche material model (Chaboche, 1886 and 1989) was applied accounting for kinematic hardening, which is implemented in ABAQUS software. Steel reinforcement was modelled as one-dimensional truss elements, which are embedded in the surrounding concrete sections (see Fig. 2-58). In this way each reinforcement bar is explicitly modelled, adding stiffness to the concrete blocks. The displacements of the rebar nodes are determined by an average of the nearest concrete nodes. Thus, a perfect bond is modelled with no relative slip between reinforcement bar and concrete. The stress strain curve for the steel reinforcement bars was evaluated based on tension loading tests conducted at UNITN. Fig. 2-59 shows a comparison between simulation and test results for different bar diameters showing an excellent fit.

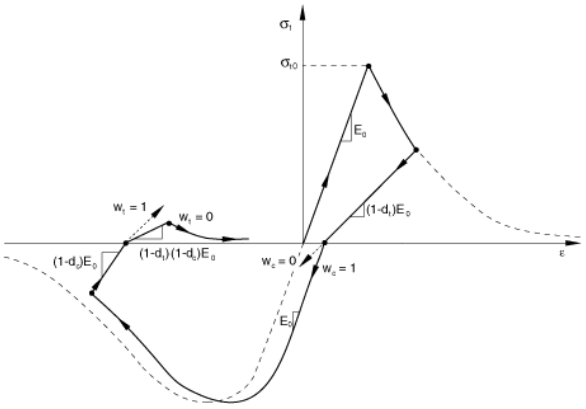

Fig. 2-57 Explicit modelling approach for steel reinforcement (truss elements embedded within concrete solid elements) (ABAQUS)

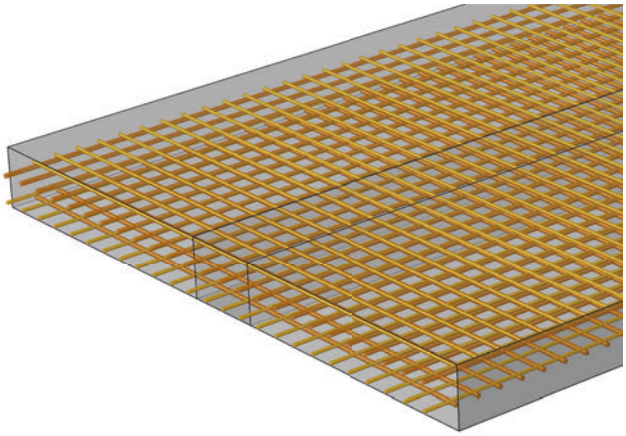

Fig. 2-58 Explicit modelling approach for steel reinforcement (truss elements embedded within concrete solid elements)

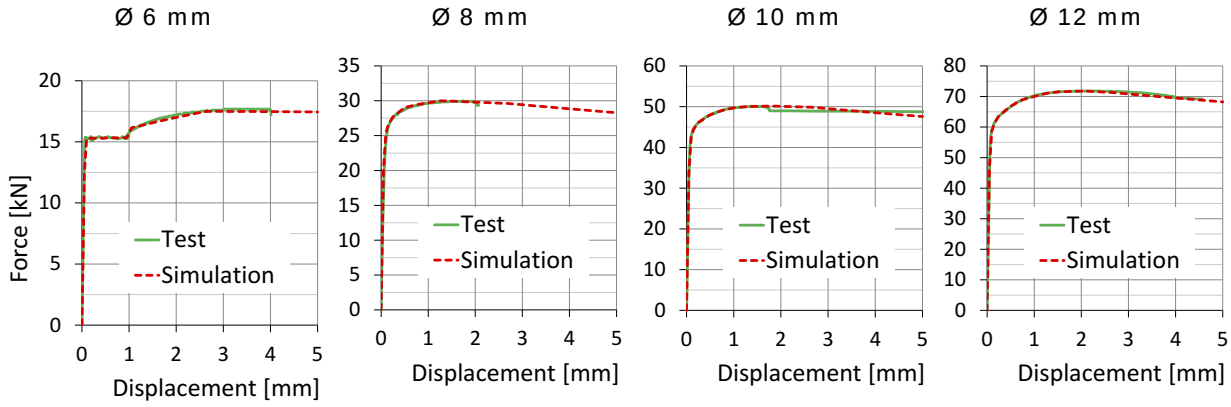

Fig. 2-59 Validation of reinforcement material input – comparison of force displacement curves obtained by tests and output of Abaqus simple bar simulations for all four diameters.

The connection in the shear interface between steel and concrete – in reality provided by shear studs – was modelled with three different approaches (see Fig. 2-60: perfect bond, i.e. both surfaces are tied together allowing no slip between both surfaces; using nonlinear springs representing the shear studs phenomenologically; and finally a detailed modelling approach modelling each shear stud explicitly by solid elements. The latter approach however exposed to be not applicable for the investigated specimens due to meshing, convergence and computational efficiency issues. The first approach showed to be the easiest and robust approach. The spring model approach was of practical importance only if relative slip between steel and concrete was observed in the tests and thus had to be modelled.

Interaction and contact modelling

Contact interaction had to be modelled if two surfaces are allowed to separate from each other, as for example in the case of the spring modelling approach illustrated in Fig. 2-60b) regarding steel and concrete surfaces. In such a case penetration of both surfaces had to be prevented. From the two generally available methods (Penalty method or Lagrange multiplier approach) the first one was used. This method inserts high stiffness terms between the two contact pairs to simulate the contact conditions. The finite sliding option (i.e. large displacement considerations) and hard contact option were used wherever contact interaction had to be modelled.

a) Perfect bond modelling approach

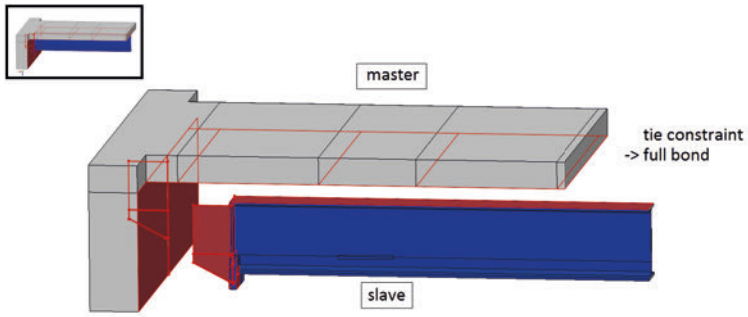

b) Spring modelling approach

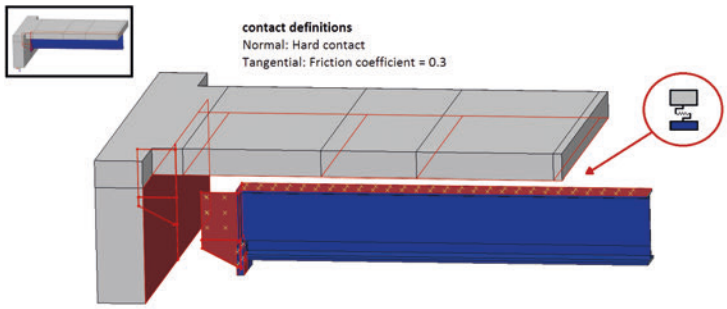

c) Detailed solid element modelling approach

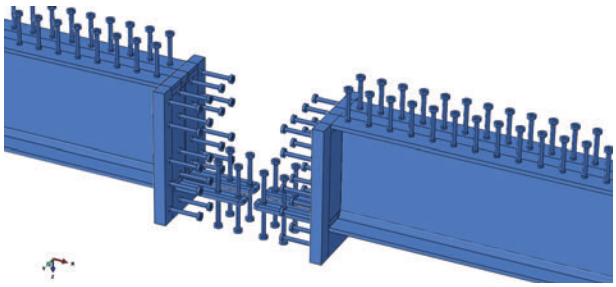

Fig. 2-60 Different modelling approaches for modelling of bond between steel and concrete

Meshing

For all the models a high quality mesh was desired. Convergence problems were always initiated in the concrete material elements and not in the steel elements. The smaller the elements the more convergence problems occurred. Additionally, as a matter of fact computational time increased exponentially. Thus, an average element size of 40 to 50 mm was used for the concrete parts as the best compromise between local accuracy, computation time and convergence. Related to the overall specimen dimensions, this can be still regarded as relatively fine mesh. Two different meshes are shown exemplarily in Fig. 2-61. The steel parts were modelled with a finer mesh, due to the fact that steel parts were usually more slender than the concrete parts. Exemplary meshes of all of the three joint typologies for the girder and inserted plates are shown in Fig. 2-62. If needed, single parts had to be separated and finally combined by tie constraints (see red dotted lines in Fig. 2-62) to achieve a high quality of all elements.

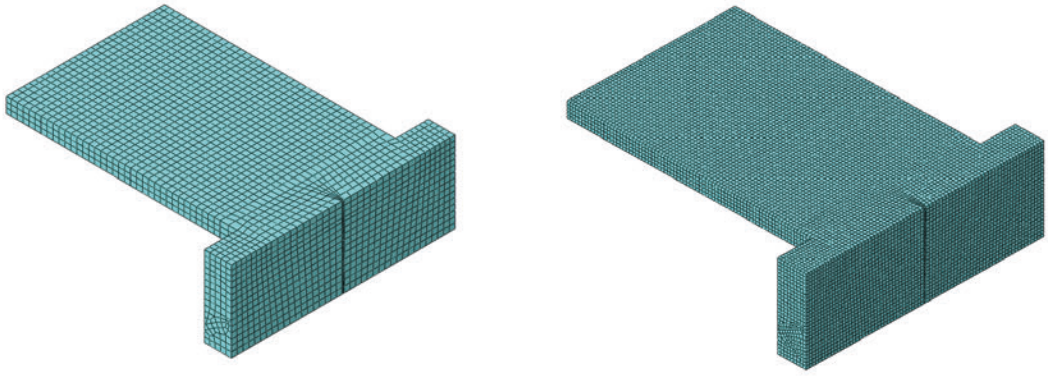

Fig. 2-61 Meshes of concrete parts – slab and concrete cross beam – medium (default) mesh with 50 mm (left) and 25 mm (right) element average size

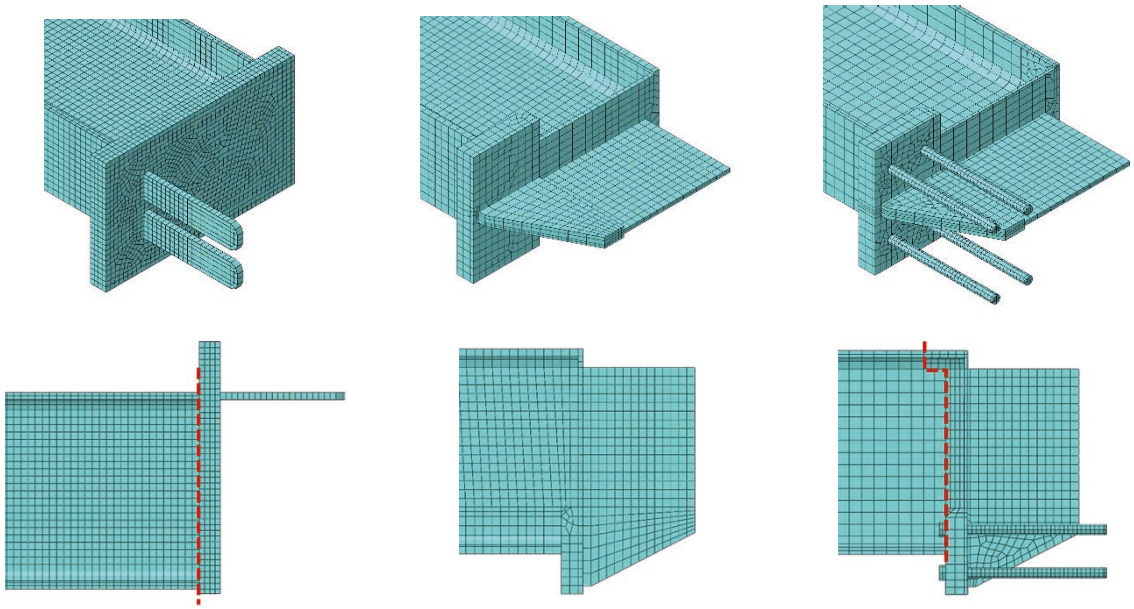

Fig. 2-62 Meshes of the steel parts of all three joint typologies: DIN-FB (left), DOMI-1 (middle) and DOMI-2 (right)

Element Types

The default element types used for different geometries of the subassembly are listed in Table 2-14. Usually reduced integrating elements were used for computational efficiency reasons but also to reduce unintentional stiffening due to locking phenomena. Solid elements have been used for all concrete parts and all steel parts of the specimen. Steel parts of the test setup were modelled by shell or beam elements. For the numerous reinforcement bars truss elements were used to reduce the overall amount of degrees of freedom. Rigid, thus non-deformable elements, were used for e.g. the ground on which the transversally loaded specimen was sliding on.

Table 2-14 Default element types for different geometrical parts of the numerical models

Structure type	Element type	Example
Solid parts	linear solid elements with reduced integration (C3D8R)	Concrete cross beam, steel girder
Solid parts with curvatures	quadratic solid elements with reduced integration (C3D20R)	Pretension bolts inside concrete cross beam
Shell like parts	linear shell elements with reduced integration (S4R)	Beams in setup
Beams	linear beam elements (B31)	Bars in setup
Trusses	linear truss elements (T3D2)	Reinforcement
Rigid surfaces	rigid shells (R3D4)	Contact plates

2.3.3.2 Validation of 3D nonlinear FE models of tested I-girder subassemblies; verification of scale effects (Task 3.2)

Transversally loaded subassemblies

Fig. 2-63 shows the full numerical model of the transversally loaded test specimen including the relevant parts of the test setup. As explained in detail in Deliverable 3.1 (2016) the test setup flexibility had a strong influence on the measured responses. The reason is that the tested specimen was extremely stiff in the tested direction, and thus although the deflection and slip effects of the setup were small, the relative contribution was very important. Detailed measurements of the test setup deflections have been conducted during the last test SQ3C, the cyclic test for the DOMI-2 joint typology. With these additional measurements it was possible to quantify the contribution of the test setup to the overall response. In general two strategies could be followed to compare the test results with simulation results: either exclude the test setup contributions by post-processing the test results or include the test setup flexibility in the numerical model by including for example additional springs.

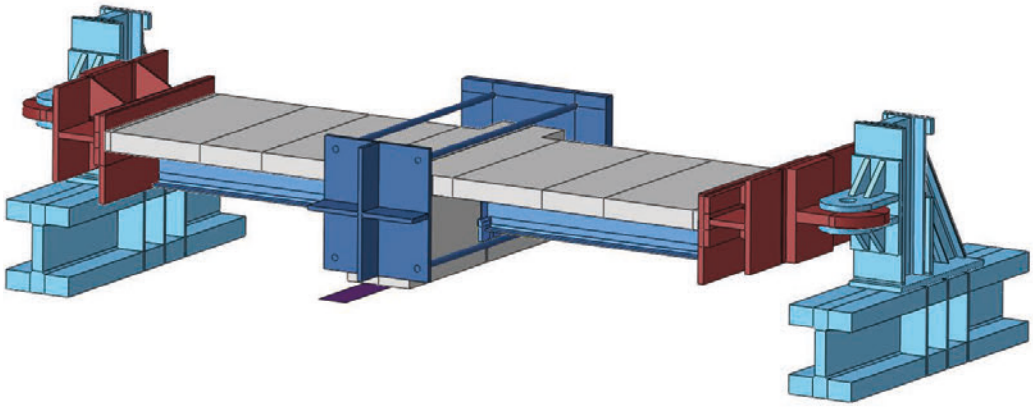

Fig. 2-63 Isometric view of full subassembly including specimen and almost full test setup.

Fig. 2-64 shows the same model as Fig. 2-63 from different views along with a labelling of different parts. The concrete part (coloured in grey) consists of the concrete slab and the concrete cross beam. The general steel specimen part consists of the steel girder and the connection detail inside the concrete cross beam shown in Fig. 2-62 for the three different joint typologies. All other

parts of the model belong to the test setup, which did not necessarily need to be modelled explicitly and some parts were excluded and replaced by spring in later models. It is worth mentioning that the longitudinal flexibility (perpendicular direction of load introduction) of the setup construction (see Fig. 2-64) had an important influence on the post-elastic load displacement curve and had to be taken into account.

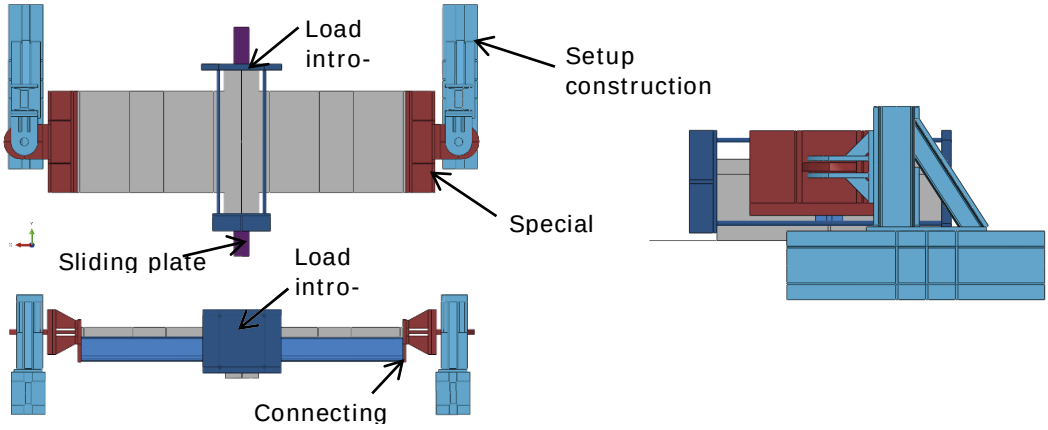

Fig. 2-64 Top, front and side view of test subassembly including test setup. Labelling of different parts.

Loading

The transversal loading was applied on the load introduction plate by enforcing a displacement. Reaction forces could be evaluated at the load introduction point or as sum of the reaction forces introduced into the ground left and right. A contact interaction was introduced between load introduction plate and concrete cross beam. By this approach, during cyclic simulations, the load introduction plates were just allowed to push the specimen, and not to pull it. The additional load on the top of the slab introduced in reality by steel plates acting as additional gravity loads at a real bridge were modelled by equivalent vertical pressure forces.

Boundary conditions

Concrete and steel surfaces were ideally tied together, thus, a full bond was assumed, according to the tests observations, where no noteworthy slip occurred. The test setup left and right was fixed to the ground at its bottom surface. The load introduction plate and concrete cross beam interface was modelled by contact interaction – hard contact in perpendicular direction of the tow surfaces and friction with a coefficient of 0.3 in tangential direction. The connection of the special beam and the test setup construction was idealized as hinged connection, as was the load pin cell in reality. Between the concrete slab and the connecting plate also a contact interaction was applied, in order not to exert tension on the concrete surface. The reinforcement bars inside the concrete slab in contrary were ideally tied to the connecting plate.

Longitudinally loaded subassemblies

In order to obtain also the displacements and behaviour of the test setup, a very detailed model was set up. In such a way all displacements measured during the tests could be directly compared to that one obtained in the simulation. The specimen consists of the concrete pier, slab and cross beam and of the structural steel parts, i.e. girders and steel plates forming the connection detail. The DOMI-2 subassembly with pre-tensioned bolts is shown in Fig. 2-65. A detail of the typology along with the applied mesh is shown in Fig. 2-66. The pier foot was placed inside the steel shoe, which was able to rotate freely. Four tension bars are hinged to the ground and connected to the two transverse beams, which were tied to the concrete slab. A contact definition between transverse beam and concrete slab showed no different results than the more simple tying technique. Due to the beam assembly the desired moment was introduced into the specimen left and right. Circular hollow sections transmit approximately half of the force to the other side of the specimen. Ideal hinges are modelled at all spots where hinges exist in reality. The corresponding deformation shape showing the correct modelling of hinges is shown in Fig. 2-67.

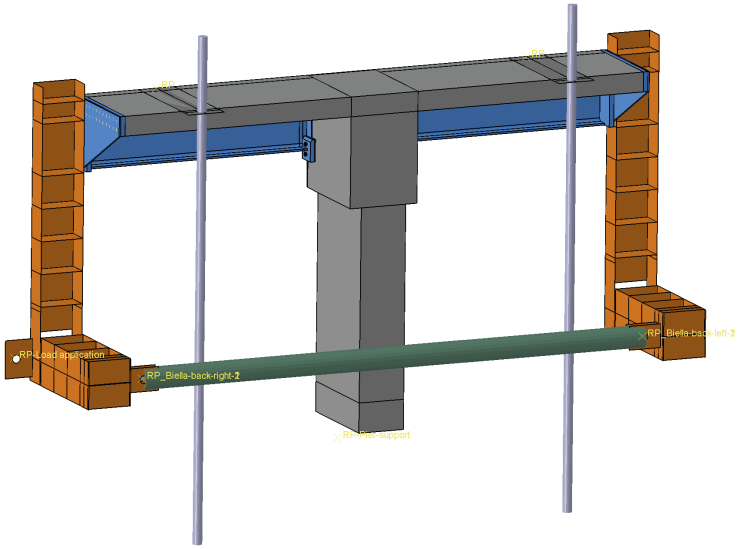

Fig. 2-65 Complex model of longitudinally tested specimen and setup

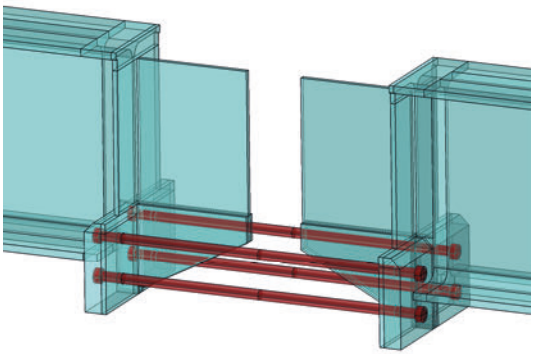

Fig. 2-66 DOMI-2 joint typology with pre-tensioned steel bars

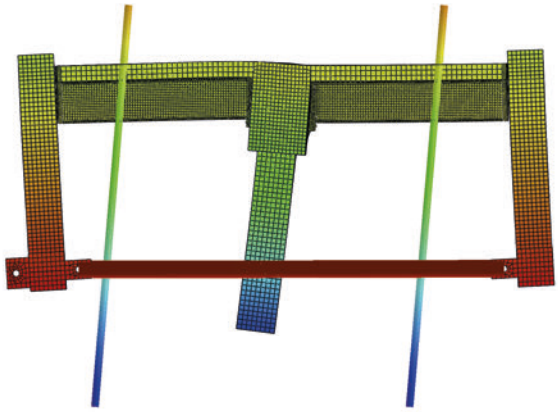

Fig. 2-67 Deformation shape of specimen and test setup (deformation scale factor of 3)

2.3.3.3 Damage analysis of I-girders of Case Studies (Task 3.3)

Transversally loaded subassemblies

Parametric analyses for studying the influence and sensitivity of various parameters may be found in Deliverable 3.1 (2016). In this section just the final calibrated model will be presented which simulates the behaviour of the test in very good agreement to the test observations. During the calibration of the model the material parameters listed below in Table 2-15 were found to be the most reasonable. The concrete strength characteristics have also been based on the concrete cube tests conducted during the project. A Sargin parameter D of 0.6 has been chosen to account for the higher ductility due to the confined conditions of the concrete.

The global displacement-load curve is shown in Fig. 2-68. Due to the fact that the joint typology had no effect on the test results, because it was merely stressed during the tests, just one connection typology is shown. The different test cases in the graph differ in the fact whether flexibility and slip effects have been taken into account or not. Starting with case a) which is the virgin displacement data obtained at the load actuator to case d), where all known flexibility contributions have been eliminated by post processing of the data. The full information (case c) and d)) has been gathered only for the last test, which was not run until failure due to the additional vertical load tests foreseen for the last specimen. As can be seen, initial stiffness, post cracking behaviour as well as peak load are captured very well by the numerical model.

Table 2-15 Material parameters used for the simulations

Concrete			Structural steel		
Young's modulus	[N/mm²]	32 000	Young's modulus	[N/mm²]	210 000
f_{cm}	[N/mm²]	63.0	v	[-]	0.3
f_{ctm}	[N/mm²]	4.3	Element type	[-]	C3D8R
G_f	[N/m]	155			
b_c	[-]	0.8	**Reinforcing Steel**		
k	[-]	1.37	Young's modulus	[N/mm²]	200 000
Sargin parameter D	[-]	0.6	v	[-]	0.3
v	[-]	0.2	Element type	[-]	T3D2
Element type	[-]	C3D20R			
Average element size	[mm]	40			

Fig. 2-69 shows the load-displacement curve in perpendicular direction to the load introduction. The asymmetric behaviour of forces which occurred during the tests could of course not been modelled with a prefect numerical model. This is why an additional load of approximately 37 kN was applied gradually to the specimen. This simulates a skewing of the load actuator, which seems to be the main reason for the observed unsymmetrical forces measured during the tests. Because of the flexibility and slip effects of the test setup, which play an important role on the level of longitudinal forces developed during the load application, the stiffness has been calibrated. The displacement of the flexible test setup has been in very good accordance with that one additionally measured in the last test. With these adjustments, the load displacement curve is very similar to the tests and also the unsymmetrical damage pattern could be captured very well.

The patterns of damage evolution in compression are sketched in Fig. 2-70 for several displacement values. 28 mm is the displacement where the peak load has been reached. The concrete crushes at the highest stressed region – the corner where the concrete slab and cross beam connect to each other. The final concrete crushing at this corner is the initiator of the sudden drop in the load displacement curve. In Fig. 2-71 it can be seen that also in the test the same failure modes were observed. Thus, the numerical model captures the real behaviour of the test both quantitatively and qualitatively.

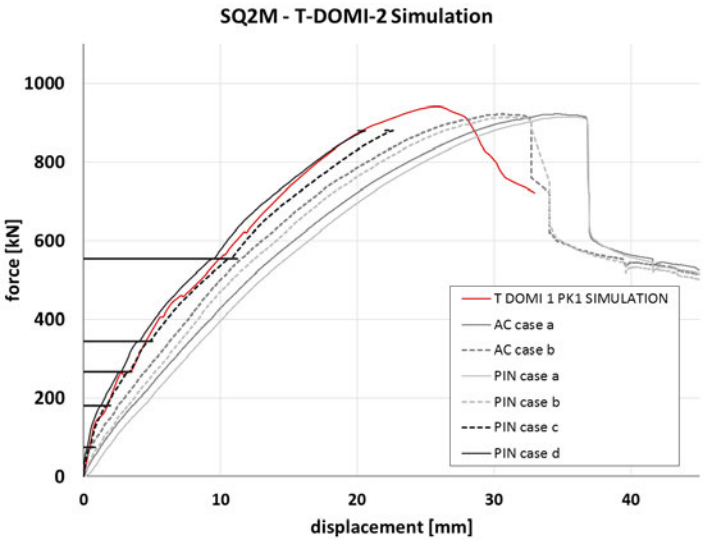

Fig. 2-68 Load-displacement curve in transversal direction using final parameter combination (red: simulation, black/grey: evaluation of test results)

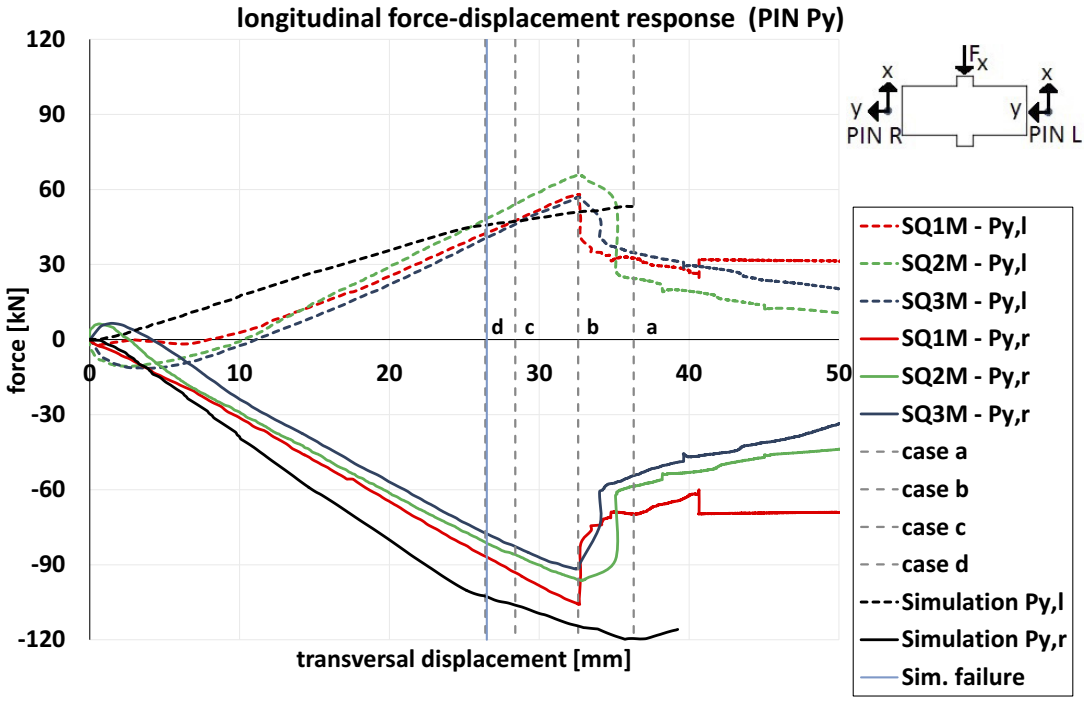

Fig. 2-69 Longitudinal load-displacement curve with final parameter combination

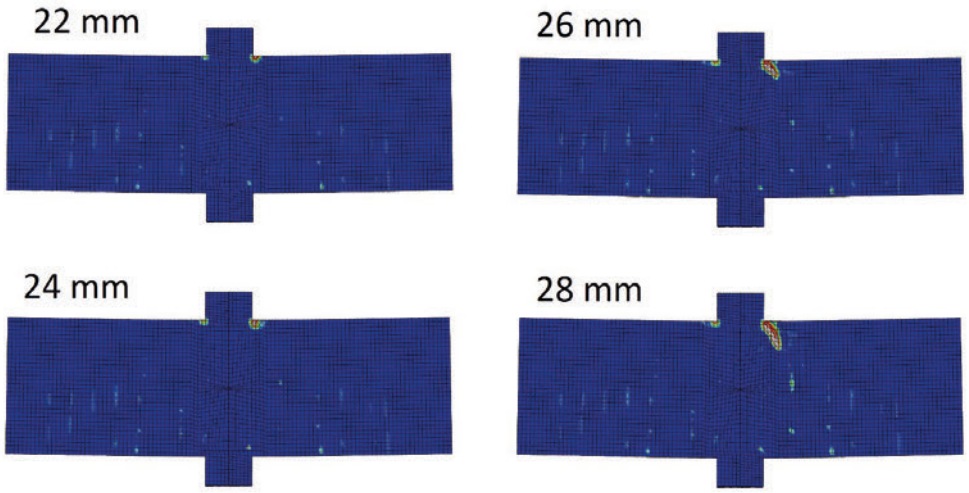

Fig. 2-70 Development of concrete crushing during the simulation at different specimen displacements

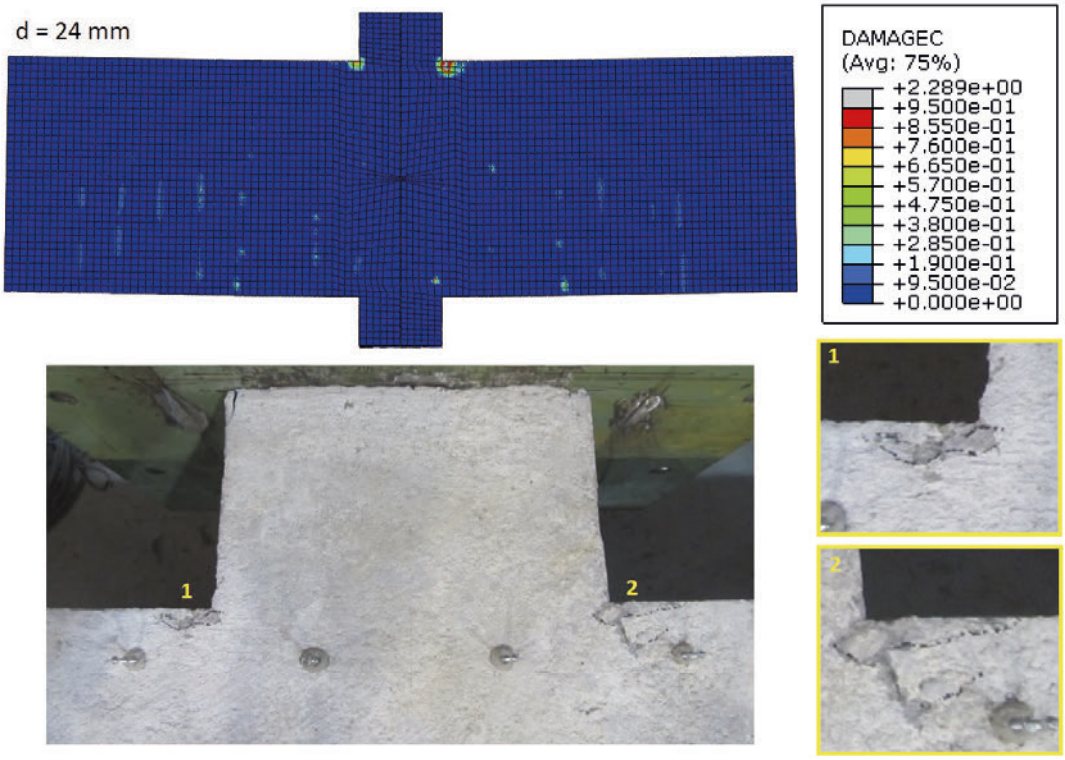

Fig. 2-71 Simulated damage pattern compared to visible damage during the test at a corresponding displacement of 24 mm (test pictures courtesy of UNITN)

Damage evolution in tension for the concrete slab is shown in Fig. 2-72. First cracks appear at the transition of concrete slab and concrete cross beam. With higher displacements more and more cracks develop towards the supported ends of the bridge deck, yielding a balanced cracking pattern at failure of the specimen. Cracks in tension develop much earlier before the peak load and do not cause a sudden decline in load capacity. Chronological development of cracks as well as the final crack pattern resemble the observations made during the tests. A comparison between real and simulated crack pattern at peak load can be seen in Fig. 2-73.

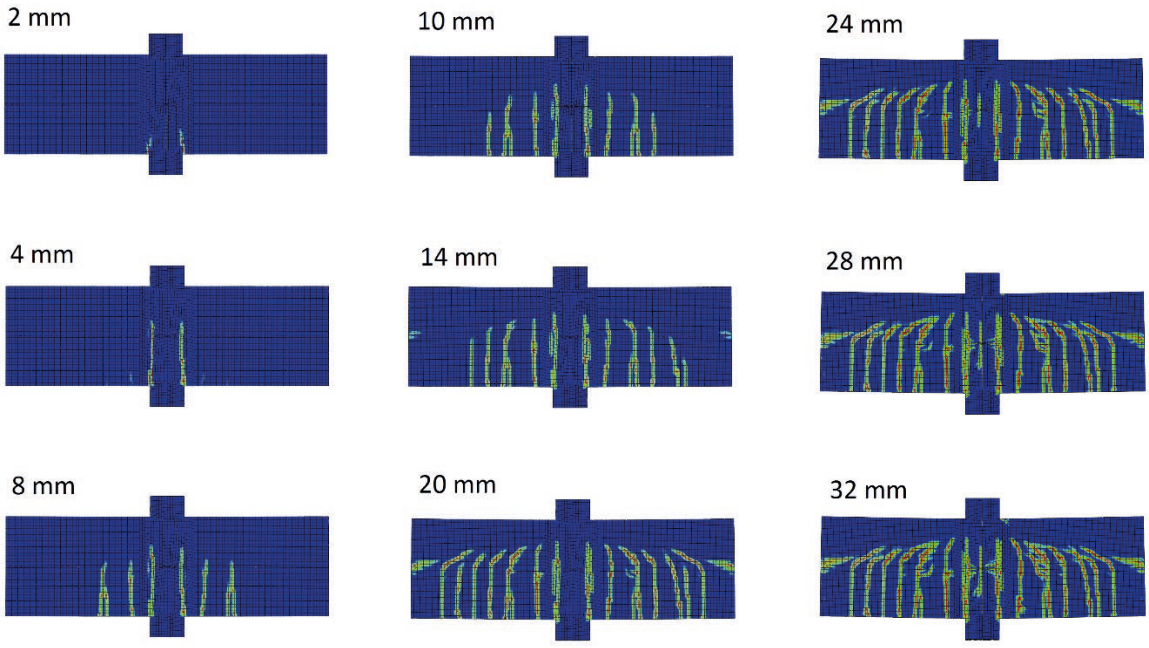

Fig. 2-72 Development of concrete cracks during the simulation

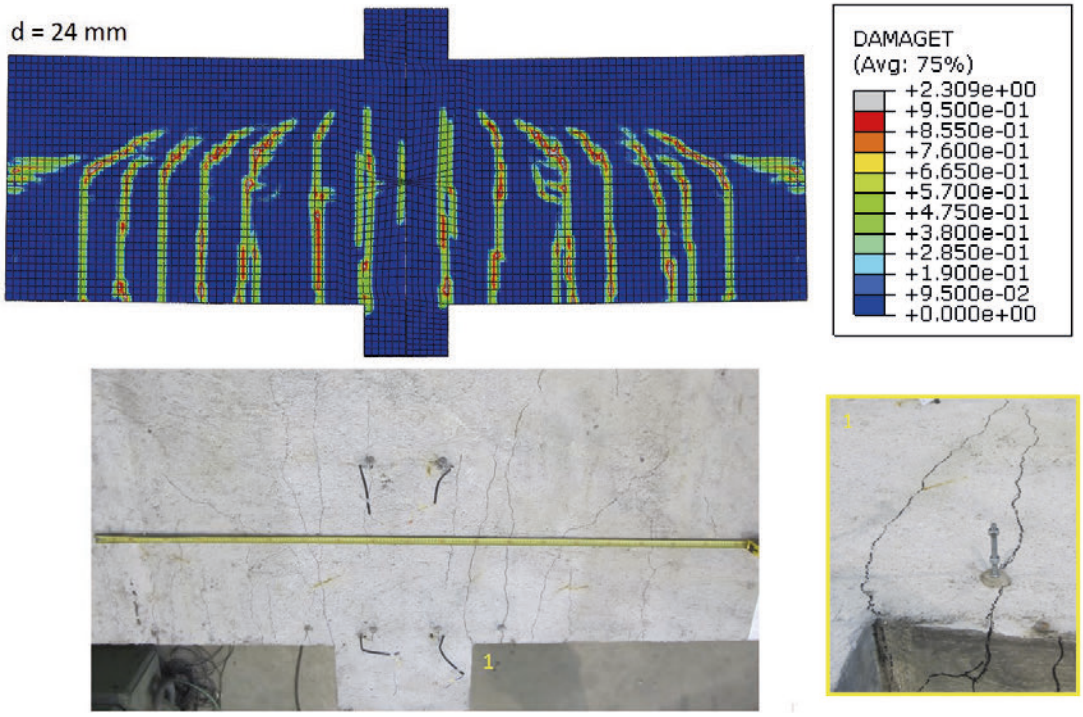

Fig. 2-73 Comparison between simulated and observed cracking patterns (test pictures courtesy of UNITN)

Yielding of the reinforcement took place at the longitudinal bars of the concrete slab reinforcement as can be seen in Fig. 2-74 (yielding bars are coloured red). Inside the concrete cross beam no significant yielding phenomena could be observed. This is in accordance with the strain measurements, which have been conducted during the tests at some of the reinforcement bars. Yielding of the structural steel – girders as well as connection detail plates within the concrete cross beam – did not occur except at some singular points. Also during the test no structural steel yielding was observed.

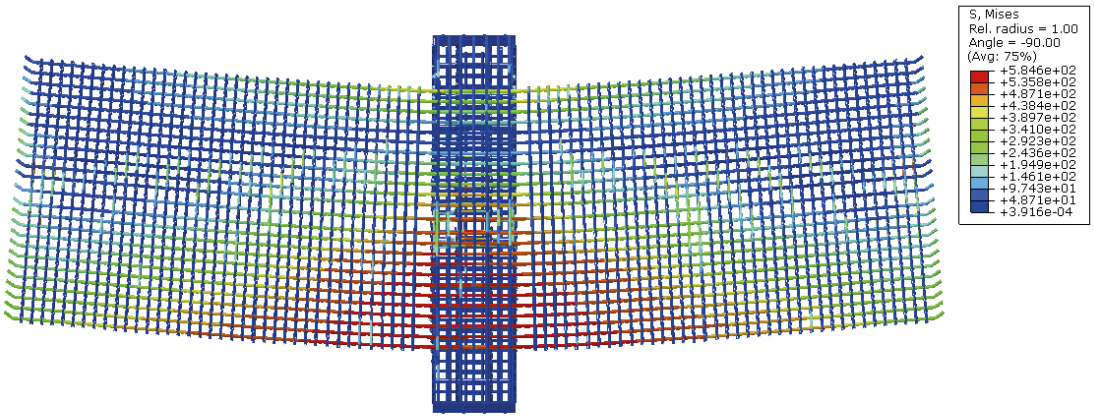

Fig. 2-74 Yielding of reinforcement bars (red) at peak load of the simulation.

Cyclic simulations

Parametric studies on the cyclic response have been conducted. For the cyclic loadings, the load displacement time histories measured during the tests have been applied on the model. Due to the modelling approach just pushing was used to move the specimen from both sides, since the contact interaction did not allow for any tension forces to be transmitted. The most influencing parameter was found to be the stiffness recovery factor. If it was chosen to high, the developing load was increasing

from cycle to cycle and was finally far too high. A very small stiffness recovery factor showed to generate the most reasonable response. The corresponding hysteresis loop compared to the SQ3C cyclic test (DOMI-2 joint typology) is shown in Fig. 2-75. In general, the tested response can be captured quite well. As in the monotonic simulations the damage patterns match very well with the test observations. The simulation runtime was 6 days on a 12-core / 64GB RAM machine, what prohibited comprehensive parametric studies. Moreover, often no convergence lead to premature abortion of the simulations.

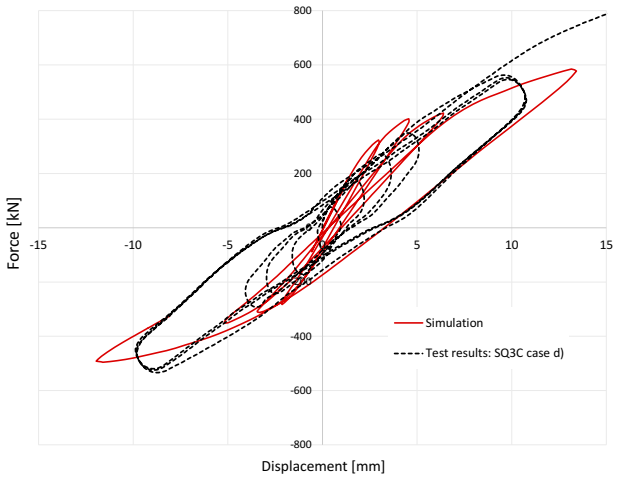

Fig. 2-75 Comparison of cyclic load displacement curve for SQ3C test (case d) with response obtained by calibrated model

Longitudinally loaded subassemblies

In general the same material parameters have been used for the longitudinal loaded subassembly model, as shown in Table 2-15. Just the mean concrete strength has been slightly increased, in order to account for the longer hardening time of the concrete since the longitudinally tested specimens were tested much later after concreting than the transversally loaded ones. Fig. 2-76 shows the current numerical model force displacement behaviour compared to the test results. As can be seen the force level at failure is captured very well whereby the stiffness of the numerical model is too high. Parametric studies have been conducted, whereby all investigated parameters showed no significant influence on the stiffness. Further investigations are needed to assess on the divergent force displacement behaviour until peak load.

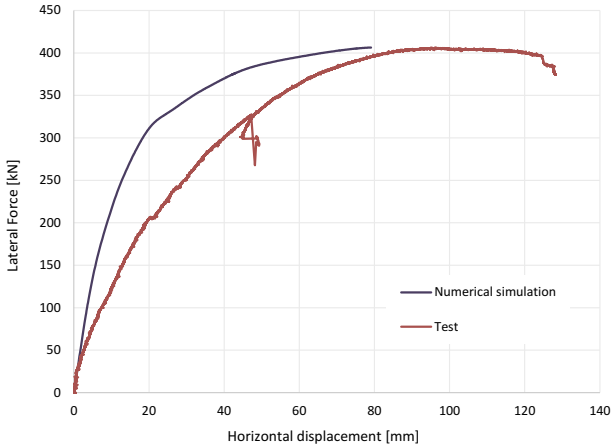

Fig. 2-76 Comparison between best-fit numerical model and test result

Although the load displacement curve of the numerical model does not fit perfectly that one of the test for lower displacements, the observed damage patterns equal the observed ones, as will be shown in the following. Evolution of the cracking of the concrete is illustrated in Fig. 2-79. As observed during the tests, cracking starts in the slab at the transition to the concrete cross beam followed by cracks forming in the pier. With higher loads the cracking pattern broaden more and more. At higher displacements of about 30 mm, also inside the concrete cross beam damage in tension occurs, resulting in severe damage at peak load. Evolution of concrete crushing is shown in Fig. 2-77. As can be seen, the most severe damage occurs inside the concrete cross beam, due to interaction with the steel plates inside the concrete cross beam, what could be also observed during the tests.

45 mm displacement – 57% of peak load

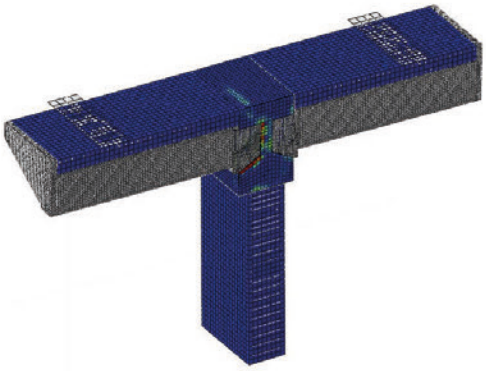

80 mm displacement – at peak load

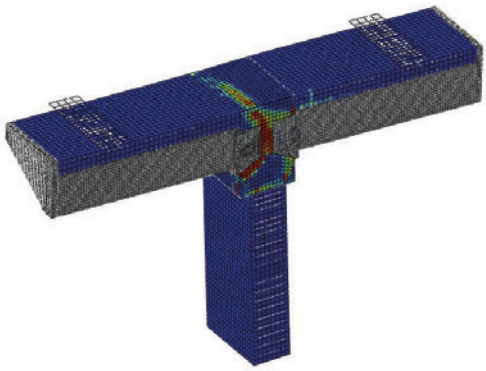

Fig. 2-77 Evolution of damage in compression (concrete crushing)

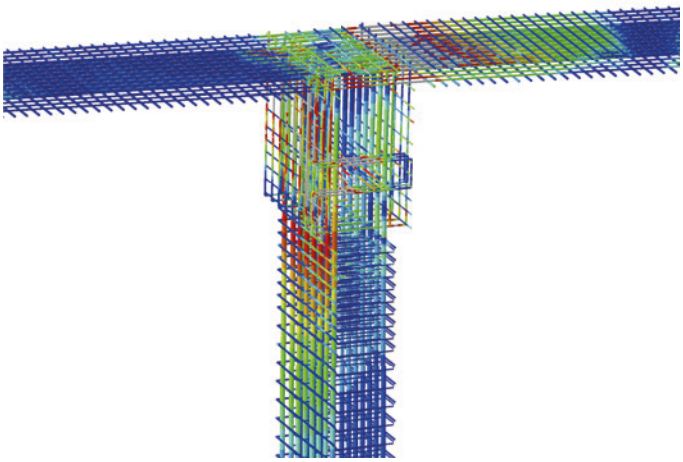

Fig. 2-78 Stresses in reinforcement at peak load

Demands on the reinforcement are illustrated in Fig. 2-78 for the deformation shape at peak load. Bars colored in grey indicate yielding. The most stressed regions coincide with the cracking patterns shown in Fig. 2-79. Firstly, the hoops inside the concrete cross beams start to yield at 30 mm displacement, followed by the transversal (38 mm) and vertical (50 mm) reinforcement bars inside the concrete cross beam. The longitudinal reinforcement bars inside the slab start to yield at a displacement of 45 mm.

8 mm displacement - 9% of peak load

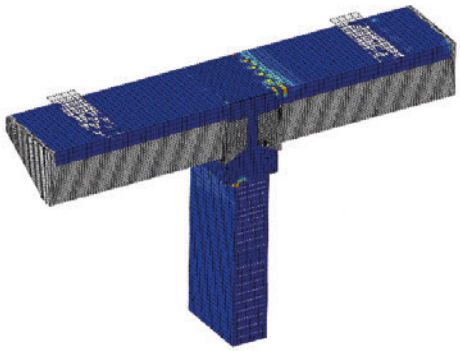

15 mm displacement – 19% of peak load

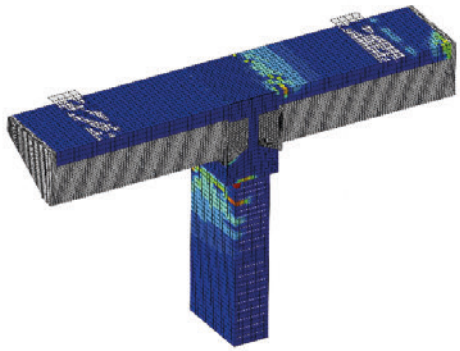

23 mm displacement – 28% of peak load

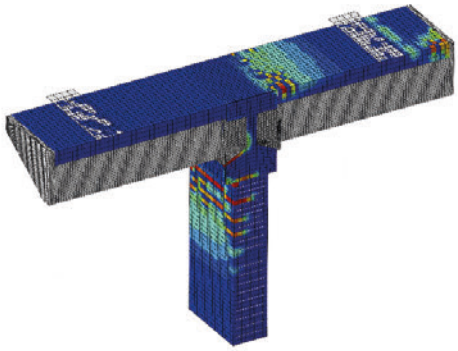

30 mm displacement – 38% of peak load

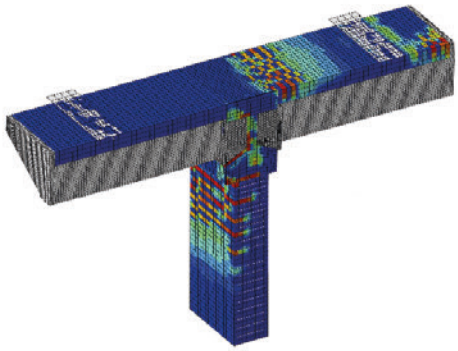

38 mm displacement – 47% of peak load

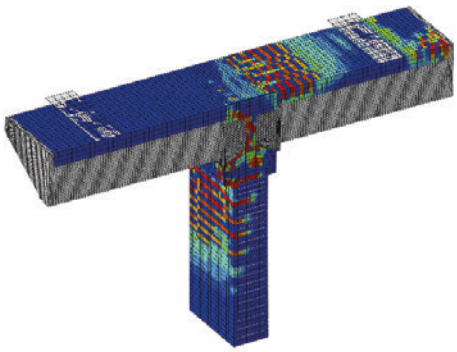

45 mm displacement – 57% of peak load

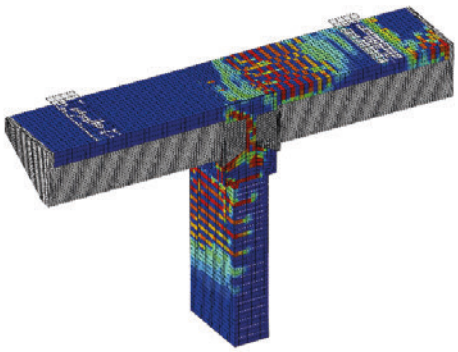

60 mm displacement – 75% of peak load

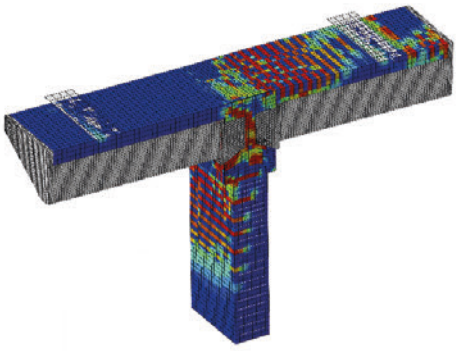

80 mm displacement – at peak load

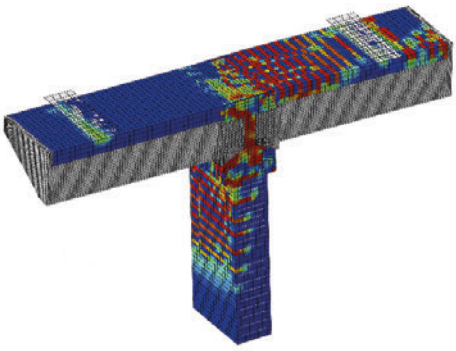

Fig. 2-79 Evolution of damage in tension (cracking patterns)

The buckling phenomenon on the lower steel flange at the side of the load introduction which was observed during the tests could also be reproduced in the numerical simulation, as is shown in Fig. 2-80.

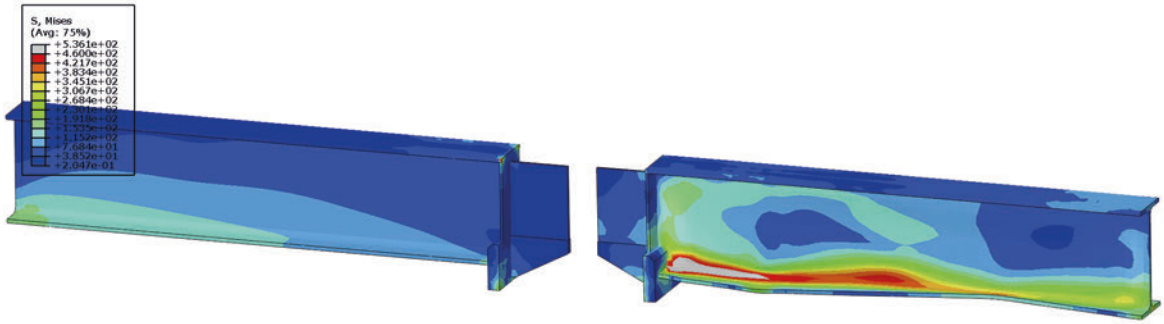

Fig. 2-80 Severe local buckling of lower flange; grey areas indicate yielded steel; unscaled deformation shape.

In summary, fine tuning of the longitudinal specimen simulations has still to be done. Especially the joint interaction has to be deeper investigated, also under cyclic loading, which is a difficult task due to several convergence problems occurring during the simulations. However, the force level, failure mode and damage patterns could be well reproduced in the numerical simulations.

2.3.4 *Work Package 4: Application of the PBEE methodology to selected case studies*

In this WP, the probabilistic analysis of the case studies selected in task 1.1 and subject to seismic loading has been carried out by means of the PBEE methodology, sketched in Fig. 2-81 and analytically summarized in Fig. 2-82 (Porter 2003). This WP is of paramount importance for the project because it realize the fourth element of the PEER methodology, namely the Loss or Cost-effective risk analysis. As a result, the probability of economic losses has been evaluated. For this purpose, the repair cost ratio (RCR) has been selected as Decision Variables (DV), which represents a meaningful factor for various bridge stakeholders, in view of deciding whether a bridge design is acceptable or not.

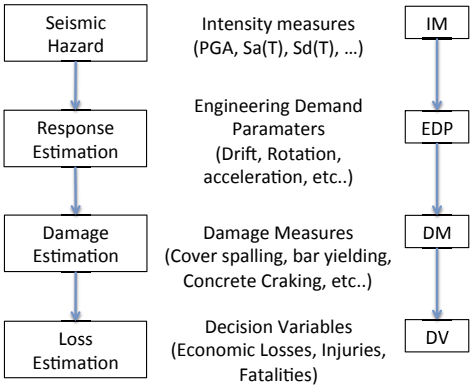

Fig. 2-81 Components of a probabilistic performance-based methodology

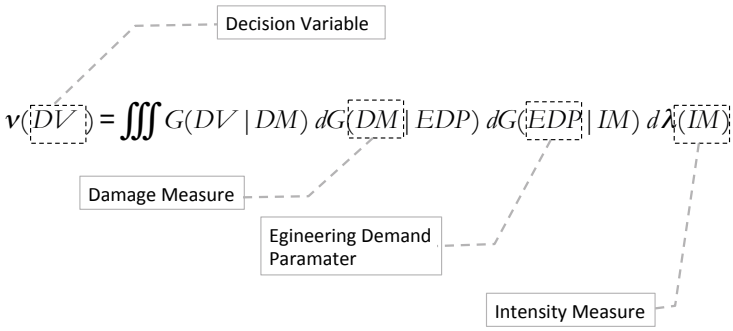

Fig. 2-82 The Pacific Earthquake Engineering Research Center (PEER) Framework integral

The full development of this activity has been carried out in the third year of the project. To show the potentiality of the PBEE method, it has been fully applied to assess the vulnerability of one of the case studies defined in WP1 (CS 2.1.2), already designed according to Eurocodes. In fact, the availability of the comprehensive set of experimental and numerical results gather in WP2 and WP3 made the selected case study the most suitable one to fully show the potentiality of the method. The Performance Based Earthquake Engineering (PBEE) is composed by four distinct steps, and it is illustrated in Fig. 2-83.

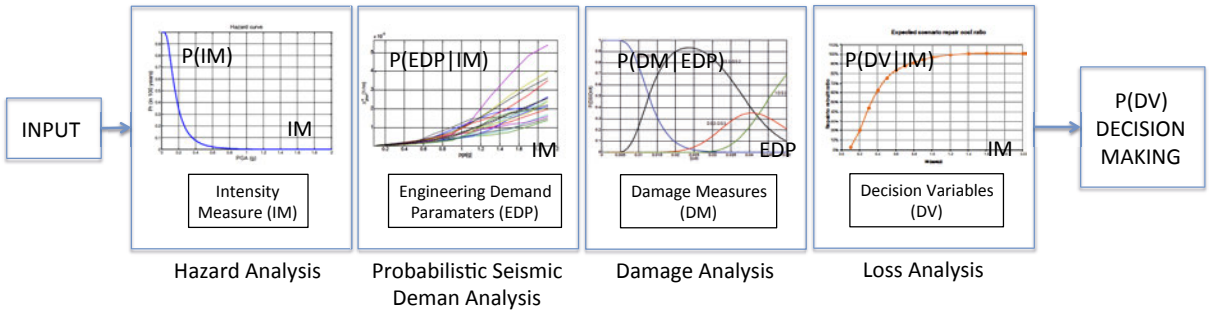

Fig. 2-83 PBEE framework for the seismic assessment of structures

Hazard Analysis: The rate (or probability) of exceeding various ground-motion levels at a site is evaluated. The main variable of this phase is the intensity measure, (IM), that for the further analyses it has been identified with Peak Ground Acceleration (PGA), even though a wide literature investigated other possibilities (Evangelos et al. 2010).

Structural Analysis: The effect (demand) of site-specific ground motions with a given intensity (IM) on a structure is evaluated in terms of engineering demand parameters (EDPs). This is determined using a mathematical model of a structure and an appropriate structural analysis method. The probability of exceedance of an Engineering Demand Parameter, P(EDP|IM) given an IM is derived

using the response data for each of the ground motions relative to the selected site-specific suite. This aspect has been treated in Deliverable D4.1 (2014) and D4.2 (2014).

Damage Analysis: The damage analysis intends to provide a model describing the probable damage state of a structure in terms of damage measures (DMs), given a level of engineering demand parameters (EDPs), by using a mathematical relation between EDPs and DMs. DMs are usually discrete rather than continuous quantities, defined as observations of the onset of certain damage states. The most common source of data comes from experimental tests of structural components, subassemblies, or systems where observed damage and measured capacity of the specimens are correlated to the level of applied demand. In this context, damage models are often termed capacity models. This step has been fully discussed in Deliverable D4.3 (2015). The results of experimental tests, described in Deliverables D2.2 (2014), D2.3 (2015) and D2.4 (2015) permitted to better define the relation between the several DMs and EDPs.

Loss (Cost-Effective Risk) Analysis: Cost-effective risk evaluation is the very last step of the global integrated probabilistic performance-based evaluation procedure. The result of this phase is a decision model, which based on Decision Variables (DV) pertaining to the use of a structure given a level of sustained damage. Decision models are mathematical relations between damage measures (DMs) and decision variables (DVs). Commonly used DV describe losses in terms of money (repair cost), interruption in service (downtime or repair time), or loss of life: thus, decision models are also called loss models. The decision model may have several parts—those that relate DMs to repair quantities (Q) and those that relate Q back to repair cost or repair time. A completely different set of decision variables focuses on the remaining capacity of the structure to function as intended. For example, the return of a highway bridge to differing degrees of functionality in a highway network is also an important loss criterion. Functionality may be measured in terms of lateral load resistance in aftershocks, traffic volume, lane and speed reductions, or access for emergency vehicles. As explained in the following chapters in SEQBRI project the main DV adopted in this context is the repair/construction cost ratio (Direct cost). This choice comes from the goal to provide an immediate economic measure of earthquake performance of the structure. Indirect costs like downtimes, even if mentioned, are not explicitly considered in the analysis. All the steps of this phase have been systematically reported in Deliverable D4.3 (2015) and in the second annual report (2015).

2.3.4.1 Hazard Analysis (task 4.1)

In order to evaluate the probability of exceeding a damage threshold in a given time interval a probabilistic seismic hazard analysis is usually adopted. The seismic hazard gives the probability that a selected scalar measure of the seismic intensity IM, (usually the peak ground acceleration PGA or the spectral acceleration at the natural period of the structure $S_a(T)$), exceeds a given value in a given a time interval.

The classical PSHA method used for the evaluation of the seismic hazard curve H(IM) has been proposed by Cornell (Cornell 1968). It consists of 5 steps (Deliverable D4.1, 2014):

1. Identify all earthquake sources capable of producing damaging ground motions;
2. Characterize the distribution of earthquake magnitudes;
3. Characterize the distribution of source-to-site distances associated with potential earthquakes;
4. Predict the resulting distribution of ground motion intensity as a function of earthquake magnitude, distance, etc., (attenuation Law);
5. Combine uncertainties in earthquake size, location and ground motion intensity, using the total probability theorem;

They have been discussed and summarized in the mid-term report (SEQBRI 2013). Because earthquake-shaking hazards are dependent on site location with respect to causative faults and sources and regional and site-specific geologic characteristics, the above-mentioned steps have to be referred to a specific site, identifying:

- Location
- Local Soil Effects (Shear wave velocity)
- An appropriate attenuation relationship

Concerning the local soil effect, the first 30 m of soil are usually enough to identify the shear wave velocity based on which the soil amplification factor can be determined.

As attenuation laws, it should be better to use next-generation relationships like the one proposed by Atktinson and Boore (2006), Campbell and Bozorgnia (2007) and Chiou and Youngs (2008). At this purpose useful tools like the Open Seismic Hazard Analysis website (http:/www.opensha.org/) could be used. These relationships provide the probabilistic distribution of the Intensity Measure (IM) for a given distance R and thus the distribution of ε.

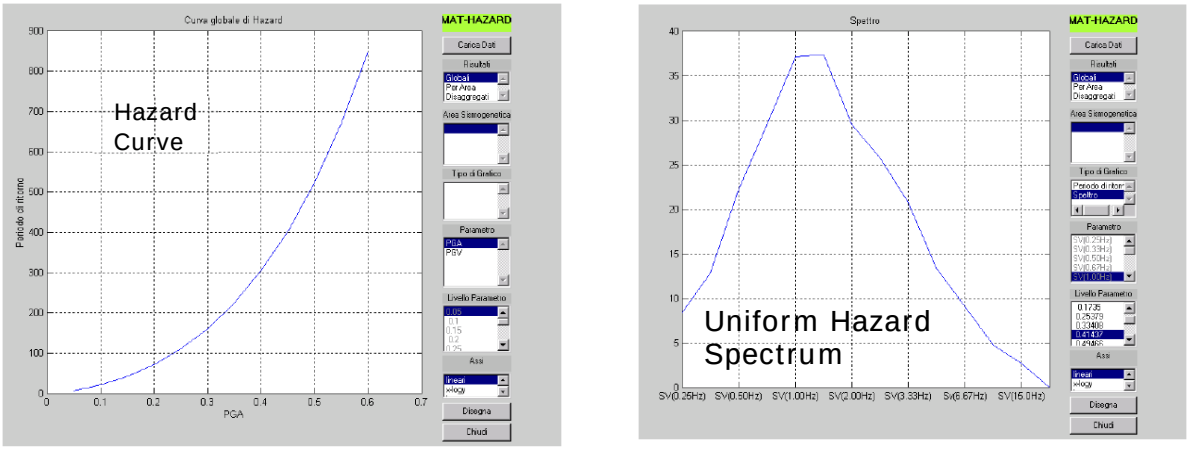

Fig. 2-84 Mathazard - Output Environment after (Giannini 2015)

Another goal of PSHA is to identify a response spectrum to be used for structural or geotechnical analysis. One approach for developing a spectrum is to compute a uniform hazard spectrum (UHS). This spectrum is determined by performing the above PSHA calculations for spectral accelerations at a range of periods. Then, a target rate of exceedance is chosen, and for each period the spectral acceleration amplitude, S_a, corresponding to that rate is identified. This spectrum can be used to select input signals for the fragility analysis, even though code spectra are used at this purpose as for SEQBRI bridges (Deliverable D4.1). Typical outputs of PSHA analysis are depicted in Fig. 2-84, where for a given zone, hazard curve and Uniform Hazard Spectrum are reported (Giannini 2015).

For the scope of SEQBRI a high seismicity zone has been selected that is located in Priolo Gargallo (Italy), whose seismic hazard maps for a return period of 475 years in 50 years is shown in Fig. 2-85. The maximum PGA in the selected zone is in the range 0.225-0.25g for soil A. For the evaluation of the hazard curve (Fig. 2-87) and the corresponding uniform hazard spectra the Mathazard program developed by UNIRM3 (Giannini 2015) has been employed. Specifically, the uniform hazard spectrum corresponding to a probability of exceeding of 10% in 50 years has been built (Fig. 2-86). The normalized form of this spectrum fits well the response spectrum of EC8 type 1. Therefore, the selection of natural records carried out in task 1.3 appears reasonable and represents well the frequency content of the structural response.

To represent the damage potentiality of the seismic action, the PGA has been often used as intensity measure (IM). However, many works dedicated to the efficiency of this IM demonstrated the weakness of this choice. Therefore, a different IM has been specifically defined for SEQBRI. In particular, it is defined as the acceleration at zero period of the target response spectrum scaled at a specific PGA value. Consequently, the selected accelerograms are affected by the same scaling factor. This scaling procedure has been adopted in task 4.3 for the probabilistic seismic demand analysis of the SEQBRI bridges. More details can be found in the Mid Term Report (2013) and Deliverable D4.1 (2014).

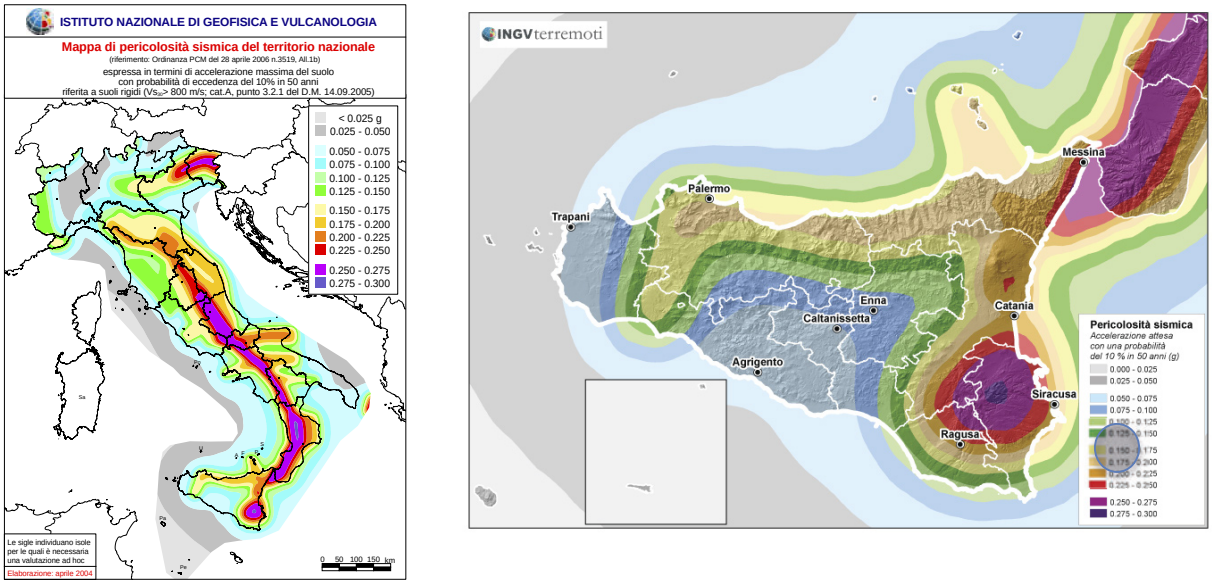

Fig. 2-85 Seismic Hazard maps: a) Italian territory, b) Sicily

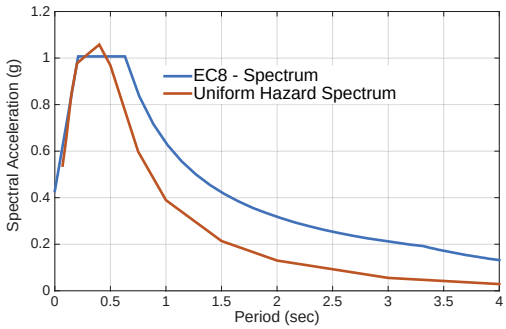

Fig. 2-86 Response Spectra of Priolo Gargallo (Siracusa, Sicily, Italy)

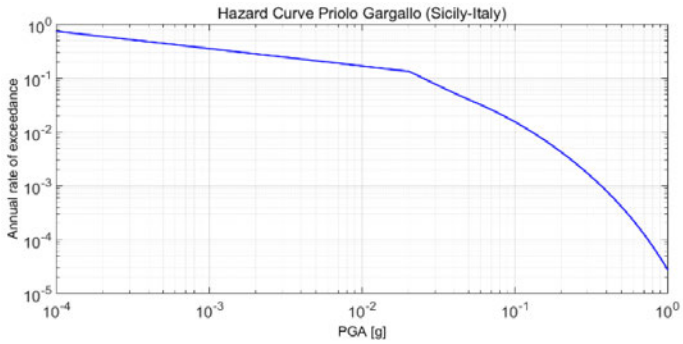

Fig. 2-87 Hazard curve of Priolo Gargallo (Siracusa, Sicily, Italy)

2.3.4.2 *Refinement of FE models for Case Studies (Task 4.2)*

This task is dedicated to the refinement of the stick models already defined in WP1 for the simulation of the case studies (Task 1.2). At this purpose the results of WP2 and WP3 has been used. In greater detail, stick models based on uniaxial beam elements with appropriate hysteretic laws have been validated in the OpenSees software, an open source finite element software platform developed by the Pacific Earthquake Engineering Researcher Centre (PEER, http://peer.berkeley.edu). This model employs standard non-linear beam and link elements. In particular, piers, CCB, bearings and composite girders have been modeled by using classical literature models (fiber elements for the piers, CCB and composite girders, linear and non-linear springs for bearings).

Instead, a component-based approach has been proposed for the deck-pier connection of SCC bridges with CCB. In this respect, a similar model has been already proposed and detailed in the past SEQBRI reports. In this task a refined version is defined and integrated in a full 3D stick model of the bridge. This model concerns the three different typologies of CCB illustrated in Fig. 2-88, experimentally tested in WP2 and numerically simulated in WP3 by using ABAQUS. Because the behaviour of the CBB in longitudinal and transversal direction is different, in what follows the two models will be treated separately.

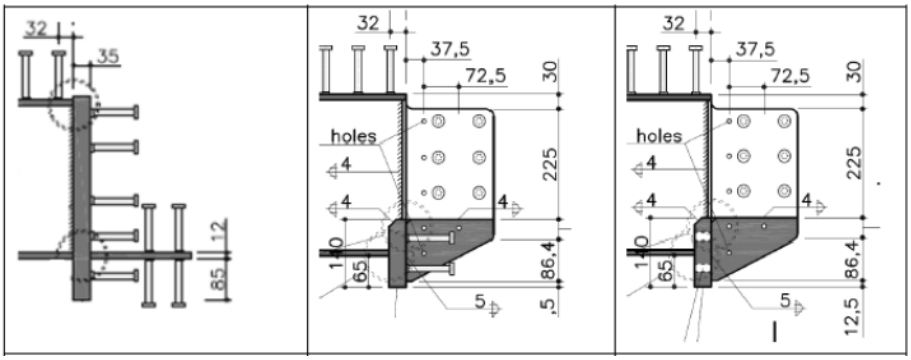

(a) (b) (c)

Fig. 2-88 CCB configurations: a) DIN FB 104 Type C, b) DOMI 1, c) DOMI 2

Component-based model for CCB in longitudinal direction

The components considered for the deck-pier connection in longitudinal direction are different for the three CCB configurations of Fig. 2-88, whose description is provided in Table 2-16. Details and models are illustrated in Fig. 2-89, Fig. 2-90, Fig. 2-91, Fig. 2-92, Fig. 2-93, Fig. 2-94.

Table 2-16 Main elements of the Component-based Mechanical Model in longitudinal direction

	CCB configuration			
Component	**DIN-FB104**	**DOMI1**	**DOMI2**	**Description**
TC1	✔	✔	✔	Shear studs – Vertical (shear)
TC2	✔	✔	-	Shear studs – Longitudinal (axial)
TC3	-	✔	✔	Shear Studs – Longitudinal (shear)
TC4	✔	✔	✔	CCB
TC5	✔	✔	✔	Head steel plate
TC6	-	-	✔	Prestressing bars

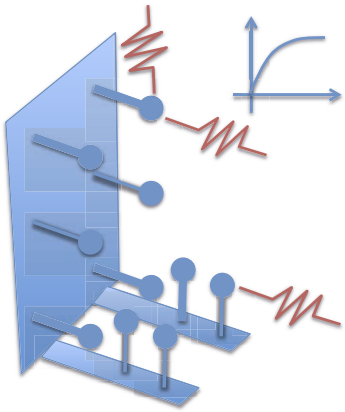

Fig. 2-89 Non-linear spring models for shear studs - DIN FB104 – Var C.

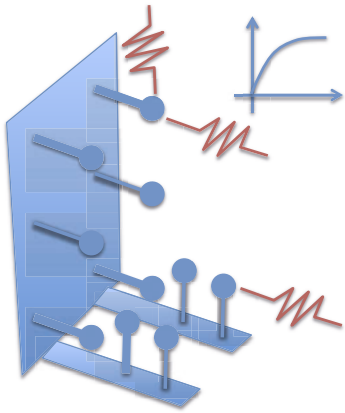

Fig. 2-90 Non-linear spring models for shear studs - DOMI 1 or DOMI2.

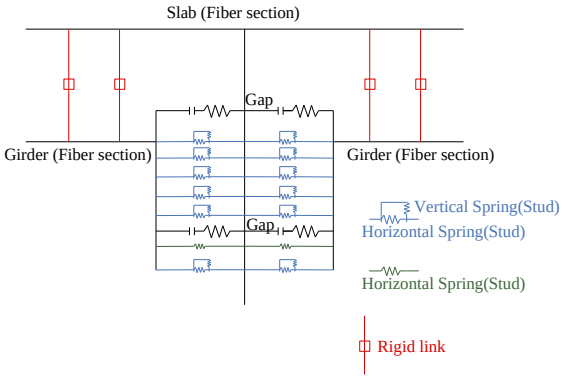

Fig. 2-91 Detail of CCB joint model for DIN FB-104 Type C configuration

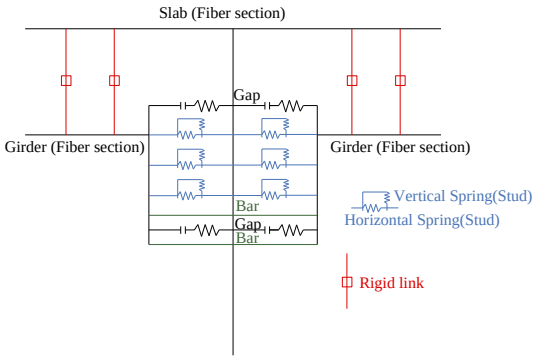

Fig. 2-92 Detail of CCB joint model for DOMI 2 configuration

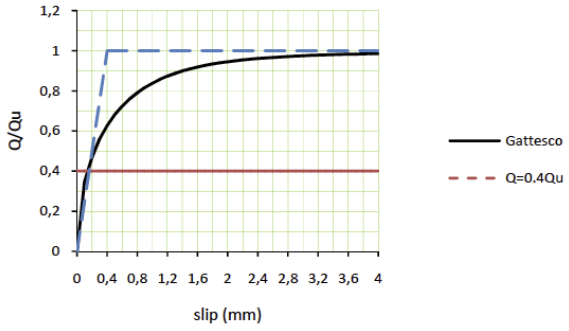

Fig. 2-93 Shear force-slip constitutive law of headed stud

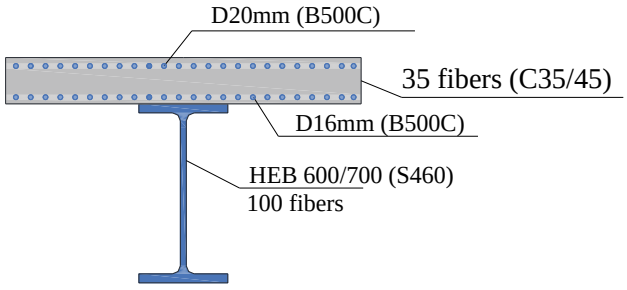

Fig. 2-94 Fiber sections of slab and girder

Components TC1 – Vertical (shear)

This component is present in all CCB configurations. In the DIN-FB104 it represents the shear behaviour in vertical direction of the longitudinal shear studs. In DOMI1 and DOMI2 represents the vertical shear behaviour of the transversal shear studs welded on the insertion of the web into the CCB. They are modeled using nonlinear links with elasto-plastic behaviour. The strength of the single shear stud Q_u, has been calculated according to EN 1994-2, while the related stiffness K_s has been evaluated by mean of the shear load-slip curves (Q-s). The relationship defined in Gattesco et al. (1996) has been used, even though different other recent proposal could be adopted (Viest 1967, Shim et al. 2004, Lee et al. 2005). Based on this shear force-slip constitutive law, the stiffness can be assumed as the slope of the line that crosses the distribution around 0.4Qu (Fig.

2-93); this component is simulated with nonlinear links in the vertical direction connected to the beam elements representing the head plate of steel girders and the CCB. They connect the head plate of the steel girders to the middle of the CCB

Components TC2 – Longitudinal (axial)

This component is present in DIN-FB104 and DOMI 1 configurations. In the DIN-FB104 it represents the axial behaviour in tension of all shear studs and in the DOMI1 the axial behaviour of the longitudinal shear studs welded on the bottom head plate. In the DIN-FB104 configuration the axial strength can be modeled using the procedure proposed in *PCI Design Handbook Precast and Prestressed Concrete* and reported in Deliberable D5.1. For the DIN-FB104 the formula is referred to the single shear stud whereas for the DOMI1 the strength of the group of studs at the bottom of head plate should be considered.

Components TC3 – Longitudinal (Shear)

This component is present in DOMI 1 and DOMI2 configurations. It represents the shear behaviour of the transversal shear studs welded on prolongation of web within the CCB. Their behaviour is similar to the behaviour of the component TC1. Therefore, also in this case stiffness and strength can be evaluated according to relationship defined in Gattesco et al. (1996).

Components TC4 – CCB

In order to reproduce the constraint in compression due to the presence of the CCB, four compression gap elements have been modeled both at left and right sides of the joints at two different levels, as shown in Fig. 2-91 and Fig. 2-92. The compression gaps of the numerical models link the vertical head plates to the axis of CCB beam at mid-support, both in the left and right side of the joint. Gap element is a link element whose axial stiffness is activated only when the absolute value of the negative deformation of its two end-nodes becomes greater than an initial gap. A simplified evaluation of the stiffness can be performed, assuming that the compressive force coming from the girder would act uniformly on a surface equal to the area of the vertical head-plate and considering the deformability of the related portion of CCB.

Components TC5 – Head steel plate

The head steel plates of each steel girder can be modeled using linear or non-linear beam elements. DIN-FB104 configuration employs a thick plate that usually can be considered as rigid. Conversely, in case of DOMI1 and DOMI2 configurations, only the bottom plate is particularly thick and can be considered rigid. The remaining part may be subjected to deformation also in non-linear filed. In this case a beam element with non-linear capability should be used.

Components TC6 – Prestressing bars

This component is present only in DOMI2 configuration. It can be modeled by using a non-linear links. A classical elastoplastic relationship can be employed, which is characterized by stiffness, strength and hardening of the steel bars.

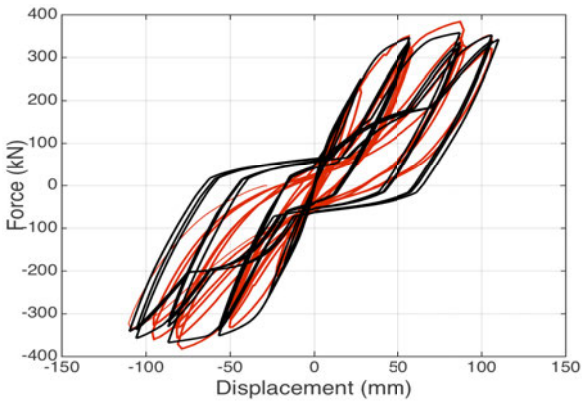

Fig. 2-95– Comparison of the component model (OpenSEES) with the experimental results (DOMI1) – red (experimental), black (numerical)

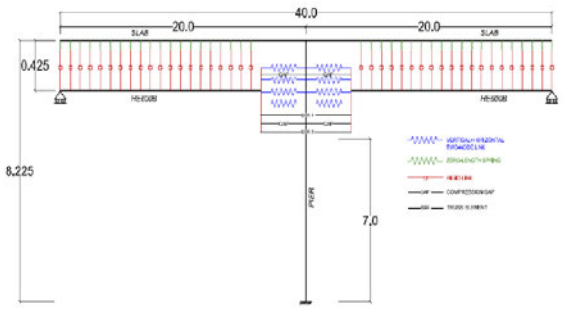

Fig. 2-96 – 2D component-based model of the case study 2.1.2

The above-mentioned components have been tuned based on experimental test. An example is shown in Fig. 2-95 where the experimental cyclic behaviour of DOMI1 specimen is reproduced by using the proposed component model.

This component-based model has been implemented in a 3D stick model of the entire bridge. This represents a refinement of the model used in WP1 and WP2 for the simulation of the cyclic behaviour of the subassembly. In this respect, each 2D component-based model (Fig. 2-96) is assembled as in Fig. 2-97 and Fig. 2-98 where both the cases of wall piers and column piers have been considered.

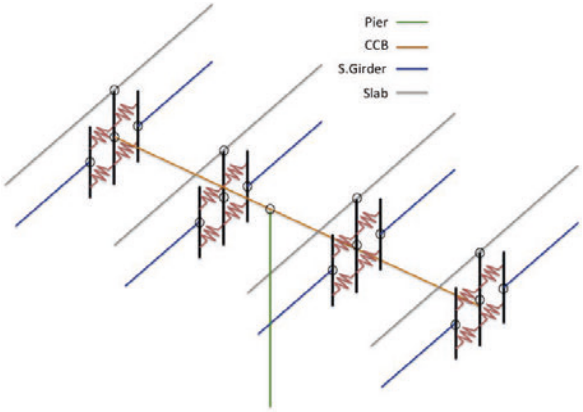

Fig. 2-97 - Wire frame model of the pier-beams-CCB connection for shear wall pier

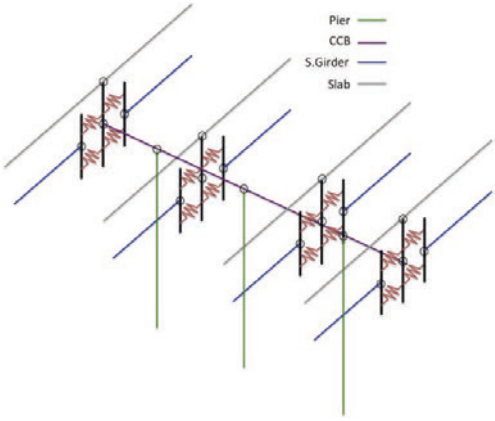

Fig. 2-98 - Wire frame model of the pier-beams-CCB connection for column piers

Component Based model for CCB in Transversal direction

As in the previous case, a component-based model has been proposed for the transversal behaviour. In order to do this, the following set of components has been considered (Table 2-17). The analogy with the components implemented to model the longitudinal behaviour can be easily appreciated.

Table 2-17– Main elements of the Component-based Mechanical Model in transversal direction

Components of the component-based mechanical model of DOMI2 connection		
Component	**Description**	**Direction**
TTC1t	Concrete and rebars top layer - axial response in the slab	X
TTC1b	Concrete and rebars bottom layer - axial response in the slab	X
TTC2	Shear of the concrete slab	Z
TTC3u	Shear on the upper group of studs in the inner plate	X
TTC3l	Shear on the lower group of studs in the inner plate	X
TTC4	Shear on all the studs of the inner plate	Y
TTC5	Shear on the inner plate	Z
TTC6	Prestressing bars and compression zone of CCB	X

Components TTC1t/TTC1b

This component reproduces the top and bottom layer of rebars and concrete. The tension stiffening effect was implemented following the specifications of CEB-FIP (1993), whilst the force displacement relationship considered for this component was based on the well-known Kent-Scott-Park model.

Components TTC2

This component represents the shear resistance of the slab in Z direction, by means of elements located in the central layer.

Components TTC3u/TTC3l

This component is one of the characteristic components of the DOMI2 type connection shown in Fig. 2-99, i.e. the Nelson studs welded on the girder web protrusion. In detail, this component is the one implemented to take into account the shear resistance in the horizontal (X) direction. It

represents the shear resistance of six studs, i.e. three studs on each side of the web panel on the top layer of studs.

Components TTC4

This component has been implemented to take into account the shear resistance and stiffness of Nelson studs in the vertical (Y) direction, conversely from the TC3 relevant to the horizontal (X) direction.

Components TTC5

The component reproduces both the shear stiffness and strength of the web plate in the Z direction evaluated accordingly with EN1993-1-1 (2005).

Components TTC6

This component represents the prestressing bars connecting the head plates on both sides of the CCB and the compression zone, under the hypothesis of uniform compression distribution, of the CCB.

Fig. 2-99 depicts the details of the component-based mechanical model for the DOMI-2 solution with the complete set of springs. In Fig. 2-100 the comparison between the experimental results and the numerical response of the mechanical model is shown. This refined mechanical model, since allows the designer to detect the local response of the structural components, is suitable to be employed in a model of the complete bridge and to be used for performing Incremental Dynamic Analysis.

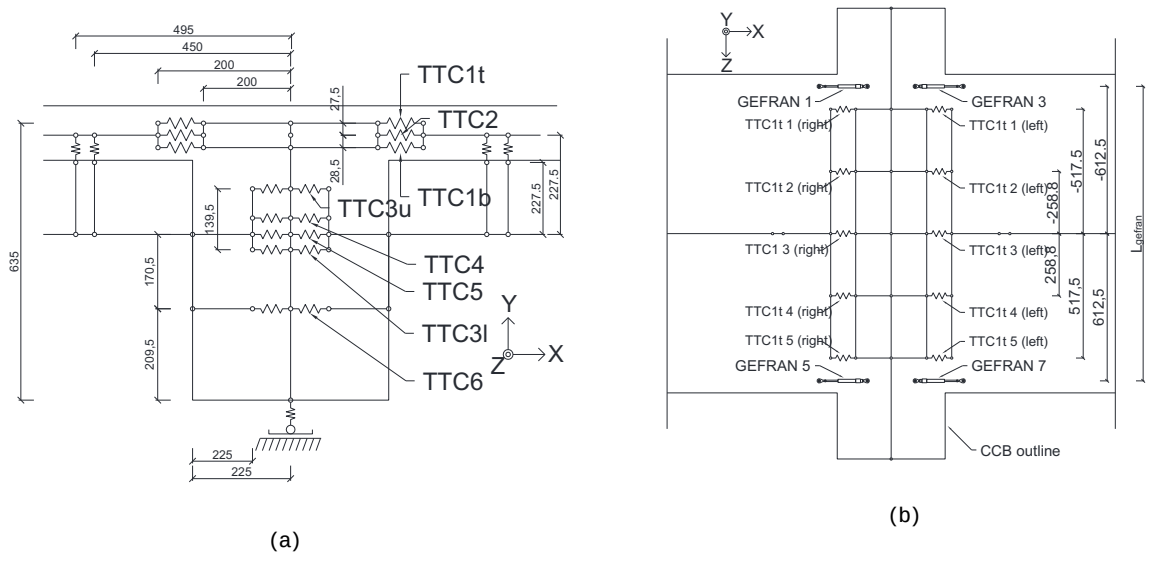

Fig. 2-99 - Refined model of Case Study 2 based on experimental results: a) Mechanical model of the connection; b) Plane view of the component-based mechanical model ideally positioned on the tested specimen.

a) b)

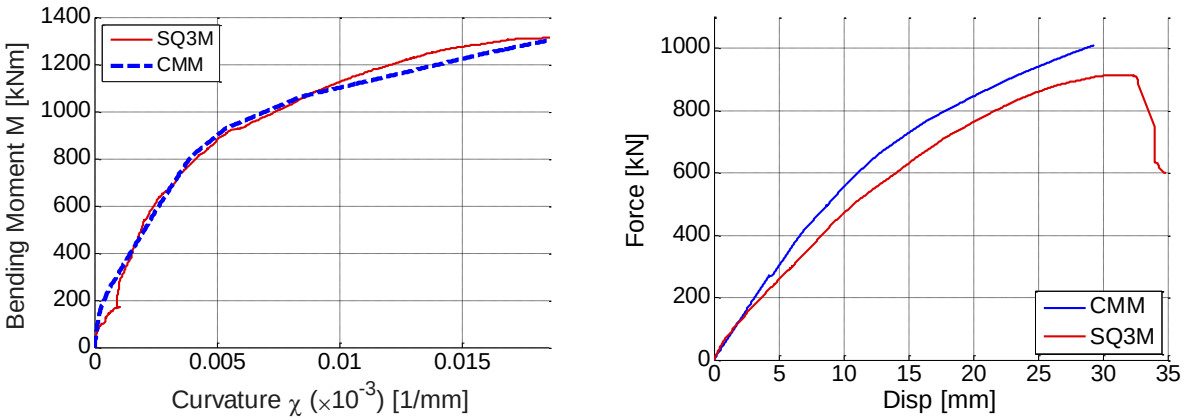

Fig. 2-100– Comparison between component-based mechanical model and experimental SQ3M test: a) Moment-Curvature at the left interface of the CCB; b) Global force-displacement.

2.3.4.3 Probabilistic Seismic Demand evaluation of Case Studies (Task 4.3)

Nonlinear time history analyses have been performed on the computational model of the bridges defined in task 4.2, to estimate the structural response in terms of engineering demand parameters (EDP). These latter have been calculated by using the Incremental Dynamic Analysis (IDA) method (Vamvatsikos and Cornell, 2002). For this purpose the ground motions selected in Task 1.3 and 4.1 and scaled at various levels of intensity measures (IM) have been utilized. The scaling procedure has been described in section 2.3.4.1 (task 4.1).

More in detail, non-linear bidirectional dynamic analyses have been performed with the ground motions at increasing levels of IM (PGA). Each accelerogram have been scaled at the same level of the intensity expressed in g. Thus, formally, PGA is the scaling factor of the spectral ordinate of the normalized target spectrum (ZPA=1) and the IDA curves represent the variation of the response measure (EDP) as a function of that PGA, for each accelerogram used.

The distribution of EDPs, conditioned on the intensity measure, is assumed to have a lognormal distribution. Two statistical measures are required to describe the EDP distribution: a central tendency measure and a measure of variation. The central tendency is described by the geometric mean, which is the mean of the natural logarithms of the EDPs, is given by:

$$\mu_{EDP|PGA} = \frac{1}{n}\sum_{i=1}^{n} ln(EDP|PGA) \tag{2.2}$$

where *n* is the number of observations. The geometric mean assumes that a data set is normally distributed in log-space. The variation around the central tendency of a data set is the standard deviation of the natural logarithm of the EDPs and is given by:

$$\sigma_{EDP|PGA} = \sqrt{\frac{1}{n-1}\sum_{i=1}^{n}\left(ln\,EDP|PGA - \mu_{EDP|PGA}\right)^2} \tag{2.3}$$

Possible EDPs can grouped into three different categories: a) global EDPs describe overall bridge behaviour, (e.g. maximum column displacement, motion at the abutments, residual displacements, etc..), b) intermediate EDPs describe performance of bridge structural components, (e.g maximum column curvature, shear force in the abutment shear tabs, etc..), c) local EDPs describe material level responses (e.g. stress and strain) in the bridge. For the specific case of SCC bridges with CCB selection of EDPs includes, according to the classification of (Mackie at a. 2008) and (Tubaldi et a. 2010):

1. Global EDPs
   - Pier drift;
2. Intermediate EDPs
   - Moment and curvature relationship at the bottom section of the pier;
   - Moment and rotation of the CCB-deck connection. These EDPs have been obtained for both the left and right sides of the joint. The bending moment of the composite section just before the side of interest, has been defined as follows:

$$M_{tot} = M_{slab} + M_{girder} + \Delta N \cdot z \tag{2.4}$$

with M_{slab} is the bending moment of the slab, M_{girder} is bending moment of the girder, ΔN is the axial force in the slab and z is the level arm (distance between girder and slab), Fig. 2-101;

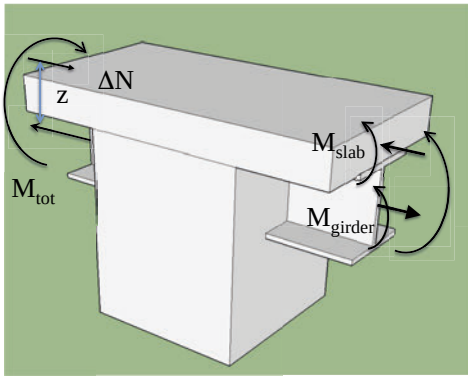

Fig. 2-101 Statics of the composite beam

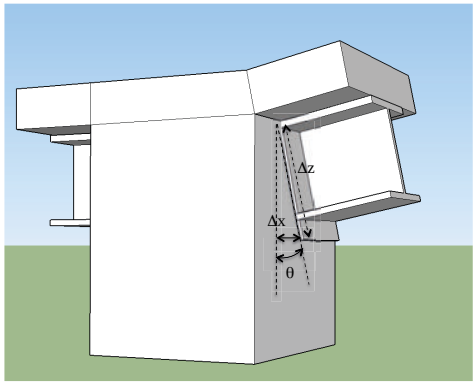

Fig. 2-102 Kinematics of the CCB-girder joint

The rotation of one side of the CCB-girder joint is given by the rotation of the vertical end plate with respect to the undeformed configuration:

$$\theta = \frac{\Delta x}{\Delta z} \tag{2.5}$$

where Δx is the relative displacement between top and bottom node of the vertical end plate and Δz is the height of the vertical end plate (Fig. 2-102);

- Axial strain of steel reinforcement and concrete at bottom section of the pier;
- Maximum horizontal slip in the CCB studs.

Only the EDPs that are relevant for the damage analysis have been considered for the evaluation of the fragility curves. Engineering demand parameters are plotted versus the Intensity Measure (IM). Since the properties of the seismic response depend on the intensity of the seismic shaking, a comprehensive assessment requires numerous nonlinear dynamic analyses at various levels of intensity in order to represent different possible earthquake scenarios. The selected range of PGA is 0.1 g - 2.0 g. This large range has been chosen to evaluate all possible damage levels and the corresponding probability of occurrence and thus the seismic risk of the bridge.

Case Study 2.1.2 – Straight two spans bridge

In this and the following section the complete set of IDA results of Case Study CS2.1.2 and CS2.2 (2-spans straight and skew bridges), endowed with DOMI2 detail are reported and discussed. For the other case studies only a synthesis of the results is provided; more details can be found in Deliverable D4.1 (2014).

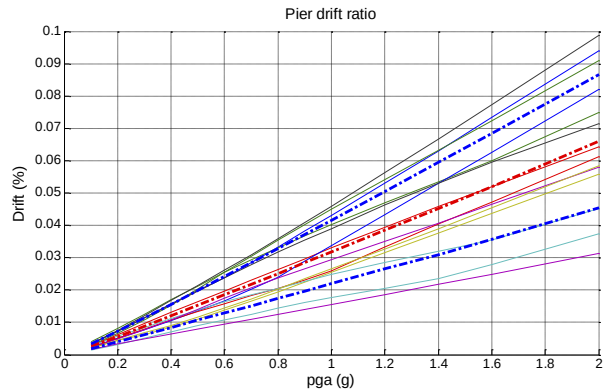

Fig. 2-103 Drift ratio of the pier in longitudinal direction (CS 2.1.2)

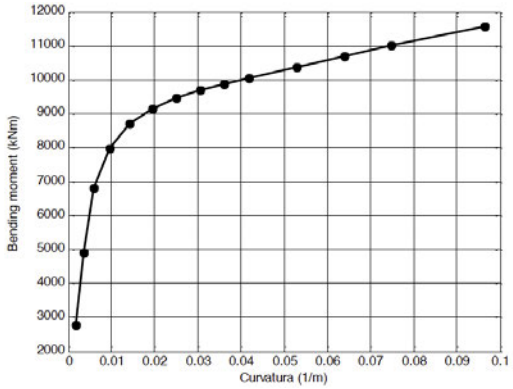

Fig. 2-104 Moment-curvature at bottom section of the pier in longitudinal direction (CS 2.1.2)

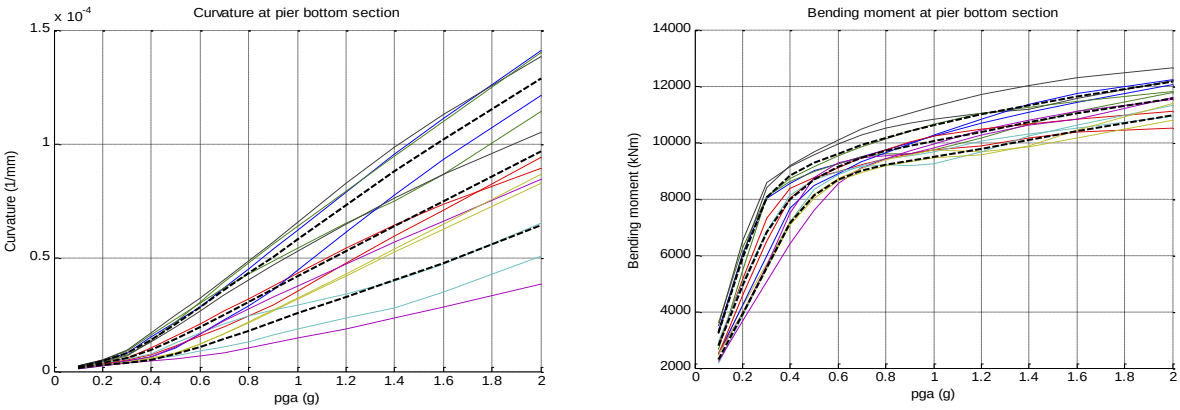

Fig. 2-105 Curvature and bending moment at bottom section of the pier in longitudinal direction (CS 2.1.2).

The maximum absolute value of the pier drift and bending moment-curvature at the bottom section of the pier in the longitudinal direction, obtained as mean value of the multi-record IDA analyses, are shown in Fig. 2-103 and Fig. 2-104, respectively. The black dashed lines represent the mean value and the mean ± standard deviation lines.

The typical collapse ratio of 4% for RC structures (FEMA 356) is reached in the pier (in mean) around 1.2g, which corresponds to the ultimate curvature at the bottom section, whereas the yielding condition (in mean) occurs for a PGA=0.4g (Fig. 2-105). However, the variance due earthquake randomness is particularly high (> 50%).

The IDA curves for bending moment of composite beams and rotation θ at the CCB-girders joint are plotted in Fig. 2-106. It can be seen that the onset of nonlinear behaviour takes place well "after" the yielding of the pier, both at left and right side. A careful reader can notice the full agreement with the experimental results. For example, the yielding moment that in the experimental tests was about 120 kNm, in full scale, for 4 beams, becomes about 3900 kNm that corresponds to the yielding moment in Fig. 2-108. The compatibility can be also noted in terms of rotation θ, even though the precision is reduced (Fig. 2-107).

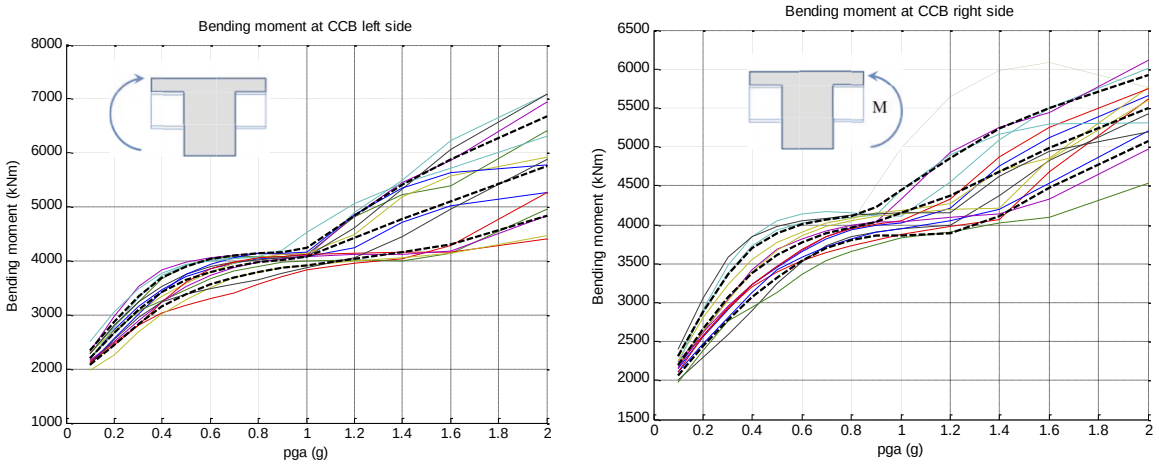

Fig. 2-106 Bending moment at CCB left and right side (CS 2.1.2).

The maximum horizontal displacement between the steel girder and the CCB at 1st and 3th row of non-linear links, which represent the slip of the shear headed studs within the CCB (Fig. 2-91), are shown in Fig. 2-109. Representative force-slip curves have been plotted using the mean values (Fig. 2-110). It can be noticed that the yielding condition (slip = 0.5 mm) in the shear studs occurs in mean for a PGA=0.5g.

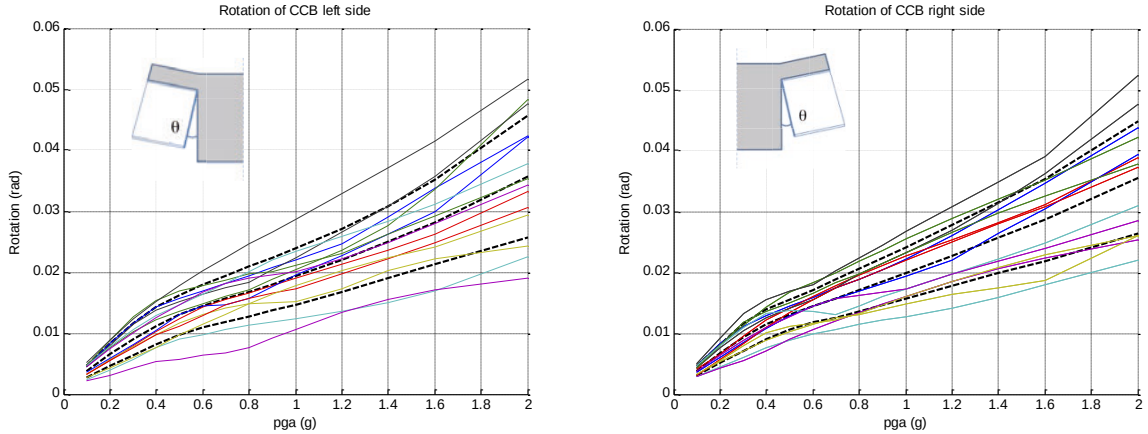

Fig. 2-107- Rotation of CCB left and right side (CS2.1.2)

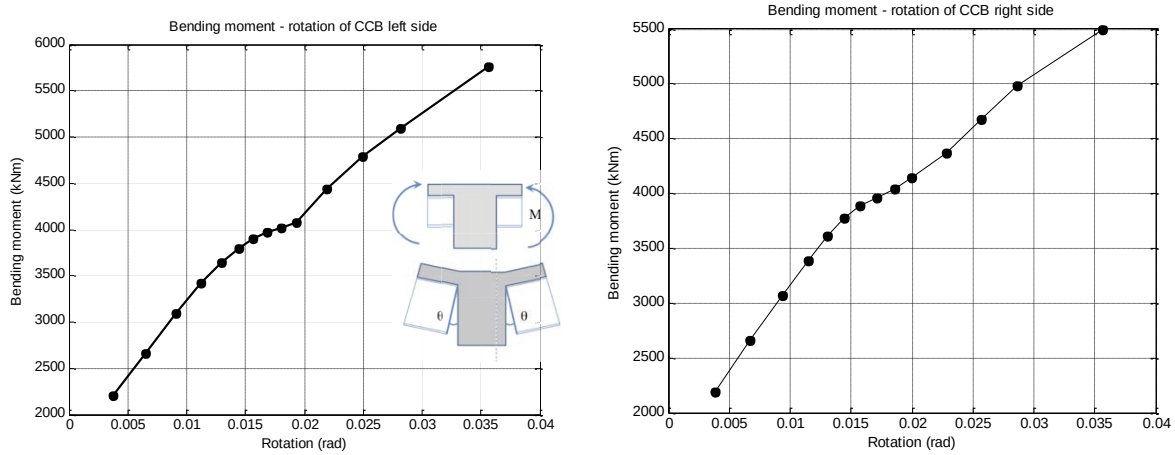

Fig. 2-108 Moment - rotation curves (mean) of CCB at left and right side (CS 2.1.2)

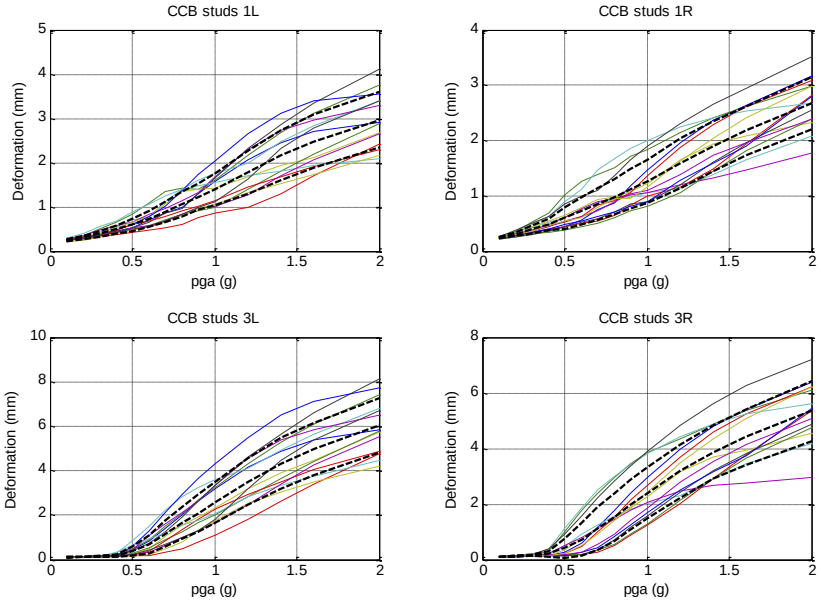

Fig. 2-109 - CCB shear studs deformation in longitudinal direction (CS 2.1.2).

The IDA curves of maximum longitudinal strain for concrete and steel rebars at bottom section of the pier are shown in Fig. 2-111. Mean value of maximum axial steel strain increases up to 4.5%, while mean value of maximum concrete axial strain is around 1.5%. At the ultimate condition (drift 4%) the maximum strain of rebars and concrete is about 2,7% and 0,35% respectively.

Case Study 2.2 – Skew two spans bridge

In the following, the results for the case of skew bridge are briefly reported and discussed. In this analysis, the ultimate condition of the bearing has not accounted for.

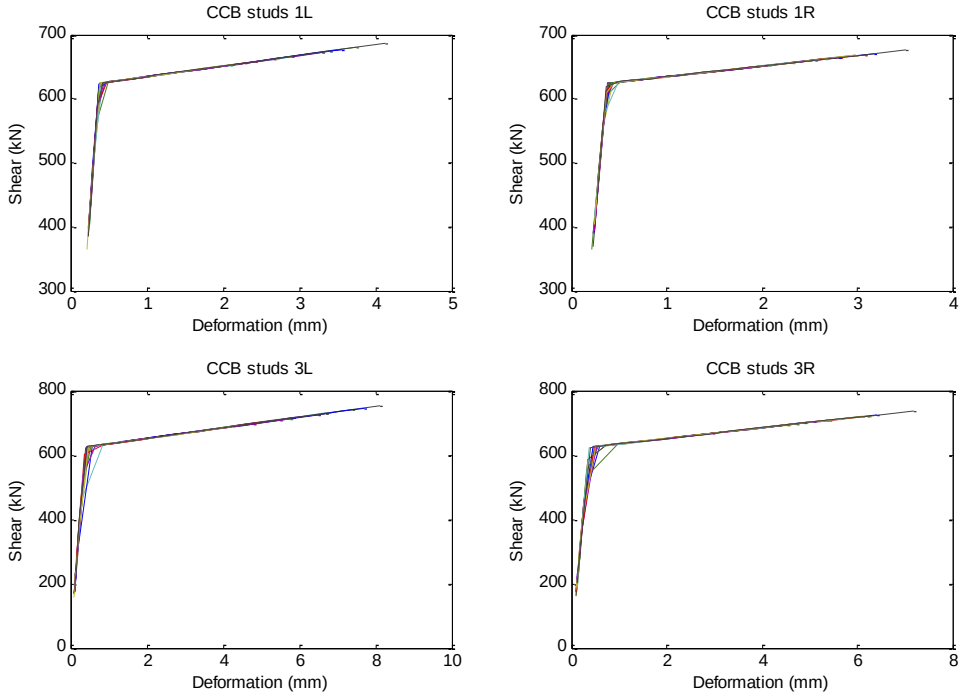

Fig. 2-110 Force - slip of CCB studs (CS 2.1.2).

The IDA curves of pier drift, bending moment and curvature at the bottom section of the most stressed column (left) in the longitudinal direction, are shown in Fig. 2-112, Fig. 2-113, Fig. 2-114, Fig. 2-115. A collapse drift ratio of 4% is reached for a PGA=1.3g, similarly to the CS 2.1.2. For a PGA=0.3g (design PGA) the drift ratio is less than 1.0%, well under the yielding condition. This is the positive effect of the deck on deformable bearings (NDB), for which behaviour factor q=1 has been adopted.

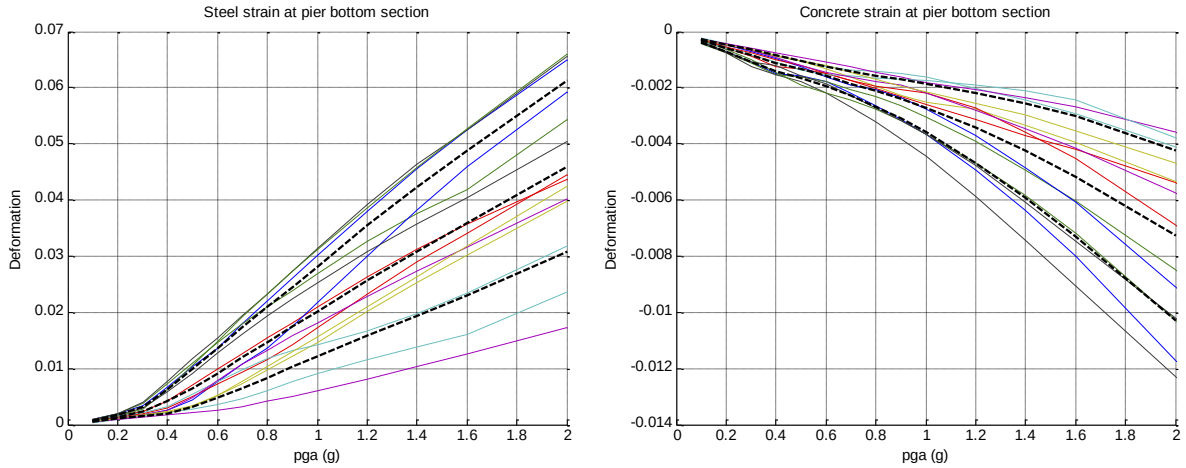

Fig. 2-111 - Steel and concrete strain at pier bottom section (CS 2.1.2).

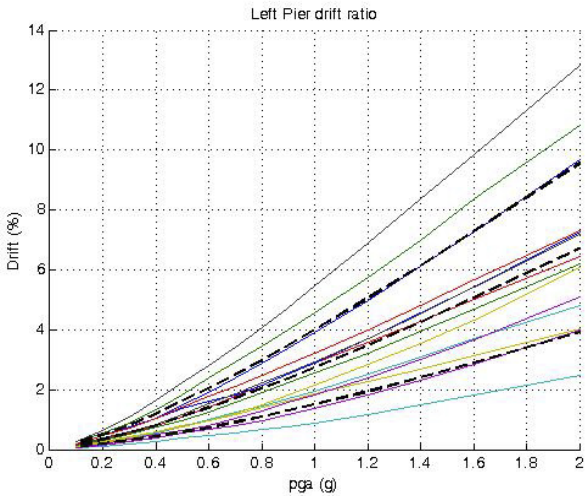

Fig. 2-112 Drift ratio of the left pier – Longitudinal direction (CS2.2)

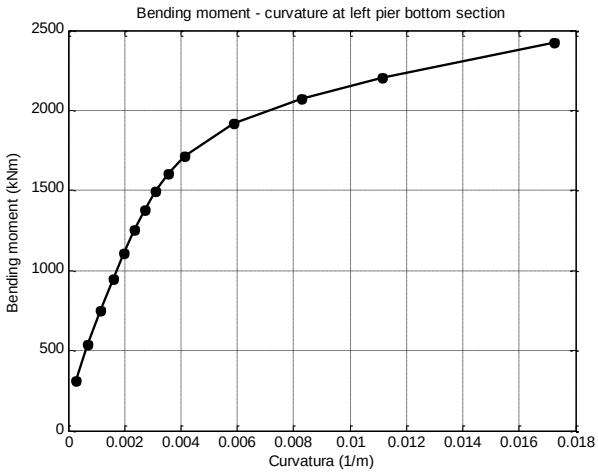

Fig. 2-113 Moment-curvature plot at bottom section – left pier (CS2.2)

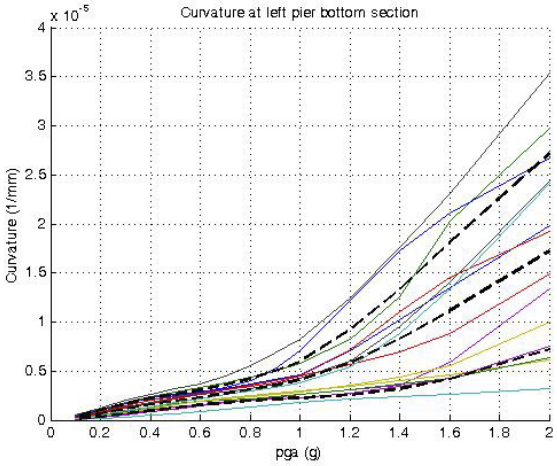

Fig. 2-114 Curvature at bottom section - left pier (CS2.2)

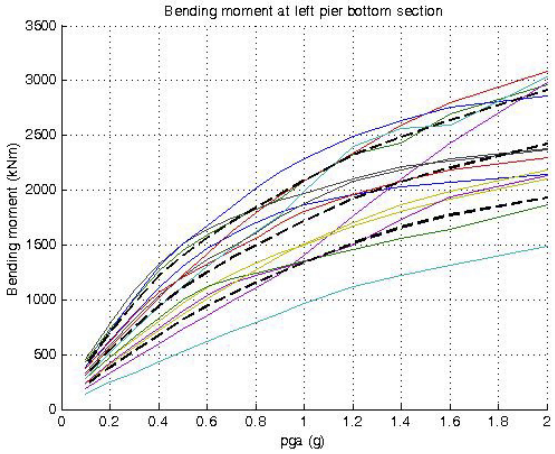

Fig. 2-115 Bending moment at bottom section - left pier (CS2.2)

Maximum absolute values of bending moment and rotation at the CCB-girders joint have been also recorded during dynamic analysis. It has been noticed a substantial linear behaviour of the joint. Conversely, the yielding condition of the shear studs within the CCB has been recorded, in mean, for a PGA=0.5g, similarly to the CS 2.1.2. Finally, the maximum longitudinal strain in the steel at bottom section of the left pier increases up to 0.25% in correspondence of the design PGA=0.3 g, while mean value of maximum concrete axial strain is around 0.1%. This confirm, as expected, that the pier remains elastic for design conditions. The yielding condition occurs in mean for a value of PGA=1g. Thus, this bridge appears, as expected, less vulnerable of the CS2.1.2 due to the different configuration in which the NDB have a predominant role.

Case Study 1.1 and 1.2 – Three spans bridge

The bridge object of these case studies is a three spans steel-concrete composite bridge. It is divided in two sub-cases.

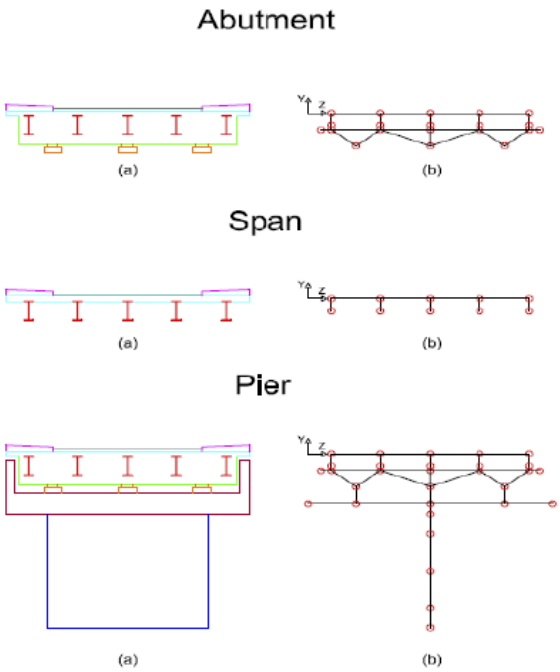

Fig. 2-116 (a) Actual bridge and (b) stick model of abutment, span and piers of the CS 1.1

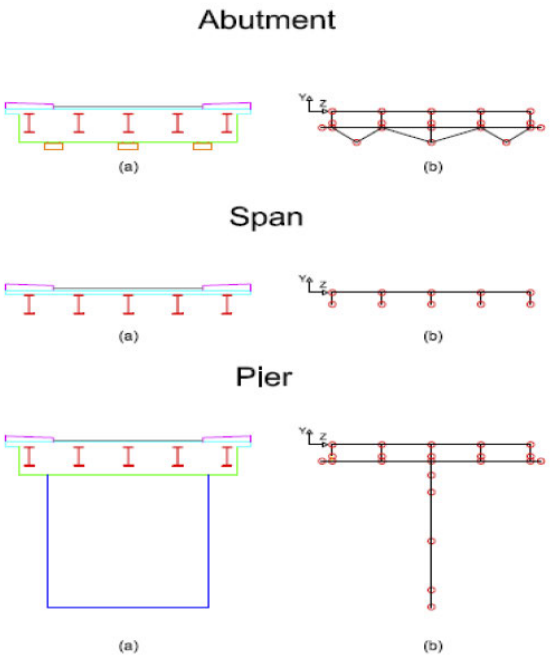

Fig. 2-117 - (a) Actual bridge and (b) stick model of abutment, span and piers of the CS 1.2

In the Case Study 1.1, the support of the deck on piers is characterised by a set of normal damping rubber bearings, whilst in the Case Study 1.2 a monolithic connection between CCB and piers is employed. The analytical models used in the analysis are shown in Fig. 2-116, Fig. 2-117 and Fig. 2-118. More details on modeling assumptions can be found in Deliverable D4.1 (2013). Fig. 2-118 shows the 3D model adopted for the analysis.

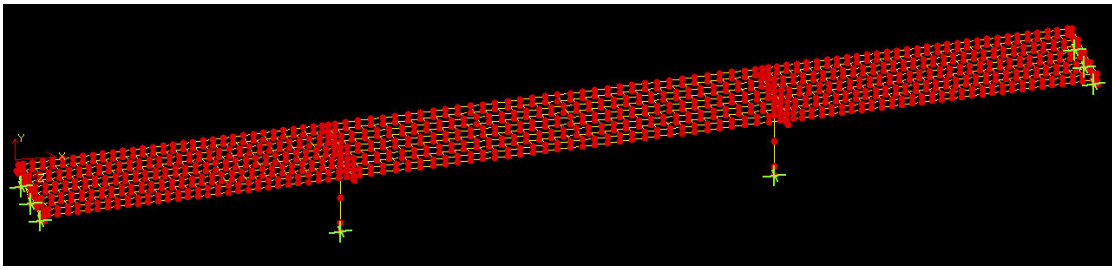

Fig. 2-118- 3D view of the stick model - Case Study 1

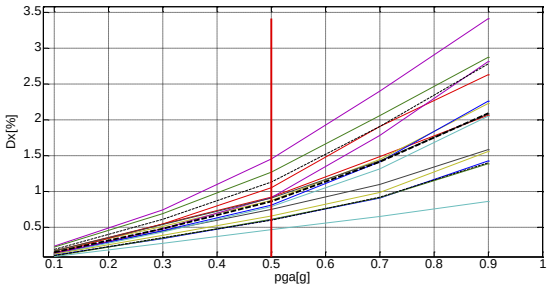

Fig. 2-119 - Results for EDP 1 (CS1.1).

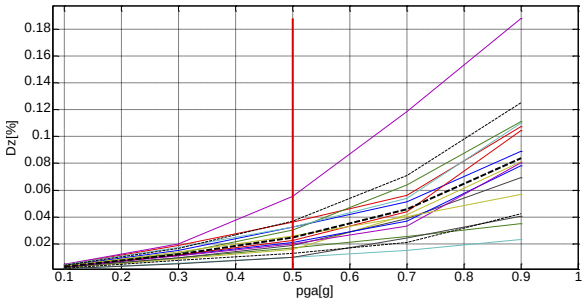

Fig. 2-120- Results for EDP 2 (CS.1.1)

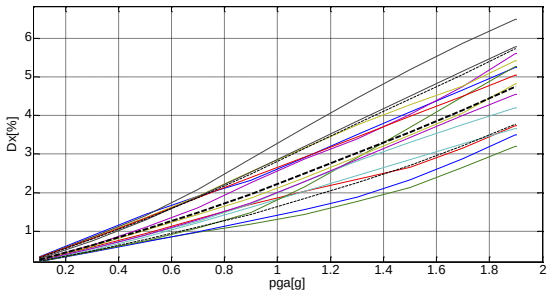

Fig. 2-121 Results for EDP 1 (CS1.2)

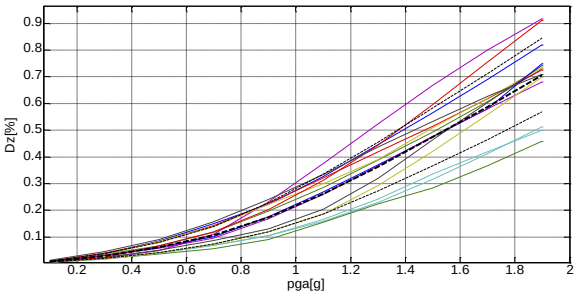

Fig. 2-122 Results for EDP 2 (CS1.2)

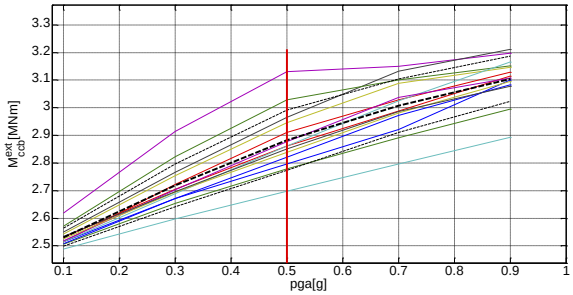

Fig. 2-123 Results for EDP 4 (CS1.1)

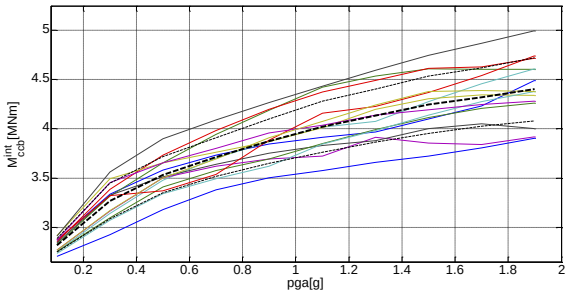

Fig. 2-124 Results for EDP 3 (CS1.2)

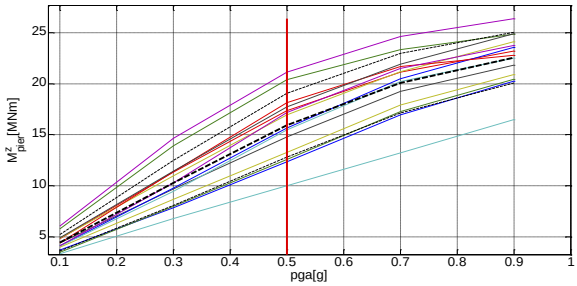

Fig. 2-125 Results for EDP 5 (CS1.1)

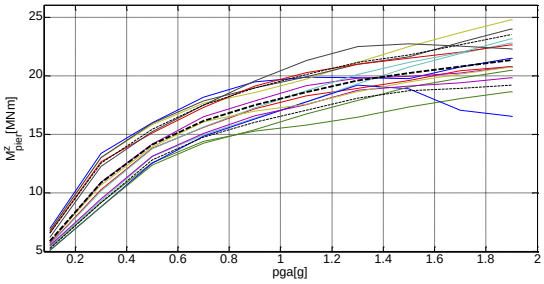

Fig. 2-126 Results for EDP 6 (CS1.2).

The full set of results for all EDPs is reported in deliverable D4.1 (2014): the drift of the pier in longitudinal (x) and transversal (z) direction (EDP1, EDP2), the bending moment (EDP5, EDP6) and the corresponding curvatures of the pier at bottom section (EDP7, EDP8), the maximum bending moment in the composite section near the CCB in the middle and external span (EDP3, EDP4), the maximum deformation of concrete and steel in the pier (EDP9, EDP10).

Here only a summary of the most significant results is presented (Fig. 2-119-Fig. 2-126). The IDA curves for the two considered case studies, shown how the two solutions are quite similar although different support configurations are used. The reason of this similarity lies in the fact that both case studies were designed in order to reduce the seismic action. CS 1.1 with an appropriate isolation system whilst CS 1.2 by plastic dissipation in the piers. In particular, the design values of the structural factors in x and z direction for CS1.1 are both equal to 1, whereas they are equal to 3.5 and 1 for CS1.2. It is evident that the yielding condition in the pier occurs in CS1.1 for values of PGA ranging between 0.3 and 0.5g, whereas for CS1.2 the behaviour of the pier is practically elastic. It is interesting to note that the moment transferred from the deck to the CCB for a PGA=0.3g is in the range 2.5-2.7 MNm for the CS1.1, and 3-3.5 MNm for the CS1.2. According to the component-based model developed in task 4.2, DOMI-2 detail develops a plastic moment of about 5000 kNm. Therefore, for the seismic design action no plastic deformation is expected in the deck-pier joint and consequently no damage. Anyhow, the moment value remains under the plastic value in the entire range of investigated PGA.

In conclusion, from the analysis of CS1.1 and CS1.2 only important damage in the piers is expected for both the typologies as function of the behaviour factor adopted. The CCB remain practically undamaged in the wide range of investigated IMs.

Case Study 3 – Six spans bridge

The bridge of these case studies is a six spans steel-concrete composite bridge. It is divided in two sub-cases. In the Case Study 3.1, the support of the deck on piers is characterised by a set of normal damping rubber bearings, whilst in the Case Study 3.2 a monolithic connection between CCB and piers is achieved. The analytical models used in the analysis are shown in Fig. 2-127, Fig. 2-128 and Fig. 2-129. Modeling assumptions are similar to the ones adopted for the other bridges.

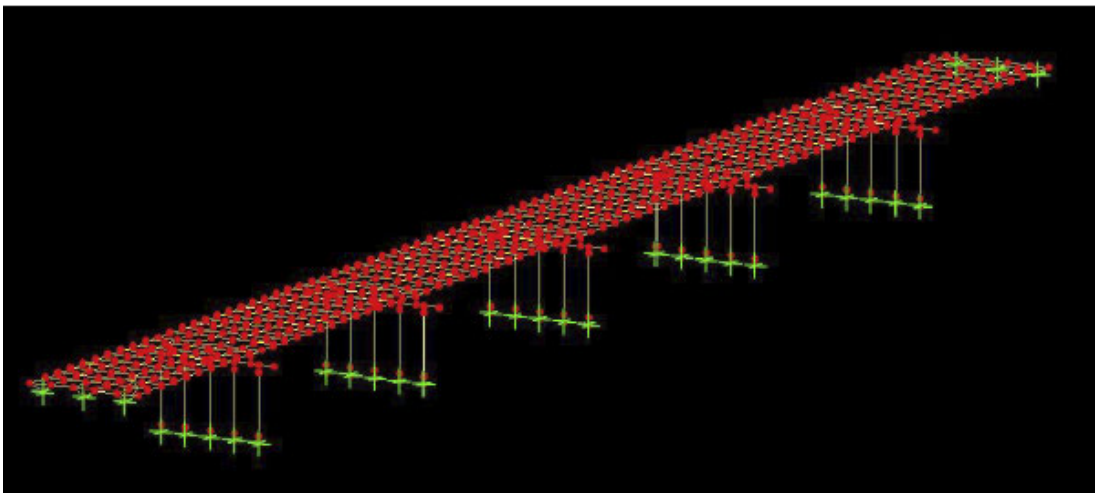

Fig. 2-127 3D view of the stick model - Case Study 3

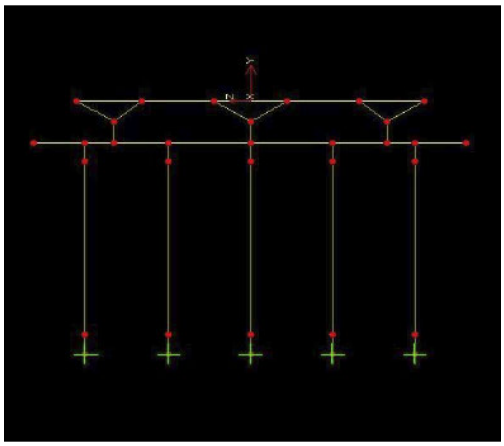

Fig. 2-128 Stick model of piers – CS 3

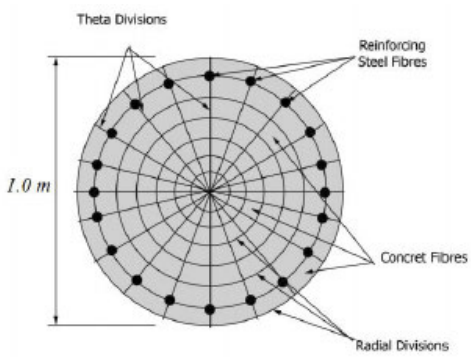

Fig. 2-129 Fiber model adopted for the piers

As in the previous cases the vulnerability of this bridge typology was found rather limited. Fig. 2-130 and Fig. 2-131 show for one of the most demanding input signals the moment-curvature response of one piers' columns (CS 3.2). It is evident that for the design PGA the column remains elastic, whereas only from PGA=0.5g the damage takes place. From the fragility analysis of the bridge it was noticed that for a damage level that corresponds to the concrete spalling (DS1), a slight damage, the probability of exceedance is greater than 60%, corresponding to the design conditions (PGA=0.3g). For higher damage states (DS2 and DS3) the probability decrease to 2-10%.

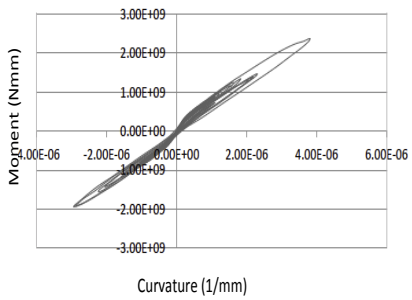

Fig. 2-130 Moment-Curvature for PGA=0.3 g – CS 3-2

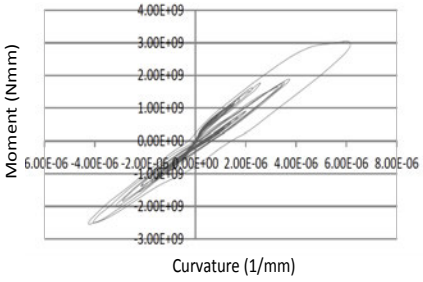

Fig. 2-131 Moment-Curvature for PGA=0.5 g – CS 3.2

2.3.4.4 Damage Analysis and determination of fragility curves (task 4.4)

The purpose of the damage analysis is to estimate physical damage at the component or system levels as a function of the structural response. Damage measures, DMs, are typically defined in terms of damage levels corresponding to the repair measures needed to restore the components of a facility to the original conditions (Porter 2003).

Damage level of a damageable group shows variance, even for the same value of EDP. This is mainly due to two reasons. The first reason is the uncertainty in the material characteristics, which translate into the uncertainty in the corresponding EDP capacity term that defines the damage level. The second reason is the differences in the pattern and history of the structural response. EDPs are generally represented as peak quantities. However, differences in the path of achieving the same peak value introduce differences in the observed damage and these differences contribute to the variance of the DM corresponding to an EDP. Accordingly, a specific value of EDP corresponds to various DMs with different probabilities.

The damage is therefore expressed in probabilistic term. The tool used to determine the above probabilities are the "capacity fragility functions," as commonly referred to in the literature, that represents the probability of a structure to exceed a damage threshold conditioned to the ground motion IM.

With this aim, the collapse mechanisms must be defined for each structural component together with the progressive Damage States (*DS*). The Damage State (*DS*) are addressed in terms of probabilistic quantities and conditioned to an *EDP* that quantifies the response of the structure to the input ground motion. A relationship between *DS* and *EDP* must be developed, which account for uncertainty in damage prediction; this relation is usually developed from experimental data. It provides the average value, the coefficient of variation and the correlation of the EDP_i corresponding to the DS_k (k =1,2,…). Assuming that the DS occur in sequence (with DS_1 preceding DS_2 which, in turn, precedes DS_3 and so on), the corresponding *EDP* can be ordered ($EDP_1 \le EDP_2 \le EDP_3 \le ....$).

Assuming, for example, three *DS*, the joint probability density function of the variables EDPs can be assumed as follows (Deliverable 4.3, Alessandri et al 2013).

$$P_{EDP_1,EDP_2,EDP_3}\left(EDP_1,EDP_2,EDP_3\right)=\begin{cases} \dfrac{1}{k}\,p_L\left(EDP_1,EDP_2,EDP_3\right) & if\ \ EDP_1 \le EDP_2 \le EDP_3 \\ 0 & Otherwise \end{cases} \tag{2.6}$$

where $p_{EDP_1,EDP_2,EDP_3}(EDP_1,EDP_2,EDP_3)$ is the joint lognormal distribution function of three random variables. The constant κ in the previous equation is the normalization constant that takes into account the truncation of the distribution and can be evaluated by the following expression:

$$\kappa = \int_0^{\infty}\int_{EDP_1}^{\infty}\int_{EDP_1}^{\infty} p_{EDP_1,EDP_2,EDP_3}(EDP_1,EDP_2,EDP_3)\,dEDP_1,dEDP_2,dEDP_3 \tag{2.7}$$

The probability of damage conditioned to EDP is given by the following equations:

$$\begin{aligned}
\Pr(\mathrm{DS}_0 \mid \mathrm{EDP}) &= \frac{1}{\kappa}\int_{\frac{\ln \mathrm{EDP}-\mu_{X_1}}{A_{11}}}^{\infty}\left\{\varphi(u_1)\int_{\alpha_{11}u_1+\beta_1}^{\infty}\varphi(u_2)\left[1-\Phi(\alpha_{21}u_1+\alpha_{22}u_2+\beta_2)\right]du_2\right\}du_1 \\
\Pr(\mathrm{DS}_1 \mid \mathrm{EDP}) &= \frac{1}{\kappa}\int_{-\infty}^{\frac{\ln \mathrm{EDP}-\mu_{X_1}}{A_{11}}}\left\{\varphi(u_1)\int_{\frac{\ln \mathrm{EDP}-A_{21}u_1-\mu_{X_2}}{A_{22}}}^{\infty}\varphi(u_2)\left[1-\Phi(\alpha_{21}u_1+\alpha_{22}u_2+\beta_2)\right]du_2\right\}du_1 \\
\Pr(\mathrm{DS}_2 \mid \mathrm{EDP}) &= \frac{1}{\kappa}\int_{-\infty}^{\frac{\ln \mathrm{EDP}-\mu_{X_1}}{A_{11}}}\left\{\varphi(u_1)\int_{\alpha_{11}u_1+\beta_1}^{\frac{\ln \mathrm{EDP}-A_{21}u_1-\mu_{X_2}}{A_{22}}}\varphi(u_2)\left[1-\Phi\left(\frac{\ln \mathrm{EDP}-A_{31}u_1-A_{32}u_2-\mu_{X_3}}{A_{33}}\right)\right]du_2\right\}du_1 \\
\Pr(\mathrm{DS}_3 \mid \mathrm{EDP}) &= \frac{1}{\kappa}\int_{-\infty}^{\frac{\ln \mathrm{EDP}-\mu_{X_1}}{A_{11}}}\left\{\varphi(u_1)\int_{\alpha_{11}u_1+\beta_1}^{\frac{\ln \mathrm{EDP}-A_{21}u_1-\mu_{X_2}}{A_{22}}}\varphi(u_2)\left[\Phi\left(\frac{\ln \mathrm{EDP}-A_{31}u_1-A_{32}u_2-\mu_{X_3}}{A_{33}}\right)-\Phi(\alpha_{21}u_1+\alpha_{22}u_2+\beta_2)\right]du_2\right\}du_1
\end{aligned} \tag{2.8}$$

where $\varphi(u)=e^{-u^2/2}\sqrt{2\pi}$ is the PDF of the normalized Gaussian variable *u* and Φ is the corresponding CDF,

$$\alpha_{11} = \frac{\left(A_{11} - A_{21}\right)}{A_{22}}$$
$$\alpha_{21} = \frac{\left(A_{21} - A_{31}\right)}{A_{33}}, \quad \alpha_{22} = \frac{\left(A_{22} - A_{32}\right)}{A_{33}} \tag{2.9}$$

and

$$\beta_1 = \frac{\mu_{X_1} - \mu_{X_2}}{A_{22}}, \quad \beta_2 = \frac{\mu_{X_2} - \mu_{X_3}}{A_{33}} \tag{2.10}$$

where μ_{Xi} is mean value of X_i and A_{ij} is the generic element of the diagonal of matrix **A**, which comes from the Cholesky decomposition of the covariance matrix $\mathbf{C_X = AA^T}$. The damage state DS0 corresponds to the onset of damage; a damage less then DS0 is assumed to be insignificant and not needing repair.

One or more collapse mechanism must be defined for each structural component together with the relevant progressive damage states.

Finally the *P(DS|IM)* is evaluated by convolution of the structural demand probability *P(EDP|IM)* and the damage model *P(DS|EDP):*

$$Pr\left(DS \mid im\right) = \int_{EDP} Pr\left(DS \mid EDP\right) \cdot dG\left(EDP \mid IM\right) dEDP \tag{2.11}$$

In the evaluation of the fragility curves the structure has been assumed to be deterministic because of uncertainty in structural geometry, mechanical characteristics of materials and analytical models for structural behaviour could be considered negligible, compared to that of the input ground motion. The randomness of the seismic action has been taken into account in the demand evaluation by using several accelerograms selected so as to reduce the dispersion of the structural response. The uncertainties of the demand, therefore, is dominated by the dispersion of the response due to different input ground motions. Given the completeness of the data of CS 2.1.2, including non-linear model and experimental tests, in what follows, this example will be fully analysed.

In the perspective of the evaluation of the expected losses, that is the final goal of the application of the PBEE procedure, the elements of the bridge, whose damage could be considered significant, are the piers, the CCB and the deck. For the reinforced wall-type pier a flexural damage mechanism has been considered with three different DSs: a) concrete cover spalling, b) bar buckling, c) bar fracture.

Fig. 2-132 Cover Spalling (DS1)

Fig. 2-133 Bar Buckling (DS2)

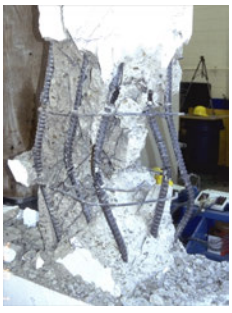

Fig. 2-134 Bar Fracture (DS3)

Concrete cover spalling represents the first flexural damage state (Fig. 2-132), in which there are marginal safety implications, there may be a possible short-term loss of function, and the cost to repair concrete spalling could be significant. Buckling (Fig. 2-133) and fracture (Fig. 2-134) of the longitudinal bars represent damage states in which safety implications are significant, partial replacement may be required, and a longer term loss of function may occur.

To quantitatively implement PBEE the three events above mentioned in this work have been considered as damage measures and related to the EDP (represented by the column drift ratio), by the relathionship developed by Berry and Eberhard (2003). They developed empirical equations to estimate deformations at concrete cover spalling, bar buckling and bar fracture based on theoretically expected trends in drift ratios. The models were calibrated with existing experimental results from the UW-PEER reinforced concrete column performance database, which includes the performance of over 400 columns. Drift ratio equations proposed by Berry and Eberhard for damage estimation are the following:

$$\frac{\Delta_{sp}^{calc}}{L}(\%) = 1.6\left(1-\frac{P}{A_g f'_c}\right)\left(1+\frac{L}{10D}\right) \qquad \text{Concrete cover spalling}$$

$$\frac{\Delta_{bb}^{calc}}{L}(\%) = 3.25\left(1+k_e\rho_{eff}\frac{d_b}{D}\right)\left(1-\frac{P}{A_g f'_c}\right)\left(1+\frac{L}{10D}\right) \qquad \text{Bar buckling} \qquad (2.12)$$

$$\frac{\Delta_{bf}^{calc}}{L}(\%) = 3.5\left(1+150\rho_{eff}\frac{d_b}{D}\right)\left(1-\frac{P}{A_g f'_c}\right)\left(1+\frac{L}{10D}\right) \qquad \text{Bar fracture}$$

with $k_e=40$ for rectangual sections, $\rho_{eff}=\rho f_{ys}/f_c'$ (where ρ_{eff} is the volumetric transverse reinforcement ratio, f_c' the concrete compressive strength, f_{ys} the yeld stress of the tranverse reinforcement), d_b diameter of the longitudinal reinforcement, D column depth, P axial load at the column base, A_g gross area of the cross-section and L distance from the column base to the point of contraflexure. Table 2-18 shows the mean value of the EDP at the onset of the considered damage and the relevant C.o.V evaluated for the C.S. 2.1.2. The DS0 in the table corresponds to a negligible damage for which no repair items is considered.

Fig. 2-135 and Fig. 2-136 presents the four probabilities of the DS conditioned to the EDP for each performance group PG (see section 2.3.4.5). The correlation between the DSs has been considered assuming that the DS occur in sequence (with concrete spalling preceding bar buckling, which, in turn, precedes bar fracture).

Table 2-18 Pier damage states – CS 2.1.2

	DS description	**EDP description: median drift ratio for limit state**
DS0	Negligible damage with initial cracking	Drift ratio associated with cracking moment M_{cr}
DS1	Cover concrete spalling	Δ_{sp} Equation from Berry and Eberhard (2003)
DS2	Longitudinal reinforcing bar buckling	Δ_{bb} Equation from Berry and Eberhard (2003)
DS3	Longitudinal reinforcing bar fracture	Δ_{bf} Equation from Berry and Eberhard (2003)

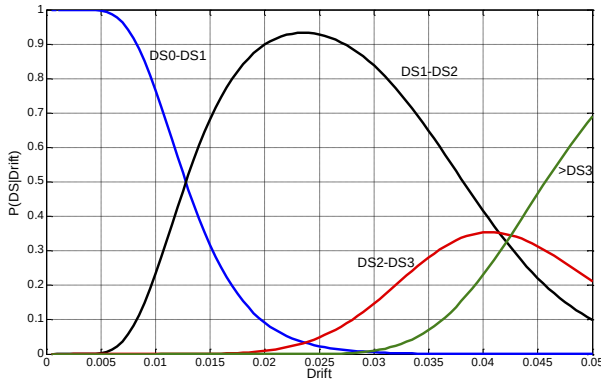

Fig. 2-135 Conditional probability functions of DS for PG1 and PG2.

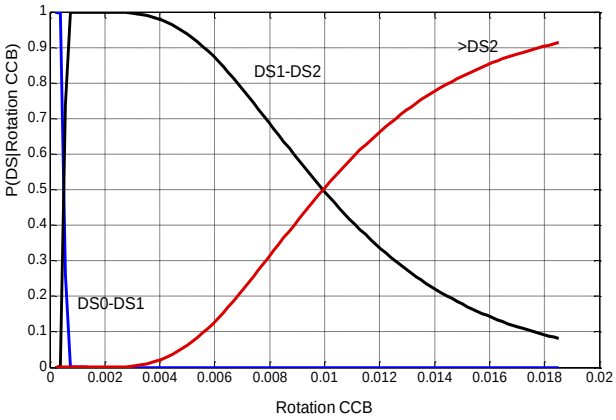

Fig. 2-136 Conditional probability functions of DS for PG3

A flexural damage models has been considered also for the CCB. The DSs are represented by the yielding (DS1) and the ultimate (DS2) deformation of the shear studs. The associated EDP is represented by the rigid rotation of the steel head plates of the joint. In this case, based on the results of experimental tests performed by several authors (Viest 1967, Gattesco et al. 1996, Shim et al. 2004, Lee et al. 2005) and listed in Table 2-19, the mean value and the dispersion of the yielding and ultimate slip deformation of the shear studs have been evaluated; it is assumed that there is no correlation between the two variables. The mean value of the slip of shear studs at yielding is about 0.28mm; under the hypothesis that the head plate of girders, herein considered as rigid, can rotate around one extremity (Fig. 2-102), its rigid rotation can be calculated as follow:

$$\theta_y = \frac{\Delta x}{\Delta z} = \frac{0.28}{540} = 5.31 \cdot 10^{-4} (rad) \tag{2.13}$$

where Δx is the relative displacement between top node and bottom node of the vertical end plate and Δz is the height of the head plate.

Table 2-19 Push-out test results

Authors	Yielding slip (mm)	Ultimate slip (mm)
Viest (1956)	0.249	4.32
	0.305	7.08
	0.259	9.70
	0.335	2.51
	0.299	3.50
	0.333	2.54
Gattesco e Giuriani (1997)	0.3	9.7
Shim Lee & Yoon 2004 and Lee Shim & Chang 2005	0.25	6.78
	0.25	7.21
Mean	**0.28**	**5.93**
CoV	**0.12**	**0.47**

Table 2-20 CCB damage states

	DS description	EDP description: median rotation
DS1	Yielding	Rotation associated with yielding of the shear stud
DS2	Ultimate	Rotation associated with ultimate deformation of the shear stud

Assuming that the failure slip of the shear studs is about 5.93 mm, the rigid rotation, which determines a horizontal displacement of 5.93 mm at the other extremities, reads:

$$\theta_u = \frac{\Delta x}{\Delta z} = \frac{5.93}{540} = 1.1 \cdot 10^{-2} (rad) \tag{2.14}$$

They are listed in Table 2-20. The correlation between the DS has been neglected and it has been assumed that the DSs occur in sequence (with yielding of studs preceding stud fracture).

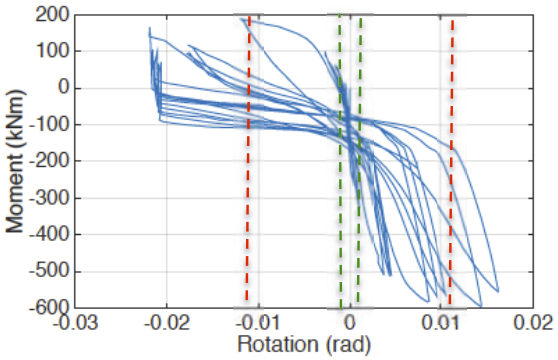

Fig. 2-137 Experimental moment-rotation response of DOMI2 – C1 specimen and limit states (green: yielding - DS1), red: ultimate – DS2)

Fig. 2-138 Detachment of the steel plate from the CCB (DOMI2-C1) – Limit state DS2

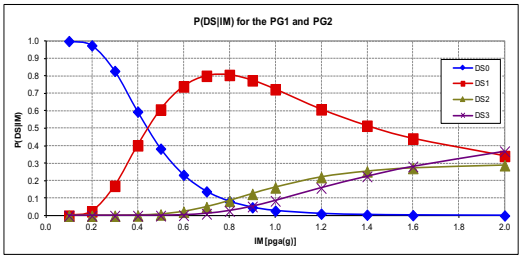

Fig. 2-139 Capacity fragility curves of PG1 and PG2

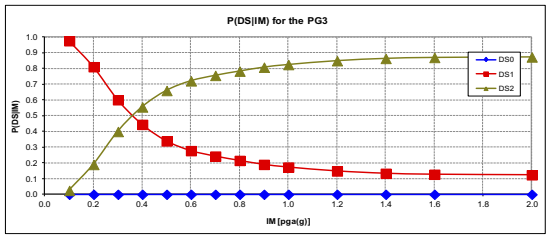

Fig. 2-140– Capacity fragility curves of PG3

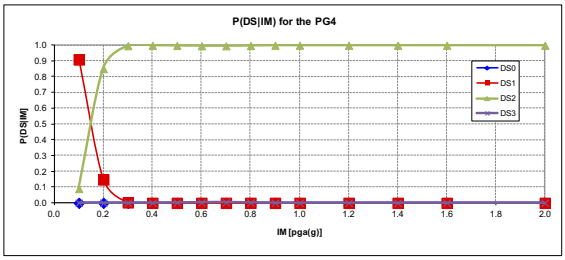

Fig. 2-141 Capacity fragility curves of PG4

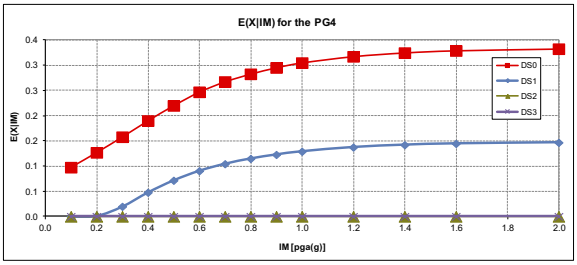

Fig. 2-142 Mean value of the maximum distance from the CCB at which DS in the deck occur

Concerning the damage in the deck, it can be associated to the flexural deformation of the slab. Taking into account that yielding of steel bars in the slab is rarely achieved; damage states are defined in terms of progressive concrete cracking in the slab. Three levels of damage have been considered: a) 0.2mm cracking width (DS1), b) 0.4mm cracking width (DS2) and c) the yielding of the top bars (DS3). The EDP is represented by the distance of the crack from the CCB, where the DS occurs (Fig. 2-143). The link between EDPs and damage is based on relationships between the percentage of deck concrete slab area that needs to be repaired and maximum values of the demand parameter.

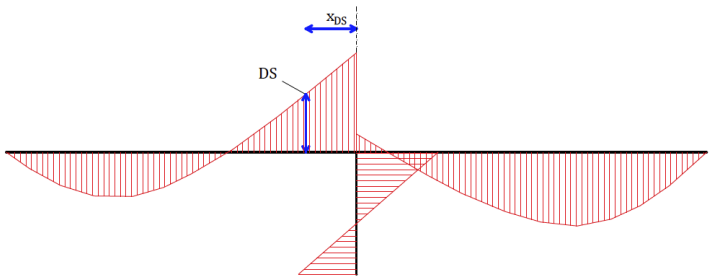

Fig. 2-143 Definition of the EDP for Deck

By assuming that the EDP is log-normally distributed, the capacity fragility curves P(DS|IM) are evaluated by the convolution of the P(DS|EDP) and P(EDP|IM):

$$Pr\left(DS_{PG_i} \mid im\right) = \int_{EDP} Pr\left(DS_{PG_i} \mid EDP\right) \cdot dG\left(EDP \mid IM\right) dEDP \tag{2.15}$$

The capacity fragility curves, P(DS|IM), are shown in Fig. 2-139, Fig. 2-140, Fig. 2-141. In Fig. 2-142 the mean value of the maximum distance from the CCB at which the DS occurs are listed and plotted as a function of the PGA.

2.3.4.5 Loss (Cost-effective risk) Analysis (Task 4.5)

Cost-effective risk evaluation is the very last step of the global integrated probabilistic performance-based evaluation procedure used for SEQBRI project, that explores all aspects of the problem: a) global earthquake demand to local engineering demand parameters (EDP), b) associated damages, which are based on a detailed non-linear analysis of each case study including the experimental evaluation of the joint, c) the loss analysis. The result of this phase is a decision model, which is based on Decision Variables (DV) pertaining to the use of a structure given a level of sustained damage. Decision models are mathematical relations between damage measures (DMs) and decision variables (DVs). Commonly used decision variables describe losses in terms of repair cost, interruption in service (downtime or repair time), or loss of life: thus, decision models are also called loss models. The decision model may have several parts—those that relate DMs to repair quantities (Q) and those that relate Q back to repair cost or repair time. A completely different set of decision variables focuses on the remaining capacity of the structure to function as intended. For example, the return of a highway bridge to differing degrees of functionality in a highway network is also an important loss criterion. Functionality may be measured in terms of lateral load resistance in aftershocks, traffic volume, lane and speed reductions, or access for emergency vehicles.

The main DV adopted in **SEQBRI** is the repair/construction cost ratio (Direct cost). This choice comes from the goal to provide an immediate economic measure of earthquake performance of the assessed structure. Indirect costs like downtimes, even if mentioned, are not explicitly considered in the analysis.

Global earthquake demand is defined in terms of peak ground acceleration (PGA), which represents the most commonly used entrance parameter for structural seismic analysis and design issues. Local engineering demand parameters (EDP) consist in more representative variables related to structural elements deformation or load, such as pier drift, bending moments, shear stress for examples. Damage states are expressed in terms of EDP limit values and associated

damage or repair amounts expressed in terms of percentage of structural quantities (concrete cracking surface and/or volume, percentage of broken or yielded reinforcement rebars, percentage of broken studs or rotation angle for example for what concerns CCB).

At the end, the ultimate goal is to evaluate the cumulative probability distribution function of the decision variables DV (cost and/or repair duration), as expressed by the PBEE framework Integral defined on Figure 2.82.

Most of those different successive analysis parameters and intermediate outcomes, result from the previous tasks, including numerical non-linear analysis and experimental evaluations. At each steps, results are addressed in terms of probabilistic quantities such as mean values, deviation or probability of exceedance (see previous paragraphs). Repair costs and duration databases are collected from different former projects, US and French repair data (see Deliverable 4.3 for further details). Additional (but rather sparse) data are also collected from road/bridges maintenance services concerning European recent « real field » seismic events such as Aquila earthquake.

Analysis preferentially focuses on direct costs related to structural damages, since indirect costs appears to be very depend on the context (country, location, proximity of big cities, economical/industrial activities, toll-roads) and are not directly related to SEQBRI project bridge typology and specificity (SCC bridges with CCB).

2.3.4.5.1 Direct cost evaluation

Direct cost evaluation is essentially based on repair quantities evaluated for different parts or elements of the structure for a given intensity measure or damage scenario and on associated unit repair costs. For this matter, the bridge system is disaggregated into individual components or ensembles, such as the columns or CCB, denoted as performance groups (PGs) that are damaged, assessed, and repaired together using a specific combination of different repair methods. Each of those performance groups is also sub-divided into individual elements or sub-PGs.

Different damage-states (DS) are defined for each performance group. A set of damage scenarios is defined for each SEQBRI case study bridge that corresponds to most probable events and relevant or representative combinations of damage states associated to the different performance groups, derived from numerical analysis or experimental tests.

2.3.4.5.2 Performance groups

Repair cost estimation (and loss modeling in general) is almost always a structural system problem, not simply determined at the component level. Therefore, it is often necessary to combine (sum) numerous scalar values in order to obtain, for example, a total cost. In the **SEQBRI** project, the problem of computing repair-related decision variables at the structural system level accounting for the correlations imposed by the selected repair methods is treated using the notion of Performance Groups. A Performance Group is a collection of discrete damage states, associated with different structural elements, correlated because they are affected by the selected repair procedure.

The tested SEQBRI case-study bridges are thus broken down into performance groups (PGs) for each major bridge component. Each performance group represents a collection of structural components that act as a global-level indicator of structural performance and that contribute significantly to repair-level decisions. Performance groups are not necessarily the same as load-resisting structural components. For example, non-structural components may also be a performance group, since they also suffer damage and contribute to repair costs. The PGs generally correspond to things that are observable as a unit. Grouping bridge components into performance groups allows for more meaningful damage assessment than grouping by component. The definition of the PGs used for the SCC bridges with CCB corresponds to the following structure disaggregation, which can be taken identical for all SEQBRI case studies. Five performance groups subdivided into a total of 84 sub-PGs have been defined for this study (foundations are excluded):

- **PG1: Piers (bottom)**: 1 performance group per pier, subdivided into individual columns for multi-column piers
- **PG2: Piers (top)**: 1 performance group per pier, subdivided into individual columns for multi-column piers
- **PG3: Concrete Cross beams** (specific elements of the analyzed bridge typology): 1 performance group per pier
- **PG4: Deck** (including concrete slab, steel girders and superstructures/equipment): 1 performance group per pier (associated tributary length, counted from mid-span to mid-span), subdivided into concrete slab (including asphalt layers and sidewalk), edge

(external) steel girders, central (internal) steel girders and non-structural elements (barrier rail)

- **PG5: Bearings**: 1 performance group per pier or abutment, including all bearings
- **PG6: Expansion joint and associated fuse blockouts at abutments**: 1 performance group per abutment

2.3.4.5.3 Damage States and associated repair methods and quantities

Each damage state corresponds to only one repair method. Selection of repair methods is a crucial step in computing the repair-related decision variable, repair cost ratios and repair time. A selection of repair methods specific for the damage states of the benchmark bridges has been stated (see Deliverable 4.3 for details). This selection is made based on Caltrans database (Mackie et al. 2008) of typical repair techniques, since it has been defined to be generalizable and usable for performance-based evaluation of other structures.

Each performance group contains a number of discrete damage states (DS) corresponding to repair quantities needed for restoring the bridge. The damage states are numbered from DS0 to DS3 with higher numbers indicating more severe damage. The DS0 damage state corresponds to the onset of damage when repair costs begin to accumulate. For analysis, the repair cost of the bridge is treated as 0 € below the DS0 level of damage. Damage beyond DS0 are needed to be repaired and costs begin to accumulate. Slight damage less than DS0 is assumed to be insignificant and not needing repair. Damage computation requires the definition of maximum possible repair quantities to define an upper limit to the quantities and costs. The upper limit is called DS∞, since it corresponds to the most severe possible damage state for the elements in a performance group. DS∞ usually corresponds to complete failure and replacement of all elements in the entire performance group, even sometimes leading to generalized collapse of the entire bridge structure.

Piers (PG1-bottom and PG2-top) based on maximum displacement

The performance of the bridge piers is quantified in terms of maximum displacement only since it can be assumed that maximum and residual displacement are generally linked or statistically correlated. Four damage states are defined for the piers in Table 2-21 together with the relevant repair items and quantities.

Table 2-21 Piers damage state definition and associated repair methods and quantities

	Damage state limit description	**EDP description median: drift ratio for limit state**	**Repair Method**	**Repair Item**	**Unit Computation**
DS0	Negligeable damage with initial cracking	Drift ratio associated with cracking moment Mcr	No repair	None	None
DS1	Cover concrete spalling	Δsp Equation from Berry and Eberhard (2003)	Seal cracks and minor removal and patching of concrete	Epoxy inject cracks (m)	2 x column height
				Repair minor spalls (m2)	10% x (surface area)
DS2	Longitudinal reinforcing bar buckling	Δbb Equation from Berry and Eberhard (2003)	Seal cracks, major patching	Re-center pier (per pier)	Re-center pier **(once max for both PG1 and PG2)**
				Epoxy inject cracks (m)	4 x column height
				Repair minor spalls (m2)	25% x (surface area)
DS3	Longitudinal reinforcing bar fracture	Δbf Equation from Berry and Eberhard (2003)	Replace half of column	Bridge removal, column (m3)	Total column gross volume / 2
				Structural concrete, bridge (m3)	Total column gross volume / 2
				Bar reinforcing steel, bridge (kg)	Total column gross volume / 2 x rebar weight ratio
				Temporary support, bridge (m2)	Tributary length x tributary width **(once max for both PG1 and PG2)**
				Structure excavation (m3) - **only for PG1 (bottom)**	0.90 m embedment, 1.20 m round the column
				Structure backfill (m3) - **only for PG1 (bottom)**	Same as structure excavation

Concrete cross beams (PG3)

Two damage states are associated to the concrete cross beams. The EDP is represented by the rotation of the end-plates of the joint. The left and right rotation of the end-plates of the joint have almost symmetrical fragility curves. The DS are listed in Table 2-22 where the associated repair method descriptions and repair quantities are summarized as well.

Table 2-22 CCB damage state definition and associated repair methods and quantities

	Damage state limit description	**EDP description: median rotation for limit state**	**Repair Method**	**Repair Item**	**Unit Computation**
DS1	Yielding	Rotation associated with yielding of the shear studs, based on section analysis	Seal cracks and minor removal and patching of concrete	Epoxy inject cracks (m)	1 x Beam length L (= Deck width)
				Repair minor spalls (m2)	10% x (lateral surface area)
DS2	Ultimate	Rotation associated with ultimate deformation of the shear studs, based on section analysis	Replace CCB	Bridge removal, portion (m3)	CCB gross volume
				Structural concrete, bridge (m3)	CCB gross volume
				Bar reinforcing steel, bridge (kg)	CCB gross volume x rebar weight ratio
				Shear studs (kg)	Total studs weight
				Temporary support, bridge (m2)	Tributary length x deck width

Deck concrete slab and superstructure (PG4-1)

The DS are represented by the bending moment correspond to the maximum strain of extreme fiber (or deformation), the concrete cracking, and yielding of top steel reinforcement; the EDP is expressed in terms of mean distance from the CCB where DS occurs (Table 2-23).

Table 2-23 Deck concrete slab damage state definition and associated repair methods and quantities

	Damage state limit description	EDP description: median distance from CCB	Repair Method	Repair Item	Unit Computation
DS0	No irreversible damage	median distance from CCB where DS occur	No repair	None	None
DS1	0.2mm cracking width	median distance from CCB where DS occur	Seal cracks, clean deck and apply methacrylate	Epoxy inject cracks (m) Clean deck for methacrylate (m2) Furnish methacrylate (lt) Apply methacrylate (m2)	unit cost
DS2	0.4mm cracking width	median distance from CCB where DS occur	Seal cracks, clean deck and apply methacrylate	Epoxy inject cracks (m) Clean deck for methacrylate (m2) Furnish methacrylate (lt) Apply methacrylate (m2)	unit cost
DS3	yelding of top steel reinforcement	median distance from CCB where DS occur	Seal cracks, clean deck and apply methacrylate	Epoxy inject cracks (m) Clean deck for methacrylate (m2) Furnish methacrylate (lt) Apply methacrylate	unit cost

Deck steel girders (PG4-2)

Two damage states are associated to deck steel girders. The EDP is represented by the bending moments associated respectively with local buckling or tearing and heavy damage (shear fracture, global instability...). Table 2-24 summarizes repair method and repair quantities for this PG.

Table 2-24 Steel girders damage state definition and associated repair methods and quantities

	Damage state limit description	EDP description: Bending moments which determine limit state	Repair Method	Repair Item	Unit Computation
DS0	Negligeable damage	Longitudinal: Transversal:	No repair	None	None
DS2	Local buckling or tearing	Longitudinal: Transversal:	Steel girder, repair	Welding additional steel plates (kg)	2% x tributary deck length x steel girder sections x 7850 kg/m3
DS3	Heavy damage	Longitudinal: Transversal:	Steel girder, replace	Replace steel girder (kg)	Tributary deck length x steel girder sections x 7850 kg/m3

Barrier rail (PG4-3)

A portion of the barrier rail is often replaced when there is anything more than a 10 cm offset anywhere along the length. Although offsets this small are not indicative of structural deficiency, the barrier rail is often replaced at this level anyway because of public perception. Two damage states are associated to barrier rail, corresponding respectively to 10% and 25% replacement along deck tributary length (Table 2-25).

Table 2-25 Barrier rail damage state definition and associated repair methods and quantities

	Damage state limit description	EDP description: median axial strain for limit state	Repair Method	Repair Item	Unit Computation
DS0	Negligeable damage		No repair	None	None
DS1	10% deck segment length damaged		Barrier rail, replace (m)		10% x tributary deck length
DS2	25% deck segment length damaged		Barrier rail, replace (m)		25% x tributary deck length

Bearings (PG5)

The bearing is what the deck rests on in a seat-type abutment or at pier locations. The bearing is typically made of elastomeric material. It is manufactured to undergo large displacement demands without degrading strength. Therefore, only a single damage state was provided that corresponds to the shear failure of the bearing (Table 2-26).

Table 2-26 Bearings rail damage state definition and associated repair methods and quantities

	Damage state limit description	EDP description: median shear strain for limit state	Repair Method	Repair Item	Unit Computation
DS0	No bearing yield:	Shear starin < 200%	No repair	None	None
DS2	Bearing failure:	Shear strain > 300%	Deck uplifting and repositionning + replace bearings	Normal damping rubber bearings (lt)	Total bearing volume at pier/abutment
				Deck uplifting (actuators)	2 x nb of bearings on the pier or abutment
N/A	No bearing on the pier under scope				

2.3.4.5.4 Damage scenarios

Cost and repair time data were collected using two damage scenarios representing a range of different damage states for each performance group and for the different cases studies, named respectively minor and major damage scenarios and representing the principal damages to the bridge structure. The damage scenarios do not correspond to a particular earthquake ground motion. Rather, they are designed to cover the range of damage state possibilities in order to refine the unit cost and repair time estimates used in the analytical decision model. Damage scenario that include the repair methods and repair quantities corresponding to the different performance group damage states can be derived from both analytical and experimental results

2.3.4.5.5 Loss analysis of SEQBRI bridges

In what follows the loss analysis of case study 2.1.2 is carried out in terms of repair cost ratio for different damage scenarios, according to section 2.3.4.5.4. The results for other case studies, are not reported here for brevity

Loss analysis of case study 2.1.2

The method has been effectively implemented in Excel and uses as input the unit repair costs for each damage state and the probability of exceedance of each damage state, for each IM. Subsequently, according to each damage scenario definition, the expected repair cost is evaluated as function of IM. In addition, the special formulation of the problem allows the disaggregation of this cost for the several Performance Groups. Finally, the probability of each scenario is provided along with overall expected repair cost conditioned to IM. The procedure has been applied to Case Study 2.1.2.

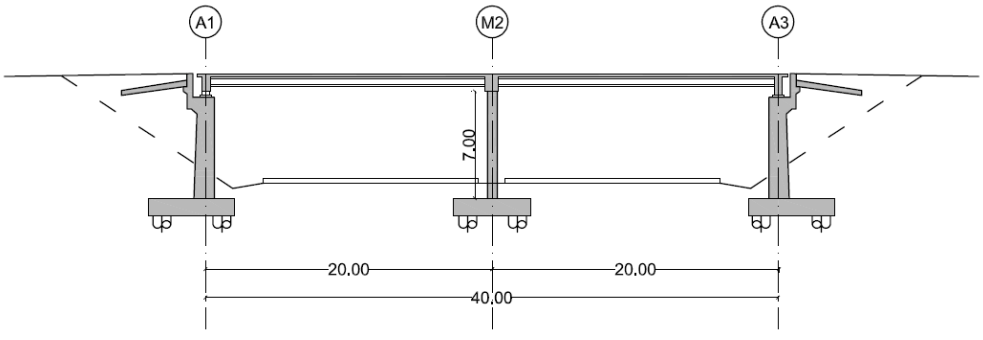

Fig. 2-144 Longitudinal section of the case study 2.1.2.

To compute repair quantities data about geometry, dimensions and materials of the structure are collected and reassumed in deliverable D4.3 (2014). Information about the bridge is subdivided into 4 major areas: Deck and Superstructure, Piers, CCB and Abutments. This subdivision is necessary to individuate the repairing items and, consequently, the performance groups. The evaluation of the expected repair cost of a structure as a consequence of a seismic event requires the identification of the elements (structural or finishing) whose damage and repairing item could

be significant. With this aim, the collapse mechanisms must be defined for each structural component together with the progressive damage states. Structural components are classified into performance groups according to the repair methods corresponding to their damage states. As stated in the previous paragraph, a Performance Group (PG) is a collection of discrete damage state associated with one or more structural elements. The damage states are defined by limit states conditioned on an engineering demand parameter (EDP). Fig. 2-145 shows the PG considered in the case study, whose description is reported in Table 2-27.

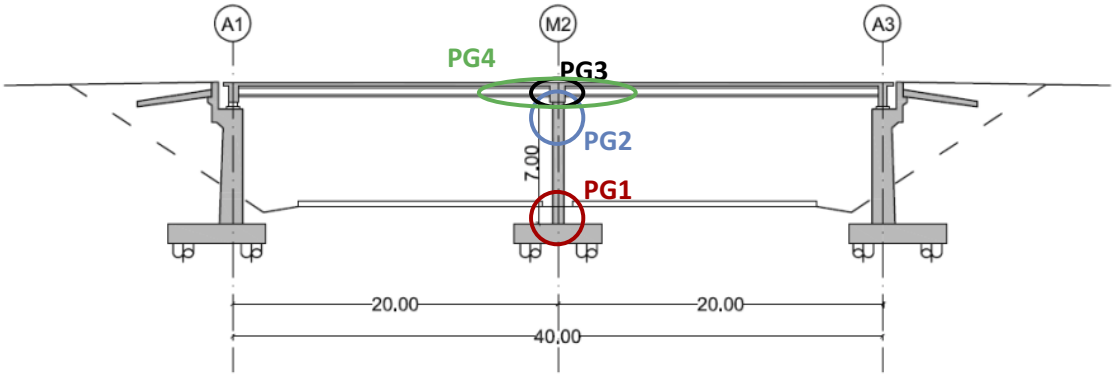

Fig. 2-145 Performance groups

Table 2-27 Description of the PG

Performance groups	
PG1	Bottom pier based on maximum displacement
PG2	Top pier based on maximum displacement
PG3	Cross beam
PG4	Deck

Four damage states are defined for the pier. Table 2-28 shows the DS description together with the associated EDP.

Table 2-28 Pier damage states (PG1 and PG2)

	DS description	**EDP description: median drift ratio for limit state**	λ **(median %)**	β (C.o.V.)
DS0	Negligible damage with initial cracking	Drift ratio associated with cracking moment M_{cr}	0.066	0.2
DS1	Cover concrete spalling	Δ_{sp} Equation from Berry and Eberhard (2003)	1.2	0.43
DS2	Longitudinal reinforcing bar buckling	Δ_{bb} Equation from Berry and Eberhard (2003)	3.8	0.25
DS3	Longitudinal reinforcing bar fracture	Δ_{bf} Equation from Berry and Eberhard (2003)	4.4	0.2

The repair methods associated to each DS and the relevant repair items and unit costs are listed in Table 2-29. Two DS are associated to the PG3 (Table 2-30), represented by the CCB. The EDP is the rigid end-plate rotation and the DS are the yielding of the shear studs (DS1) and the ultimate deformation of the same shear studs (DS2). The mean value and the dispersion of the yielding and ultimate slip have been evaluated based on results of experimental tests executed by several authors. The repair methods associated to each DS and the relevant repair items and unit costs are listed in Table 2-31.

Table 2-29 Pier repair methods and items (PG1 and PG2)

	DS description	Repair Method	Repair Item	Unit Computation	Unit cost
DS0	Negligible damage with initial cracking	No repair	None	None	
DS1	Cover concrete spalling	Seal cracks and minor removal and patching of concrete	Epoxy inject cracks (m)	2 x column height	560 €
			Repair minor spalls (m2)	10% x surface area	407 €
DS2	Longitudinal reinforcing bar buckling	Seal cracks, major patching	Re-center pier (per pier)	Re-center pier (once max for PG1 and PG2)	790 €
			Epoxy inject cracks (m)	4 x column height	560 €
			Repair minor spalls (m2)	25% x surface area	407 €
DS3	Longitudinal reinforcing bar fracture	Replace half of column	Bridge removal, column (m^3)	Total column gross volume / 2	209 €
			Structural concrete, bridge (m^3)	Total column gross volume / 2	183 €
			Bar reinforcing steel, bridge (kg)	Total column gross volume / 2 x rebar weight ratio	1-6 €
			Temporary support, bridge (m^2)	Tributary length x tributary width (once max for both PG1 and PG2)	328 €
			Structure excavation (m^3) - only for PG1 (bottom)	0.9m embedment + 1.2m round the column	15-26€
			Structure backfill (m^3) - only for PG1 (bottom)	Same as structure excavation	15-35 €

Table 2-30 CCB damage states (PG3)

	DS description	EDP description: median rotation	λ (median mrad)	β (C.o.V.)
DS1	Yielding	Rotation associated with yielding of the shear stud	0.593	0.12
DS2	Ultimate	Rotation associated with ultimate deformation of the shear stud	11	0.47

Table 2-31 CCB repair methods and items (PG3)

	DS description	Repair Method	Repair Item	Unit Computation	Unit cost
DS1	Yielding	Seal cracks and minor removal and patching of concrete	Epoxy inject cracks (m)	1 x beam length L (= Deck width)	560 €
			Repair minor spalls (m^2)	10% x lateral surface area	407 €
DS2	Ultimate	Replacement of CCB	Bridge removal, portion (m^3)	CCB gross volume	154 €
			Structural concrete, bridge (m^3)	CCB gross volume	183 €
			Bar reinforcing steel, bridge (kg)	CCB gross volume x rebar weight ratio	1-6 €
			Shear studs (kg)	Total studs weight	2 €
			Temporary support, bridge (m^2)	Tributary length x deck width	328 €

Four DS are associated to the PG4 (deck). The EDP is represented by the distance from the CCB where the DS occurs. The DS and their descriptions are listed in Table 2-32. The repair methods associated to each DS and the relevant repair items and unit costs are listed in Table 2-33.

Table 2-32 Deck damage states (PG4)

	DS description	EDP description
DS0	No irreversible damage	median distance from CCB where DS occur
DS1	0.2mm cracking width	median distance from CCB where DS occur
DS2	0.4mm cracking width	median distance from CCB where DS occur
DS3	yielding of the top steel reinforcement	median distance from CCB where DS occur

To evaluate the expected repair cost of a structure as consequence of a seismic event in a given reference time period, one or more damage scenario must be defined. Its definition, that considers repairing items more or less large, reflects a level of the intensity measure (IM) of the ground motion at the site. Two damage scenarios have been defined and described in Table 2-34 and Table 2-35.

According to the methodology developed in Deliverable 4.3 (2015), once the scenario has been defined its average cost can be calculated by summing the costs of the repairing items associated to each PG. Fig. 2-146 and Fig. 2-147 show $C_{TOT|IM}$ for both minor and major scenarios along with the expected repair cost disaggregated for PGs. From the results it clearly appears that PG1 (base of piers) contributes most to minor damage scenario expected cost at high value of the PGA, while peak contribution is from PG3 (cross beams) at lower values of PGA for the minor scenario and over the whole range of PGA for the major damage scenario.

From this curves it appears that the contribution for the minor damage scenario is mainly from epoxy inject cracks and repairing minor spalls, independently of earthquake intensity. For major damage scenario temporary support of the deck begins to rise rapidly as a contributing cost for higher intensities. In the analysis it also can be noted that one repair quantity can dominate because several performance groups require that item in the associated repair methods for that group.

The method has been finally applied to the case study showing that:

- Significant probability of occurrence of the minor damage scenario are due to 0.3g < PGA < 0.6 g;
- Significant probability of occurrence of the major damage scenario are due to PGA > 0.7 g;
- An overall expected repair ratio between 5-8% is obtained for the minor damage scenario and >20% for PGA > 0.2 g for major damage scenario;
- PG1, PG2 (pier) and PG3 (CCB) mainly govern the decision-making analysis given that their associated costs results particularly important. Therefore, any optimization action should act on these elements.

Table 2-33 Deck repair methods and items (PG4)

	DS description	Repair Method	Repair Item	Unit Computation	Unit Cost
DS0	No irreversible damage	No repair	None		
DS1	0.2mm cracking width	Seal cracks, clean deck and apply methacrylate	Epoxy inject cracks (m)	mean damage length	560 €
			Clean deck for methacrylate (m^2)	mean damage length x deck width	3 €
			Furnish methacrylate (lt)	mean damage length x deck width	20 €
			Apply methacrylate (m^2)	mean damage length x deck width	204 €
DS2	0.4mm cracking width	Seal cracks, clean deck and apply methacrylate	Epoxy inject cracks (m)	mean damage length	560 €
			Clean deck for methacrylate (m^2)	mean damage length x deck width	3 €
			Furnish methacrylate (lt)	mean damage length x deck width	20 €
			Apply methacrylate (m^2)	mean damage length x deck width	204 €
DS3	yielding of top steel reinforcements in the slab	Seal cracks, clean deck and apply methacrylate	Epoxy inject cracks (m)	mean damage length	560 €
			Clean deck for methacrylate (m^2)	mean damage length x deck width	3 €
			Furnish methacrylate (lt)	mean damage length x deck width	20 €
			Apply methacrylate (m^2)	mean damage length x deck width	204 €

Table 2-34 Minor damage scenario details

Performance Group	Damage State	Description
PG1 (Pier at base)	DS1	Seal cracks and minor removal and patching of concrete
PG2 (Pier at top)	DS0	----
PG3	DS1	Seal cracks and minor removal and patching of concrete
PG4	DS2	Seal cracks, clean deck and apply methacrylate

Table 2-35 Major damage scenario details

Performance Group	Damage State	Description
PG1 (Pier at base)	DS2	Seal cracks, major patching
PG2 (Pier at top)	DS1	Seal cracks and minor removal and patching of concrete
PG3 (CCB)	DS2	Replacement of CCB
PG4 (Deck)	DS2	Seal cracks, clean deck and apply methacrylate

Mean expected repair cost conditioned to IM associated with damage scenario costs by Performance Groups

Disaggregation of expected repair costs by Performance Groups

IM [pga (g)]	PG1: Piers (base)	PG2: Piers (top)	PG3: Cross Beams	PG4: Deck	Total	Repair Cost Ratio
0.1	0.0k€	- €	7.5k€	0.0k€	**7.5k€**	5%
0.2	0.3k€	- €	6.2k€	0.0k€	**6.5k€**	5%
0.3	2.1k€	- €	4.6k€	0.0k€	**6.7k€**	5%
0.4	4.9k€	- €	3.4k€	0.0k€	**8.3k€**	6%
0.5	7.4k€	- €	2.6k€	0.0k€	**10.0k€**	7%
0.6	9.0k€	- €	2.1k€	0.0k€	**11.1k€**	8%
0.7	9.7k€	- €	1.9k€	0.0k€	**11.6k€**	8%
0.8	9.8k€	- €	1.6k€	0.0k€	**11.5k€**	8%
0.9	9.4k€	- €	1.5k€	0.0k€	**10.9k€**	8%
1.0	8.8k€	- €	1.3k€	0.0k€	**10.1k€**	7%
1.2	7.4k€	- €	1.1k€	0.0k€	**8.5k€**	6%
1.4	6.3k€	- €	1.0k€	0.0k€	**7.3k€**	5%
1.6	5.4k€	- €	1.0k€	0.0k€	**6.4k€**	5%
2.0	4.2k€	- €	0.9k€	0.0k€	**5.1k€**	4%

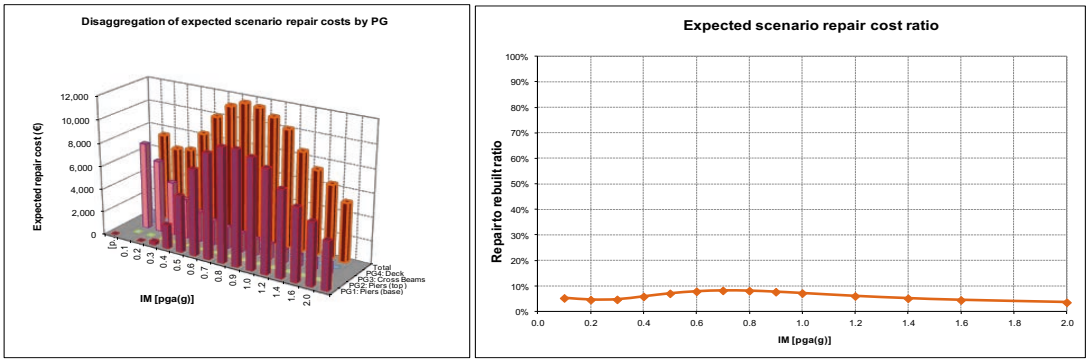

Fig. 2-146 Expected repair cost conditioned to IM for the minor damage scenario - Case-Study 2.1.2 (based on mean unit costs, from different sources)

Mean expected repair cost conditioned to IM associated with damage scenario costs by Performance Groups

Disaggregation of expected repair costs by Performance Groups

IM [pga (g)]	PG1: Piers (base)	PG2: Piers (top)	PG3: Cross Beams	PG4: Deck	Total	Repair Cost Ratio
0.1	0.0k€	0.0k€	3.6k€	0.0k€	**3.6k€**	3%
0.2	0.0k€	0.3k€	28.1k€	0.0k€	**28.4k€**	20%
0.3	0.0k€	2.1k€	59.1k€	0.0k€	**61.2k€**	44%
0.4	0.0k€	4.9k€	82.3k€	0.0k€	**87.2k€**	62%
0.5	0.2k€	7.4k€	97.7k€	0.0k€	**105.3k€**	75%
0.6	0.6k€	9.0k€	106.9k€	0.0k€	**116.5k€**	83%
0.7	1.3k€	9.7k€	112.0k€	0.0k€	**123.1k€**	88%
0.8	2.3k€	9.8k€	116.0k€	0.0k€	**128.1k€**	92%
0.9	3.4k€	9.4k€	119.7k€	0.0k€	**132.5k€**	95%
1.0	4.4k€	8.8k€	122.2k€	0.0k€	**135.4k€**	97%
1.2	6.0k€	7.4k€	125.8k€	0.0k€	**139.3k€**	100%
1.4	6.9k€	6.3k€	128.0k€	0.0k€	**141.2k€**	101%
1.6	7.4k€	5.4k€	128.9k€	0.0k€	**141.7k€**	101%
2.0	7.9k€	4.2k€	129.4k€	0.0k€	**141.4k€**	101%

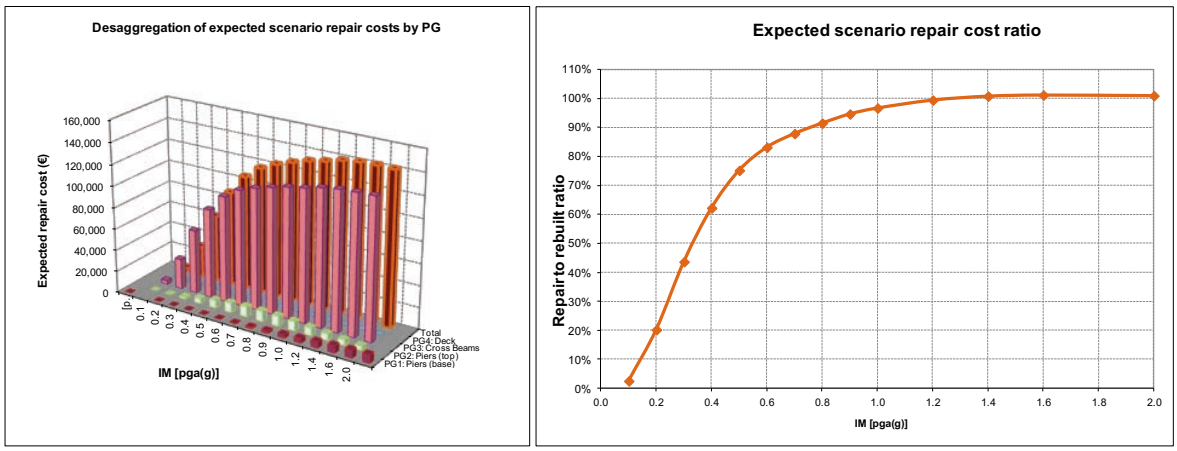

Fig. 2-147 Expected repair cost conditioned to IM for the major damage scenario in the example of case-study 2.1.2 (based on mean unit costs, from different sources)

2.3.4.6 Comparison between standard Eurocode 8-based and PBEE-based bridge design solutions (Task 4.6)

The contribution of **SEQBRI** on the design improvement of the SCC bridges with CCB has been done by the detection and comprehension of the vulnerable points of the deck-pier joint, through the experimental and analytical process, as well as the design guidelines proposed, which are resulted by a re-design focused on the joints. The verification of the advantages of the connection configuration with the prestressed bars (DOMI2) is a significant contribution of **SEQBRI** project towards the improvement of the seismic behavior of SCC bridges with CCB increasing both safety and construction simplicity. Finally, the integration of the MITKI (Chabrolin et al 2008) procedure for bridges in seismic prone areas along with the use proper component models appears an indubitable advancement with respect to a code-based approach. This has been fully proved through the PBEE methodology.

2.3.4.7 Comparison between SCC composite bridges and RC bridges based on prestressed concrete beams (Task 4.6)

Steel-concrete composite bridges in a PBEE framework have been rarely investigated in the past. Therefore, a comparison with the most frequent RC bridge typology is important to show the convenience in using the bridge typology proposed in the SEQBRI project. The definition of damage states for the two bridge solutions is different but consistent with the general definition of light, moderate and extensive damage.

For example, in Tubaldi at al (2009), the authors performed a parametric investigation on typical steel-concrete composite bridges. They observed that, differently from the most typical RC bridges, the performance of multi-span steel-concrete composite (SCC) bridges in recent seismic events has shown that these structures are very sensitive to earthquake loading. Extensive damage may occur not only in the substructures (piers), which are expected to yield, but also in the other components (e.g., deck, bearings, and abutments) involved in transferring the seismic loads.

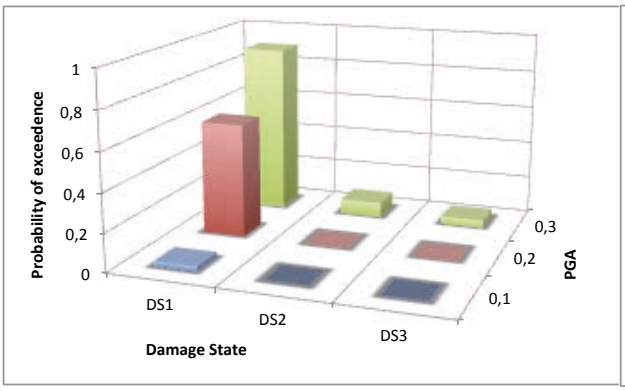

Fig. 2-148 Probability of exceeding different damage states (DS) in the pier MSC concrete beam) after Mackie & Stojadinovic (2008)

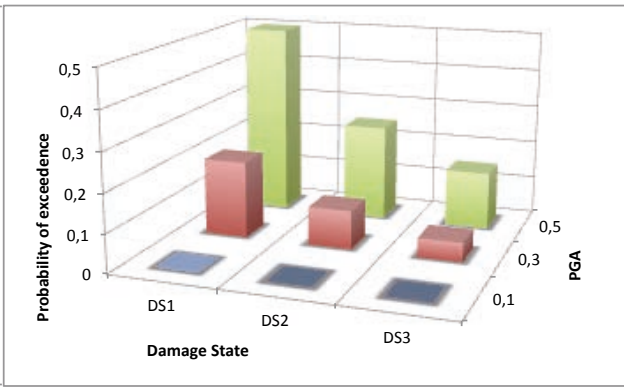

Fig. 2-149 Probability of exceeding different damage states (DS) in the pier (MSC concrete beam), after Nielson & DesRosches (2006)

In Nielson and DesRoches (2006), the authors analysed a large bridge portfolio, in which SCC bridges were included. The results show that the multispan simply supported (MSSS) and multispan continuous (MSC) steel girder bridges are the most vulnerable bridge types. This vulnerability is largely due to the steel fixed and rocker bearings typically used in these classes of bridges. However, MSC continuous steel girder bridges with pier-deck monolithic connection were not investigated, even though they represent 32% of the entire bridge stock of Central and Southern United States (First annual Report, 2013). Fig. 2-149 shows the probability of exceeding of the several damage states for three different seismic hazard levels, PGA=0.1, 0.3 and 0.5 corresponding to a probability of occurrence of the earthquake of 50%, 10% and 2% in 50 years.

In Borzi et al (2015) the vulnerability of a large portfolio of Italian bridges (485 bridges) has been analysed for DS2 and DS3 limit states. They observed that in Italy, most of the bridges along the roadway network were built in the 1960s and 1970s (Pinto and Franchin 2010), almost exclusively in reinforced (RC) or pre-stressed concrete. In spite of the rather simple seismic design regulations in force at the time (low, nominal forces with no capacity design provisions) the generally conservative bridge design practice resulted in a moderate seismic vulnerability against collapse observed in the last major events (from Irpinia 1980 to Emilia 2012). Lower degrees of damage, however, causing closure to general traffic and in some cases even to emergency traffic, were instead observed. A general large variability of probability of damage was observed, especially for the damage state DS3. The probability exceeding of a less severe damage state like DS2 resulted less dispersed, with PGA values confined in a range of PGA=0.1-0.3g.

The study of Moschonas et al (2009) focussed on the estimation of seismic fragility curves for all common bridge types found in modern Greek motorways. Among the analysed case studies, a RC bridge typology with monolithic pier-deck connection was analysed. No modeling of this detail was employed and the connection was considered, as in most of the cases, to be rigid.

The probability of exceeding the damage states DS1, DS2 and DS3 is plotted in Fig. 2-150 and Fig. 2-151 for two of the analysed bridges, both with three spans with length variable between 19 and 45m, with the employment of single or multi column piers. The bridges are particularly sensitive to slight damage states (DS1) with probability of damage greater then 60% for PGA=0.3g and 90% for a beyond-design level of PGA (0.5g).

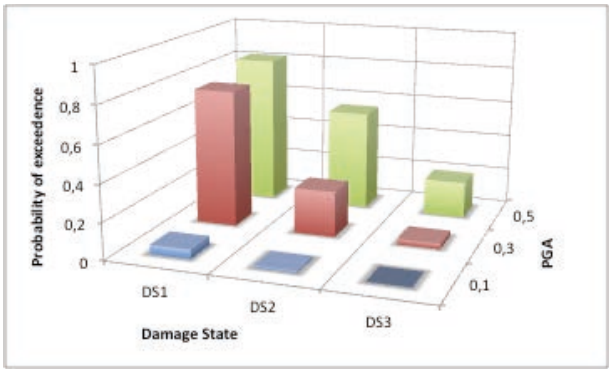

Fig. 2-150 Probability of exceeding different damage states (DS) in the pier of Siatista Bridge in Greece (MSC concrete beam with monolithic pier-deck connection), after Moschonas et al (2009)

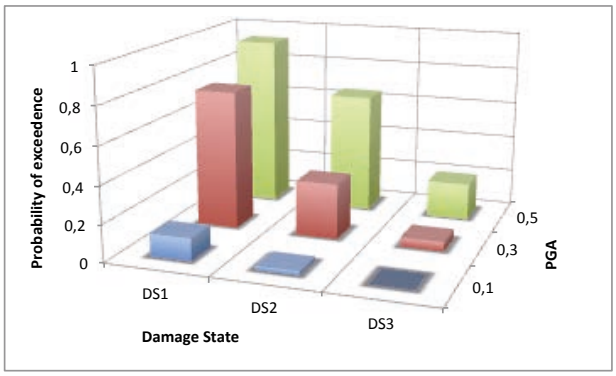

Fig. 2-151 Probability of exceeding different damage states (DS) in the pier of T7 bridge in Greece (MSC concrete beam with monolithic pier-deck connection), after Moschonas et al (2009)

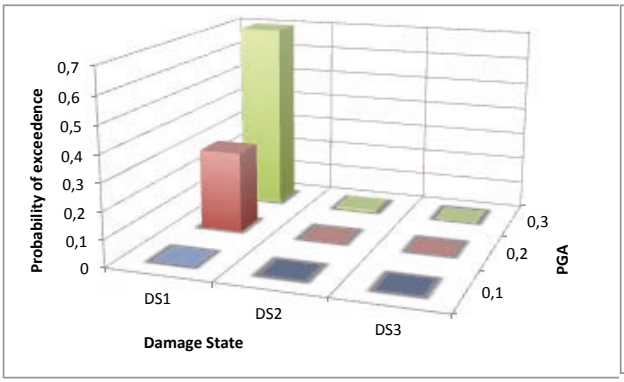

Fig. 2-152 Probability of exceeding different damage states (DS) in the pier (SEQBRI Bridges – CS 2.1.2

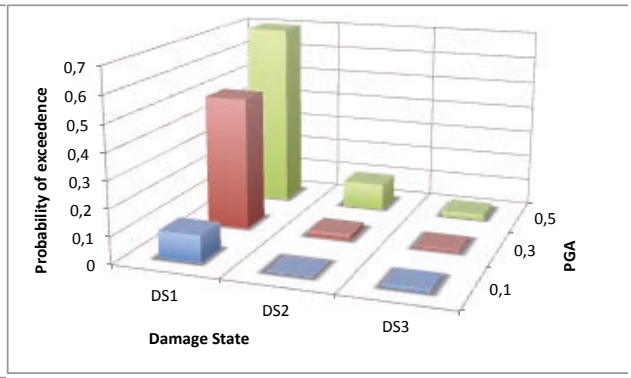

Fig. 2-153 Probability of exceeding different damage states (DS) in the pier (SEQBRI Bridges – CS 3)

Mackie and Stojadinovic (2008) evaluated the vulnerability of a set of RC bridges with a large investigation of the probabilistic seismic demand analysis using both Cloud and IDA analysis. Differently form the work of Nielson and DesRoches, they found the analysed stock of bridges (California highway overpass, single or multi bent, bridges,) less sensitive to the seismic action. In this respect, Fig. 2-148 shows the probability of exceeding the damage states for the considered three levels of seismic hazard. Only for PGA=0.5g the probability of exceeding DS2 and DS3 is of a certain importance, 8 and 4%, respectively. DS1 is instead attained with a probability of 60 and 90% for PGA=0.3g and 0.5g, respectively.

Concerning the SEQBRI bridges, Fig. 2-152 shows the probability of exceeding all damage states as function of PGA. The results are referred to CS 2.1.2, even though similar results have been obtained for the other typologies, despite the typology of piers and span lengths. Only for the CS 3 the probabilities were slightly higher (see Fig. 2-153). It can be observed that the probability of exceeding severe damage states (see DS3) is particularly limited (< 1%) for the two spans bridge and higher for the 6 spans bridge (2-10%). The probability of exceeding DS1 is instead particularly high for both the examined typologies (30% for PGA=0.3g and 60% for PGA=0.5g).

A synthesis of the above framework is illustrated in Fig. 2-154 where the probability of exceeding the damage states is plotted versus PGA, for different bridge typologies. The superiority of the SEQBRI SCC bridges is evident, at least in terms of probability of occurrence, and for any DS.

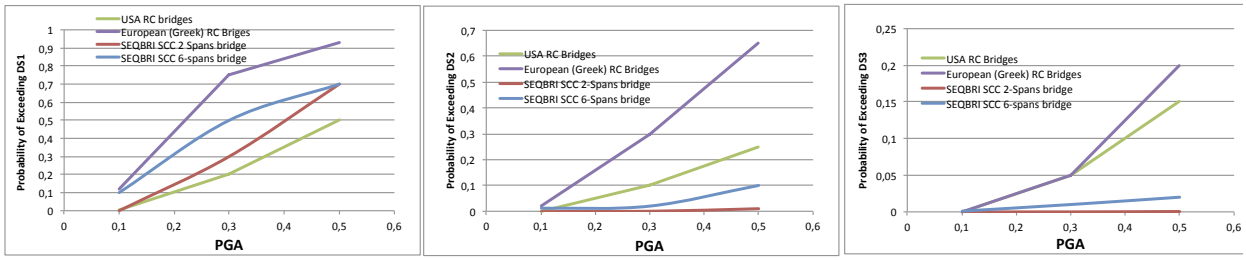

(a) (b) (c)

Fig. 2-154 Probability of exceeding different damage states (DS): Comparison between RC bridges (USA and EU) and SEQBRI SCC bridges. a) DS1, b) DS2, c) DS3 state.

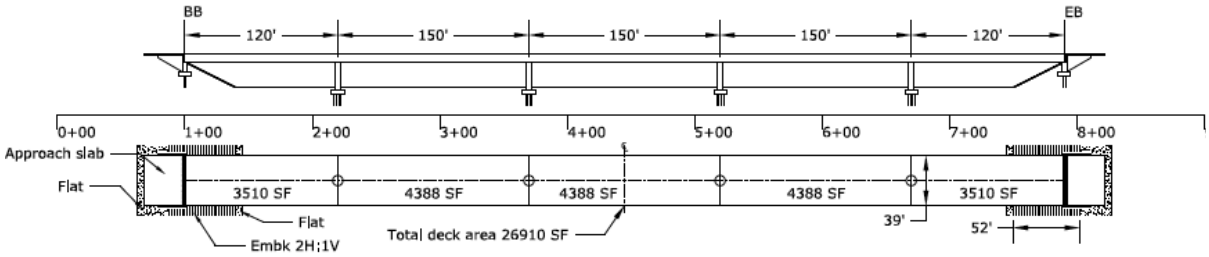

Fig. 2-155 Testbed bridge used for the RCR analysis in Mackie & Stojadinovic (2008)

From the design point of view, SCC bridges have the advantage of having reduced dead loads compared to the RC ones. A typical deck of a RC bridge has overall dead load (i.e. self-weight and superimposed dead loads) in the range of 22 to 25kN/m^2, while a typical SCC bridge from 13 to 15kN/m^2. This 40% reduction of the effective dead load of the bridge causes an almost proportional reduction of the induced seismic actions, which significantly affects the design of the whole bridge (i.e. piers, foundation etc).

To better appreciate the advantage of the SEQBRI SCC bridge typology, the application of the PBEE methodology to RC bridges has been performed. This application follows Mackie and Stojadinovic (2008), where the repair cost ratio (RCR) was calculated for a specific type of RC bridge (Fig. 2-155). The bridge is a 5-spans box girder bridge with length variable between 40 and 50 m. Two single column pier cases were considered, each with a different height h_1=7 and h_2=16m. For the comparison, only the first case is considered.

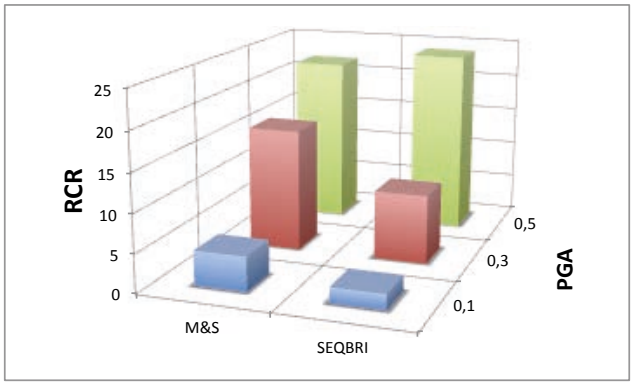

Fig. 2-156 Repair Cost Ratio: comparison between the testbed bridge used in Mackie & Stojadinovic (2008) and SEQBRI bridges (CS 2.1.2)

For the sake of brevity, Fig. 2-156 shows the comparison in terms of repair cost ratio performed on the testbed bridge by Mackie & Stojadinovic (2007) and on the SEQBRI bridges (CS 2.1.2). It is evident a certain advantage in using the SCC bridges, especially for low-medium seismic intensity. For example, for PGA=0.3g RCR is 9% for the SEQBRI bridge and 16% for the standard RC bridge. For the beyond-design PGA, the RCR is slightly higher for the SCC solution, i.e. 24% against 20%.

A useful comparison can also be made in terms of disaggregation of repair costs. For both the bridge typologies to hand, in case of low seismic intensity the major source of cost is related to epoxy injection and repair minor spall. Differently, for the major damage scenario, the temporary support of the deck begins to rise rapidly as a contributing cost for higher intensities. However, in the RC bridge it is necessary for the replacement of the columns whilst in the SCC bridge it comes from the CCB that needs to be repaired and partially replaced. In summary, for medium-to-high seismic hazard conditions (PGAs corresponding to probability of exceedance of 50% and 10% in 50 years) the SCC bridge typology clearly appears to be more convenient, saving more than 40% of costs with respect to the RC bridges solutions. Conversely, the SCC bridge solutions present similar repair costs for beyond-design seismic hazard conditions (PGAs corresponding to probability of exceedance of 2% in 50 years).

2.3.5 *Work Package 5: Issuing of design guidelines and recommendations for improving European seismic code for bridges.*

WP5 represents the finalization of the technical achievements of the **SEQBRI** project. In this respect, a contribution to a new generation of seismic codes for design bridges is provided and design guidelines and recommendation for the extension of Eurocodes have been developed.

The main objectives of WP5 are:

- Contribution to the foundation of a new generation of European seismic codes for bridges
- Issuing of design guidelines and recommendations useful to enhance Eurocodes
- Dissemination of project results.

An attempt to collect all the aspects of the Performance Based Earthquake Engineering (PBEE) methodology (Seismic Hazard, Modeling and Seismic Response Analysis, Damage Analysis, Decision Making analysis), is proposed, specializing them for the case of Steel Concrete Composite Bridges endowed with Concrete Cross Beam. All these aspects are presented in the form of guidelines to help code-writing bodies in implementing it in a new generation seismic code.

Given that PBEE methodology includes so many aspects that its full implementation in a new code requires time, some of the aspects of this new approach, and in particular some issues on the seismic design of SCC bridges with CCB are treated and design guidelines and recommendations are provided to help technicians to correctly design this bridge typology in seismic prone areas according to the current code-based approach. In doing this, the main outcomes of numerical and experimental activities developed in the previous WPs have been considered.

The activities of this WP concerning the first two objectives are presented in detail in Deliverable D5.1 (2016), whereas the dissemination results are included in Deliverables D5.2 (2016) and D5.3 (2016).

2.3.5.1 Contribution to a new generation of European seismic codes for bridges (Task 5.1)

In task 5.1 general performance-based provisions have been issued for seismic design of bridges according to the PBEE approach, whose response under common and extreme earthquake loads would comply, as demonstrated in Deliverable D4.3 (2015) with diverse needs and objectives of owners, users and society. On this basis, code-writing bodies could base the development of a new generation of European seismic codes for bridges.

In this respect, a brief overview of the PBEE methodology is provided and all the relevant aspects (Modeling issues, Seismic Hazard, Probabilistic response analysis, Damage and Fragility analysis, Loss analysis) have been specialized for the case of **SEQBRI** bridges. A comprehensive contribution toward this direction, but limited to the case of building, has already been provided by the American Technology Council (ATC 58-1, 2), recently included in a more recent documents

issued by FEMA (P-58-1, P58-2). In these two documents, generated after a long period of research and awarded by the Federal Emergency Management Agency (FEMA) to develop Next-Generation Performance Based Seismic Design Guidelines, all the above-mentioned aspects are specialized for the case of buildings. Unfortunately, similar documents have not yet published for the case of bridges for which only single cases have been analysed.

Even thought, many examples of application of PBEE methodology to Reinforced Concrete Bridges can be easily found in literature (Kunnath 2006), there are not examples of applications of PBEE to steel-concrete composite bridges (SCC) in literature. This is the main reason to propose the application of the PBEE method to SCC bridges.

Given that the bridge typology studied in SEQBRI project is very particular, because of the presence of a new solution that use a concrete cross beam (CCB) as connection element between deck and piers, the PBEE method is here specialized for this particular typology summarizing the following characteristic aspects of PBEE and how to apply them for the SEQBRI bridge typology

- Seismic Hazard Analysis
- Non-linear Modeling of SCC bridges with CCB
- Probabilistic Seismic Response Analysis and response fragility curves calculation
- Damage Analysis
- Loss Analysis

They are synthetized in Fig. 2-157, where the well-known PEER framework Integral is reported:

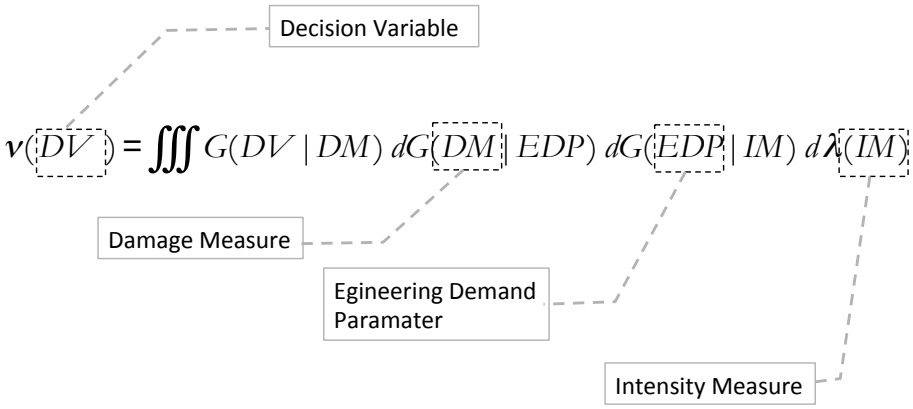

Fig. 2-157 The PEER Framework integral

On this basis, code-writing bodies could base the development of a new generation of European seismic codes for bridges. Deliverable D5.1 (2016) is dedicated to this, where all the aspects (modelling issues, Seismic Hazard, Probabilistic response analysis, Damage and Fragility analysis, Loss analysis) are explained and summarized.

All these aspects are then specialized for the case of Steel Concrete (SCC) Bridges with Concrete Cross Beams (CCB). To better explain each step, the most important results obtained have been developed for case study CS 2.1.2, leaving to further research activities the development of other case studies. The novelty of this approach is related to the fact that differently from a code-based approach the assessment/design is performed with the aim at explicitly evaluating the economic losses and the related probability of occurrence, rather than implicitly accounting for in predefined safety factors. In addition, this information in a form of repair cost ratio or any other decision variable can be utilized as a tool to communicate the design/assessment result to all stakeholders and take a decision about the goodness of the design. In SEQBRI project the main novelty stands in the definition of proper damage states for SCC bridges with CCB in seismic prone that have been never defined before. This definition has been fully supported by a wide numerical/experimental activity that allowed for a reliable calculation of damages and repair costs. All the identified steps have been developed in WP4 for the simple case study CS 2.1.2 to show the potentiality of the method.

2.3.5.2 Development of design guidelines and recommendations for extension of Eurocodes (Task 5.2)

The design approach of a steel-concrete composite (SCC) bridge with concrete cross beams (CCB) on reinforced concrete piers, exhibits many similarities with the one of the same bridge utilizing typical steel cross beams. The deck and pier design, in both cases, is performed according the standard provisions of the EN1993 for the steel girders, EN1992 for the r/c slab and EN1994 for the composite system. Regarding the earthquake design, the current EN1998 philosophy, in relation to the PBEE approach, is aiming to achieve the basic performance objective for certain levels of the design earthquake:

- prevention of structural and non-structural elements from any damage under frequent earthquakes
- limitation of the damage in non-structural elements (e.g. expansion joints) under occasional earthquakes (e.g. T_r=60 years),
- Life safe and prevention of the overall or partial collapse of the structure under rare and very rare earthquakes (i.e. $T_r \geq 475$ years).

However, when the design seismic action has a substantial probability of exceedance within the design life of the bridge, the design should aim at a “damage tolerant” structure. Parts of the bridge, susceptible to damage due to their contribution to energy dissipation, should be designed to enable the bridge to be used by emergency traffic, after the design seismic event, and to be easily repairable. Such kind of repairable damages are allowed to occur only in the piers, whilst the bridge deck shall be designed to avoid any damage, remaining within elastic range (EN1998-2). With these provisions, EN1998 is trying to control and localize the energy dissipation of the structure to specific areas (i.e. potential plastic hinges), and minimize the amount and the spreading of the expected damage and consequently to reduce economic losses due to downtime, repair costs etc.

The CCB and the connection detail between the reinforced concrete cross beam and the longitudinal composite girder constitutes the most crucial detail of the structure; this detail has to remain practically undamaged under the design seismic action, otherwise significant and hardly repairable damages inside the CCB body will occur. All the numerical results, which were carried out within the frame of SEQBRI, verified that the design of the case studies, which were based on the current Eurocodes, provided a high level of safety. For the cases with seismically isolated deck, no damages were exhibited at the structural elements, which remained elastic, at least under the design seismic action. What adjusts the level of structure’s overstrength is primarily the capacity of the isolation system, and secondary the capacity of the individual structural elements.

But even for the cases with monolithic connection between deck and pier, the results are quite encouraging. Up to the design seismic levels i.e. PGA≤0.30g, the critical part of the bridge is the piers, with the formation of a plastic hinge at their base, accompanied with bar yielding and cover spalling; significant probability of occurrence to obtain severe damages like bar buckling or bar fracture is expected at high seismic intensities (i.e. PGA>0.80~1.00g). On the contrary, the concrete crossbeam does not seem to be affected by any relevant damage at PGA ranges near the design one (i.e. 0.30g). Actually, the first level of damage in the intermediate CCB started to arise at PGA>0.50~0.60g, for which the lower group of shear studs within the CCB yielded.

In terms of repair costs, from the results of the loss analysis at case studies with integral connection between deck and piers, it is clearly shown that the significant probability of occurrence of the minor damage scenario is due to 0.30g < PGA < 0.60g, where an overall expected repair to rebuilt cost ratio is less than 10%. On the other hand, the significant probability of occurrence of the major damage scenario is due to PGA > 0.70g; for this level of PGA values, the overall expected repair to rebuilt cost ratio is more than 85%, while even for PGA > 0.30g repair ratio is more than 40%.

Combining all the above, it is concluded that it is much preferable for the designer to invest in the appropriate strengthening of the CCB and avoid damages, instead of trying to ‘optimize’ its design. Actually, the cost for such kind of strengthening is not important compared to the overall cost for the construction of the bridge, and moreover, it would be directly compensated by the lack of significant costs caused to damages in CCB after a major seismic event. The aim of damage minimization in the CCB can be achieved through two design approaches: either seismically isolating the deck or applying capacity design, providing to the CCB significant overstrength compared to the pier, even for systems with limited ductile behavior.

However, in order to do so, the designer should comprehend the vulnerable details of the CCB configuration. Towards this aim, SEQBRI experimental campaign provides valuable information on

the behavior of the CCB and its details under low-cyclic fatigue. Three different configurations of the steel girder-CCB connection were investigated; DIN-FB104-Variant C, and two new ones called DOMI-1 and DOMI-2 proposed by SEQBRI project (see detailed description at Deliverables D1.2, D5.1 and Mid-Term Report, 2014). In order to provoke significant damages to the CCB and extract its inelastic behavior, the piers of the test subassemblies were intentionally overdesigned to remain fully elastic during the tests.

According to the experimental results, the pattern of the damage development in the test subassembly joint is quite similar for the three variants:

(1) Onset of cracking in the slab (i.e. crack width ≤0.2mm) at a drift of 0.30~0.40%.
(2) Development of cracking in the slab (i.e. crack width 0.4mm) at drift of ~1.00%. This type of damage, is also caused by the bending moment distribution around the joint, is not affected by the type of connection and can be repaired with rather low cost.
(3) Onset of cracking in the pier at a drift of 1.00~1.20%. Up to this drift range, the behavior of the three CCB configurations is quite similar, and the level of the exhibited damage is acceptable and repairable.
(4) Onset of cracking in the CCB. The behavior of the three CCB configurations is starting to alter. DIN-FB104-C exhibits cracks in the CCB at a drift of 1.60%, lower than DOMI-1 with ~2.00%, and DOMI-2 with ~2.25%. The onset of cracking in the CCB is mainly imposed by the force flow within it, and is somewhat affected by the type of connection. From the design point of view, this level of damage for DIN-FB104-C and DOMI-1 configurations should be assumed as the ultimate accepted damage stage, as the exhibited damages can marginally be repaired without reconstruction of the CCB.
(5) Yield of bottom shear studs in the CCB and detachment of the head plate. Significant pull-out phenomenon and detachment of the head plate from the CCB are exhibited, due to the yielding of the bottom shear studs inside the CCB. Although, DOMI-1 configuration is locally underdesigned compared to the DIN-FB104-C (i.e. 8 bottom shear studs instead of 16, respectively), as it was not designed for significant tension in bottom flange, this type of damage is exhibited at similar levels of drift (i.e. 3.20% for DIN-FB104-C and 3.00% for DOMI-1). This underdesign could explain the reduced maximum force which was undertaken by DOMI-1 compared to the DIN-FB104-C (i.e. reduction in the order of 10%). However, from a practical point of view, both configurations should be assumed unrepairable, and need reconstruction at this damage stage. On the contrary, at DOMI-2 the bottom shear studs have been substituted by prestressing bars, which remain fully elastic, thus the only problem in this stage is the ongoing damage in the CCB, which however, still can be assumed as repairable.
(6) Buckling of steel girder's bottom flange. This type of damage occurred to all specimens (more pronounced to DIN-FB104-C and DOMI-1), though it was not expected, and other causes than imperfections at steel plates, have not been clearly identified. Such kind of damage must be avoided, because it induces significant deterioration of the structure's remaining stiffness and strength and furthermore its repair cost is too high. Fortunately, the buckling of bottom flange can be avoided very easily and with a negligible cost, if some local stiffeners (i.e. near the head plate) are foreseen.
(7) Failure of CCB. It was accompanied with extensive crack openings and significant detachment of the head plate (~9mm). It was exhibited at high levels of drift (i.e. 5.00% for DOMI-2, 4.15% for DOMI-1 and 3.80% for DIN-FB104-C). The severe cracks in the CCB are caused mainly to the bending moment distribution around the joint, and secondary to the connection variant. On the contrary, the detachment of the head plate is exclusively induced by the yielding/failure of the shear studs (i.e. irreversible damage at DIN-FB104-C and DOMI-1) or the elastic deformation of the prestressing bars (i.e. intended behavior of DOMI-2 configuration).

Concluding, given the intended elastic behavior of the piers, significant ductile inelastic behavior of the rest system and especially of the CCB was exhibited. High levels of drift were achieved (4%~5%), even though the damage levels at this stage are assumed irreversible. Variant DOMI-2 showed the most effective behavior, even for bridge types with monolithic connection between deck and pier, exhibiting no damage at the prestressing bars and reduced damages at the CCB, even at high drift levels. For cases where no or light tension is anticipated at the bottom flange near the CCB, DOMI-1 is might be preferable compared to DIN-FB104-C due to its simplicity.

Table 2-36 – CCB design procedure

Step 1	Geometry and material definition
Step 2	Joint configuration selection
Step 3	Definition of the design forces and moments acting on the joint by the composite beam cross-section and its support (e.g. pier or bearing)
Step 4	Definition of the joint internal forces
Step 5	Design of the additional reinforcing bars in the slab
Step 6	Design of the additional shear connection between slab-steel girder near the joint
Step 7	Design of the additional transverse reinforcement in the slab near the joint
Step 8	Resistance of fastening elements in the compression zone
Step 9	Resistance of the web fastening zone subjected to vertical shear V_{Ed} and to additional forces N_{ad} and M_{ad}
Step 10	Design of welding of the butt-plate
Step 11	Design of CCB reinforcements
Step 12	Fatigue resistance verification

Considering that there are no particular provisions to the existing codes for the design for such kind of connection, and taking into account the MIKTI project, and the conclusions reported previously, resulted by the various actions of SEQBRI project, a design procedure of the CCB-steel girder connection is proposed. A detailed description of the procedure is presented at Deliverable D5.1 (2015), whilst an outline of 11 steps is given herein. The provided guidelines are based on the three types of CCB investigated in SEQBRI Project (i.e. DIN-FB104-C, DOMI-1 and DOMI-2, where steps from 8 to 9 are particularized for each case), however they can be used with minor adjustment also to other CCB configurations.

2.3.5.3 Issuing of reports for the application of PBEE methodology to Case Studies (Task 5.3)

As demonstrated in the previous sections, PBEE methodology can be a very powerful and performant approach for seismic assessment of structures, by providing stakeholders with information about the structure (usually expressed in probabilistic terms) that facilitates informed decision making for risk management.

In **SEQBRI** project, results obtained from PBEE methodology applied to Case Studies for short-medium span I-girder bridges were summarized and organized in suitable formats, using fully interactive Excel spreadsheets (see Annex of Deliverable D4.3), on the same framework as the one defined by Mackie et al (2008). This type of format was preferentially chosen because of simplicity of use, because it allows easy parametric analysis (different possible assumptions on Damage States of different parametric groups), and because easy and explicit fast links between the different steps of the analysis for direct costs evaluation, from earthquake damage scenario and structure description, to repair costs and duration. Moreover, such tool can be very easily adapted by any designers to fit with any specific type of structure or analysis context.

The Excel spreadsheet tool is sub-divided into 7 different sheets: structure info & quantities, damage scenario, results and outcomes, detailed repair quantities, detailed expected repair costs, damage States definitions, and repair cost database. This makes it easy to capture the dependencies between pieces of information through the use of cell references, and makes the relation-ship between the successive steps of the loss analysis quite explicit.

Once unit repair costs are defined, along with detailed repair quantities associated with each damage states of individual elements and performance groups, the resulting repair amounts associated with the considered damage scenario are thus stored in the “Detailed repair quantities” sheet. This Repair Quantities table contains a view showing all the repair quantities and their corresponding costs for each

performance group at the assumed damage state for the chosen Damage Scenario. The expected repair cost associated with the assumed damage state of each performance group, conditioned to IM for the studied damage scenario is then obtained by summing the products of the repair items costs and the associated damage probabilities P(DS|IM).

In **SEQBRI** project the main decision variable adopted was the repair direct cost, expressed both in Euros (€) and repair to construction cost (in percent), because it provides an immediate economic measure of earthquake performance of the assessed/designed structure. However other decision variables mainly due to indirect costs like bridge closure downtimes, repair delay, human losses and crisis management or regional economical perturbations for instance, could also be analysed on the same format. The remaining capacity of the structure to function as intended, including different degrees of functionality (traffic volume, lane and speed reductions, or access for emergency vehicles) could also be an interesting loss criterion to be addressed.

Besides the already presented results expressed in terms of repair cost evaluation associated with a given damage scenario for a range of intensity measures (Mean expected repair cost conditioned to IM for each damage scenario), other interesting ways to present results can also be proposed, such as:

- The total repair cost associated with the different damage scenarios and probability of exceeding a given damage scenario conditioned to IM (fragility curves);
- The overall expected (probable) repair cost conditioned to IM

Minor damage scenario	
IM [pga (g)]	Probability of exceeding damage scenario conditioned to IM (fragility curve)
0.1	0.000
0.2	0.017
0.3	0.085
0.4	0.107
0.5	0.079
0.6	0.048
0.7	0.027
0.8	0.014
0.9	0.007
1.0	0.004
1.2	0.001
1.4	0.000
1.6	0.000
2.0	0.000
Major damage scenario	
IM [pga (g)]	Probability of exceeding damage scenario conditioned to IM (fragility curve)
0.1	0.000
0.2	0.000
0.3	0.000
0.4	0.000
0.5	0.003
0.6	0.012
0.7	0.030
0.8	0.053
0.9	0.078
1.0	0.097
1.2	0.114
1.4	0.113
1.6	0.105
2.0	0.086

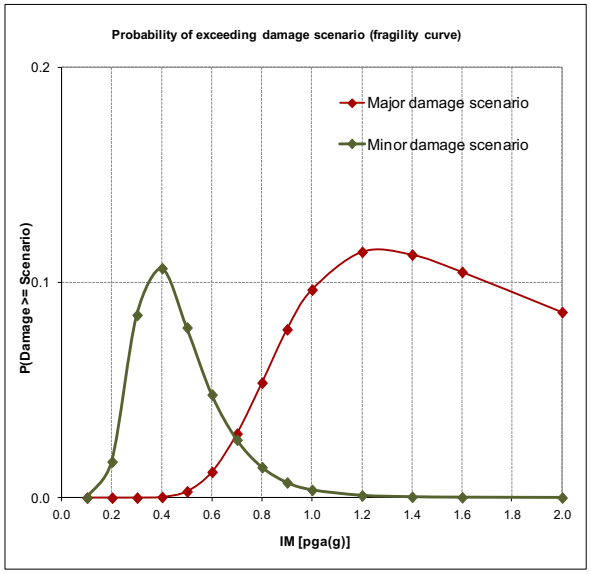

Fig. 2-158 Probability of exceedance of damage scenarios conditioned to IM (fragility curves) in the example of Case Study 2.1.2

The first one is evaluated by multiplying the individual probabilities $P(DS_{PGl}/IM)$ conditioned to *IM* of the PG_l to be in the relevant *DS* defined in the scenario (assuming that those probabilities are independent from each other):

$$P(\,Damage \geq Scenario / IM\,) = \prod_{l=1}^{N_{PG}} P(\,DS_{PG_l} / IM\,) \tag{2.16}$$

The second one is given by the following equation:

$$C_{tot-overall/IM} = \sum_{l=1}^{N_{PG}} \left(\sum_{n=1}^{DS} Q_{n,l}.P(\,DS_{PG_l} / IM\,) \right) \tag{2.17}$$

where the products of probabilistic distribution of the different damage states conditioned to intensity measure, *P(DS|IM)*, of each performance groups and the repair cost associated with each damage state of each performance group are summed over all possible damage states of all

defined performance groups. Probability of exceeding damage scenarios and overall repair cost ratio for CS 1.2.1 are presented in Fig. 2-158 and Fig. 2-159, respectively.

Performance-Based Earthquake Engineering (PBEE) implies assessment of a structure whose performance complies with objectives expressed by stakeholders (owner, user, and society). Implementation of PBEE in quantitative evaluation of the performance of a given structure is denoted here as Performance-Based Assessment (PBA). Performance-Based Design (PBD) is another implementation of PBEE that incorporates desired performance in the design of a new structure and they are usually optimization-based. In the context of PBD, various design methodologies have been proposed in the framework of structural optimisation with deterministic as well as probabilistic formulations.

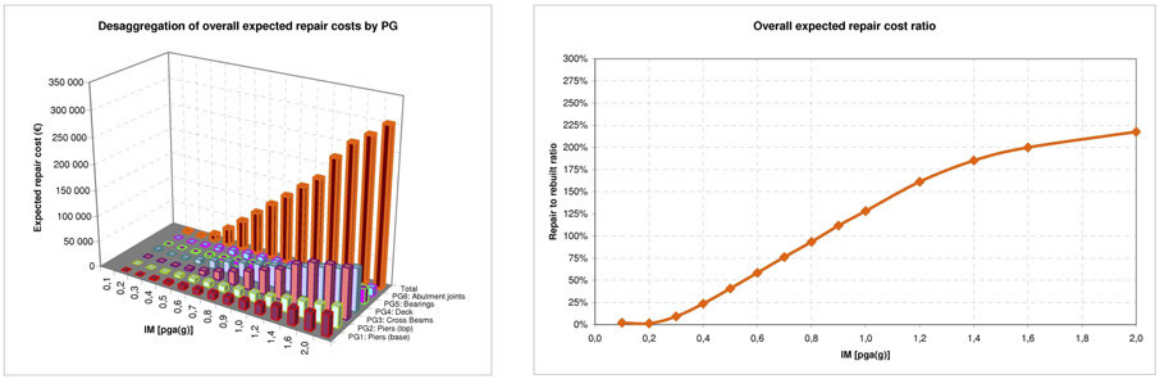

Fig. 2-159 Overall expected (probable) repair cost conditioned to IM and disaggregation by performance groups (based on mean unit costs, from different sources)

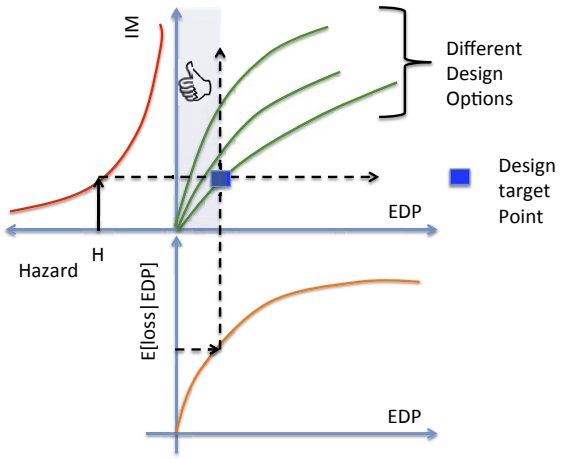

Fig. 2-160 Design Decision Support System after (Zareian et al 2009)

As a further step to the aforementioned design methodologies, life-cycle cost analysis has been also incorporated in the framework of PBD for assessing the various designs resulting from the optimization procedure. In all cases, computationally efficient optimization algorithms are usually incorporated in order to achieve fast convergence to the optimum. According to the above-mentioned framework, two possible approaches could be adopted: a) Performance-based design based on deterministic objectives, b) Performance-based design based on vulnerability objectives.

Given the general complexity that involves the second approach, the deterministic approach is generally preferred. In this approach, the main part is the definition of the deterministic performance objectives. A deterministic performance objective is defined as a desired target level of decision variables (DV) that corresponds to a specific hazard level. In this context the proposal formalized by Zareian and Krawinkler (2009), called *Design Decision Support System*, could be an example of attractive and applicable methods to the case of SEQBRI type of bridges. The proposal

is summarized in Fig. 2-160. This approach is beyond the scope of **SEQBRI** Project and will be developed in further studies.

2.3.5.4 Dissemination of project achievements (Task 5.4)

The transfer of knowledge and expertise achieved during the course of the SEQBRI project was attained through a round table, as well as dissemination of documents and other information through a dedicated webpage, developed and maintained for this purpose.

This dissemination of projects achievements is by nature susceptible to interest any potential bridge engineering owners and designers both at the European and at Worldwide level as well as representatives of key organisations/institutions, industry and technical associations.

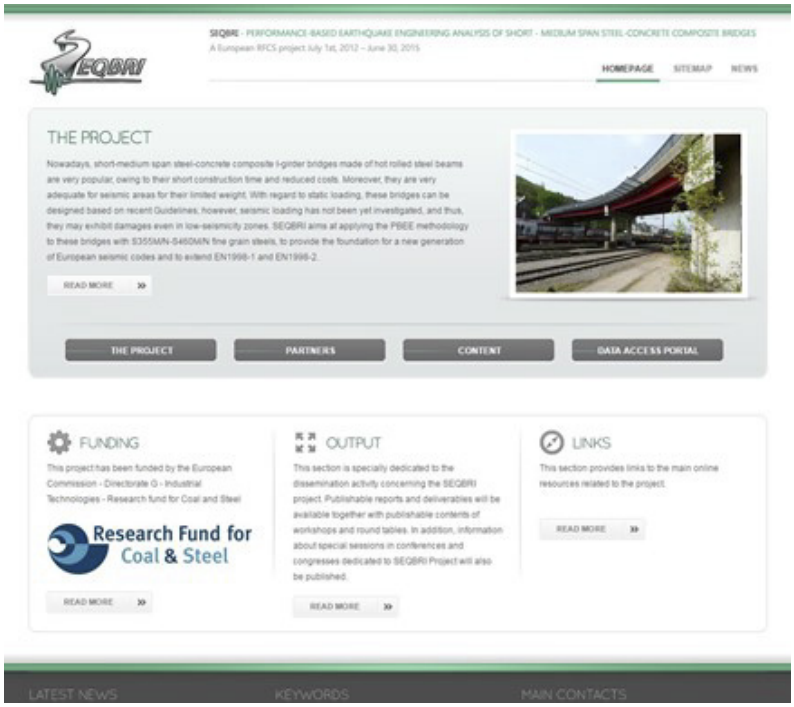

Fig. 2-161 Homepage of the SEQBRI website, www.seqbri.it

The round table was organized at Ministry of Ecology, Sustainable Development and Energy, at La Defense business district Paris, France, on Wednesday 17th June, 2015. The discussions objective was to provide a clear overview of the research activities carried out during the three years and the main goals achieved. The event was subdivided in five sessions, each one dedicated to a specific aspect of the problem and the research activities performed. Two moments of discussion with external experts (Prof. Tatjana Isakovic - Faculty of Civil and Geodetic Engineering, Ljubljana, Slovenia and Dr. Daniel Bitar - Centre Technique Industriel de la Construction Métallique – France) were organized, during which experts were invited to express their opinion about the main achieved results. The documents presented during this day by the partners of the project [**APRL, RWTH, DOMI S.A., CEREMA, UNITN, UNIRM3**] are available under request for download on the SEQBRI website (www.seqbri.it). They present main experimental and numerical results as well as technical reports.

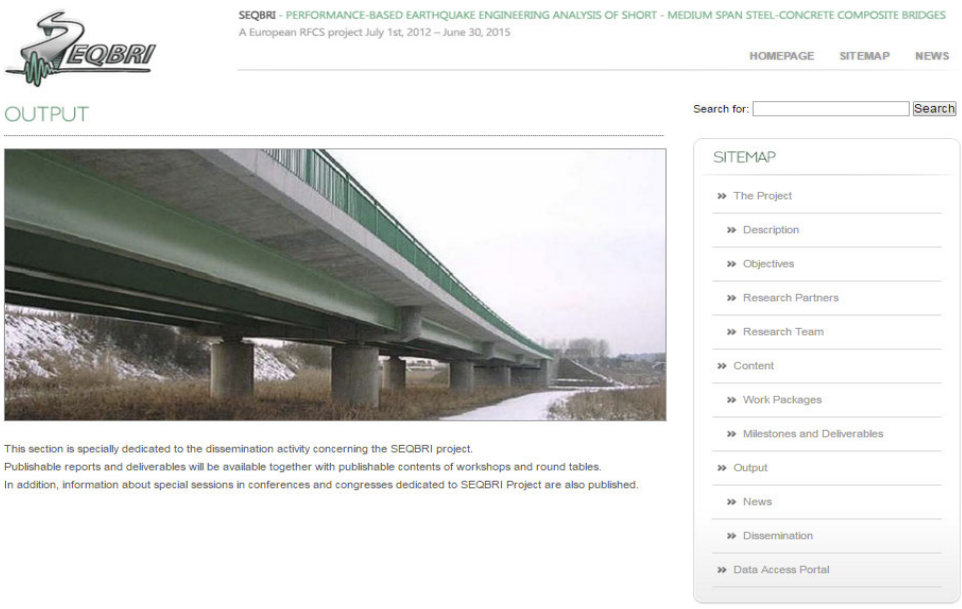

Fig. 2-162 Dedicated webpage for the dissemination of project results

2.3.6 *Work Package 6: Project coordination and management*

The main objectives of the WP6, as described in Tasks 6.1, 6.2, 6.3 and 6.4 were to establish an efficient management process, to define standard protocols, to carry out both a SWOT evaluation and the monitoring of activities of the project, towards successful completion.

2.3.6.1 Establishment of an efficient management process (Task 6.1)

SEQBRI project comprises several partners and specific objectives. The coordinator (Roma Tre University) has been responsible to manage the project activities to complete successfully on time. In order to manage the project work certain necessary steps were taken.

(a) The representatives of each partner meet once in approximately every almost six-month for work-progress, discussing the technical issues of the project, and planning the next activities. The meetings were provided an opportunity for formal discussion in detail among partners. Seven meetings were held among partners of the project during the period of concern, i.e. 01 July 2012-30 June 2015.

(b) Roma Tre University created a Drobox folder. Each partner could access this directory downloading and uploading necessary information and documents related to the project work, i.e. research papers, thesis report etc., the agenda and minutes of the meeting, experimental as well as simulation data and reports. This provides an efficient distribution of the urgent and necessary information helpful to the progress of the project.

(c) A website of the **SEQBRI** project (www.seqbri.it) was created by the Roma Tre University, to disseminate the results of the project.

(d) The coordinator and all the partners were in regular contact via e-mail. The necessary issues were also discussed by using phone or Skype. E-mail was the communications medium that was used at the large and preliminary scale. If more than two partners were involved in discussion, teleconferencing was used.

2.3.6.2 Definition of standard protocols (Task 6.2)

In the course of **SEQBRI** project, the coordinator, together with partners, set standard protocols for the tests regarding specimen order/manufacturing and test performance. SEQBRI project involved several types and number of laboratory tests to be performed by the different partners. It is necessary, in this situation to follow a common set of procedures to prepare the tests. This reduces the discrepancy in the test results as well as increases the efficiency. The following steps have been taken in this respect:

- The same company was employed to build the specimens in order to obtain the desired quality and homogeneity
- The same procedure to test all specimens were adopted
- A similar data analysis procedure was adopted to obtain as much as possible comparable results

2.3.6.3 SWOT evaluation of the project (Task 6.3)

A SWOT analysis must first start with defining a desired end state or objective. A SWOT analysis may be incorporated into the strategic planning model.

- Strengths: attributes of the person or company that are helpful to achieving the objective.
- Weaknesses: attributes of the person or company that are harmful to achieving the objective.
- Opportunities: external conditions that are helpful to achieving the objective.
- Threats: external conditions, which could do damage to the objective.

Identification of SWOTs is essential because subsequent steps in the process of planning for achievement of the selected objective may be derived from the SWOTs.

First, the decision makers have to determine whether the objective is attainable, given the SWOTs. If the objective is not attainable a different objective must be selected and the process repeated.

The SWOT analysis is often used in academia to highlight and identify strengths, weaknesses, opportunities and threats. It is particularly helpful in identifying areas for development.

If, on the other hand, the objective seems attainable, the SWOTs are used as inputs to the creative generation of possible strategies, by asking and answering each of the following four questions, many times:

- How can we use and capitalize on each Strength?
- How can we improve each Weakness?
- How can we exploit and benefit from each Opportunity?
- How can we mitigate each Threat?

Ideally a cross-functional team or a task force that represents a broad range of perspectives should carry out the SWOT analysis. For example, a SWOT team may include an accountant, a salesperson, an executive manager, an engineer, and an ombudsman.

SEQBRI Project- SWOT Analysis

The concept of determining strengths, weaknesses, threats, and opportunities is the fundamental idea behind the SWOT model. To present the model in a more understandable way, scholars came up with so-called SWOT matrix. SWOT matrix is only a graphical representation of the SWOT framework, shown in Fig. 2-163.

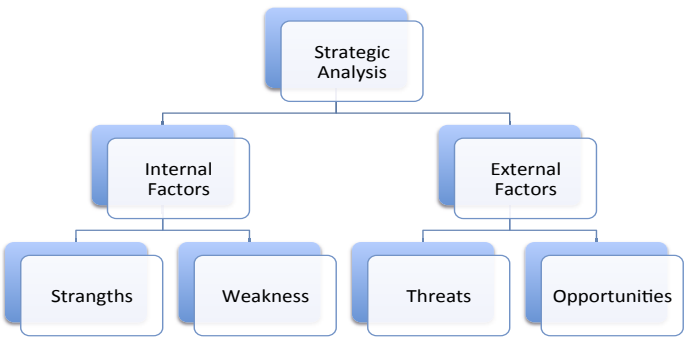

Fig. 2-163 SWOT Matrix

The SWOT analysis of the SEQBRI project is as follows:

1. Strengths

1. **University-Industry partnership:** The working partners of **SEQBRI** project belong to universities (UNIRM3, UNITN and RWTH), industries (APRL), Designer (DOMI) and a center of excellence in infrastructure and transport engineering (SETRA). This enabled a better exchange of theoretical and practical knowledge and experience.
2. **Earlier experience on similar (European) projects:** Most of the partners of the SEQBRI project had already been involved in European projects, so it was easier for them to understand and to adopt the EC guidelines, rules and regulations.
3. **All partners located in Europe:** All the partners of SEQBRI project are located in Europe, so it is easy for them to communicate and to meet efficiently. They have almost similar work schedule and work culture. This smoothens the overall work process.
4. **Partners specialized in their work area:** The different partners of SEQBRI are highly specialized in their fields, for e.g. APRL is specialized in steel constructions, DOMI is specialized in bride design and SETRA is specialized in infrastructure and transport engineering. This increases reliability of results of the project.
5. **Innovation: SEQBRI** project is aimed at working on the investigation of the seismic capacity of a new type of composite concrete-steel bridge. This field has not been explored enough, and the **SEQBRI** project aimed to explore it. The partners were motivated to work in the new area.
6. **Selection of case studies:** Several case studies were chosen (straight and skew, 2-span and multi-span bridge) with the aim at giving the opportunity to study the seismic behaviour of this new type of bridge.
7. **PBEE as new assessment/design method:** A new assessment method, based on PBEE method, is proposed for the typology of bridges analysed. The method is not yet widespread in Europe.
8. **New guideline:** At the end of the **SEQBRI** project new guidelines for this new type of bridge have been provided.
9. **Synergy:** Working on the seismic behaviour of this new type of composite bridge will establish synergy between partners with different professionality.
10. **Most of the tests performed:** Most of the experimental activities are completed.

2. Weaknesses

1. **Many-Partners:** SEQBRI project involves many partners. It puts a big challenge on efficient co-ordination among the partners.
2. **Delay in tests:** Due to the delay in the delivery of specimens to the partners, some of the tests were not completed on time according to the bar chart. The test data are the prerequisite for the validation of numerical models.

3. Opportunities

1. **Gain in experience**: The SEQBRI project offers several kinds of experience to the working partners. Working on the composite steel-concrete bridge they will build their own confidence toward the use of this new type of composite bridges in seismic prone areas. Apart from technical experience, it offers an experience to work in a team for a single objective.
3. **Round table**: During the round table, discussion related to the seismic behaviour of this new type of bridge, has attracted interest of scientific community and bridge designers.
4. **Publications:** Many conference papers and journal papers were submitted and/or published.

2. Threats

No specific threats were identified.

2.3.6.4 Monitoring of activities of each research unit (Task 6.4)

The monitoring of activities of each research unit was regularly performed through the co-ordination meetings. Seven meetings were held among partners of the project during the period of concern, i.e. 01 July 2012-30 June 2015.

In the kick-off meeting in Esch sur Alzette, Luxembourg, on 2-3 October 2012, the objectives of the project was recalled together with the distribution and content of the work in different WPs related to the concerned period.

The second meeting was held in Sourdun, France, on 31 January – 1 February 2013. During the meeting, the case studies were chosen and the I-girder subassemblies to be tested, were selected. Mechanical characterization and low-fatigue modelling of fine grain steels adopted for I-girder subassemblies was proposed and a preliminary discussion on design and construction of I-girder specimens was started. Finally, seismic design of case studies according to Eurocodes was discussed.

The third meeting was held in Rome, Italy, on 4-5 July 2013. During the meeting, testing protocols for I-girder subassemblies to test in the Laboratory of the University of Trento and Roma Tre University were defined. Some issues on the selection of seismic input for PBEE were also discussed.

In the fourth project meeting, was held in Rome, Italy, on 3 October 2013, a review of specimen typologies to be tested was made. Overall dimensions of the mock-ups, local details of each mock-up (reinforcement, shear studs, etc..) and test setup were discussed.

In the fifth project meeting, was held in Trento, Italy, on 20-21 February 2014, the monotonic and cyclic fatigue test results for the mechanical characterization of fine grain was presented and discussed. Preliminary results of the FE-modelling of I-girder subassemblies were presented and the application of the PBEE methodology to selected Case Studies was discussed.

In the sixth meeting, was held in Athens, Greece, 06-07 November 2014, the design and the construction (details about stages of construction and instruments) of I-girder subassembly specimens in transversal and longitudinal directions were presented. The results of the experimental tests in Transversal direction were presented. Preliminary results of tests in longitudinal direction were also discussed. A preliminary discussion of WP5 concerning issuing of design guidelines and recommendations for improving European seismic code for bridges was started.

In the last project meeting, was held in Paris, France, on 16-17 June 2015, the experimental results were discussed and the remaining tests were recalled and discussed. The simulation results were also discussed. Finally, the format of the draft final report and contents of the design guidelines were presented and discussed.

Roma Tre University created a Dropbox server directory. Each partner can access this directory and download and upload the necessary information and documents related to the project. The documents related to the project work, i.e. research papers, thesis report etc., the agenda and minutes of the meeting, reports are uploaded on the server. This provides an efficient distribution of the urgent and necessary information helpful to the progress of the project.

The coordinator and all the partners were in regular contact via e-mail. The necessary issues have also discussed by phone. E-mail is the communications medium that is used at the large and the fast level. A website, properly dedicated to the project was created (Fig. 2-161, Fig. 2-162).

Publications/conference presentations were produced; in greater detail, 1 paper was submitted on a reputed international journal; 3 papers under preparation; 5 papers presented on international conferences.

Finally, the following reports have been prepared and uploaded to CIRCABC:

1. 1st annual report March 2013.
2. Mid-Term report March 2014.
3. 2nd annual report March 2015.
4. Final report March 2016.

The deliverables of the project have also been uploaded to CIRCABC. In addition, minutes of each meeting have been held, and are available upon request.

2.4 *Conclusions*

THE **SEQBRI** project dealt with the full application of the next-generation Performance-Based Earthquake Engineering methodology (PBEE) employed for the assessment of a new type of steel concrete composite (SSC) bridges endowed with a special pier-to-deck connection (Concrete Cross Beam).

Expertise in earthquake and mechanical engineering, transportation and infrastructure engineering, steel constructions and design of bridges allowed to fully develop the PBEE framework through a wide experimental and numerical investigation for a reliable definition of numerical models, damage states and repair actions and costs.

The development of the PBEE framework for SCC bridges can be considered a novel contribution to the foundation of a new generation of earthquake engineering seismic codes for bridges in Europe. However, given that it will need time to be fully employed in a code, it has been used to improve current codes with some integration that could help technicians in designing SCC bridges with CCB in seismic prone areas, for which specific guidelines have been developed. The results and deliverables are both novel and unique. In particular, they entail:

- ✓ A better understanding of the seismic behaviour of SCC bridges with CCB
- ✓ A reliable definition of limit states for this new type of bridges
- ✓ A proposal of a decision-making tool based on next-generation PBEE methodology for SCC bridges with CCB in moderate/strong seismic prone areas.
- ✓ A significant improvement of seismic design state-of-the-art of SCC bridges with CCB, through the development of design guidelines for improving Eurocodes for the assessment of bridges in seismic prone areas.
- ✓ A contribution to the foundation of a new generation of seismic engineering codes for SCC bridges

In summary, the comprehensive experimental and numerical investigation performed during The **SEQBRI** project allowed to bring out the excellent behaviour of SCC with CCB under seismic action. This has been proved by the fact that significant mean damages start only for PGA>0.25g, and in particular at the bottom section of bridge piers. Furthermore, damages in CCB are exhibited only for PGA > 0.5g (initial cracking), whereas collapse conditions due to the rupture of piers and CCB occurred only for PGA > 1.2g. This is a clear demonstration of the earthquake-proof behaviour of small-medium span SCC bridges with CCB. It has also been demonstrated that the use of CCB in small-medium span SCC bridges appears highly favourable and represent an economic, fast and reliable way to realize an efficient pier-to-deck connection for SCC bridges in seismic prone areas.

It is recalled that these results have been carried out applying the PBEE methodology for assessing the seismic behaviour of SCC bridges with CCB designed in accordance with Eurocodes, which clearly demonstrate the role of Eurocodes in obtaining safe and robust bridges. It has also been demonstrated that a more efficient design could derive from the application of the PBEE as design decision support system, even though the applicability by practitioners appears of a certain complexity and requires more studies and dissemination. The issue of a specific report on the applicability of PBEE to small-medium span SCC bridges with CCB will certainly help the designers to fully understand the basic ingredients of PBEE and how this tool can provide stakeholders with information that facilitate decision making for risk management. This report offers a contribution for a new generation of seismic engineering codes.

It is evident that the application of this complex framework can be totally justified only when important damage conditions are expected and for which the adoption of non-linear models and probabilistic analyses appear justifiable. Given the fact that small-medium SCC bridges with CCB exhibit in mean important damage conditions only for PGA > 0.25 g, it appears reasonable to employ the PBEE methodology only for PGA values of 0.35g or greater. These PGA values characterize the most active prone-areas in Europe. For lower PGA values the design approaches to be adopted can rely on current design approaches prescribed by Eurocodes, where partial safety factors cover aleatory uncertainties. In sum, no specific rules are provided by Eurocodes to design CCBs, so, the design procedure proposed in the **SEQBRI** project can be profitable used.

2.5 *Exploitation and impact of the research results*

The main outcomes of SEQBRI project have been the development of design guidelines and recommendation for the seismic design of SSC bridges with CCB and the provision of a contribution to a new generation of seismic engineering codes in Europe.

Those guidelines have been developed in close cooperation with end-users partners (DOMI SA, ARCELOR MITTAL, CEREMA) and are expected to contribute significantly in a reliable seismic design of SCC bridges with CCB.

Furthermore, the scientific research on this topic and associated with experimental and numerical work in research laboratories of partners (UNIRM3, UNITN, RWTH), has significantly improved the know-how at the international level. The high quality of the research reflected in the numerous scientific publications of the research group, which will rapidly increase during the next year, especially in high ranked journals.

As a result, it is believed that all the research work conducted in **SEQBRI** has been novel and innovative, and will have a significant impact in both the scientific and the professional community.

2.6 Acronyms and Abbreviations

Symbol	Meaning
C	Cost
CCB	Concrete Cross Beam
CDP	Concrete Damage Plasticity
CS	Case Study
d_c	Damage Variable in Compression
DM	Damage Measure
DS	Damage State
d_t	Damage Variable in Tension
DV	Decision Variable
E	Young Modulus
EDP	Engineering Demand Parameter
eps	flow potential eccentricity
f_{bo}/f_{co}	invariant stress ratio
IM	Intensity measure
$\lambda(IM)$	rate of exceeding of IM
LC	longitudinal component
PG	Performance Group
$PSHA$	Probabilistic Seismic Hazard Analysis
RCR	repair cost ratio
SCC	Steel Concrete Composite
TC	Transversal Component
ν	Poisson ratio
$\nu(DV)$	rate of exceeding of DV
$w_{t,c}$	recovery factor in tension/compression
ψ	dilatation angle
μ	Mean
σ	Variance
θ	Rotation of one side of the CCB-girder joint

3 ANNEXES

3.1 Annex of WP1

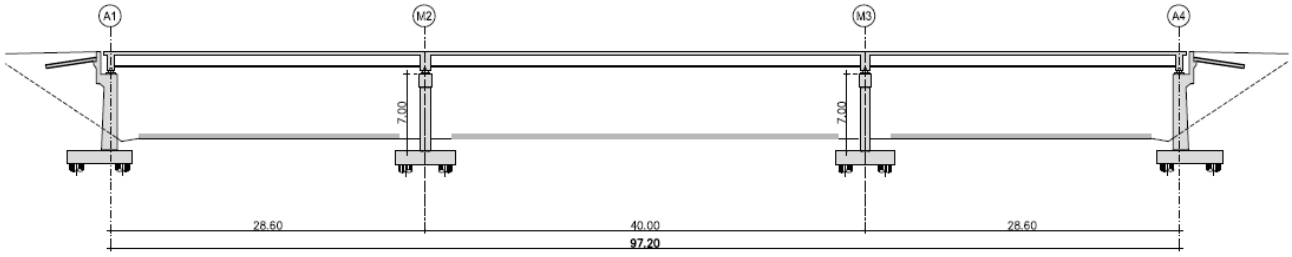

Fig. A3.1:-1 Case study 1

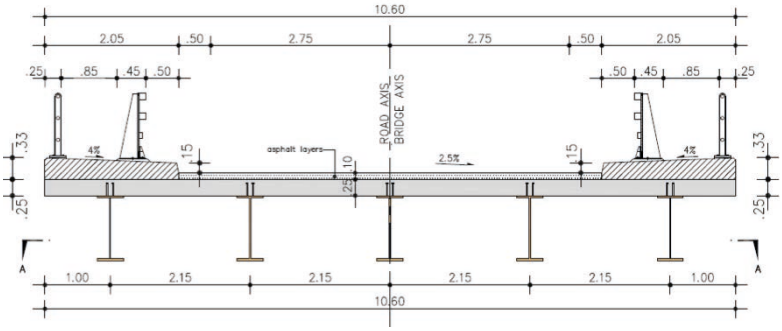

Fig. A3.1-2: Case study 1 - Cross section (5HLB1000/S460)

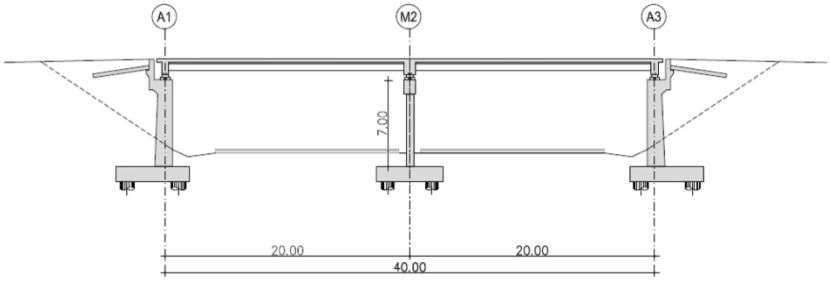

Fig. A3.1-3: Case study 2

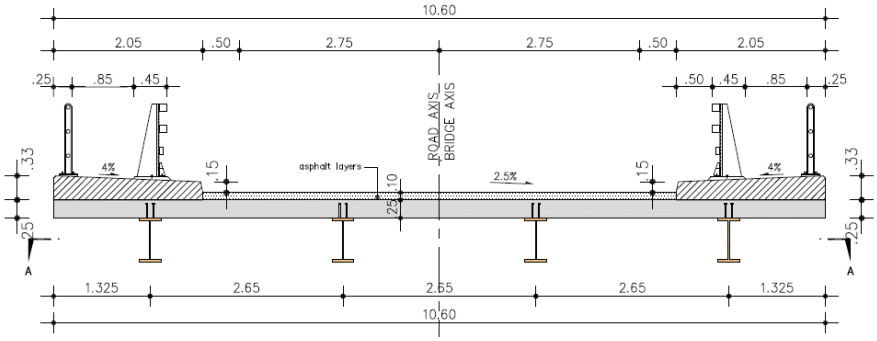

Fig. A3.1-4: Case study 2.1 - Cross section (4HEB600/S460)

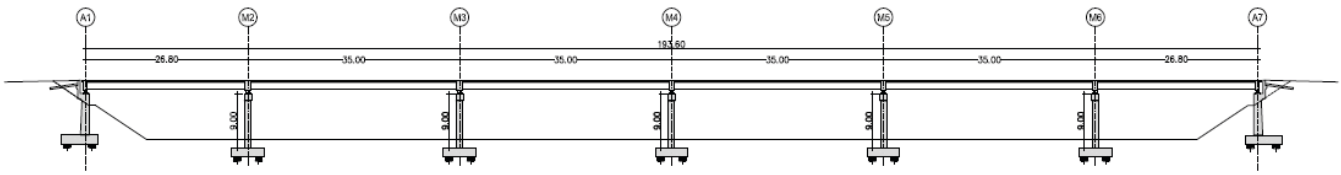

Fig. A3.1-5 Case study 3

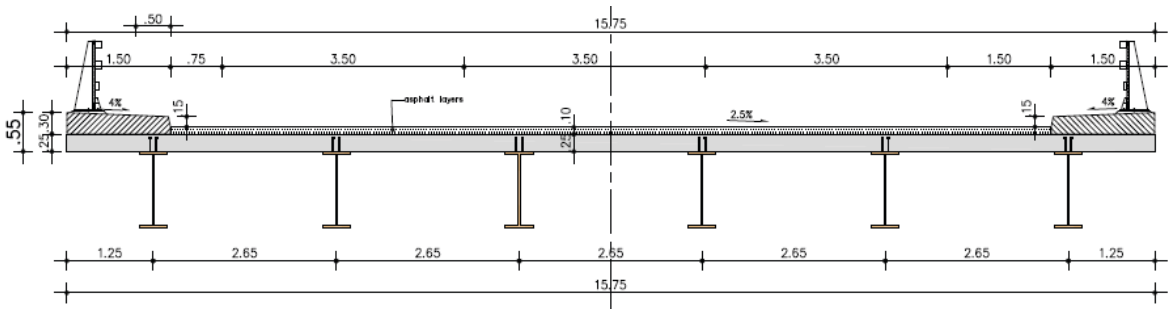

Fig. A3.1-6: Case study 3 - Cross section (6HLB1100/S460)

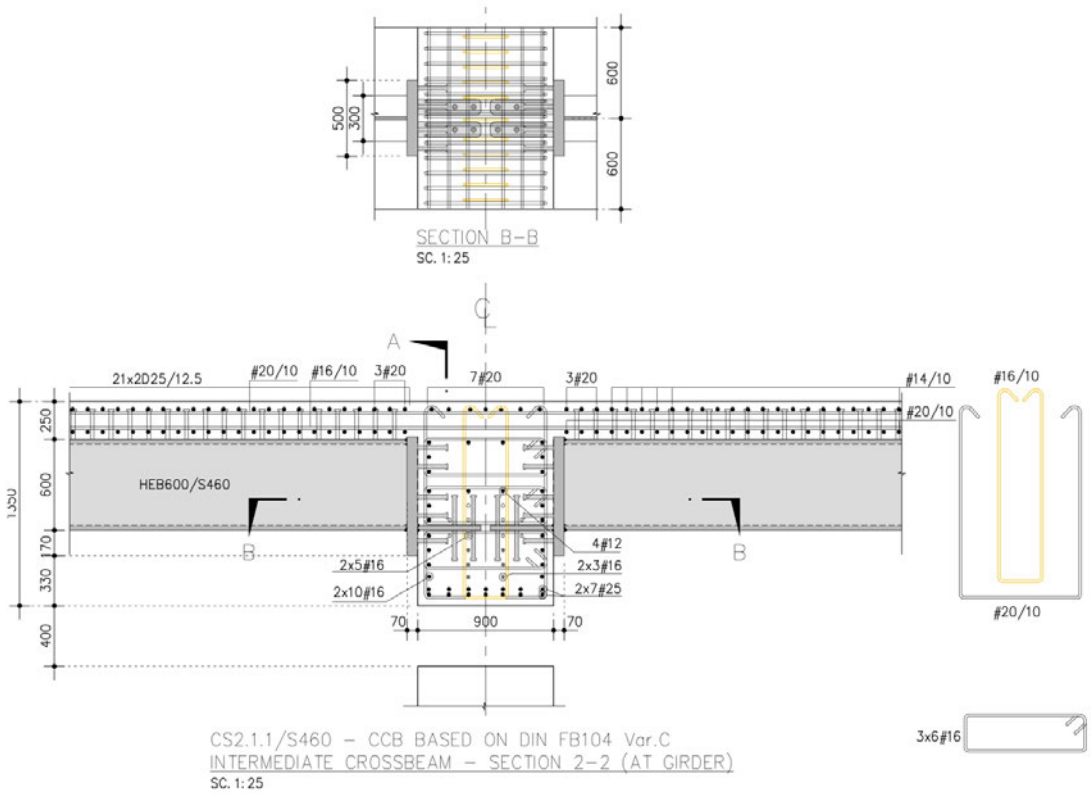

Fig. A3.1-7: Detailing of DIN FB-104 Type C Concrete Cross Beam

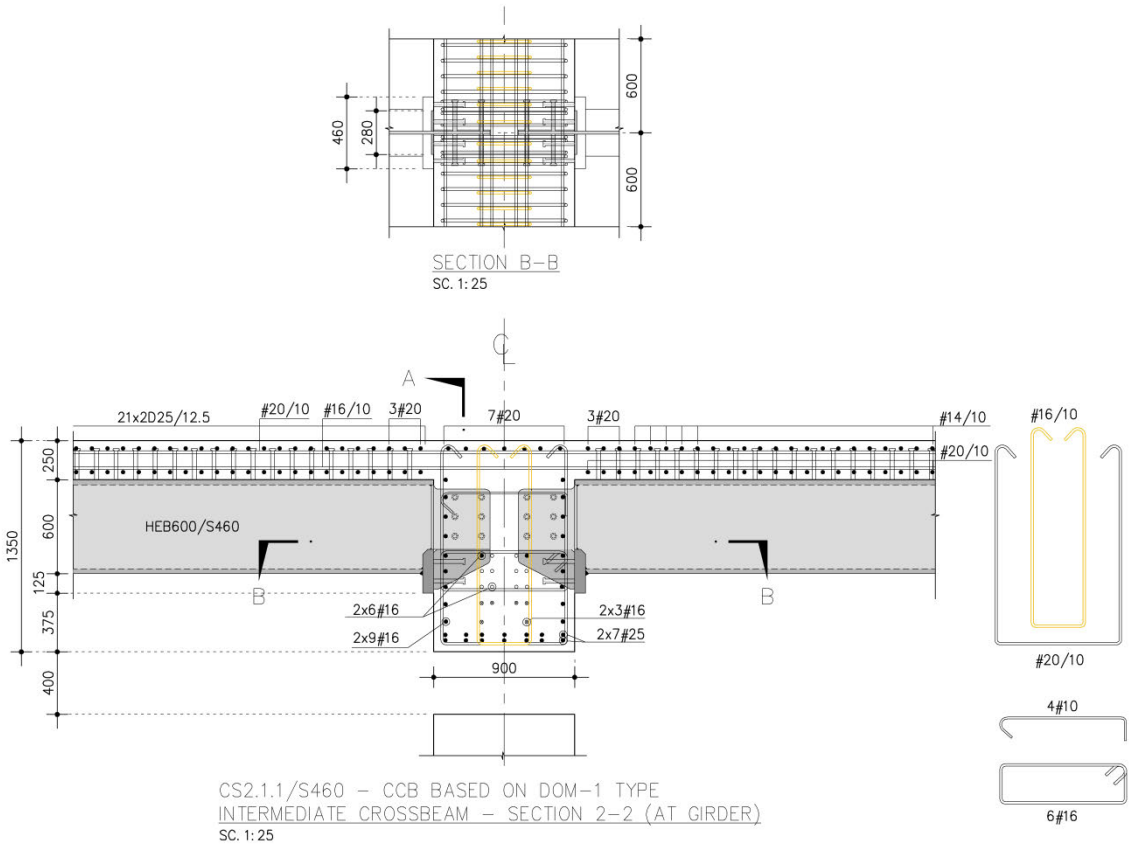

Fig. A3.1-8: Detailing of DOMI-1 Type C Concrete Cross Beam

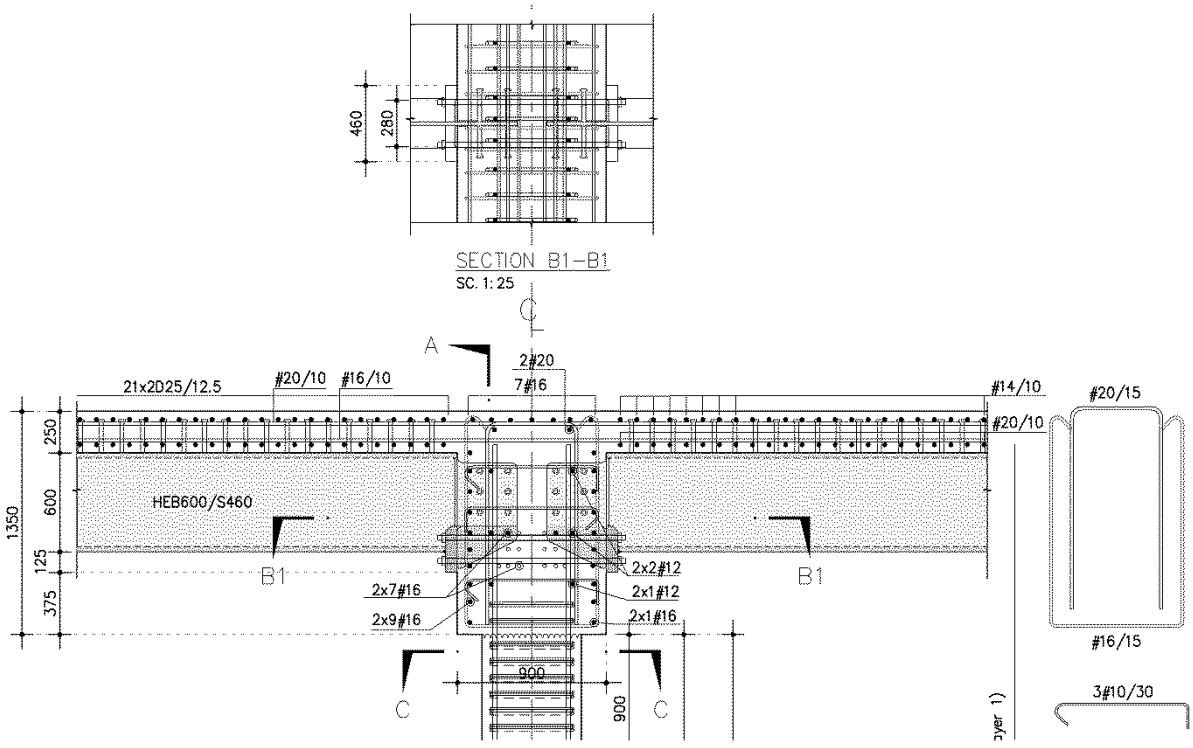

Fig. A3.1-9: Detailing of DOMI-2 Type Concrete Cross Beam

3.2 Annex of WP2

Task 2.3 - Experimental evaluation of the capacity of I-girder subassemblies subjected to transversal actions

In order to measure the deformation of elements inside the CCB, strain gauges were fixed with a special glue on head plate shear studs, rebars and stirrups before casting. Fig. A3.2-1, Fig. A3.2-2 and Fig. A3.2-3 show the position of each strain gauge for each type of specimens.

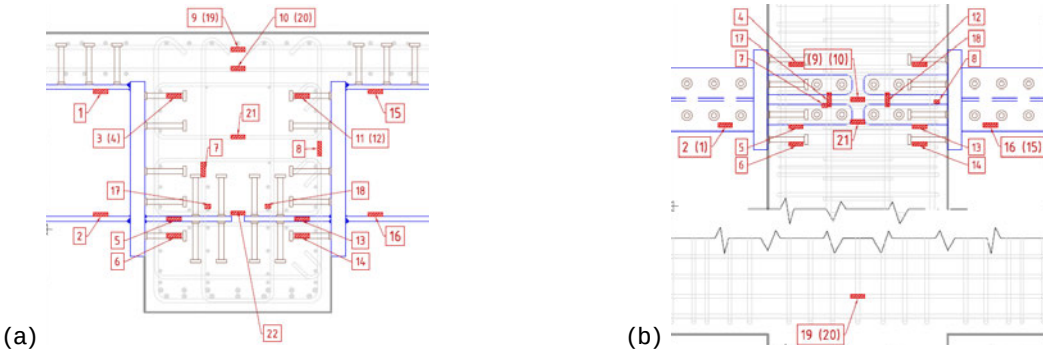

Fig. A3.2-1 - (a) front, and (b) top views of the position of strain gauges of the DIN FB104 Var.C joint detail

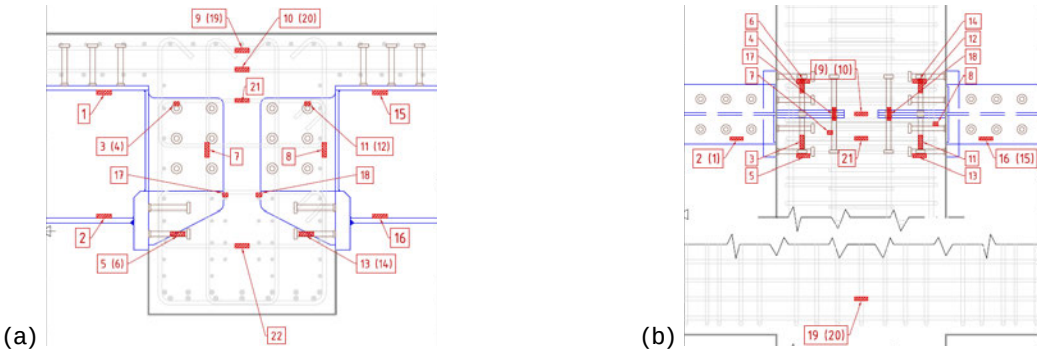

Fig. A3.2-2 - (a) front, and (b) top views of the position of strain gauges of the DOMI1 joint detail

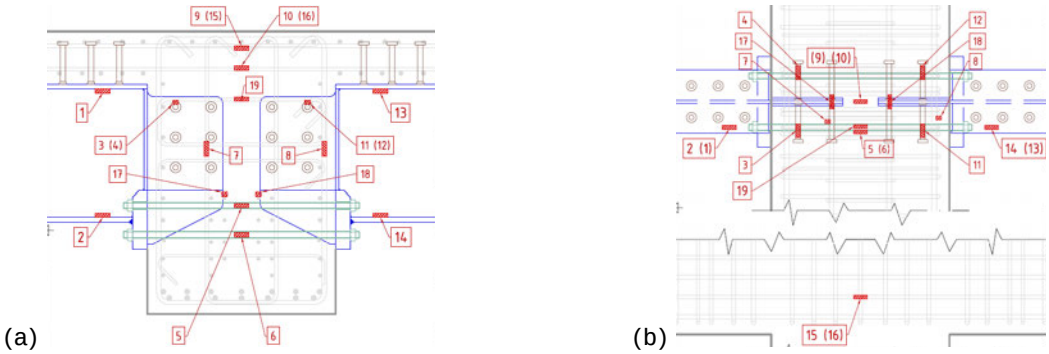

Fig. A3.2-3 - (a) front, and (b) top views of the position of strain gauges of the DOMI2 joint detail

With reference to forces measured at the actuators' load cells and transmitted to the hinges, the maximum values registered in every test are comparable, as shown in Section 2.3.2. Furthermore, the transversal displacement at which collapse of the specimen occurs varies slightly between the tests. Thus, the detail type appears not to be responsible for the bearing capacity of the specimens. In fact, the collapse mechanism develops primarily inside the concrete slab at the

girder-cross beam interface. These assertions are validated analysing crush and crack deformations on the interface between concrete slab and concrete cross-beam on different specimens. In fact, at failure displacement, on the interface, a crushing deformation range value between -3000 με and -8000 με was registered, whilst the value of cracking deformation was about between 3000 and 4500 με. Additionally, only the reinforcing steel inside the concrete slab registered a tensile deformation over the yielding point. Negligible or not important value of deformation can be read from the other measuring device fixed to specimen components. Fig. A3.2-4,56 show the most relevant results in term of deformations on steel flanges and reinforcing steel inside the concrete slab. For transversal displacements smaller than 50 mm, no detachment of head plates from the cross-beam could be visually observed, although in some cases Nelson studs suffered appreciable strain states. It is important to outline a key point of specimen design. The test specimens are representative of a small part of the bridge beam, which actually is supposed to comprise four or five lines of steel girders. The specimen longitudinal centre line passes through the girders and so does the neutral axis. Therefore, the strain state induced by horizontal transversal displacement turned out to be low.

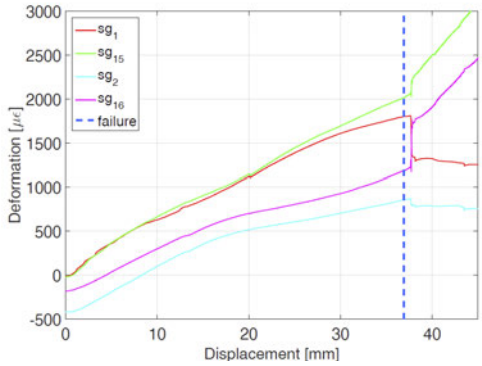

(a) Strain gauges on top and bottom flanges of steel girders

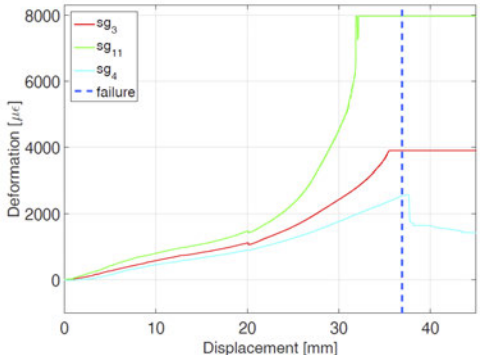

(b) Strain gauges on head plate studs

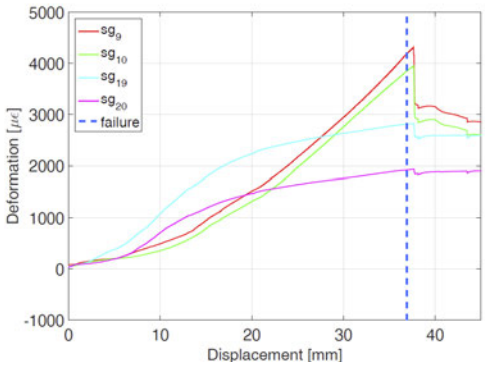

(c) Strain gauges on longitudinal re-bars of the concrete slab

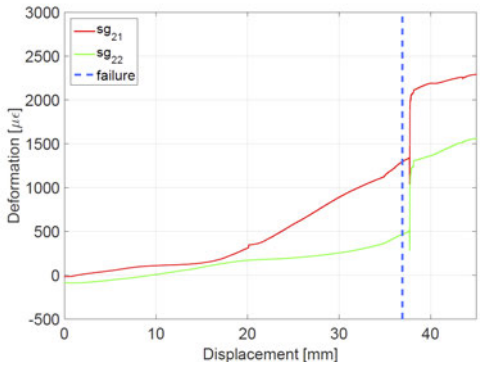

(d) Strain gauges on concrete cross beam stirrup

Fig. A3.2-4 - Strain gauges glued inside SQ1M specimen

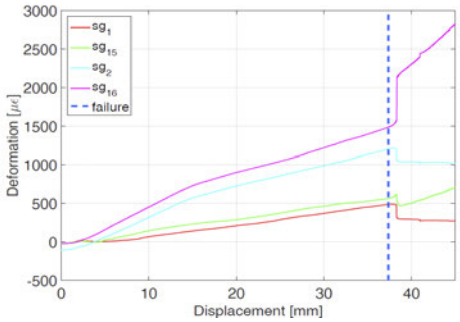

(a) Strain gauges on top and bottom flanges of steel girders

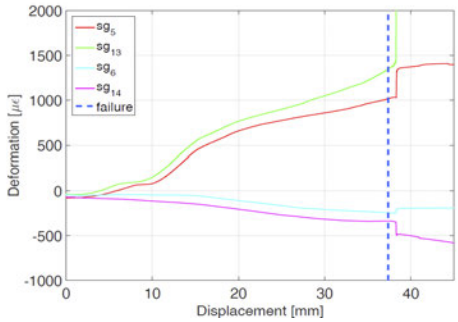

(b) Strain gauges on head plate studs

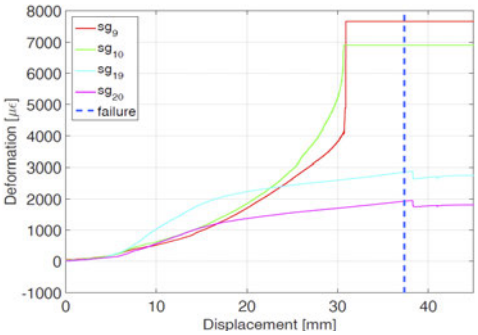

(c) Strain gauges on longitudinal re-bars of the concrete slab

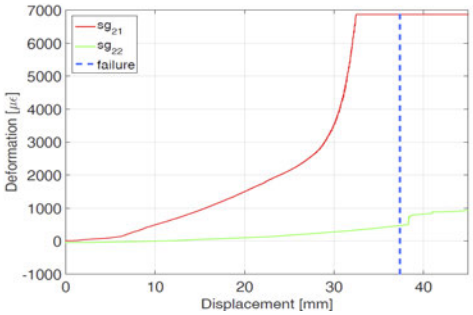

(d) Strain gauges on concrete cross beam stirrup

A3.2-5 Fig. 5 - Strain gauges glued inside SQ2M specimen

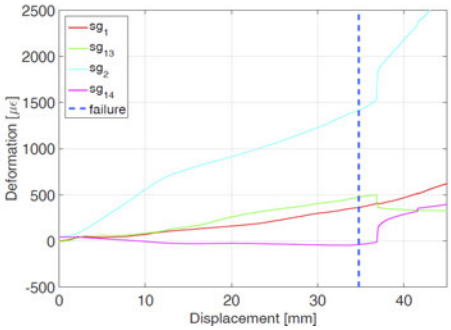

(a) Strain gauges on top and bottom flanges of steel girders

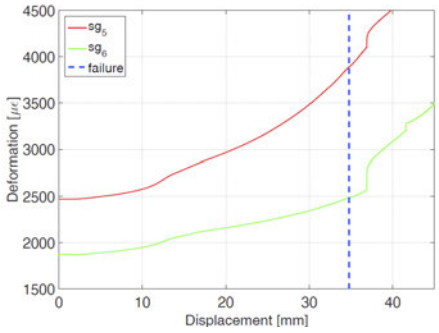

(b) Strain gauges on prestressed bars

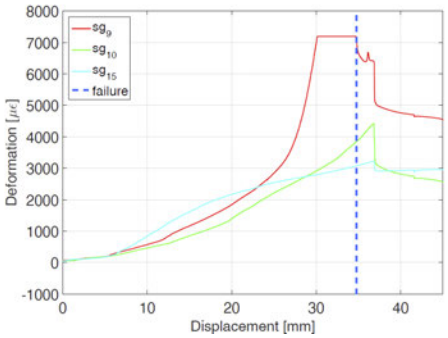

(c) Strain gauges on longitudinal re-bars of the concrete slab

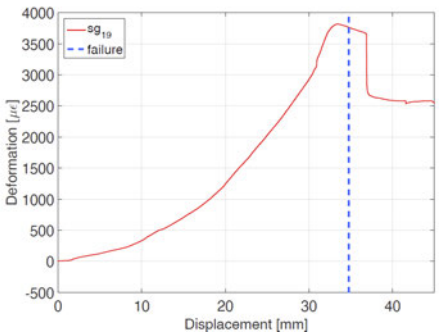

(d) Strain gauges on concrete cross beam stirrup

Fig. A3.2-6 -Strain gauges glued inside SQ3M specimen

Cracks opened in the slab mainly in the region around the cross-beam. The massiveness of the beam and the high percentage of reinforcement were responsible for its outstanding resistance.

The registered rotations of this element (around global y- and z-axis) were induced by the lever arm of actuator force. These rotations did not influence specimen response, although progressive cross-beam rotation in the x-y plane eventually led to asymmetric failure. In Fig. A3.2-7 and A3.2-8 are shown the specimens after collapse due to cyclic loads, whilst in Fig. A3.2-9 and A3.2-10 some deformations on the steel I-girders and steel headed studs during cyclic tests SQ1C and SQ2C respectively, accordingly to the positions shown in Fig. A3.2-1,3.

Fig. A3.2-7 - Damage condition of the specimen after the conclusion of the SQ1C test

Fig. A3.2-8 - Damage condition of the specimen after the conclusion of the SQ1C test

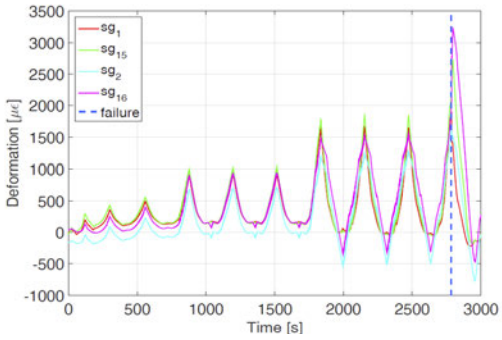

(a) Strain gauges on top and bottom flanges of steel girders

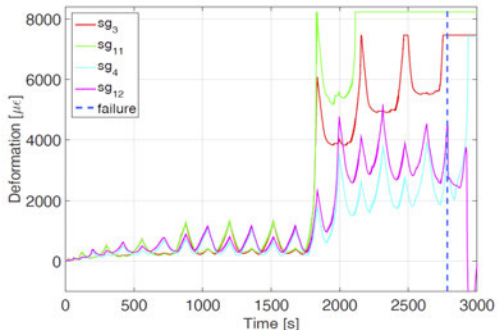

(b) Strain gauges on head plate studs

Fig. A3.2-9 - Strain gauges 1, 15, 2, 16, 3, 11, 4 and 12 during the SQ1C test

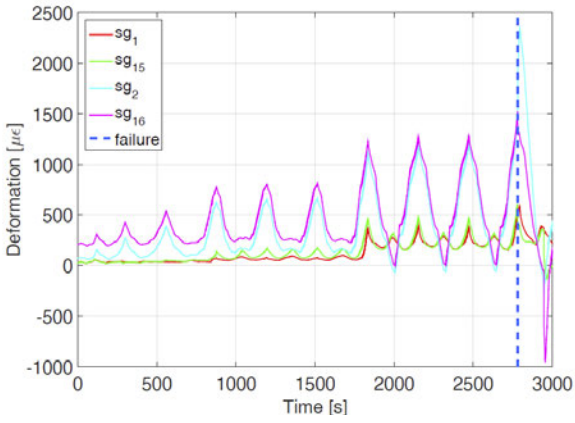

(a) Strain gauges on top and bottom flanges of steel girders

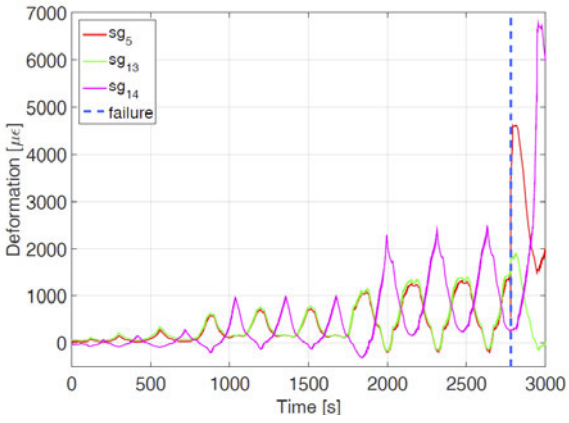

(b) Strain gauges on head plate studs

Fig. A3.2-10 - Strain gauges 1, 15, 2, 16, 3, 11, 4 and 12 during the SQ2C test

In order to measure the deformation of the elements inside the CCB, strain gauges were glued on the shear studs and steel bars before casting. Fig. A3.2-11 shows the position of each strain gauge for each type of specimens. The instruments' wires were protected with rubber tubes to prevent damage and to assure data could be acquired during the tests. Four strain gauges were glued on reinforcing steel bars of the slab for each type of connection, while eight strain gauges were placed on bottom plate for DIN FB-104 Type C, sixteen strain gauges on bottom shear studs for DOMI-1.

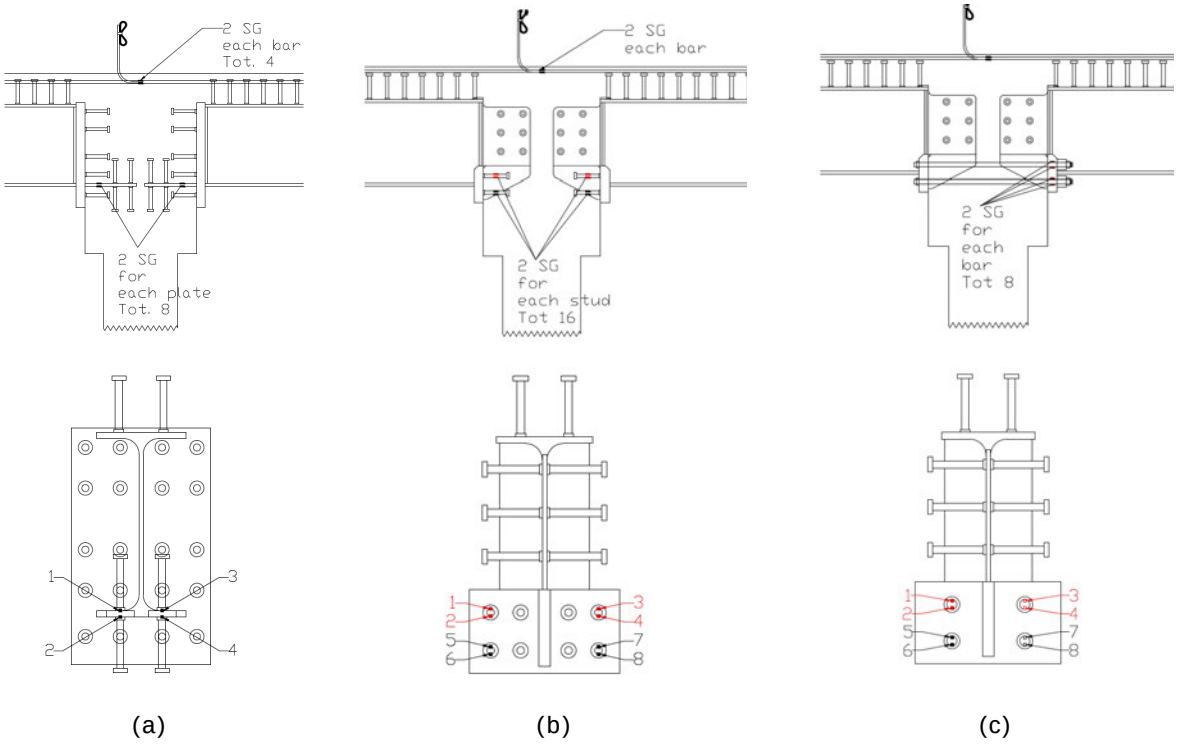

(a) (b) (c)

Fig.. A3.2-11 Internal Strain gauges on shear studs and prestressing bars
a) DIN FB-104 Type C; b) DOMI1; c)DOMI2

A2 - FBA2M (DIN FB104 Var C)

Local measures of strain were recorded to monitor the steel girders condition during the test. In Fig. A3.2-12 and A3.2-13 are plotted the time-history of the strains measured by the gauges indicated in Fig. 11. Given that the displacement has been applied along the x-direction (+), the bottom flange of steel girder on the left was subjected to a negative stress (tensile). Fig. A3.2-13 clearly shows a critical condition in the bottom flange in the last phase of the test. In fact, the sudden increasing of the strain at the bottom flange from 0.3% to 1.7% indicates a buckling problem. More details about the phenomena are reported in Deliverable 2.3 (2015).

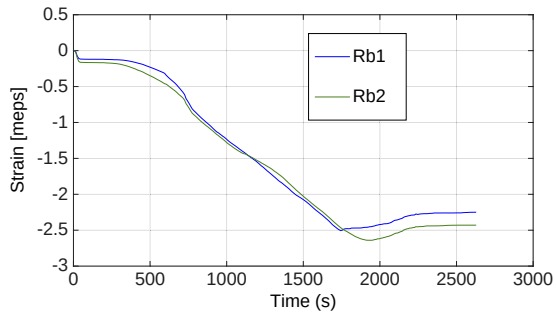

Fig. A3.2-12 Strain in the concrete slab rebars (Right)

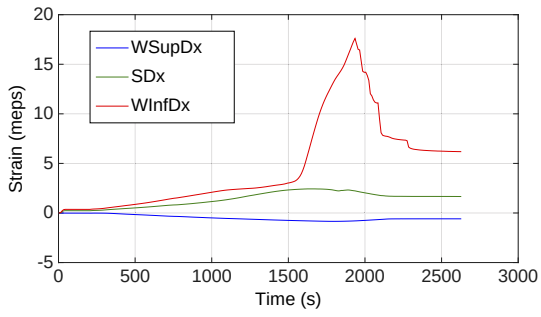

Fig. A3.2-13 Deformation in the steel girder (Right)

B2 - D1B2M (DOMI 1)

In Fig. A3.2-14 and A3.2-15 are plotted the time-history of the strain measured during test D1B2M by the gauges indicated in Fig. A3.2-11. As in the test on specimen A2, the girder on the left

remained elastic with an increasing depth of neutral axis for increasing horizontal displacement. The maximum strain was about 0.1% and thus the beam behaved elastic. On the contrary, Fig. A3.2-15 clearly shows a sudden increasing of the strain at the bottom flange that goes from 0.2% to 2%, which indicates a buckling problem. More details about the phenomena are reported in Deliverable 2.3 (2015).

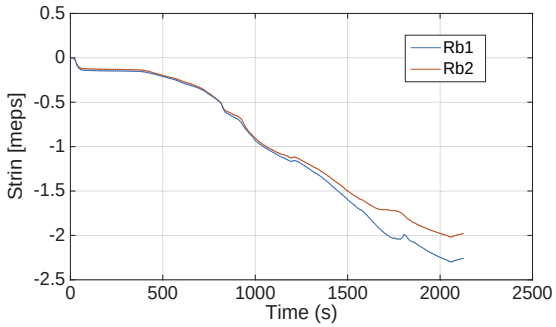

Fig. A3.2-14 Strain in the slab rebars (Right)

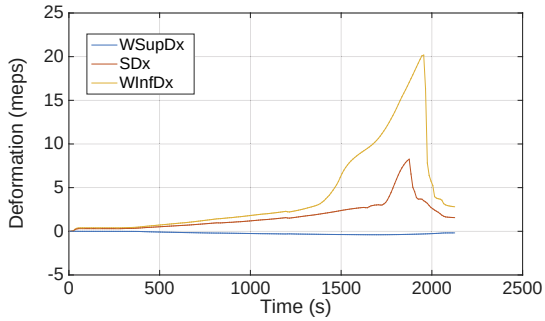

Fig. A3.2-15 – Deformation in the steel girder (Right)

CYCLIC TESTS

A2 - FBA2M (FB104 Var. c)

Fig. 16 shows the history of the strain in the slab reinforcement. After an increasing due to the vertical loads, the value changed cyclically, reaching a maximum value of 0.27%. The yielding (0.2%) occurred during the last 4 cycles for a displacement of 90 mm and a force of about 420 kN. The deformation in the steel girders is shown in Fig. A3.2-17 for the right side, the left side is not reported hereinafter but can be find in Deliverable 2.3 (2015). After the first 8 cycles the deformation in the girder on the right side increased suddenly till values of 0.9%, which indicates the occurrence buckling. As in the monotonic test the level of buckling was rather important. The distribution of the strain in the bottom shear studs is illustrated in Fig. A3.2-18 and Fig. A3.2-19. Given that the strain gauges were placed on the horizontal steel plate inserted in the CCB, this value corresponds to the behaviour of the group of shear studs welded on it. From the strain is possible to get stress and force on the plate that corresponds to the force of the group of shear studs. In the case of Fig. A3.2-19 the maximum strain is about 0.15%. Thus, the stress is about 308 MPa and being the section dimensions of the steel plate 50x12 mm, the force is 184.5 kN. Thus the steel plate is still elastic, whereas the shear studs are well beyond the elastic limits being the force of each stud equal to 46 kN whereas the elastic limit is equal to 35 kN.

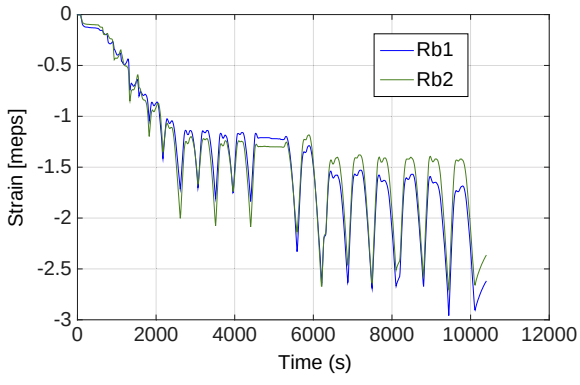

Fig. A3.2-16 Strain in the reinforcing bars (slab)

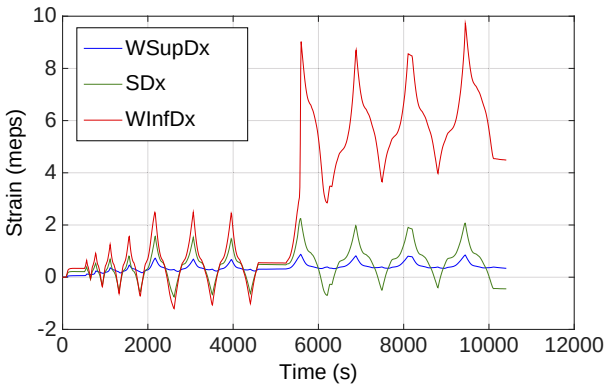

Fig. A3.2-17 Strain in the steel girder (Right)

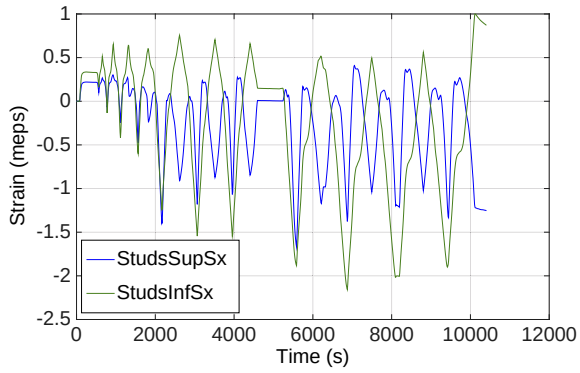

Fig. A3.2-18 Strain in the shear studs (Left)

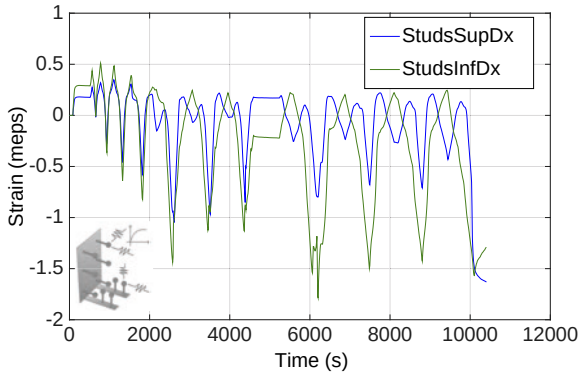

Fig. 19 Strain in the shear studs (Right)

B1 - D1B1C (DOMI 1)

Fig. A3.2-20 shows the history of the strain in the slab reinforcement. After a sudden increasing due to the vertical loads, the value increases cyclically, reaching a maximum value of 0.27%. The yielding (0.2%) occurred during the 7th cycle, for a displacement of 60 mm and a force of about 300 kN. The deformations in the right side of steel girders are shown in Fig. A3.2-21. After the first 7 cycles the deformation in the girder on the right increased suddenly till values of 1%, which indicates the occurrence of local problems, and in particular buckling. Just after, the buckling of the other steel girder happened.

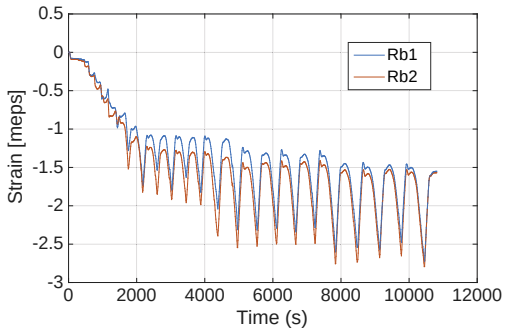

Fig. A3.2-20 – Strain in the reinforcing bars (slab)

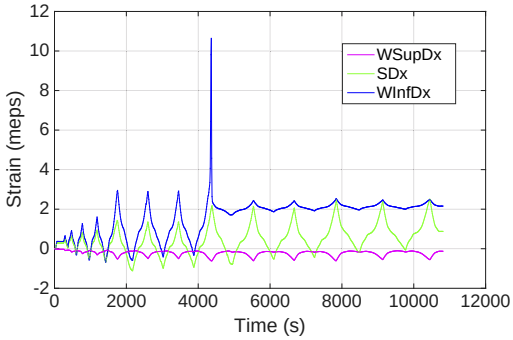

Fig. A3.2-21 – Strain in the steel girder (right)

C1, C2 and C4 – D2C1C, D2C2C and D2C4C (DOMI 2)

As in the previous tests, the strain in the steel reinforcing bars of the slab has shown a general oscillating increasing as shown in Fig. A3.2-22 for test D2C1C. A medium value starting from 0.01% of the vertical load condition to 0.2% - 0.25% in the last phase of the tests was measured, with an absolute maximum peak of 0.26% and 0.3% for the test D2C1C and D2C4C respectively. The yielding condition in the steel bars (0.2%) occurred at maximum force for both the specimens. The deformations in the steel girders are plotted in Fig. A3.2-24 and A3.2-25 for tests D2C4C, in which a sudden increasing of the strain starting from the 8th cycle is present. As in the previous connection types, this is due to the buckling phenomenon localized in the bottom flange of the steel girder as shown. However, in this case the post-buckling phenomenon has been rather limited.

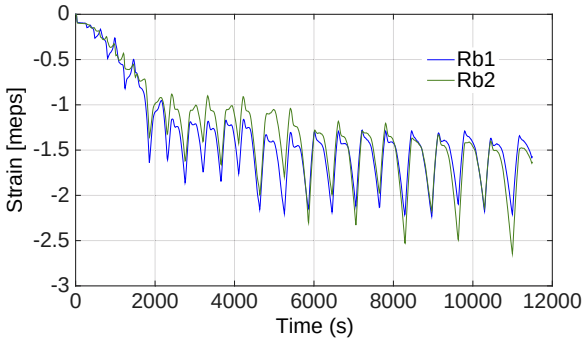

Fig. A3.2-22 Strain in the steel reinforcing bars (slab) (D2C1C)

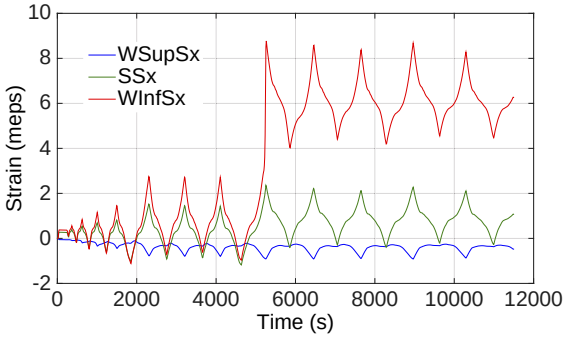

Fig. A3.2-23 – Strain in the steel girders (D2C1C): Right Girder

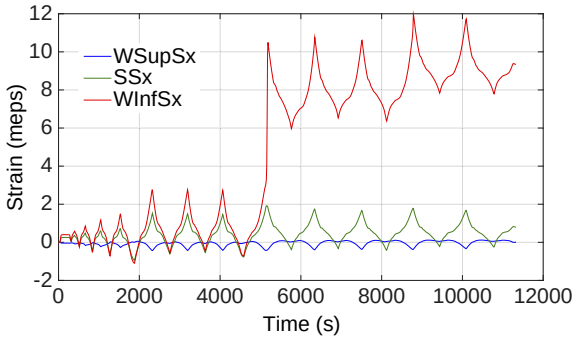

Fig. A3.2-24 – Strain in the steel girders (D2C4C)(Left)

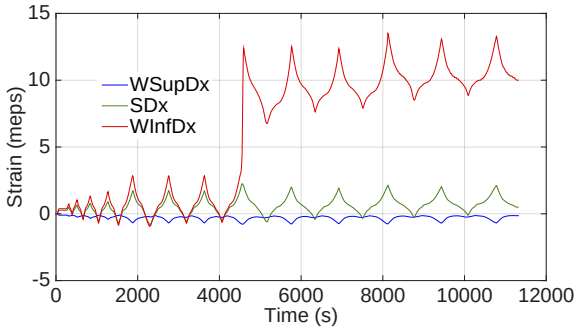

Fig. A3.2-25 – Strain in the steel girders (D2C4C) (Right)

4 LIST OF FIGURES

5 LIST OF TABLES

6 REFERENCES

ABAQUS 6.14, Dassault Systèmes, 2015.

Alessandri, S., Giannini, R. and Paolacci, F. (2013). Aftershock risk assessment and the decision to open traffic on bridges, Earthquake Engng. Struct. Dyn., 42: 2255–2275.

ASTM E606-04, Standard Practice for Strain-Controlled Fatigue Testing. West Conshohocken, PA, USA: ASTM International, 2004.

ATC-24, 1992. “Guidelines for Cyclic Seismic Testing of Components of Steel Structures for Buildings,” Report No. ATC-24, Applied Technology Council, Redwood City, CA.

ATC-58-1, (2011), Seismic Performance Assessment of Buildings Volume 1 – Methodology, Applied Technology Council.

ATC-58-2, (2011), Seismic Performance Assessment of Buildings Volume 2 – Implementation Guide, Applied Technology Council.

Atktinson G.M., Boore D., (2006), Earthquake Ground-Motion Prediction Equations for Eastern North America, Bulletin of the Seismological Society of America, Vol. 96, No. 6, pp. 2181–2205, December

Berry, M. P. and Eberhard, M., O. (2003). Performance models for flexural damage in reinforced concrete columns. Report No. 2003/18, University of California, Pacific Earth-quake Engineering Research Center, Berkeley CA.

Borzi, B., Ceresa, P., Franchin, P., Noto, F., Calvi, G.M., and Pinto, P.E., (2015). Earthquake Spectra Nov 2015, Vol. 31, No. 4 pp. 2137-2161.

Bursi, O. S., Aribert, J. M., and Lachal, A., Energy-based damage models in seismic analysis of steel-concrete composite members. The Twelfth European Conference on Earthquake Engineering, London, 2002.

Campbell K.W., Bozorgnia Y., (2007), Campbell-Bozorgnia NGA Ground Motion Relations for the Geometric Mean Horizontal Component of Peak and Spectral Ground Motion Parameters, PEER report 2007/02.

CEB-FIP Model Code 1990 – Design Code, Comité Euro-International du Béton, Lausanne, Switzerland, Thomas Telford, 1993.

CEN, Eurocode 2. “Design of Concrete Structures”, Brussels, 2004.

CEN, Eurocode 3. “Design of Steel Structures”, Brussels, 2005.

CEN, Eurocode 4. “Design of composite Steel and Concrete Structures”, Brussels, 2004

CEN, Eurocode 8. “Design of Structures for Earthquake Resistance”, Part 1: Action on Structures, European Committee for Standardization, Brussels, 2005.

CEN, Eurocode 8. “Design of Structures for Earthquake Resistance”, Part 2: Bridges, European Committee for Standardization, Brussels, 2005.

CEN, Eurocode 8. “Design of Structures for Earthquake Resistance”, Part 3: Assessment and retrofitting of buildings, Brussels, 2005.

Chaboche, J.-L., “Time-Independent Constitutive Theories for Cyclic Plasticity”, International Journal of Plasticity, 2(2), 1986.

Chaboche, J.-L., “Constitutive Equations for Cyclic Plasticity and Cyclic Visco-Plasticity”, International Journal of Plasticity, 5(3), 1989.

Chabrolin B., Kretz T., Laravoire J., Steel-Concrete Bridges. A guide for novel structures. National Program MIKTI (France), 2008.

Chai, Y. H., Romstad, K. M., and Bird, S., Energy based linear damage model for high-intensity seismic loading. Journal of Structural Engineering, ASCE, 121(5):857–864, 1985.

Chiou, B. S.-J. and Youngs R. R. (2008), An NGA model for the average horizontal component of peak ground motion and response spectra, Earthquake Spectra, 24(1), 173-215.

Cornell, C. A. (1968). "Engineering seismic risk analysis." Bulletin of the Seismological Society of America, 58(5), 1583-1606.

Deliverable D1.1 - SEQBRI Project (2013), Preliminary analysis results of Case Studies.

Deliverable D1.2 - SEQBRI Project (2013), Definition of I-girder Subassembly Specimens to be tested in laboratories and loading test protocols.

Deliverable D2.1 - SEQBRI Project (2013), Experimental data on Mechanical characterization of fine grain steels.

Deliverable D2.2 - SEQBRI Project (2014), Tests on scaled I-girder subassembly specimens-Experimental results of damaged substructures related to intermediate concrete crossbeams under transversal loading conditions.

Deliverable D2.3 - SEQBRI Project (2015), Experimental results of damaged substructures related to intermediate concrete crossbeams under longitudinal loading conditions

Deliverable D2.4 - SEQBRI Project (2015), Test on scaled I-girder Subassembly specimen-Experimental results of damaged substructures subjected to vertical loads.

Deliverable D3.1 - SEQBRI Project (2016), Calibration of numerical models based on test data.

Deliverable D4.1 - SEQBRI Project, (2014), Seismic response data of selected Case Studies.

Deliverable D4.2 - SEQBRI Project, (2014), Fragility and Damage curves of selected Case Studies.

Deliverable D4.3 – SEQBRI Project, (2015), Performance-based earthquake engineering analysis of short-medium span steel-concrete composite bridges.

Deliverable D5.1 - SEQBRI Project (2016), Report on Design Guidelines and Recommendations.

Deliverable D5.2 - SEQBRI Project (2016), Dissemination report of project achievements.

Deliverable D5.3 - SEQBRI Project (2016), Divulgation Round Table of project achievements.

DIN FB 104, DIN-Fachbericht 104 - Verbundbrücken (Composite steel and concrete bridges). Berlin, 2009

ECCS, Recommended Testing Procedures for Assessing the Behaviour of Structural Steel Elements under Cyclic Loads. Technical Committee 1, TWG 1.3, No. 45, Brussels, Belgium, 1986.

Evangelos I. Katsanos, Anastasios G. Sextos, George D. Manolis (2010). Selection of earthquake ground motion records: A state-of-the-art review from a structural engineering perspective, Soil Dynamics and Earthquake Engineering, Volume 30, Issue 4, April 2010, Pages 157-169.

FEMA 356 (2000): Prestandard and Commentary for the Seismic Rehabilitation of Buildings, Prepared by American Society of Civil Engineers, Washington, D.C. (U.S.A.), November.

Gattesco N., Giuriani E. (1996). Experimental study on stud shear connectors subjected to cyclic loading, Journal Constructional Steel Research, 38(1):1-21.

Giannini, R. MATHAZARD: A Program for Probabilistic Seismic Hazard Analysis with Matlab. (2015).

Gutenberg, R., and C.F. Richter, (1944). Frequency of earthquakes in California, Bulletin of the Seismological Society of America, 34, 185-188.

Hutchinson, T., Zhang, J., Eva, C., Development of a Drift Protocol for Seismic Performance Evaluation Considering a Damage Index Concept. Earthquake Spectra, Volume 27, No. 4, pages 1049-1076, November 2011.

ISO 12106:2003, Metallic materials - Fatigue testing - Axial-strain-controlled method. Geneva, Switzerland: International Organization for Standardization, 2003.

Kumar S., Itoh Y., Saizuka K., Usami T. (1997), Pseudodynamic Testing of Scaled Models, Journal of Structural Engineering 123:4.

Kunnath, S. K. (2006) Application of the PEER PBEE Methodology to the I-880 Viaduct, Pacific Earthquake Engineering Research Center, PEER, Report No. 2006/10.

Lee, J., Fenves, G.L., “Plastic-Damage Model for Cyclic Loading of Concrete Structures”, Journal of Engineering Mechanics, 1998.

Lee P.G., Shim C.S., Chang S.P. (2005). Static and fatigue behavior of large stud shear connectors for steel_concrete composite bridges, Journal of Constructional Steel Research, 61(9):12, 70-85.

Lubliner, J., Oliver, J., Oller, S., Onate, E., “A Plastic-Damage Model for Concrete”, International Journal of Solids and Structures (Vol. 25), S. 299–329, 1989.

Mackie K.R., Wong J.M., Stojadinovich B. (2008). Integrated Probabilistic Performance-Based Evaluation of Benchmark Reinforced Concrete Bridges, Pacific Earthquake Engineering Research Center. PEER 2007/09-report, 2008.

Maier, P., Kuhlmann, U. Tardivel, Y., Robert, N., Raoul, J., Perdigão, V., Martins, N., Barros, P., Friedrich, H., Krieger, J., (2012). Steel-composite bridges – holistic approach applied to European Case Studies. In: proceedings of the 6th International Conference on Bridge Maintenance, Safety and Management, Stresa, Italy, July 8-12.

McKenna, F., Mazzoni, S., Scott, M.H., and Fenves, G.L., OpenSees Command Language Manual. Pacific Earthquake Engineering Research Center, University of California, Berkeley, July 2007.

Moschonas, I.F., Kappos, A.J., Panetsos, P., Papadopoulos, V., Makarios, T.K., Thanopoulos, P., 2009. Seismic fragility curves for greek bridges: Methodology and case studies. Bulletin of Earthquake Engineering 7, 439–468.

Nielson B.G., DesRoches R., (2006), Influence of modeling assumptions on the seismic response of multi-span simply supported steel girder bridges in moderate seismic zones, Engineering Structures 28 (2006) 1083–1092.

Ohata, M., and Toyoda, M., Damage concept for evaluating ductile cracking of steel structure subjected to large-scale cyclic straining, Science and Technology of Advanced Materials 5, pp. 241-249, 2004.

P-58-1, (2012), Seismic Performance Assessment of Buildings Volume 1 – Methodology, FEMA, USA.

P-58-2, (2012), Seismic Performance Assessment of Buildings Volume 2 – Implementation Guide, FEMA, USA.

PEER Strong Motion Database. Pacific Earthquake Engineering Research, Available from: http://peer.berkeley.edu/smcat/).

Pinto, P.E. and Franchin, P. (2010). Issues in the upgrade of Italian highway structures. Journal of Earthquake Engineering. 14(8). pp 1221-1252.

Porter, K. A. (2003). "An Overview of PEER's Performance-Based Earthquake Engineering Methodology." 9th International Conference on Applications of Statistics and Probability in Civil Engineering, San Francisco, CA, U.S.

SAP2000, Integrated Software for Structural Analysis and Design - Analysis reference manual .

SBRI 2013. Draft Final Report. SBRI-Document No: SBRI-ALL-006-DraftFinalReport.

SEQBRI Project (2013), First Annual Report.

SEQBRI Project (2015), Second Annual Report.

SEQBRI Project (2014), Mid-Term Report.

Shim C.S,. Lee P.G., Yoon T.Y. (2004) Static behavior of large stud shear connectors, Engineering Structures, 26:18, 53-60.

SOFISTIK, A finite element software, AG, Germany.

Tubaldi, E., Barbato, M., and Dall'Asta, A. (2009). Parametric Study of continuous steel-concrete composite bridges exhibiting dual load path. Report n. 07/2009 LSU.

Tubaldi, E., Barbato, M., and Dall'Asta, A. (2010). Transverse seismic response of continuous steel-concrete composite bridges exhibiting dual load path. Earthquake and Structures 1:1,21-41.

Vamvatsikos, D., Cornell, C.A. (2002). Incremental dynamic analysis, Earthquake Engineering and Structural Dynamics, 31, 491–514.

Viest, I. M., (1956). Investigation of Stud Shear Connectors for Composite Concrete and Steel T-Beams, Journal of the American Concrete Institute, V. 27, No. 8, April 1956, 875-891.

Zareian F., Krawinkler H. (2009). Simplified performance based earthquake engineering, Report 169, The John A. Blume Earthquake Engineering Center.

HOW TO OBTAIN EU PUBLICATIONS

Free publications:

- one copy:
  via EU Bookshop (http://bookshop.europa.eu);
- more than one copy or posters/maps:
  from the European Union's representations (http://ec.europa.eu/represent_en.htm);
  from the delegations in non-EU countries (http://eeas.europa.eu/delegations/index_en.htm);
  by contacting the Europe Direct service (http://europa.eu/europedirect/index_en.htm) or calling 00 800 6 7 8 9 10 11 (freephone number from anywhere in the EU) (*).

  (*) The information given is free, as are most calls (though some operators, phone boxes or hotels may charge you).

Priced publications:

- via EU Bookshop (http://bookshop.europa.eu).

KI-NA-28-455-EN-N

Nowadays, short-medium span steel-concrete composite I-girder bridges made of hot rolled steel beams are very popular, owing to their short construction time and reduced costs. Moreover, they are particularly suitable for seismic areas due to their limited weight. With regard to static loading, these bridges exhibit a favourable behaviour testified by recent research projects. However, seismic loading has not been yet fully investigated. For this reason, SEQBRI project aimed to fill this gap investigating the applicability a new design/assessment methodology (PBEE) to a new typology of steel concrete composite bridges with S355M/N-S460M/N fine grain steel and concrete cross beams, through a comprehensive experimental and numerical investigation. The results have been used to provide the foundation for a new generation of European seismic codes for bridges and to extend Eurocodes. The research program consists of a combination of actions performed by experts in different fields (Academic Institutions (UNIRM3, UNITN, RWTH), designers (DOMI SA), a Center of excellence in Infrastructure and Transportation engineering (CEREMA, ex SETRA), a world's number one Steel Company (ARCELOR MITTAL) for the purpose of developing guidelines for the application of PBEE methodology for the design/assessment of steel concrete composite (SCC) bridges with concrete cross beams (CCB). Towards this purpose, an extensive experimental analytical and numerical work has been conducted within the project, under the synergy of all partners. The proposed guidelines are novel incorporating modern aspects of earthquake-resistant design for the design/assessment of SCC bridges with CCB.

Publications Office

ISBN 978-92-79-65612-5
doi:10.2777/48012